AIT IIT

DES-RP/88/1

FINAL REPORT

RESEARCH AND DEVELOPMENT OF SOLAR-POWERED DESICCANT

REFRIGERATION FOR COLD STORAGE APPLICATIONS (4.180)

By

Illinois Institute of Technology
Chicago, Illinois

and

Asian Institute of Technology
Bangkok, Thailand

February, 1988

SUMMARY

The objective of the present work was to develop efficient thermally activated desiccant cooling systems for cold storage applications. Since the required temperatures are below 0°C, open cycle desiccant systems (where the refrigerant is water) are not suitable.

It is therefore necessary to utilize closed cycle desiccant systems with a suitable fluid refrigerant-desiccant pair. To this end, we first modeled an available zeolite-water system and compared the predictions to experimental data. We then studied methanol-zeolite and methanol- activated carbon system.

Finally, we analyzed an advanced system which is based on a heat regeneration concept. This system seem to yield coefficients of performance which are two to three times higher than those of conventional thermally driven cooling systems.
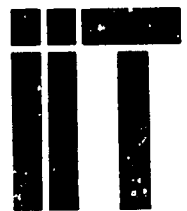
REPORT ORGANIZATION

Research and Development of Solar Powered Desiccant
Refrigeration for Cold Storage Applications

The work of this contract was a combined effort by IIT Chicago and AIT Bangkok. The present report is organized in two parts:

- Part I is analytical studies carried out by IIT Chicago

- Part II is mostly experimental studies carried out at AIT Bangkok

iiT

3

RESEARCH AND DEVELOPMENT OF SOLAR-POWERED DESICCANT REFRIGERATION FOR COLD STORAGE APPLICATIONS

(Grant No. DPE-5542-G-SS-4057-00)

Final Report

by

Zalman Lavan
Ali Hajji
Illinois Institute of Technology

and

William M. Worek
University of Illinois at Chicago

1988

H

TABLE OF CONTENTS

NOMENCLATURE

Symbol	Term
a	Activity
A	Area of adsorbing interface in Chapter II, area of the solar collector in Chapter IV
a_1, a_2, a_3	Coefficients defined in equations (6.34,a,b,c)
A_1, A_2	Constants defined in equations (7.54,a,b)
a_L	Constant defined in equation (2.72)
a_n, b_n	Coefficients introduced in equations (6.5a,b)
$a(t)$	Function introduced in equation (2.57)
$A(w)$	Function introduced in equation (2.32)
b	Channel width in Chapter VII
B_1, B_2	Constants defined in equations (7.42,a,b)
$b(t)$	Function introduced in equation (2.57)
$B(w)$	Function introduced in equation (2.32)
C	Specific heat in Chapters II-V, Concentration in VI
C_1, C_2	Constants defined in equations (7.61,a,b)
COP	Coefficient of performance
d	Depth of the absorption film in Chapter VI
D	Constant introduced in equation (2.29), Coefficient of mass diffusivity in Chapter VI
E_i	Dimensioless parameter defined in section 4.2
$f(T)$	Function introduced in equation (2.33)
$F(T,w)$	Function introduced in equations (2.32) and (4.1)
g	Acceleration of gravity

Symbol	Term
$g(T,w)$	Function introduced in equation (2.38)
G	Gibbs's free energy
G	Absorptivity function defined in equation (2.47)
Gr	Grashoff Number
h	Coefficient of heat transfer
h_m	Coefficient of mass transfer
H	Enthalpy, dimensionless heat in Chapter VII
I_i	Dimensionless integral defined by equations (5.17)
$I(t)$	Incident solar flux at time t
I	Length of the regenerator in Chapter V
I	Channel Length in Chapter VII
L	Characteristic length in section 4.4, Dimensionless channel length in Chapter VII
$L(T)$	Latent heat of vaporization at temperature T written in the form $L(T)=L_o + a_L T$
k	Thermal conductivity
K	Equilibrium constant
m,M	Mass in Chapters II-V, Dimensionless Mass Flux in Chapter VI
n	Number of adsorbed moles in Chapter II, Mass Flux in Chapter VI
N	Ratio β^*/β
Nu_L	Nusselt Number based on L
p	Pressure
P	Perimeter of the cross section of the regenerator, Dimensionless pressure in Chapter VII

Symbol	Term
Pr	Prandtl Number
q	Heat Flux in Chapters VI-VII
q_{st}	Isosteric heat of adsorption
Q	Heat quantity in Section II-V, Dimensionless Heat Flux in Chapter VI, Dimensionless flow rate in Chapter VII
r	Ideal gas constant for the adsorbate (R/Molar mass), Quantity defined by equation (6.13)
R	Universal ideal gas constant=8.314 (J/mol.K), Constant defined in equation (7.20b)
S	Entropy, Constant defined in equation (7.39)
Sc	Schmidt Number
Sh	Sherwood Number
t	Time, Temperature in Chapter VII
T	Temperature, Dimensionless temperature in Chapter VII
u(y)	Velocity
U(Y)	Dimensionless velocity
V	Velocity of the fluid
V	Volume
w	Uptake (mass of adsorbated speies/mass of adsorbent) in Chapters II-V, Mass fraction of the diffusing component in Chapter VII
W	Dimensionless mass fraction
X	Dimensionless longitudinal coordinate
Y	Dimensionless coordinate across the channel
z	Space cordinate along the regenerator

Greek Symbols

Symbol	Term
α	Absorptance in Chapter IV, Thermal diffusivity in Chapter VI
β	Collecor inclination w.r.t. the horizontal plane, Volumetric coefficient of thermal expansion
β^*	Volumetric coefficient of mass fraction expansion
ΔH	Differential heat of absorption
ε	Adsorption potential in section2.2, Emissivity in section (4.2) and Porosity (or void fraction) elsewhere
ϕ	Angle of inclination in Chapter VII
Φ	Dimensionless F
Γ	Surface concentration in Chapter II and dimensionless G in Chapters IV and V
η	Efficiency of the solar collector or dimensionless t
$I(\eta)$	Dimensionless I(t)
φ	Dimensionless isosteric energy of adsorption
ϕ_n, ψ_n	Eigen functions
λ	Dimensionless latent heat of vaporization in Chapters II-V, Dimensionless heat of absorption in Chapter VI
μ	Chemical potential
μ_n	Eigen values in Chapter VI
ν	Kinematic viscosity

Symbol	Term
π	Spreading pressure defined in equation (2.10), Dimensionless pressure in Chapters IV and V
ρ	Mass density
θ	Degree of saturation of adsorbing surface in Chapter II, Dimensionless temperature in Chapters IV and V
τ	Transmittance in Chapter IV, Length of a period in Chapter V, Dimensionless time in Chapter VI
$(\tau\alpha)_e$	Effective transmittance.absorptance of the collector
ζ	Dimensionless space coordinate in Chapters V and VI

Subscripts

Symbol	Term
a	"Dry" adsorbent
ad	Adsorption
boil	Boiler
c	Inert parts of the collector in Chapter IV and inert parts of the regenerator or "cold" period in Chapter V
co	Condenser
ev	Evaporator
e or eq	At equilibrium
exch	At the heat exchanger
f	Fluid
g	Glass or gas phase
h	"Hot" period
i	At the interface
L	Liquid phase

Symbol	Term
o	At the reference state or characteristic value
p	At constant pressure
re	Regeneration
s	Sorbed species or saturation, At the wall in Chapter V
sp	Specific
ss	Minimum value of T_{re} for the cycle to work
t	Temperature
V	At constant volume
w	Mass Fraction
∞	Ambient

Superscript

Symbol	Term
-	Partial molar quantity
~	Integral quantity

ABSTRACT

In the first section of this thesis, a relationship for the solid-vapor adsorption equilibrium is proposed and proved to represent accurately the experimental data and to be convenient for numerical calculations. Formulas describing the processes involved in closed-cycle cooling and heating systems are also derived.

These formulas are first applied in a dynamic analysis of a closed-cycle solar adsorption refrigerator. A computer program is written to study the effect of the design parameters and operating conditions on the system performance.

The second application concerns the simulation of the regenerative adsorption cooling systems which are recently introduced to increase the performance of adsorption machines. A computer program is developed to analyze the dynamic behaviour of such systems.

In the second section, an analytical investigation of the vapor-liquid absorption is presented. Closed-form solutions are obtained where the depth of the absorbing solution is taken into account. The effect of interfacial instability on heat and mass transfer is also modeled by introducing constant heat and mass transfer coefficients. Comparison with experimental data permits the determination of Lewis, Nusselt and Sherwood Numbers.

Finally an analysis of the fully developed natural convection heat and mass transfer between two inclined parallel plates is presented. Solvability conditions are determined and closed-form expressions for the temperature and concentration obtained.

CHAPTER I

INTRODUCTION

Sorption refrigeration is based on the physical process that some gases like H_2O, CO_2 and NH_3 are "pumped" by liquids or solids at low temperature and "released" at high temperature. This phenomena is the basis of several sorption cooling/heating sytems powered by thermal energy source such as solar radiation or a waste heat source.

The first sorption systems which were studied and experimentally tested used absorption (sorption by a liquid) pairs such as Lithium Bromide-Water. Adsorption (sorption by a solid) cooling was studied in recent years because it presents the advantages of working without moving parts and avoids the difficult problem of crystallization which occurs in the liquid desiccant systems. The research effort in the field of sorption cooling/heating can be classified as follows:

1. Physical chemistry of sorption phenomena and the theoretical and experimental determination of the thermodynamic properties of various sorption pairs.

2. Thermodynamic analysis of adsorption cycles in order to optimize the performance of adsorption systems.

3. Numerical simulation of sorption cooling/heating systems.

4. Experimental testing of prototypes of such systems.

While the literature of open-cycle* desiccant systems is relatively

---

* In open-cycle systems, the adsorbate is exchanged between the desiccant and the processed stream, whereas in closed-cycle systems, the adsorbate is permanently recycled.

extensive, considerably much fewer studies have dealt with the closed-cycle technologies. The present thesis analyzes the heat and mass transfer processes that occur in closed-cycle adsorption cooling systems. Some fundamental aspects of heat and mass transfer in open-cycle liquid desiccant systems are also studied.

The phenomena of physical gas-solid adsorption which constitutes the fundamental aspect of the present research, is addressed in chapter II. The general principles of adsorption theory are briefly discussed with emphasis on recent developments. A phenomenological relationship for adsorption equilibrium is proposed which accurately represents the experimental data and is very convenient for numerical calculations. Formulas are also derived for the thermodynamic description of adsorption processes encountered in the applications of closed-cycle adsorption heating and cooling systems. These formulas are used in the numerical simulations which are presented in chapters IV and V.

A literature review of adsorption cooling/heating systems which use zeolites is presented in Chapter III. The operating principle of adsorption cooling and the thermodynamic analyses of such systems as well as the results of experimental studies on these systems are presented.

Previous analyses of closed-cycle machines considered only an idealized cycle on the (T_s, T) diagram. In chapter IV, a dynamic analysis of a solar adsorption refrigeration system is presented. This analysis is very useful from the view point of optimizing the design parameters and the operating conditions of such a system.

Recently, Tchernev suggested that by using the concept of a

regenerative heat exchanger, a closed-cycle adsorption system can provide continuous cooling/heating and and have a significantly increased performance. Previous systems were generally characterized by COP's smaller than unity and are based on intermittent cycles. Chapter V gives a detailed description of the operating principle of a regenerative adsorption cooling/heating system. A mathematical model is also presented to simulate such a system and to predict its performance.

Chapters VI and VII consist of two fundamental studies of combined heat and mass transfer. They relate to the general topic of the present thesis in the fact that the two configurations considered are frequently encountered in sorption cooling/heating.

We present in chapter VI a theoretical analysis of the transient coupled heat and mass transfer in an absorption film of finite depth. The effect of interfacial convection, artificially induced to increase the transfer rates in absorption solutions, is also analyzed by using constant heat and mass transfer coefficients.

In chapter VII, an analysis of fully-developed combined heat and mass transfer natural convection between two inclined parallel plates is presented. This geometry can represent the solar collector of an open-cycle sorption sytem. The solution obtained under the assumption of fully-developed conditions can be used to provide an appropriate initial iteration in the numerical solutions of natural convection problems. It also gives good estimates of the overall transfer quantities at small Rayleigh Numbers which can be used to verify the numerical solutions for the developing regime.

CHAPTER II

THERMODYNAMICS OF SOLID ADSORPTION

PHENOMENA AND PROCESSES

2.1 SOLID ADSORPTION PHENOMENA

Solid adsorption is the process by which molecules of a certain fluid substance ("adsorbate") adhere to the surface of a solid material ("adsorbent"). Two types of adsorption at fluid-solid interfaces are usually distinguished: physical adsorption (or physio-sorption) and chemical adsorption (or chemisorption).

Chemisorption is the result of strong binding forces comparable to those which accompany chemical reactions. Thus the energies involved are of the same order of magnitude as heats of reaction (10^4-10^5 calories per mole). As a consequence of the formation of a chemisorbed compound, the process is usually irreversible and terminates after the formation of a single layer at the interface. A typical example of chemisorption is the adsorption of oxygen by charcoal at 100 °C which when heated and exposed to low pressures releases CO.

On the other hand, physical adsorption involves forces of Van der Waals type and the energy effects are comparable to heats of phase change such as condensation. The amount adsorbed at a given temperature T increases with the relative pressure p/p_s, where p_s is the saturation vapor pressure of liquid adsorbate at the temperature T. Several superimposed layers of adsorbed substance may form. The process is essentially reversible except when capillary condensation occurs in adsorbents containing fine pores.

This usually leads to hysterisis in the sorption isotherm.

The following discussion addresses the phenomena of physical gas-solid adsorption which constitutes the fundamental aspect of the present research. First the general principles of adsorption theory are briefly discussed with emphasis on the recent developments. A phenomenological law for adsorption equilibrium is proposed and compared to known potential theories. Then formulas are derived for thermodynamic description of adsorption processes encountered in the applications of closed-cycle adsorption heating and cooling systems. The use of these formulas will be illustrated in the numerical simulations presented in this thesis.

2.2 EXPERIMENTAL AND THEORETICAL DESCRIPTION OF
ADSORPTION

Adsorption is most generally described in terms of isotherms which give the amount of gas adsorbed per unit mass of adsorbent as function of the relative pressure at constant temperature. Figure 2.1 shows isotherms of the pair chabazite-Methanol [5] as an example.

2.2.1 Experimental Determination of Isotherms. The experimental apparatus should allow to measure the amount of gas adsorbed, the pressure of the vapor phase and the temperature of the adsorbent-adsorbate system. Two experimental methods are typically used. Their basic principles are shown in figure 2.2 although the apparatus can be more sophisticated for more accurate and faster runs [1]*.

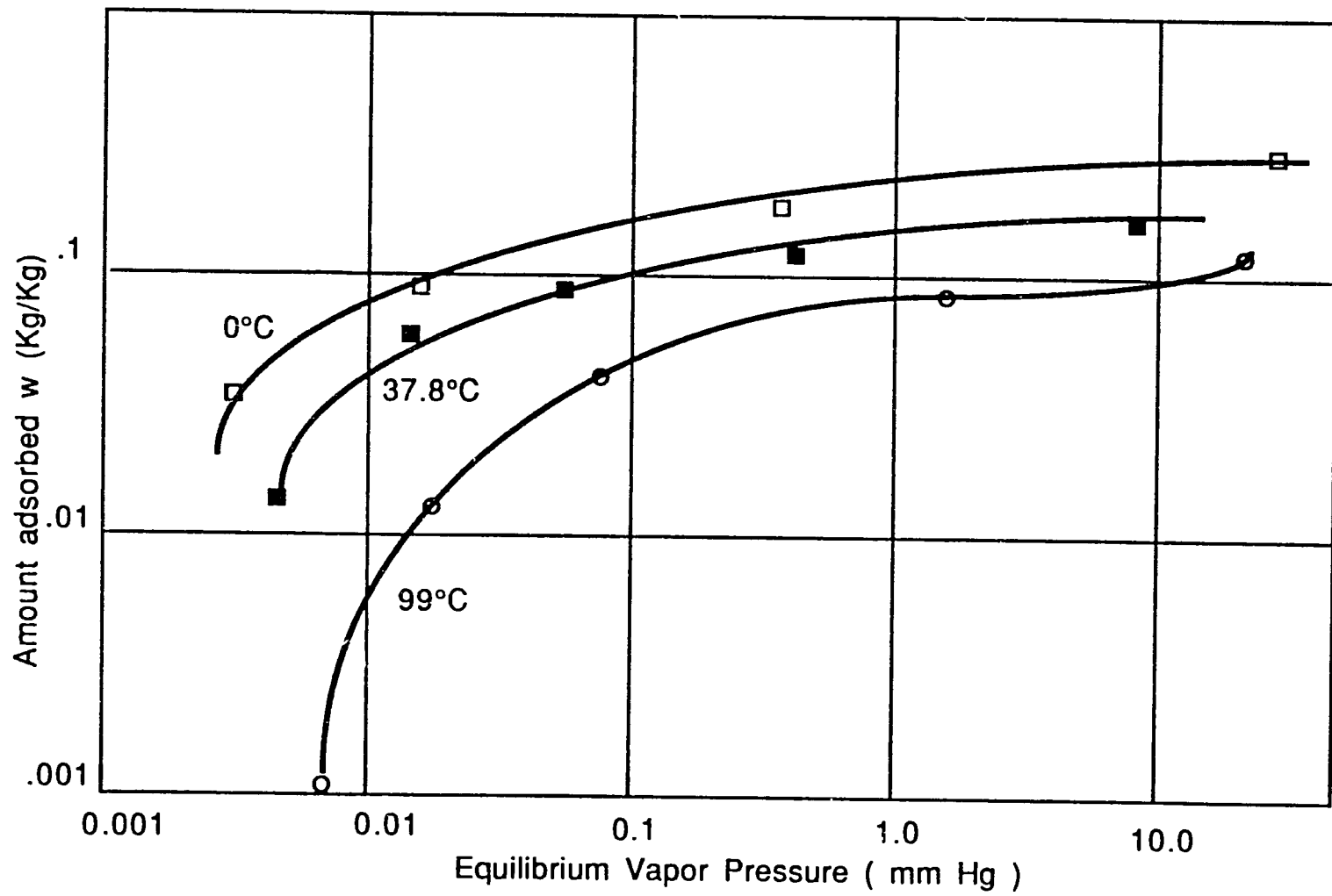* Bracketed numbers indicate numbered references.

Figure 2.1 : Isotherms for the Pair Chabazite-Methanol [5]

Adsorbent sample

Two regulated
ovens

Liquid
adsorbate

(a) Gravimetric Method

To vacuum

M
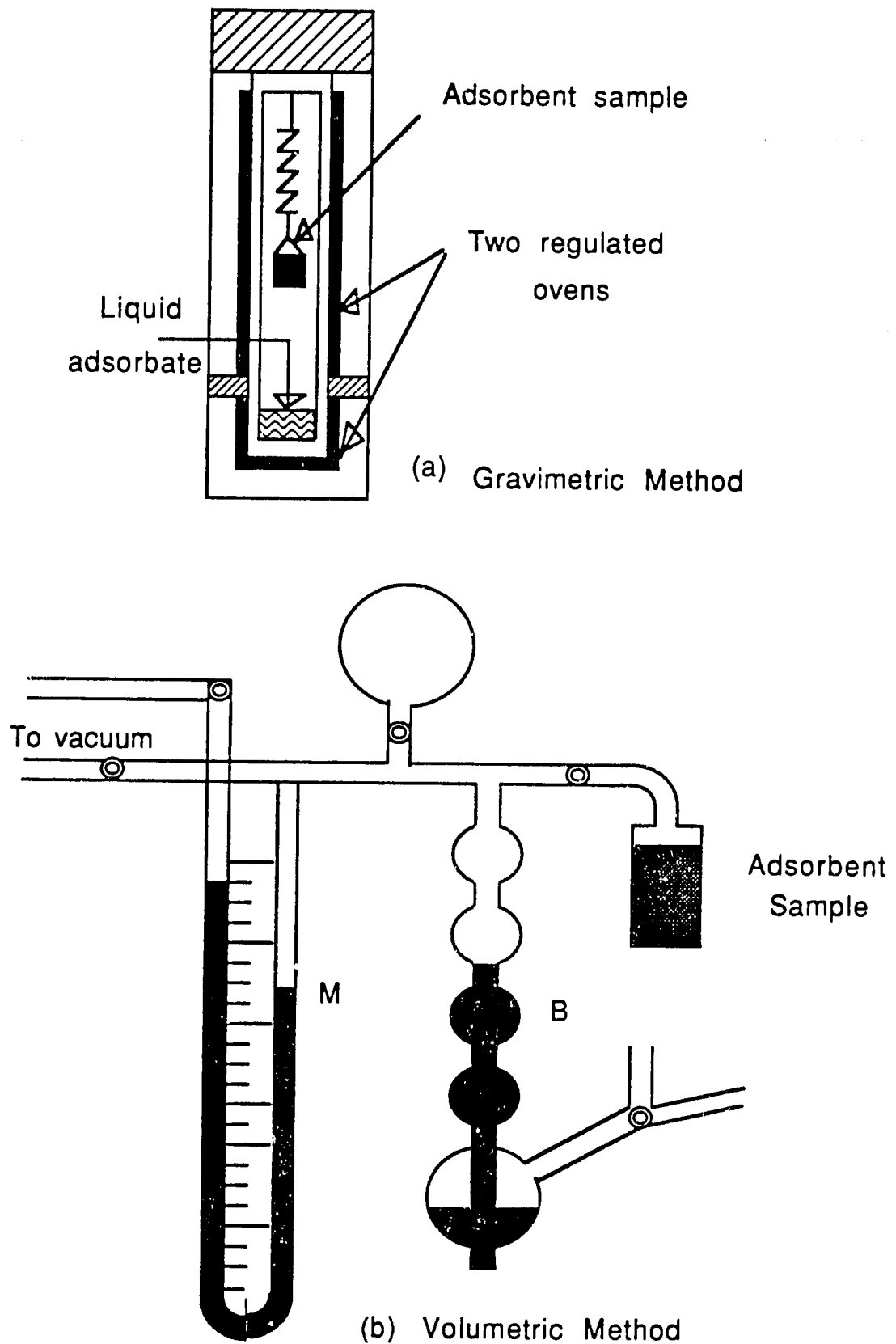
B

Adsorbent
Sample

(b) Volumetric Method

Figure 2.2: Experimental Determination of Isotherms

• Gravimetric method: the amount of gas adsorbed is measured by the gain in weight of an adsorbent sample placed in a glass tube at a preset relative pressure. In order to obtain the desired relative pressure, a large sample of initially frozen adsorbate is contained in the glass tube which is initially evacuated prior to any measurements. The temperature of the liquid adsorbate (which imposes the pressure of the gas phase) and the temperature of the adsorbent are then controlled by two regulated ovens.

• Volumetric method: All volumes in the experimental setup are calibrated. The amount of gas adsorbed is calculated from the pressure measured by a manometer M and the volume adsorbed read on a buret B. The adsorbent sample is contained in a thermostatic tube.

2.2.2 Types of Adsorption Isotherms. Figure 2.3 shows Brunauer's 5 types of adsorption isotherms. Although a qualitative interpretation of thes isotherms can be made [2], a more precise description is made difficult by overlapping phenomena involved in physical adsorption: monolayer adsorption, multilayer adsorption and capillary condensation. The type-II isotherm illustrates this difficulty as the first portion of the S.shaped curve correspondes to monolayer adsorption up to relative pressure (p/p_s) 0.1, a multilayer adsorption region follows until about $p/p_s=0.4$ and at larger values of the relative pressure, capillary condensation occurs.

2.2.3 Equilibrium Thermodynamics of Adsorption. In applying thermodynamic principles to adsorption equilibrium, two different approaches can be adopted. It is possible to regard
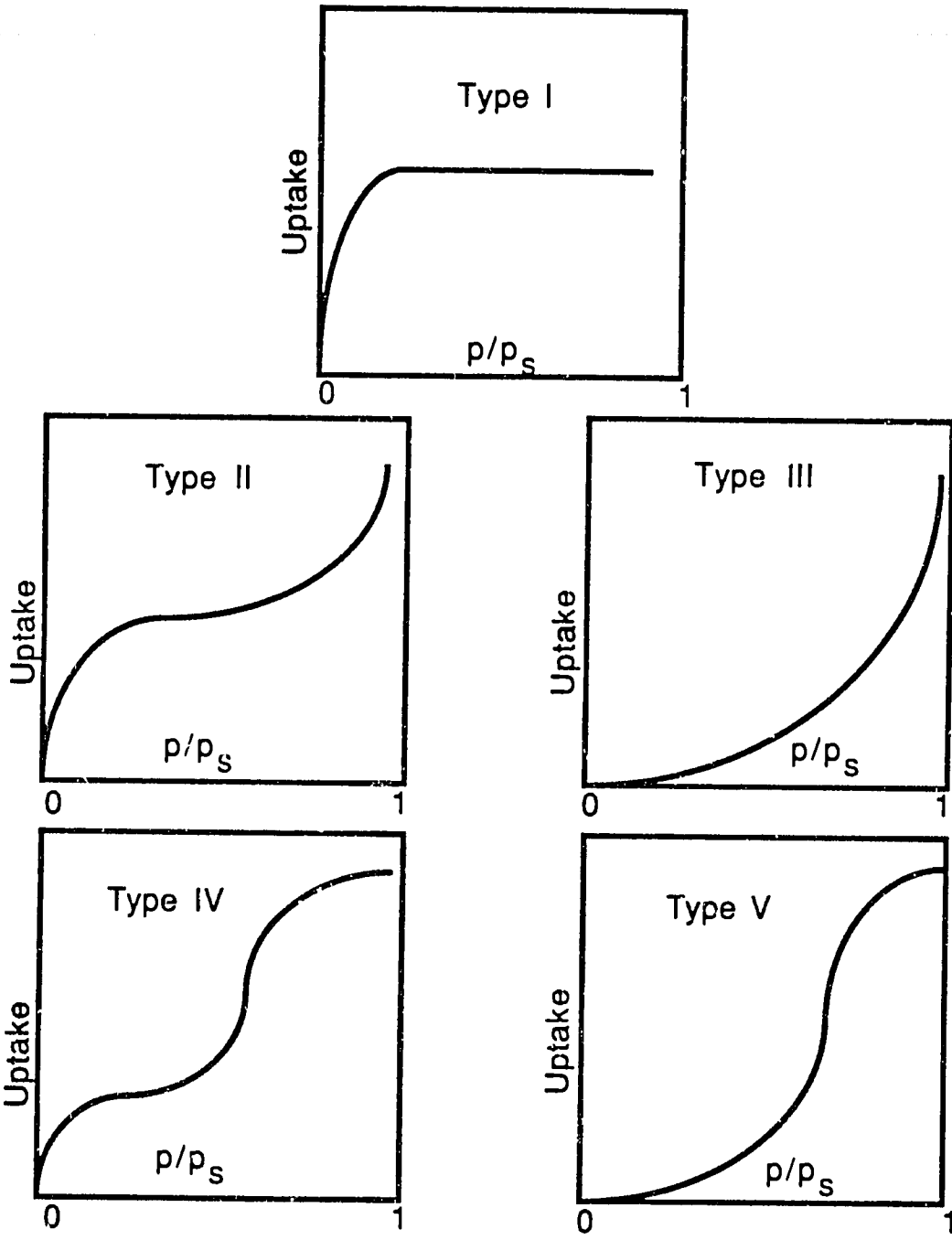
Figure 2.3 : Brunauer's five Types of Adsorption Isotherms

adsorption as a transformation from the gas phase to the adsorbed phase according to:

Gaseous molecule ⟺ Adsorbed molecule

The adsorbent is assumed to have the unique role of creating a force field and otherwise be exterior to the adsorbed phase. Another perspective considers the surface layer (adsorbent and adsorbate) as single phase comparable to a solution. In both approaches, the equilibrium condition is:

$$\mu_g = \mu_s \tag{2.1}$$

or since $\mu = \bar{H} - T\bar{S}$

$$\bar{H}_g - \bar{H}_s = T(\bar{S}_g - \bar{S}_s) \tag{2.2}$$

2.2.3.1 Equilibrium Constant. Introducing the relation $\mu = \mu^o + RTLn(a/a^o)$ where a is the activity and "o" designates a standard state, equation (2.1) yields:

$$\mu_s^o - \mu_g^o = -RT\,Ln\,K \tag{2.3}$$

where,

$$K = (a_s a_g^o)/(a_s^o\,a_g) \tag{2.4}$$

is the equilibrium constant. A simplified expression for K is obtained by choosing the standard activities to equal 1 and assuming an ideal gas phase for which $a_g = p$:

$$K = a_s/p \tag{2.5}$$

To obtain the isotherms a_s need to be determined using statistical thermodynamics [3]. To illustrate the procedure, for ideal localized

sorption:

$$a_s = \theta / (1-\theta) \tag{2.6}$$

where θ is the degree of saturation of the adsorbing surface. Substituting in (2.5) yields:

$$K = \theta / [p(1-\theta)] \tag{2.7}$$

which is the well known **Languimir isotherm** originally derived using kinetic arguments.

2.2.3.2 <u>Gibbs's Adsorption Isotherm</u>. Consider a solid-gas interface with area A, n moles of adsorbed species at temperature T and pressure p. The Gibbs free energy is given by:

$$G = -\pi A + \mu_s n \tag{2.8}$$

[2], where π is the *spreading pressure* defined by:

$$\pi = - (\partial G / \partial A)_{p,T,n} \tag{2.9}$$

Using thermodynamic principles, we can write:

$$dG = Vdp - SdT - \pi dA + \mu_s \, dn \tag{2.10}$$

Differentiating (2.8) at constant temperature and pressure and using the equilibrium condition $dG_{T,P} = 0$ yields:

$$dG_{T,P} = -\pi dA - Ad\pi + \mu_s dn + n \, d\mu_s = 0 \tag{2.11}$$

Combining equations (2.10) and (2.11) gives:

$$d\pi = (n/A) \, d\mu_s \tag{2.12}$$

Introducing the surface concentration $\Gamma \equiv n/A$ and using equation (2.1) yields:

$$d\pi = \Gamma \, d\mu_g \tag{2.13}$$

If we further assume an ideal gas phase, $d\mu_g = RT\ d(Lnp)$. Thus

$$d\pi = RT\ \Gamma\ d(Lnp) \tag{2.14}$$

This relation between the spreading pressure and the surface concentration is called *Gibbs's adsorption isotherm*. Equation (2.14) can be integrated at constant temperature from 0 to p from which one obtains:

$$p=(RT/A_{sp}) \int_0^p x\ d(Lnp) \tag{2.15}$$

where A_{sp} =A/m is the area per unit mass of adsorbent and x is the number of adsorbed moles per unit mass of adsorbent.

To obtain the isotherm from Gibbs's relation (2.14), an equation of state for the two dimensional adsorbed phase is needed. Such an equation relates the spreading pressure π to the surface concentration Γ . To illustrate the procedure, assume an equation of state in which deviation from ideality is expressed by an excluded area correction:

$$\pi(\sigma-\sigma^0) = RT \tag{2.16}$$

where $\sigma = A_{sp}w/n$. Differentiating (2.16) and substituting in (2.14) yields:

$$d\theta/[\ \theta(1-\theta)^2\ ] = d(Lnp) \tag{2.17}$$

where $\theta=\sigma/\sigma^0$. Integrating (2.17) gives:

$$Ln[\theta/(1-\theta)] + \theta/(1-\theta) = Lnp + LnK \tag{2.18}$$

which is **Volmer's isotherm**.

2.2.3.3 Other Adsorption Isotherms. An alternative method of deriving adsorption isotherms is the use of statistical

thermodynamics. The procedure is exposed in some detail in [3-4]. Another important isotherm for multilayer adsorption was drived by Brunauer, Emett and Teller. This theory and final equation are known by the initials of the authors: **BET**. The BET isotherm is the basis of an experimental method of determining the specific surface area of adsorbents. A thermodynamic analysis based on a virial equation is also available [3] and has the advantage of including nonlocalized sorption.

2.2.3.4 <u>Heats of Adsorption</u>. Barrer [3] gives the following definitions for the isosteric heat of adsorption q_{st} , the differential heat of adsorption $\Delta\overline{H}$ and the integral heat of adsorption $\Delta\tilde{H}$:

$$q_{st} = RT^2 \, (\partial Lnf/\partial T)_n \tag{2.20}$$

$$\Delta\overline{H} = \overline{H}_s - \overline{H}_g \tag{2.21}$$

$$\Delta\tilde{H} = (1/n) \int_0^n \Delta\overline{H} \, dn \tag{2.21}$$

$\overline{H}_s$ is the partial molar enthalpy of adsorbed species and $\overline{H}_g$ is the same quantity for the gas phase. Replacing μ in equation (2.1) by $\mu^0 + RTLn(f/f^0)$, dividing by T and using the Gibbs-Helmholtz relation $[\partial(\mu/T)/\partial T] = -\overline{H}/T^2$ yield:

$$-\frac{\overline{H}_s}{T^2} = \frac{\tilde{H}_g}{T^2} + R\left(\frac{\partial Lnf}{\partial T}\right)_n \tag{1-23}$$

Assuming an ideal gas phase, $\overline{H}_g = \tilde{H}_g$. Thus equation (2.23) gives:

$$\Delta \bar{H} \equiv \bar{H}_s - \bar{H}_g = R T^2 \left(\frac{\partial Lnf}{\partial T}\right)_n \equiv q_{st} \qquad (2.24)$$

This establishes the equality of ΔH and q_{st}. An application of this relation is to test equilibrium data from which q_{st} is determined by means of an independent calorimetric method allowing the measure of ΔH [4]. An other important equation involving q_{st} is derived from the following Clausius-Clapeyron type of relation:

$$\left(\frac{\partial p}{\partial T}\right)_n = \frac{\bar{S}_g - \bar{S}_s}{\bar{V}_g - \bar{V}_s} \qquad (2.25)$$

Using equation (1-2), we obtain:

$$\left(\frac{\partial p}{\partial T}\right)_n = \frac{\bar{H}_g - \bar{H}_s}{T(\bar{V}_g - \bar{V}_s)} \qquad (2.26)$$

Assuming ideal gas, $\bar{H}_g - \bar{H}_s = q_{st}$ and $\bar{V}_s << \bar{V}_g = RT/p$

and equation (2.26) becomes:

$$\left(\frac{\partial Lnp}{\partial 1/T}\right)_n = \frac{q_{st}}{R} \qquad (2.27)$$

This last equation shows that q_{st} can be obtained from the slope of the curve Lnp versus 1/T.

2.2.4 Potential Theories of Adsorption

2.2.4.1 Dubinin-Polanyi Theory. A different approach to

the theoretical determination of isotherms was developed by Polanyi and extended by Dubinin (see for example [6]) . The sorbed species is considered to be liquid like and incompressible, however the properties of this phase will be different from those of bulk fluid. The difference in free energy between the two phases is measured by the *adsorption potential* , ε , defined by:

$$\varepsilon = - RT \, Ln(p/p_s) \qquad (2.28)$$

The pressures p and p_s are the saturation pressure at temperature T for the adsorbed phase and the bulk liquid respectively. Dubinin-Polanyi theory is based on the assumption that the relationship between ε and the volume sorbed, which is estimated as liquid is temperature independent. Thus using a "characteristic curve" obtained at a suitable temperature, an isotherm can be obtained at any other sorbent temperature.

For micropore adsorbents such as activated carbon or zeolites, an empirical isotherm equation of the form :

$$w = w_0 exp(-D\varepsilon^2) \qquad (2.29)$$

with two adjustable parameters is sometimes sufficiently adequate to fit the experimental data. A posssible generalization of equation (2.29) is to replace the exponent 2 by a third adjustable parameter n. Although equation (2.29) is known to deviate from experimental data for very small and very large uptakes, it is a very useful tool in correlating adsorption data for design purposes.

2.2.4.2 "Linearized Potential" Theory. In a recent paper, Pons and Grenier [7] extended the Polanyi assumption by proposing that ε is a linear function of temperature:

$$\varepsilon = C\ (w) + D(w)\ T \qquad\qquad (2.30)$$

C(w) and D(w) are then choosen as second-order polynomials of the variable X defined by:

$$X=[Ln(w_0/w)]^{0.25} \qquad\qquad (2.31)$$

The seven parameters of the model are determined by a best fit of the experimental data. This model was applied to the pair Activated Carbon-Methanol for which they obtained:

$$C(w) = 68.619 + 199.9X - 15.489X^2$$

$$D(w) = -0.28811 - 0.52414X + 0.69153X^2$$

$$X = [Ln(0.34/w)]^{0.25}$$

Their experimental conditions were:

$$-10<T<130^{\circ}C; \qquad 0.1<p<70\ kPa; \qquad 0.007<w<0.321$$

2.2.5 A Proposed Phenomenological Relationship for Adsorption Equilibrium.

A convenient graphical representation of adsorption data is to plot the *isosters* (curves of constant uptake) in a (T_s,T) diagram; T is the temperture of the system and T_s the saturation temperature of the liquid adsorbate at the pressure of the system. Such graphs which are obtained from the isotherms (figure 2.4 gives the isosters for the pair Chabazite-Methanol obtained form data of [5]) and prove to be very convenient in the analysis of adsorption cycles encountered in heating and cooling applications .

Available data on adsorption by microporous adsorbents such as zeolites and activated carbon show that the isosters in a (T_s,T) diagram are straight lines over a sufficiently wide range of temperature and adsorbate uptake. This naturally leads to the idea
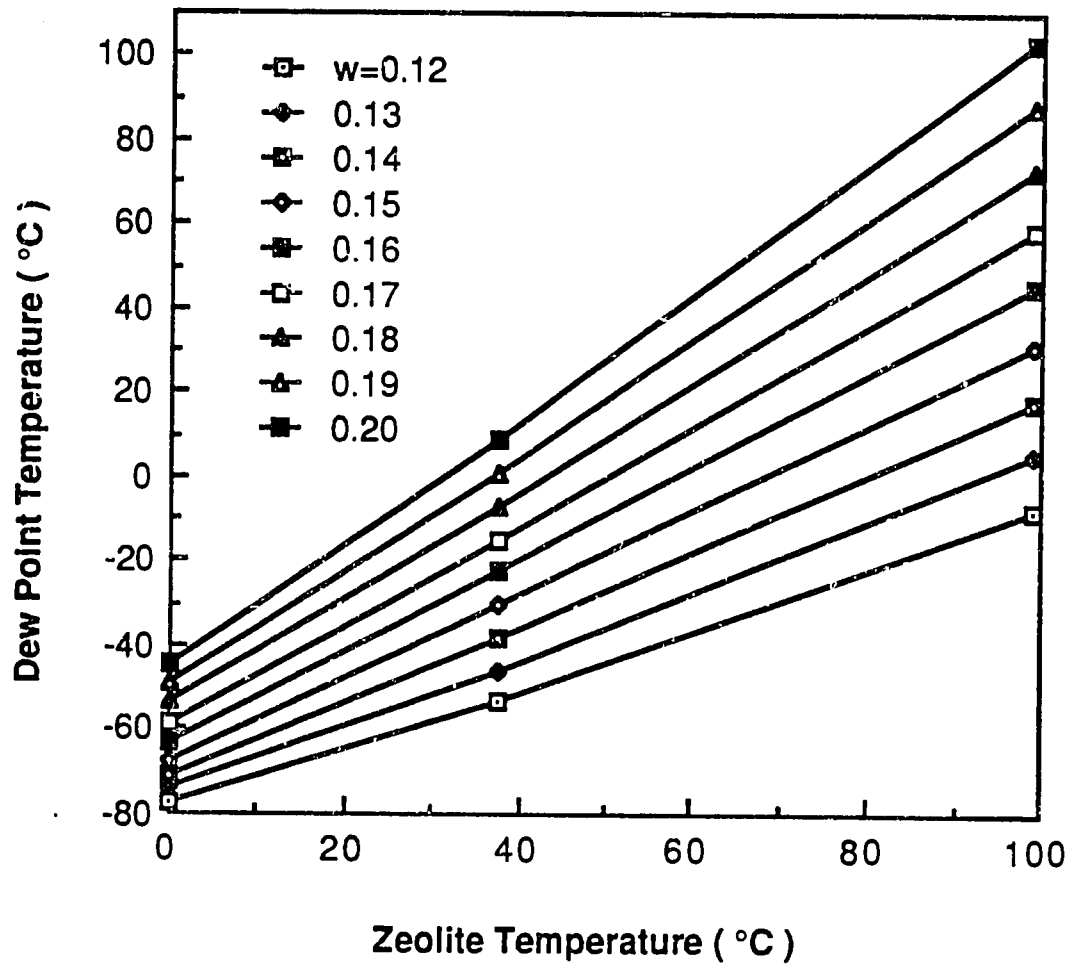
Figure 2.4: Isosters for the Pair Chabazite-Methanol

that a linear law of the form:

$$T_s = A(w)T + B(w) \tag{2.32}$$

will be suitable for representing adsorption data over a range of T and w conditions which hopefully will include the important range for engineering applications.

A linear relation such as (2.32) is obviously very convenient to numerical calculations since it is explicit in T_s and T and requires an iterative method only if w is desired. This is the advantage sought in the present thesis since we are mainly concerned with the numerical simulation of practical adsorption machines. Nevertheless an attempt is made to provide some theoretical basis for this law and to give a physical interpretation of $A(w)$ and $B(w)$.

2.2.5.1 Relation to Potential Theories. A certain theoretical justification of the proposed law can be found by investigating its relation to potential theories. Recalling Clausius-Clapeyron's equation for the bulk liquid adsorbate:

$$\frac{dLnp}{dT} = \frac{L(T)}{RT^2} \tag{2.33}$$

and writing L(T) in the functional form

$$L(T) = L_0 + f(T) \tag{2.34}$$

[f(T) need not be specified at this stage but one can think of it as the first term in a Taylor expansion of L(T)] we obtain after substitution of (2.34) in (2.33) and integration:

$$Lnp = -\frac{L_o}{RT} + \frac{1}{R} \int^T \frac{f(U)}{U^2} dU \qquad (2.35)$$

The expression of the adsorption potential becomes:

$$\varepsilon = RT \left[-\frac{L_o}{R} \left(\frac{1}{T_s} - \frac{1}{T} \right) + \frac{1}{R} \int_T^{T_s} \frac{f(U)}{U^2} dU \right] \qquad (2.36)$$

Using equation (2.32) yields:

$$\varepsilon = -L_o \left(\frac{1}{A(w)} - 1 \right) + g(w,T) \qquad (2.37)$$

where,

$$g(w,T) = \frac{L_o}{A(w)} \frac{B(w)}{T_s} + T \int_T^{T_s} \frac{f(U)}{U^2} dU \qquad (2.38)$$

Equation (2.37) indicates that when g(T,w) is constant, we have a temperature independent potential (Polanyi assumption) and if the first order term in T is considered, we obtain the " linear potential " of [7]. A more precise information about the form of the functions A(w) and B(w) can be obtained from the comparison of the present law to Dubinin-Polanyi theory. In effect, substituting (2.36) in (2.29) and taking the logarithm of each side yields:

$$Ln \frac{w}{w_o} = -DR^2 T^2 \left[-\frac{L_o}{R} \left(\frac{1}{T_s} - \frac{1}{T} \right) + \frac{1}{R} \int_T^{T_s} \frac{f(U)}{U^2} dU \right]^2 \qquad (2.39)$$

which can be rewritten as:

$$\frac{1}{\sqrt{D}} \left[Ln \frac{w}{w_o} \right]^{0.5} = T \left| -L_o \left(\frac{1}{T_s} - \frac{1}{T} \right) + \int_T^{T_s} \frac{f(U)}{U^2} dU \right| \qquad (2.40)$$

This relation illustrates the role of the quantity $[Ln(w_0/w)^{0.5}]$. To see it more clearly, let's examine the case of constant latent heat L_0 for which $f(T)=0$. In this case equation (2.40) reduces to:

$$\frac{1}{\sqrt{D L_0}} \left[Ln \frac{w}{w_0} \right]^{0.5} = \left| \frac{T}{T_s} - 1 \right| \qquad (2.41)$$

or for $T > T_s$:

$$T = \left\{ \frac{1}{\sqrt{D L_0}} \left[Ln \frac{w}{w_0} \right]^{0.5} + 1 \right\} T_s \qquad (2.42)$$

This suggests that Dubinin's equation (2.29) may reduce to the form proposed by (2.32). Furthermore the coefficients $A(w)$ and $B(w)$ should be simple functions of $[Ln(w_0/w)]^{0.5}$.

2.2.5.2 Expressions of q_{st} Using Equation (2.32). A relation between the isosteric heat of adsorption q_{st} at conditions (T,p) and the latent heat of vaporization of the bulk liquid adsorbate at conditions (T_s,p) is obtained by a simple combination of relation (2.20) defining q_{st} and Clausius-Clapeyron equation (2.33). We obtain:

$$q_{st} = L(T_s) [T/T_s]^2 (\partial T_s/\partial T)_w \qquad (2.43)$$

If equation (2.32) is used $(\partial T_s/\partial T)_w = A(w)$, thus:

$$q_{st} = L(T_s) [T/T_s]^2 A(w) \qquad (2.44)$$

This relation shows that q_{st} depends not only on w but also on T.

2.2.6 Application of the Proposed Law. Figure 2.5 is a plot of the adsorption equilibrium data for the pair synthetic Zeolite
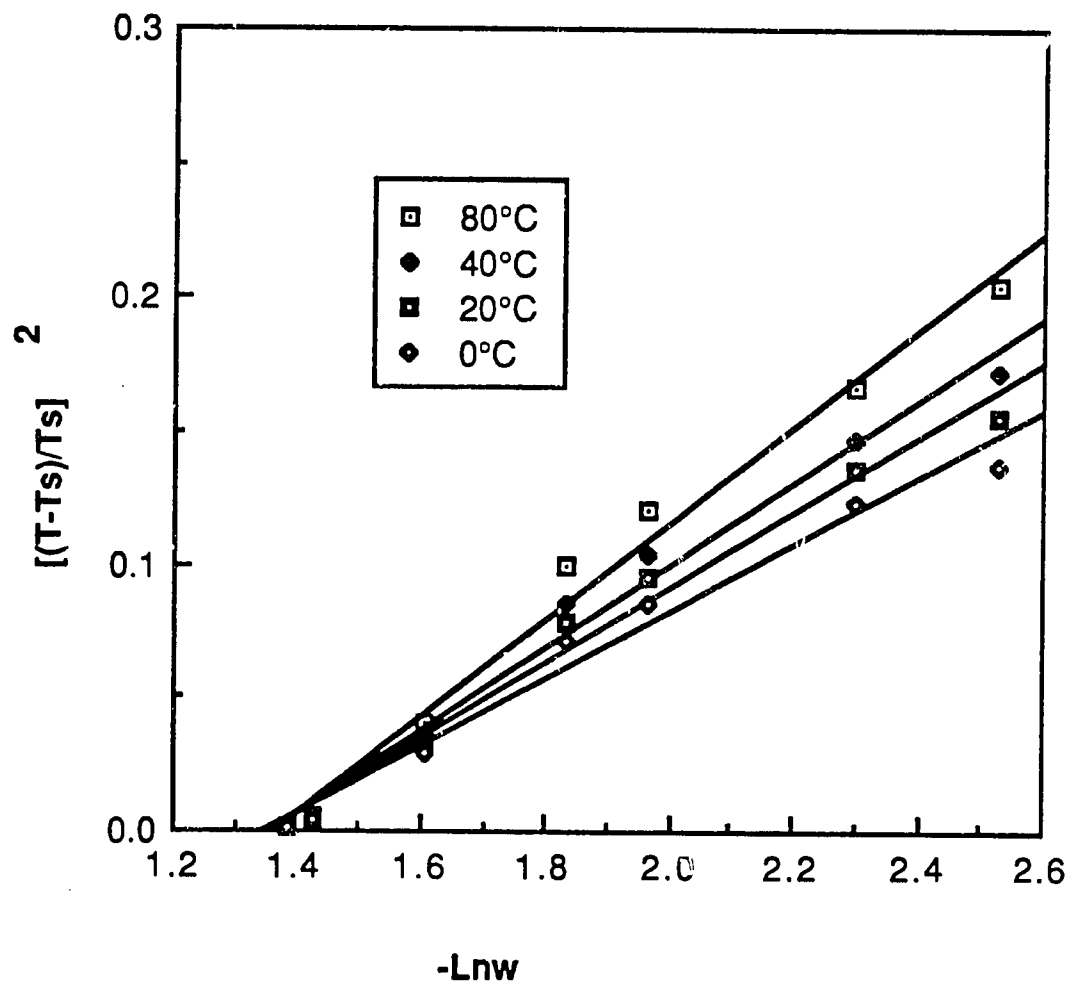
Figure 2.5: Plot of $[(T-Ts)/Ts]^2$ vs Lnw for the Data of [10]

13X-Water [9] in the $[(T-T_s)/T_s]^{0.5}$ versus $Ln(w)$ diagram. The best curvefitting of this data is given by:

$$w = 0.2578 \exp \{-6.4516[(T-T_s)/T_s]^2\}$$

According to Dubinin's formula (2.29), all the data points should fall on a straight line. This is obviously not the case even in the region apart from the limits w small and w large where such deviation is expected. This poor representation of the equilibrium data justifies the use of a more accurate equation such as Pons and Grenier's equation (2.30) or the proposed law (2.32).

Figures (2.6,7,8) show the functions $A(w)$ and $B(w)$ for three sets of adsorption equilibrium data. The fact that the curves exhibit similar trends for the three cases supports the existence of a physical significance to the functions $A(w)$ and $B(w)$. Figure (2.8) presents these functions versus the scaling term $[Ln(0.25/w)]^{0.5}$. Although the curve $A(w)$ is almost a straight line in this diagram, the curve $B(w)$ does not indicate a simple expression for this function. For this reason, third order polynomials in w are used to correlate the equilibrium data for use in the simulation of adsorption systems. The data of reference [9] for example are very well represented only by the second order expressions:

$$A(w) = 0.711 - 0.3177w + 6.003w^2$$

$$-B(w) = 220.6 - 1256.6632w + 1532.6928w^2 \; (^\circ F)$$

Figure (2.9) shows $A(w)$ and $B(w)$ for the pair Chabazite-Methanol. In this case the data points are well correlated by the following linear expressions:

$$A(w) = 10.0w - 0.5 \qquad B(w) = -2125.0w + 252.75 \; (K)$$
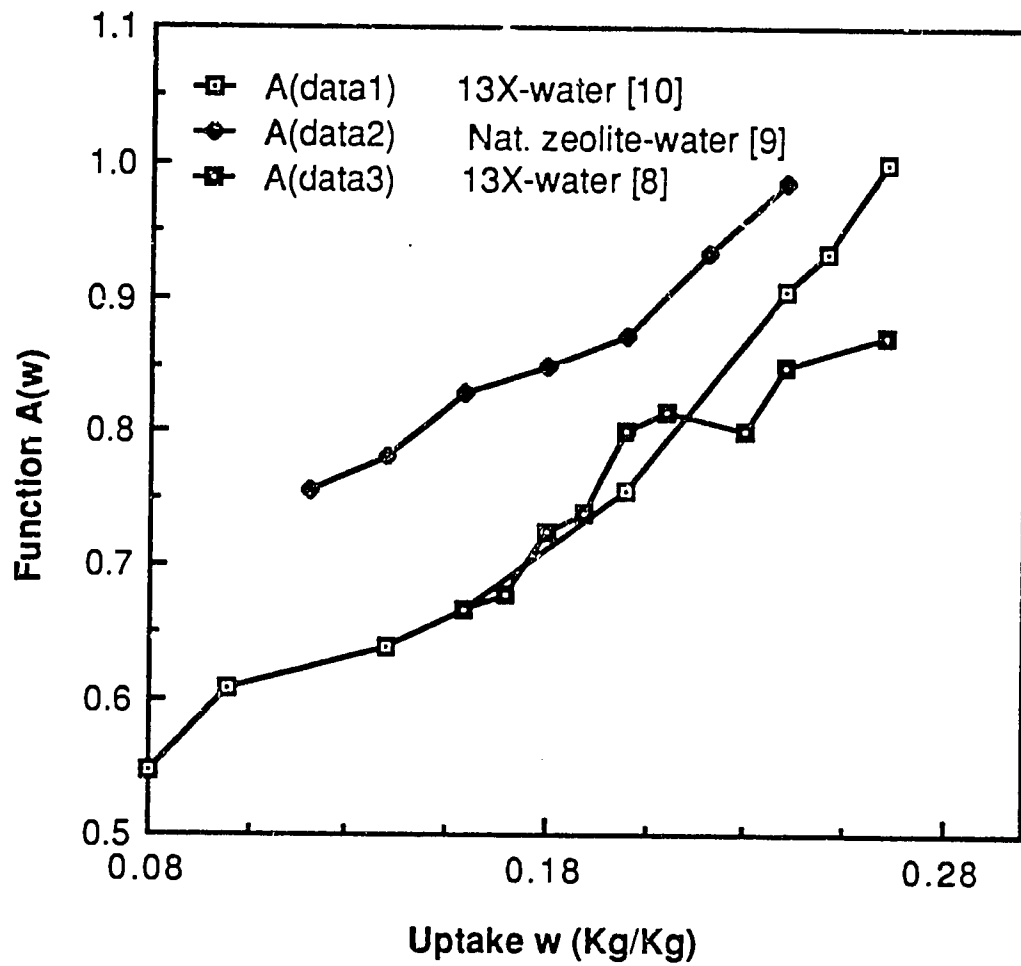
Figures (2.10) gives the variations of the isosteric heat of

Figure 2.6 : the Function A(w) For 3 Adsorption Pairs

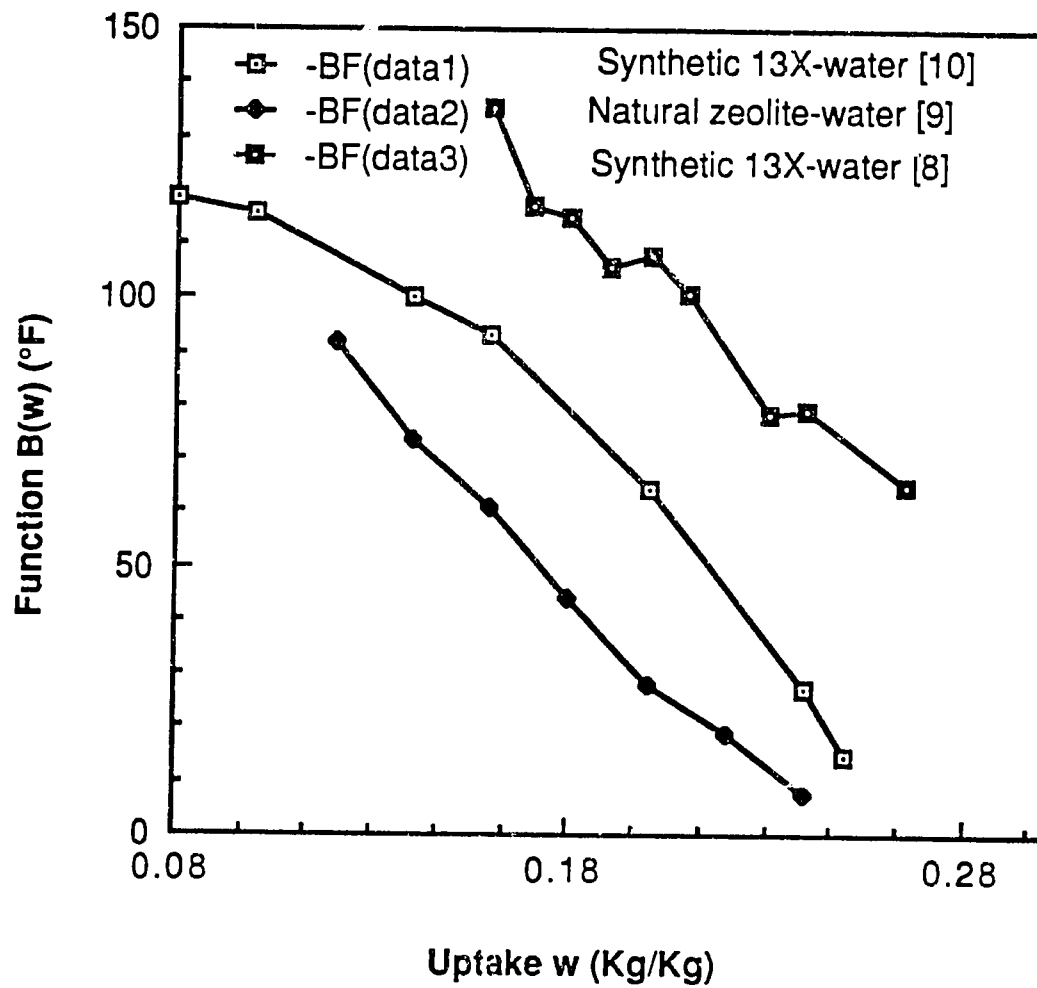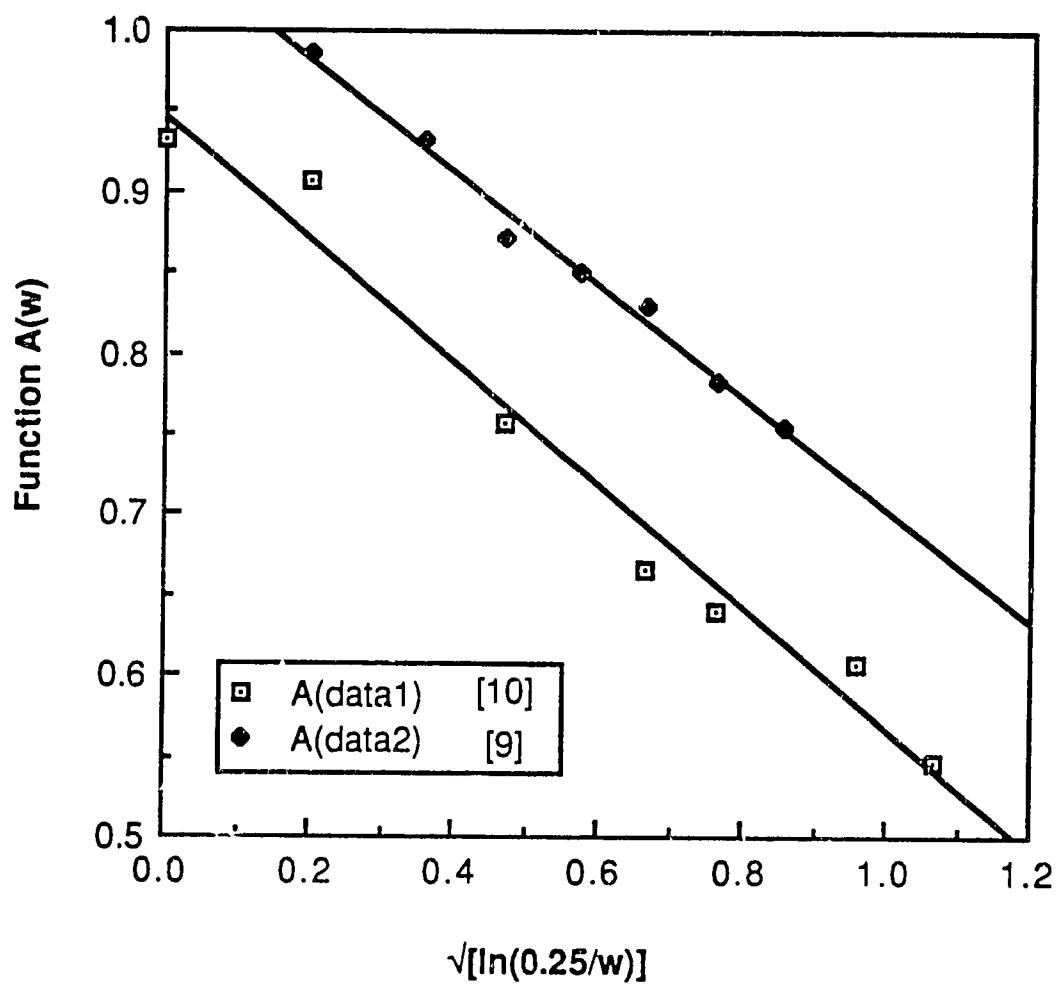Figure 2.7: the Function B(w) (°F) for 3 Adsorption Pairs
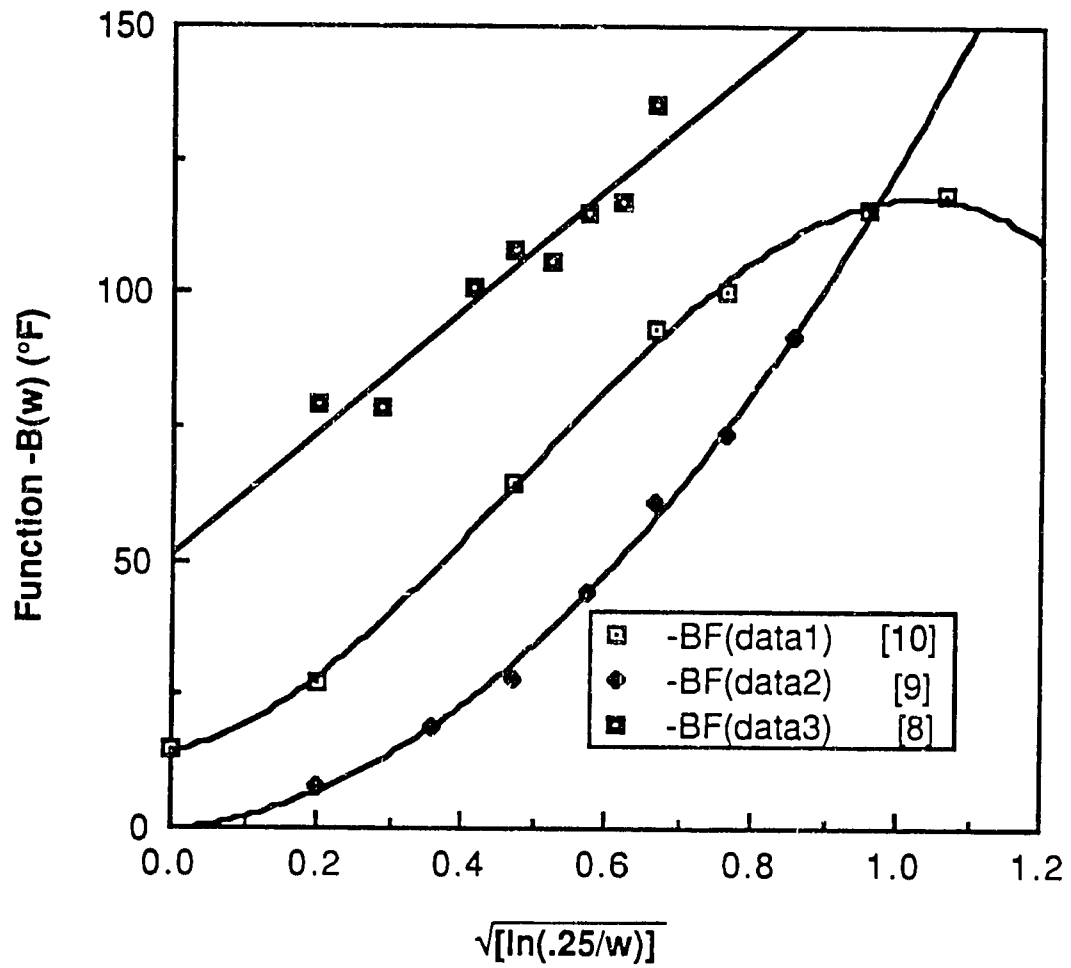
Figure 2.8a: the Function A(w) vs √[Ln(.25/w)]

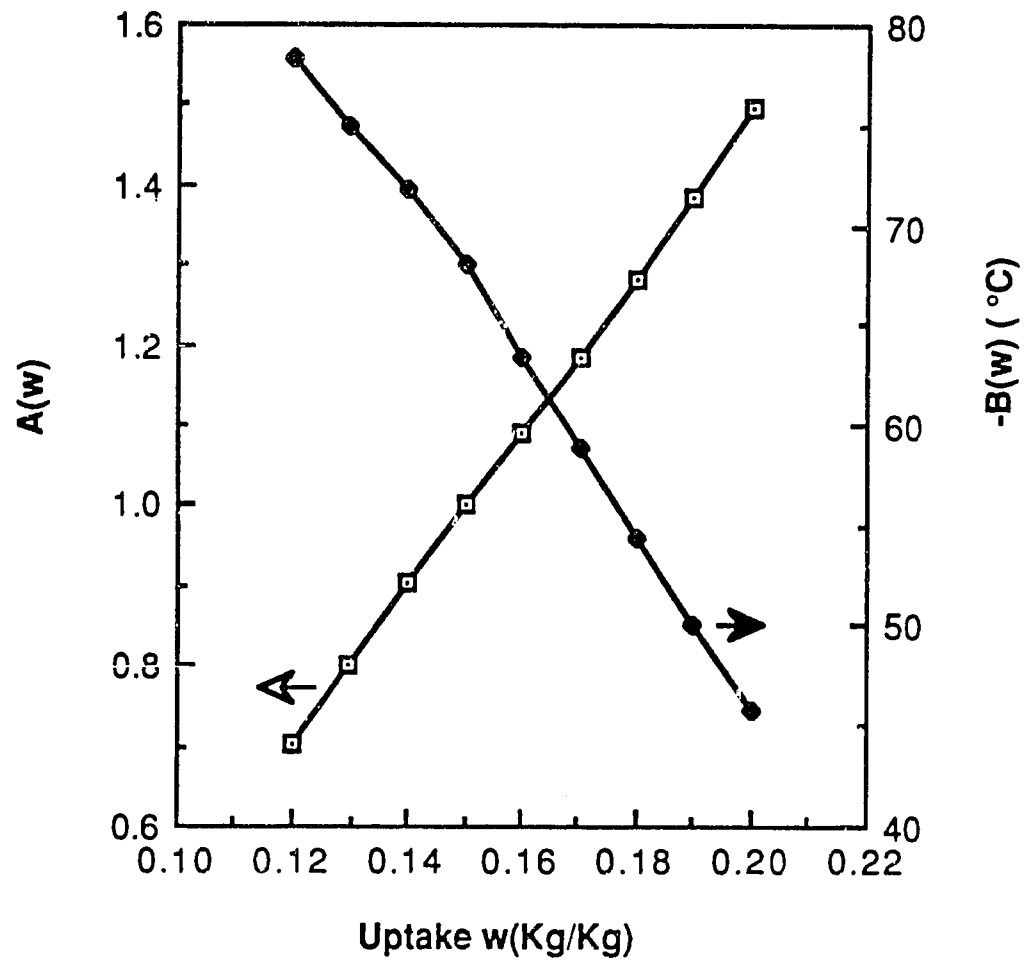Figure 2.8b: The Function -B(w) (°F) vs √[ln(.25/w)]

Figure 2.9 : Functions A(w) and B(w) for the Pair
Chabazite-Methanol

adsorption q_{st} and the ratio q_{st}/L with w at constant temperature according to equation (2.44). Figure (2.11) presents the variations of q_{st} with T and w. The data used are for the pair Synthetic 13X-Water [9]. The general features of these results are similar to the ones presented in other references such as [3] which indicate the weak dependence of q_{st} on T and the decrease of q_{st} with increasing w to approach the latent heat of condensation L near saturation.

2.3 THERMODYNAMIC DESCRIPTION OF ADSORPTION PROCESS

2.3.1 General Considerations. The important property of changing uptake with temperature and the energy effects that accompany the transformation:

Gaseous moiecule $\Leftrightarrow$ adsorbed molecule

can be used in thermal processes to produce heating and/or cooling. In such processes, the system is constrained to undergo a cycle during which the desired effect is produced. The most important phases in adsorption cycles occur at one of the following conditions:

- constant pressure (isobaric process)
- constant volume
- constant uptake (isosteric process)

A natural question that arises when modeling adsorption machines is how the parameters T, w and T_s (or p) are related during one of the above phases. It is the purpose of this section to obtain formulas describing adsorption cycles. The following assumptions are made to symplify the analysis:
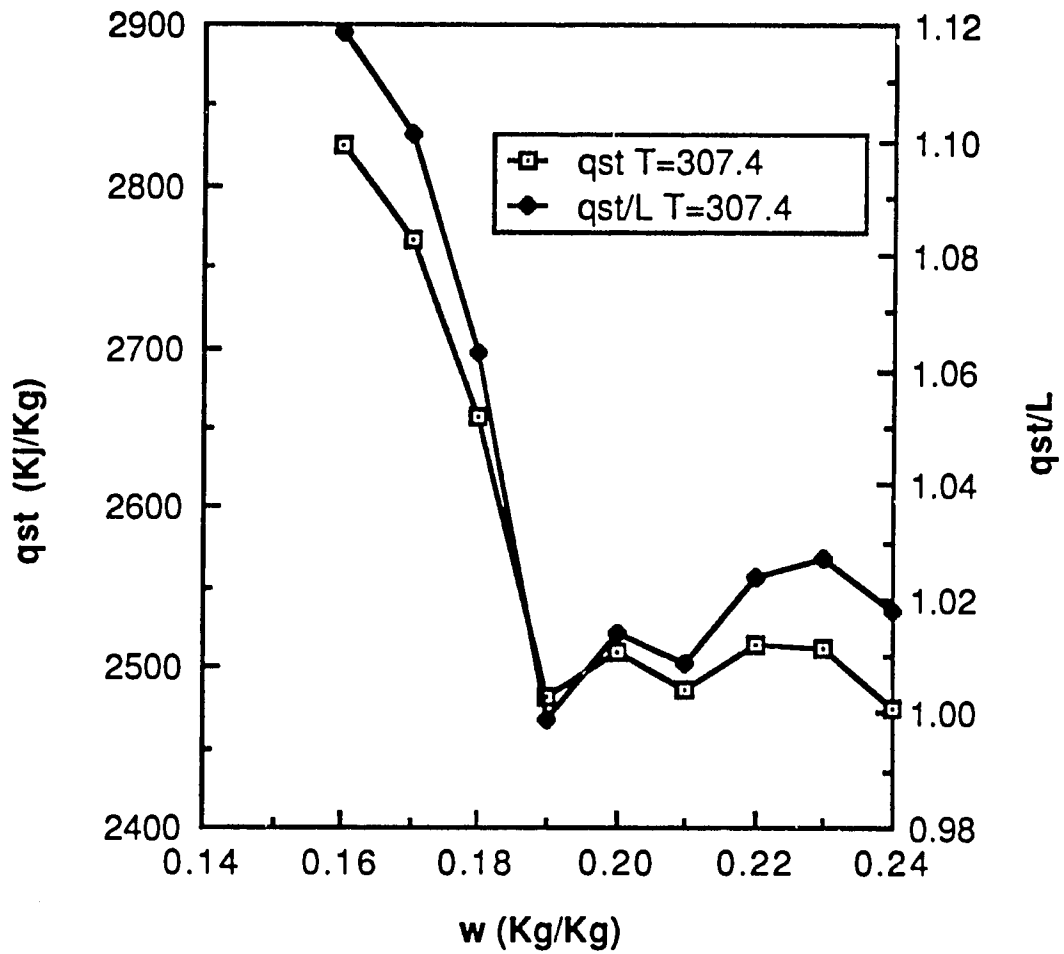
Figure 2.10: Variations of qst and qst/L with w at Constant T
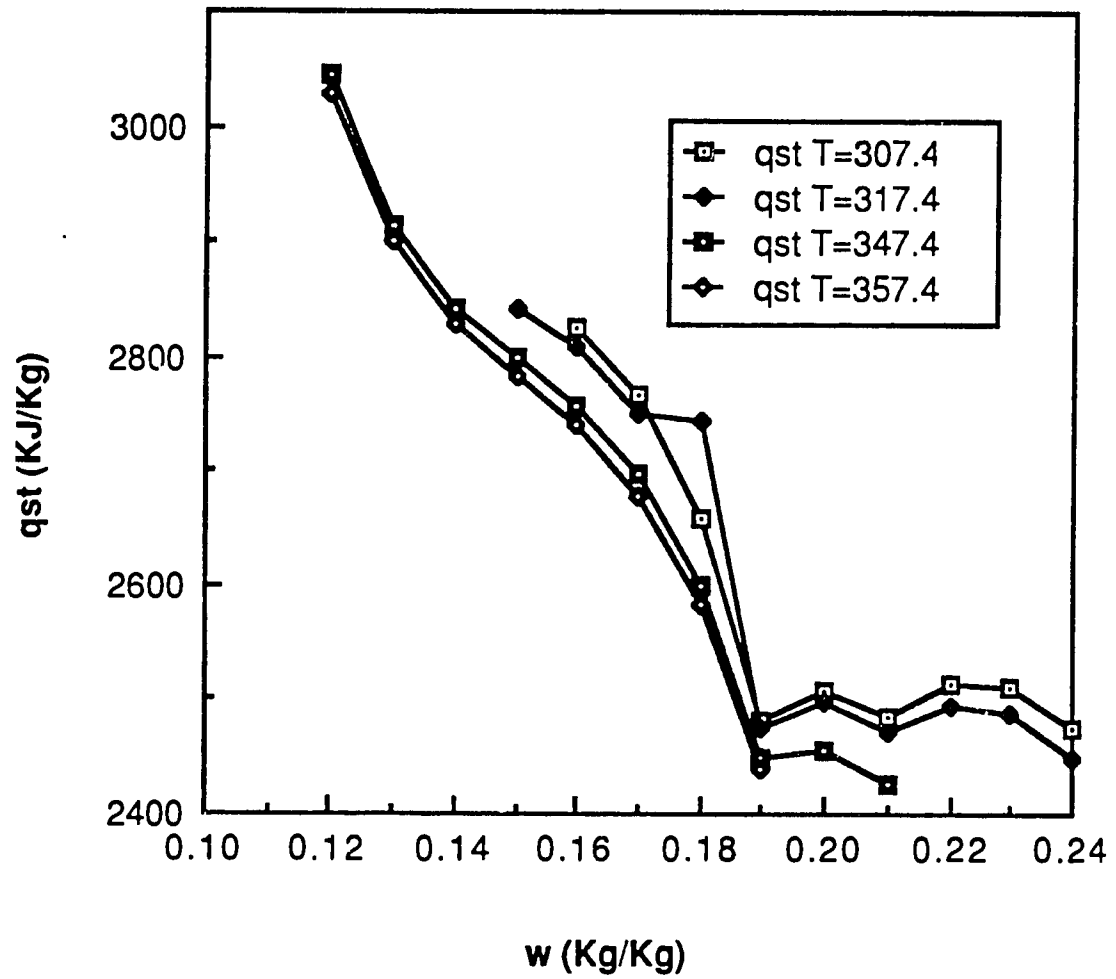as Computed Using (2.44) and the Data of [9]

Figure 2.11: Variations of qst with w and T as Computed
Using Equation (2.44) and the Data of [9]

(i)   Ideal gas phase

(ii) Uniform pressure

(iii) Thermodynamic equilibrium

Assumption (i) is valid for all heating/cooling applications given their very low pressure conditions. Assumption (ii) is acceptable for adsorbents with large intercrystalline voids such as pellets of zeolite 13X which are usually used. Assumption (iii) is equivalent to saying that mass diffusion in the adsorbent is infinitely fast. This assumption can be expected to give good results for systems with sufficiently slow temperature variations such as solar energy powered adsorption machines. However deviations from equilibrium may occur with systems operating in fast conditions. In such cases an additional mass balance equation is needed which will relate the uptake w to its equilibrium value w_{eq} under the system conditions T and T_s. A simple model of the driving force to mass transfer can be assumed to be the difference $(w_{eq}-w)$. Hence the mass flux can be written as:

$$(\partial w / \partial t) = h_m (w_{eq} - w) \tag{2.45}$$

where h_m is a constant proportional to the resistance to mass transfer. The formulas derived below using assumption (iii) will still hold if w is replaced by w_{eq} when necessary. For each phase, general formulas are derived with space dependent temperature field and simplified expressions are obtained for the case of uniform conditions. The equilibrium relation is written in the form :

$$T_s = F(T,w) \tag{2.46}$$

A function $G(T,w)$ which measures the change in uptake per degree of temperature change is introduced by:

$$G(T,w) \equiv dw/dT \qquad (2.47)$$

and called " adsorptivity function ". G characterizes the response of the adsorbent to imposed temperature variations in terms of the consequent uptake change. From the computational point of view the use of G reduces the number of unkowns by eliminating for example w. This reduction is advantageous when a convenient expression of G can be found. This is in particular the case in the simulation of a solar adsorption refrigerator presented in Chapter 3.

2.3.2 Constant-pressure Process. We assume that the pressure of the system is imposed by an external source and remains constant. Differentiating (2.46) at constant p (or T_s) yields:

$$0 = (\partial F/\partial T)_w \, dT + (\partial F/\partial w)_T \, dw \qquad (2.48)$$

This equation gives the expression of G as follows:

$$G_p(T,w) = - \frac{(\partial F/\partial T)_w}{(\partial F/\partial w)_T} \qquad (2.49)$$

when equation (2.32) is used we obtain:

$$G_p(T,w) = - A(w) / [A'(w)T + B'(w)] \qquad (2.50)$$

Since p is known, the equilibrium relation (2.46) gives T explicitly when w is known and allows the solution of w by an iterative method when T is known.

2.3.3 Constant-volume Process. In this case, the system is confined to a constant closed volume. Let V_a be the total volume

of the adsorbent and V_g the total volume of the gas phase. V_g is the sum of two terms: εV_a the void fraction of V_a , and the portion of the total volume not occupied by the solid adsorbent (Figure 2.12)
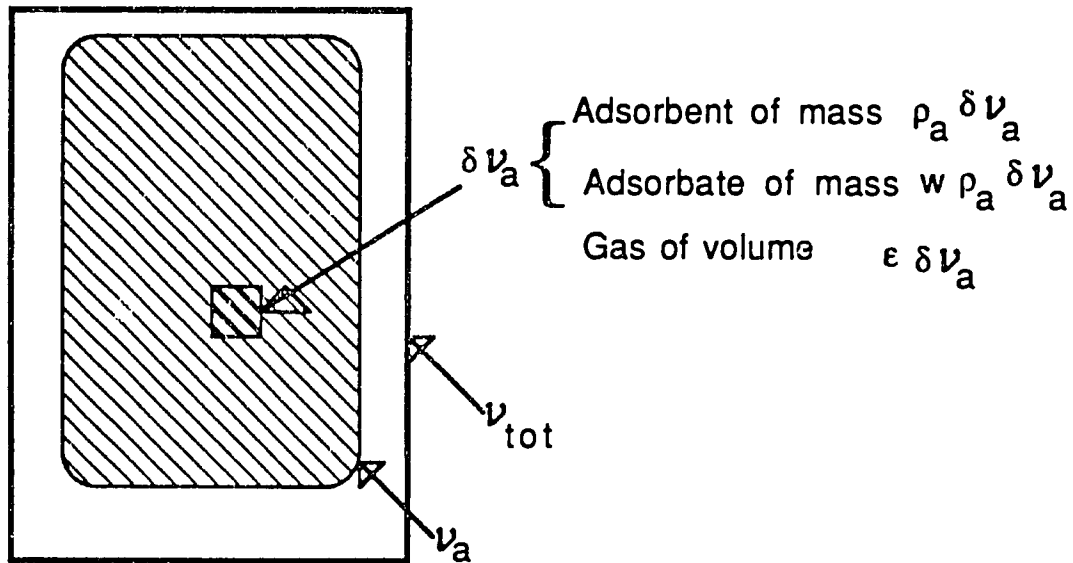
Figure 2.12: Sketch for the Model of an Adsorption System

$$V_g = \varepsilon V_a + (V_{total} - V_a) \tag{2.51}$$

The term $(V_{tot}-V_a)$ is usually small and is neglected in the following analysis. A small adsorbent element of volume δV_a is considered. It contains "dry" adsorbent of mass $\rho_a \delta V_a$, adsorbed species of mass $w\rho_a(\delta V_a)$ and gas phase of volume $\varepsilon(\delta V_a)$ and mass δm_v . The ideal gas equation for the gas phase is :

$$p (\varepsilon \delta V_a) = (\delta m_v) r T \tag{2.52}$$

Assuming constant porosity, for an infinitesimal transformation we have by differentiating (2.52):

$$\frac{dp}{p} = \frac{d(\delta m_v)}{\delta m_v} + \frac{dT}{T} \qquad (2.53)$$

An additional equation is obtained by considering that the change in the mass of the gas phase is of opposite sign and equal to the change in the mass of the adsorbed phase:

$$\int_{\nu_a} d(\delta m_v) = \int_{\nu_a} -\rho_a(dw)\, \delta\nu_a \qquad (2.54)$$

Solving for the term $d(\delta m_v)$ in (2.53) and integrating over ν_a yields:

$$\frac{dp}{p} \int_{\nu_a} \delta m_v = \int_{\nu_a} d(\delta m_v) + \int_{\nu_a} \frac{dT}{T} \delta m_v \qquad (2.55)$$

Taking into account (2.53) and (2.54) we obtain:

$$dp \int_{\nu_a} \frac{\delta \nu_a}{T} = \frac{-\rho_a{}^r}{\varepsilon} \int_{\nu_a} dw\,(\delta \nu_a) + p\int_{\nu_a} \frac{dT}{T^2} \delta \nu_a \qquad (2.56)$$

This equation is a linear equation in p which can be solved for known distributions of of dT and dw. If we call t the varying parameter and define a(t) and b(t) by:

$$a(t) = \frac{\displaystyle\int_{\nu_a} \frac{1}{T^2}\frac{dT}{dt}\delta\nu_a}{\displaystyle\int_{\nu_a} \frac{\delta \nu_a}{T}} \quad ; \quad b(t) = \frac{-\dfrac{\rho_a{}^r}{\varepsilon}\displaystyle\int_{\nu_a} \frac{dw}{dt}(\delta \nu_a)}{\displaystyle\int_{\nu_a} \frac{\delta \nu_a}{T}} \qquad (2.57)$$

we can write:

$$p(t) = [p(0) + \int_0^t b(\eta) \, e^{-\int_0^\eta a(x)dx}] \, e^{\int_0^t a(\eta) \, d\eta} \qquad (1.58)$$

An expression of the function G_v can be derived as follows. Differentiating (2.46) yields:

$$d T_s = (\frac{\partial F}{\partial T})_w \, dT + (\frac{\partial F}{\partial w})_T \, dw \qquad (2\text{-}59)$$

Making use of Clausius-Clapeyron's equation, equation (2.56) transforms to :

$$\frac{L(T_s)}{R T_s^2} \, dT_s = \frac{- \frac{\rho_a \, r}{\epsilon p} \int_{\nu_a} dw \, (\delta \nu_a) + \int_{\nu_a} \frac{1}{T^2} \, dT \, \delta \nu_a}{\int_{\nu_a} \frac{\delta \nu_a}{T}} \qquad (2.60)$$

Eliminating dT_s between (2.59) and (2.60) yields:

$$G_v = \frac{\left\{ \frac{R T_s^2}{L(T_s)} \frac{- \frac{\rho_a \, r}{\epsilon p} \int_{\nu_a} dw \, (\delta \nu_a) + \int_{\nu_a} \frac{1}{T^2} \, dT \, \delta \nu_a}{(dT) \int_{\nu_a} \frac{\delta \nu_a}{T}} - (\frac{\partial F}{\partial T})_w \right\}}{(\frac{\partial F}{\partial w})_T}$$

$$(2\text{-}61)$$

2.3.3.1 Approximation for Small Temperature Change. In most heating/cooling adsorption cycles, the change in pressure during the constant-volume phase is caused by the change in the uptake. The contribution of the temperature change (2nd term in RHS of (2.53)) can in general be neglected. Thus :

$$\delta m_v \, (dp/p) \approx d(\delta m_v) \tag{2.62}$$

Integrating over the volume $\mathcal{V}_a$ gives:

$$(dp/p) \approx (dm_v/m_v) \tag{2.63}$$

where m_v is the total mass of the vapor phase. Integrating equation (2.63) with respect to the parameter t yields:

$$p(t) = p(0) \, [\, m_v(t)/m_v(0) \,] \tag{2.64}$$

From the mass balance given by (2.54) we obtain:

$$m_v(t) = m_v(0) - \int_{\mathcal{V}_a} \rho_a \, [\, w(t) - w(0) \,] \, \delta \mathcal{V}_a \tag{2.65}$$

Thus:

$$p(t) = p(0) \, \{ \, 1 - \frac{\rho_a}{m_v(0)} \int_{\mathcal{V}_a} [w(t) - w(0)] \, \delta \mathcal{V}_a \, \} \tag{2.66}$$

Using the ideal gas law to express $m_v(0)$, we obtain:

$$p(t) = p(0) \, \{ \, 1 - \frac{\rho_a \, r}{\varepsilon} \; \frac{\displaystyle\int_{\mathcal{V}_a} [w(t) - w(0)] \, \delta \mathcal{V}_a}{\displaystyle\int_{\mathcal{V}_a} \frac{1}{T(0)} \, \delta \mathcal{V}_a} \, \} \tag{2.67}$$

2.3.3.2 <u>The Case of Uniform Conditions</u>. When the parameters T and w are constant over the volume $\mathcal{V}_a$, the previous equations (2.54) and (2.56) can be greatly simplified. The mass balance equation (2.54) when integrated with respect to t yields:

$$m_v(t) = m_v(0) - \rho_a \mathcal{V}_a \, [\, w(t) - w(0) \,] \tag{2.68}$$

Equation (2.55) becomes:

$$\frac{dp}{p} = \frac{dT}{T} - \frac{dw}{\dfrac{m_v(0)}{\rho_a \nu_a} - [\ w(t) - w(0)\ ]} \qquad (2.69)$$

or in integrated form:

$$\frac{p(t)}{p(0)} = \{\ 1 - \frac{\rho_a \nu_a}{m_v(0)}\ [\ w(t) - w(0)\ ]\ \}\ \frac{T(t)}{T(0)} \qquad (2.70)$$

Equation (2.60) reduces to:

$$\frac{L(T_s)}{R\,T^2}\,dT_s = \frac{dT}{T} - \frac{dw}{\dfrac{m_v(0)}{\rho_a \nu_a} - [\ w(t) - w(0)\ ]} \qquad (2.71)$$

Assuming a linear variation of $L(T_s)$ with T_s of the form:

$$L(T_s) = L_0 - a_L T_s \qquad (2.72)$$

We can the integrate (2.71) with respect to t to obtain:

$$\frac{L_0}{R\,T_s(t)} + Ln\ \{\ \frac{T(t)\{\dfrac{m_v(0)}{\rho_a \nu_a} - [\ w(t) - w(0)\ ]\ \}}{[T_s(t)]^{a_L / R}}\ \} = Const \qquad (2.73)$$

Equation (2.71) expresses a differential relationship between T, T_s and w for a constant-volume process whereas (2.73) gives an implicit relation between the three parameters. If starting from a known initial state characterized by two of the parameters $(T(0), T_s(0), w(0))$, we would like to determine the conditions of an adsorption system at the final state of a constant-volume process

for which one parameter (for example T_s) is specified. Equations (2.46) and (2.73) form a set that can be solved for w(t) and T(t).

The expression of the function G_v given by (2.61) reduces to:

$$G_v = \frac{- (\frac{\partial F}{\partial T}) \, w + \frac{R}{L(T_s)} \frac{F^2(T,w)}{T}}{(\frac{\partial F}{\partial w})_T + \frac{R}{L(T_s)} \frac{F^2(T,w)}{\frac{m_v(0)}{\rho_a \, \nu_a} - [\, w(t) - w(0) \,]}}$$

(2.74)

2.3.4 " Globally-Isosteric " Process. Usually a constant volume process corresponds to a very small change in the global uptake. But in general, a globally isosteric process is achieved when no adsorbate species is allowed to leave the adsorbed phase. Such a process satisfies:

$$d \int_{\nu_a} \rho_a \, w \, \delta \nu_a = 0$$

(2.75)

Since ν_a is stationary, we can write

$$\int_{\nu_a} \rho_a (dw) \, \delta \nu_a = 0$$

(2.76)

Using equation (2.59), we obtain:

$$\int_{\nu_a} \rho_a \frac{dT_s - (\frac{\partial F}{\partial T})_w \, dT}{(\frac{\partial F}{\partial w})_T} \delta \nu_a = 0$$

(2.77)

Solving for dT_s (which is uniform) and assuming ρ_a constant yields:

$$dT_s = \frac{\displaystyle\int_{\nu_a} [\,(\frac{\partial F}{\partial T})_w \,/\, (\frac{\partial F}{\partial w})\,](dT)\,\delta\nu_a}{\displaystyle\int_{\nu_a} \frac{1}{(\partial F/\partial w)_T}\,\delta\nu_a} \qquad (2.78)$$

It is obvious that for uniform conditions, equation (2.78) reduces to

$$dT_s = (\partial F/\partial T)_w\, dT \qquad (2.79)$$

Which can be directly derived from (2.59) since in this case the process is described by dw=0.

2.3.4 Verification of the Derived Formulas.

No experimental data now exists which can be used in a direct verification of the formulas derived in this section. Therefore the only method of their validation is by comparison of the results obtained from these formulas when used in the numerical simulation of adsorption systems with available test results. This indirect procedure is not rigorous as other approximations involved in such analysis are possible sources of errors.

In the simulation of a solar energy powered adsorption refrigerator, the formulas relative to uniform conditions are used along with data from reference [8]. The predicted transient regime and machine performance show sufficient agreement with the experimental results.

Using equilibrium data provided by Tchernev [9], the functions G_p and G_v are computed for a chosen set of experimental data. The results are given in figures 2.12 and 2.13 . Although Tchernev didn't specify the type of process for he determined experimentally the variations with T of a quantity analogous to G , his results of figure
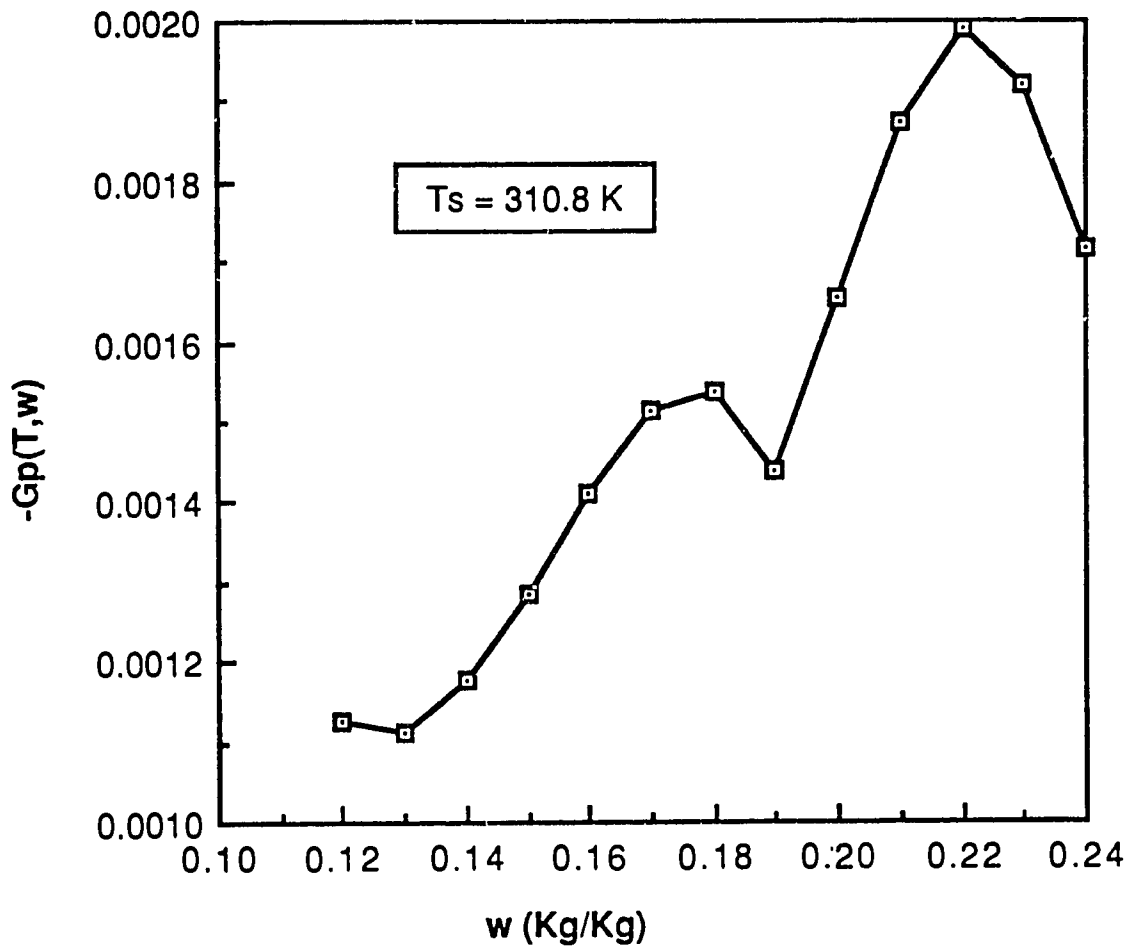
Figure 2.13: The Function G(T,w) as Computed from Equation (2.50) and the Data of [9]
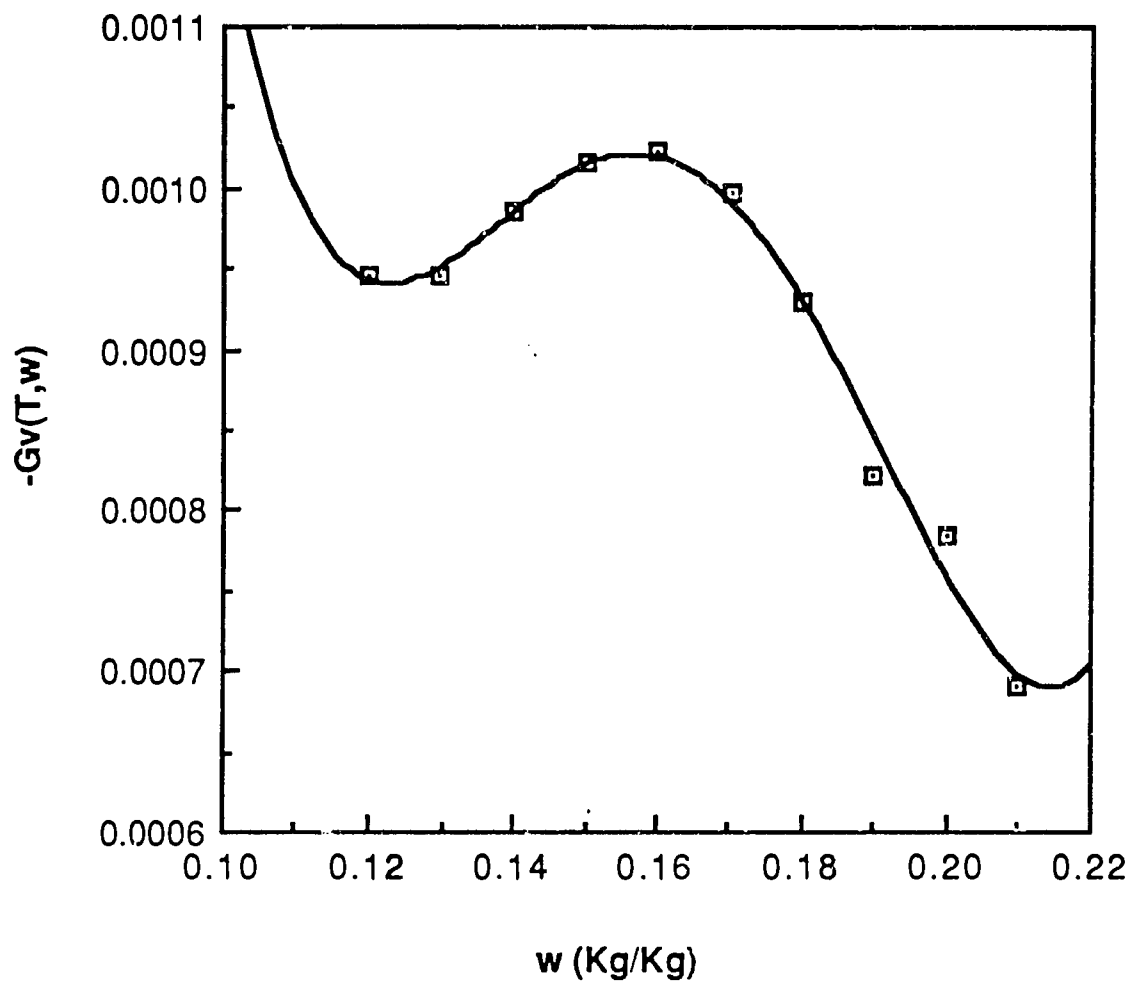
Figure 2.14: The Function Gv(T,w) as Comp_,ited from Equation
(2.74) and the Data of [9]

A15 show similar trend as figures 2.12,13.

The agreement mentioned above between the derived formulas and the available experimental results substantiate somewhat their validity. However in the absence of more direct verification, the following remarks should be made:

1. No detailed comparison with experimental data is attempted here due to lacking data in references [8,9].

2. Most of the derived formulas involve differentiations of the experimentally determined equilibrium function F(T,w), which process is known to may induce large errors. Thus these formulas will certainly be more accurate if the quantities $(\partial F/\partial T)_w$ and $(\partial F/\partial w)_T$ are determined experimentally.

2.4 CONCLUSIONS

A phenomenological law for solid adsorption is proposed and proved to lead to precise and convenient representation of equilibrium data especially for numerical calculations. Formulas describing the processes involved in heating and cooling applications of solid adsorption are also derived. These formulas are substantiated by an indirect verification through the results obtained in their application to numerical simulation of actual adsorption heating and cooling systems.

CHAPTER III

LITERATURE SURVEY ON THE USE OF ZEOLITES IN

SOLAR ADSORPTION REFRIGERATION

3.1 INTRODUCTION

Sorption refrigeration is based on the property that some gases like H_2O, CO_2 and NH_3 are "pumped" by liquids or solids at low temperature and "released" at high temperature. This phenomena discovered since 1824 [17] was the subject of intensive research in the last 30 years. The energy crises and the development of solar technology served to renew the interest in these technologies. Several pairs sorbent-sorbate such as LiBr-H_2O, LiCl-H_2O ... etc were studied theoretically and prototypes were built to test the results of these models.

Adsorption (sorption by a solid) cooling was studied in recent years and presents the advantages of working without mobile parts and avoiding the difficult problem of crystallization which handicaps the liquid desiccant systems. The closed-cycle solid desiccant cooling systems are suited only for air- conditioning applications when water is used as refrigerant. But other fluids such as alcohols can be used to provide refrigeration at temperatures below freezing. These systems can be solar energy powered in which the adsorber is incorporated to the solar collector.

The operating principle of adsorption cooling was described in the late 70's by Tchernev [13] and Meunier & al. [14]. These authors proved both on a thermodynamic basis and by building test
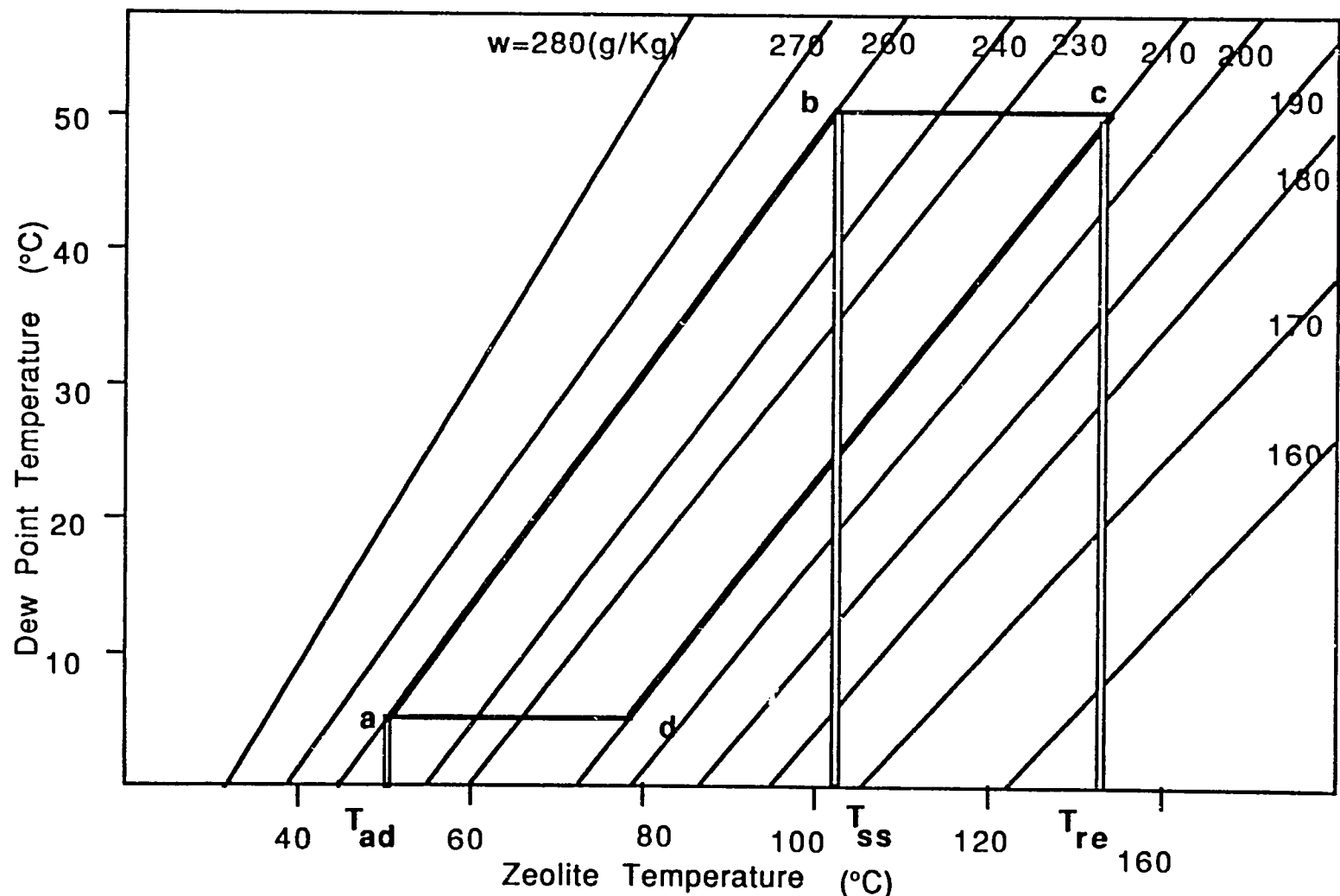
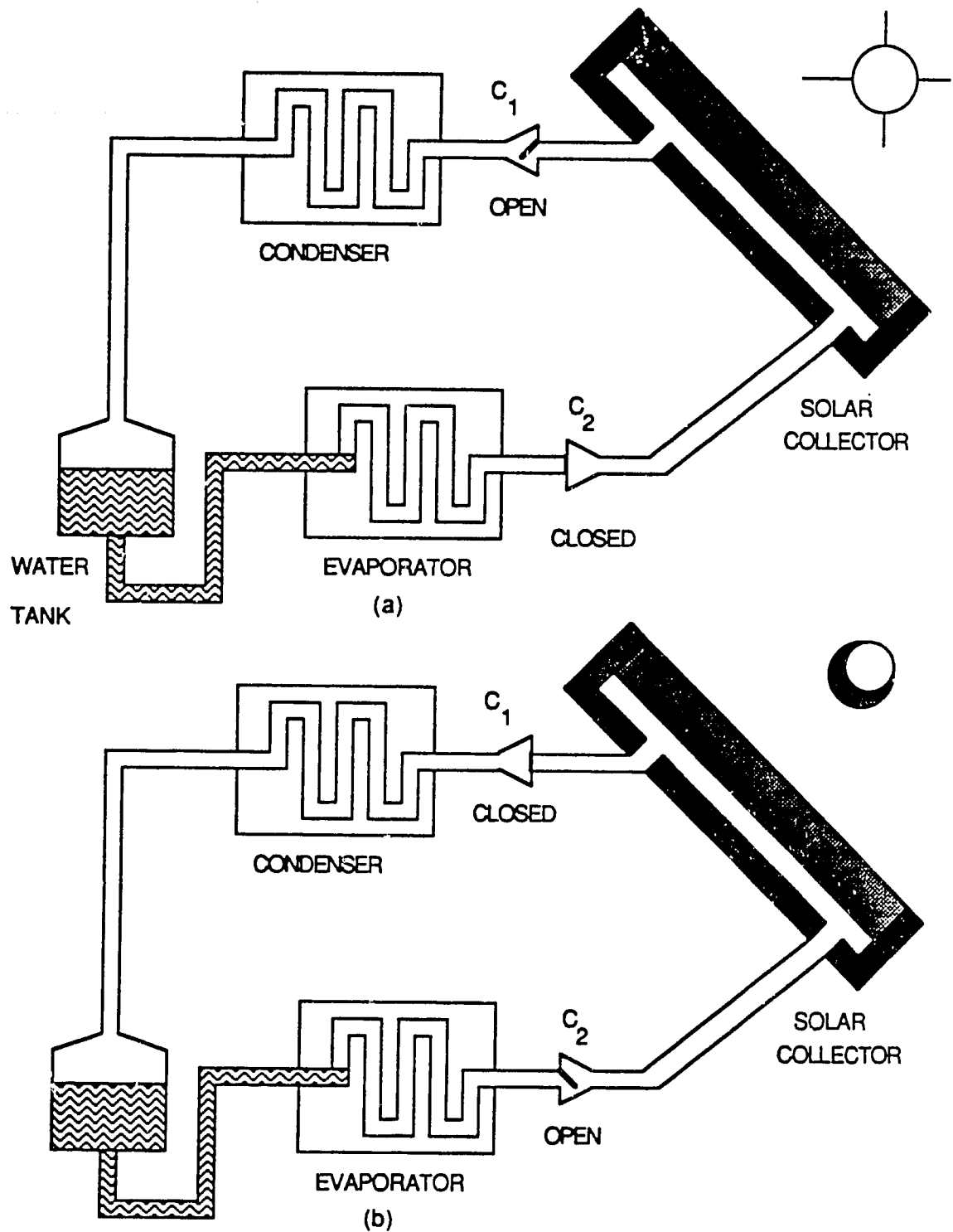Figure 3.1: Isosters for the Pair Zeolite 13X-water . Representation of an Adsorption Cycle.

Figure 3.2: The Two Operating Modes of a Solar Adsorption Refrigerator. (a) Adsorption, (b) Desorption

prototypes the reliability of such systems. The adsorbents used are different types of microporous alumino-silicates also called **zeolites** which are capable of adsorbing considerable amount of several refrigerant gases. A detailed description of the nature and use of zeolites, as well as the physics of solid sorption on these materials can be found in references [3,12,13,14]. In this Chapter we will recall the operating principle of adsorption cooling and review the thermodynamic analyses of such systems as well as the results of experimental studies obtained in this domain.

3.2 OPERATING PRINCIPLE OF ADSORPTION COOLING SYSTEMS

The principle of intermittent single effect cooling cycles using solid adsorption is described in detail in [13,14,15,16]. It is usually found convenient to represent such cycles in the (T, T_s) diagram where the isosters (lines of constant mass fraction of adsorbate w) are approximately straight lines. Figure 3.1 shows the (T,T_s) diagram for the pair Zeolite 13X-H_2O [16] on which a cooling cycle is represented by the points a-b-c-d-a. This cycle is followed daily by a solar refrigerator in a periodic regime and consists of two operating modes (figure 3.2) :

• **Regeneration mode.** At the end of adsorption (point a), the collector is at temperature T_{ad} and the gas sorbate at pressure p_{ev} of the evaporator. As solar radiation heats up the system, the pressure of the gas phase increases and the one-way valve C_2 closes. When the pressure reaches p_{co} (point b) -the temperature of the collector is then T_{ss}-, the one-way valve C_1 opens and allows

the condensation to begin and continue until the adsorbent is at its maximum temperature T_{re} (point c).

• **Adsorption mode.** When the collector is cooled down at night, the pressure of gas adsorbate decreases and the valve C_1 closes. At the value p_{ev} of the pressure, the valve C_2 opens and the evaporation starts (point d). This phase of cooling production continues until the adsorbent is at its minimum temperature T_{ad} (point a).

3.2 THERMODYNAMIC ANALYSIS OF ADSORPTION COOLING SYSTEMS

3.2.1 First Law Analysis and Coefficient of Performance

To perform a thermodynamic analysis of an adsorption cooling machine, the following data are needed:

-Equilibrium isotherms for the pair adsorbent-adsorbate used

-Adsorption enthalpies and entropies as functions of T and w

-Physical properties (p, C_p, etc) of both the sorbent and the adsorbate as pure substances and in the adsorbed state.

-Data on the inert parts of the machine (heat capacity, efficiency, etc).

-The temperatures of the cycle which are:

T_{ad} : temperature at the end of adsorption

T_{ev} : temperature of the evaporator

T_{co} : temperature of the condenser

T_{re} : temperature at the end of regeneration

It is then possible to obtain the minimum value T_{ss} of T_{re} below which the cycle does not work. Assuming constant values of the latent heat L and the isosteric heat of adsorption q_{st} and using Clapeyron-Clausius equations (1. 27) and (1.33), it is easy to obtain:

$$(1/T_{ss}) = (1/T_{ad}) - (L/q_{st})[(1/T_{ev}) - (1/T_{co})] \qquad (3.1)$$

The following heat quantites can also be calculated. If we designate by m_L the amount of cycled adsorbate , we have

$$m_L = M_a (w_{ab} - w_{cd}) \qquad (3.2)$$

The cooling effect: $\qquad Q_L = L(T_{ev}) m_L \qquad (3.3)$

The heat of regeneration : $\qquad Q_{ad} = \int_{T_{ss}}^{T_{re}} q_{st} \ (T,w) \ dm_L \qquad (3.4)$

Sensible heat to bring the condensate from T_{co} to T_{ev} :

$$Q_1 = m_L \int_{T_{ev}}^{T_{co}} C_L \ (T) \ dT \qquad (3.5)$$

Sensible heat needed to bring the collector from point a to b:

$$Q_{sen} = \int_{T_{ss}}^{T_{re}} (M_c \ C_c + M_a \ C_a + w_{ab} M_a C_s) \ d \ T \qquad (3.6)$$

Sensible heat needed to bring the collector from point b to c :

$$Q_r = \int_{T_{ss}}^{T_{re}} (M_c \ C_c + M_a \ C_a + w \ M_a \ C_s) \ dT \qquad (3.7)$$

The coefficient of performance of the machine is defined as follows:

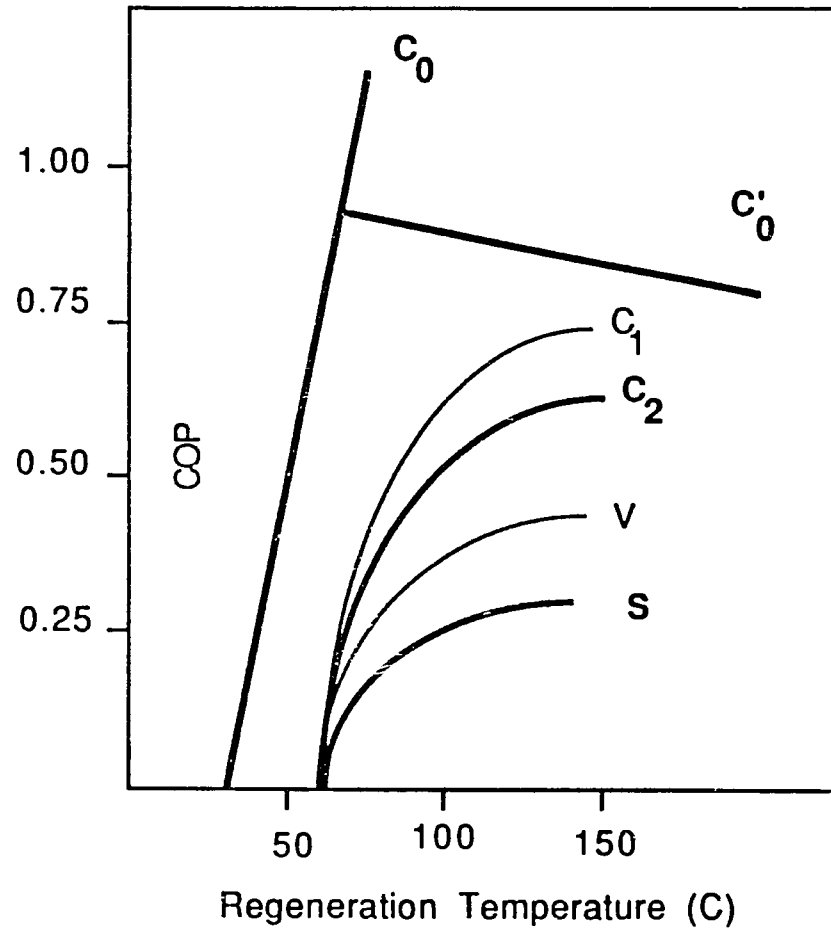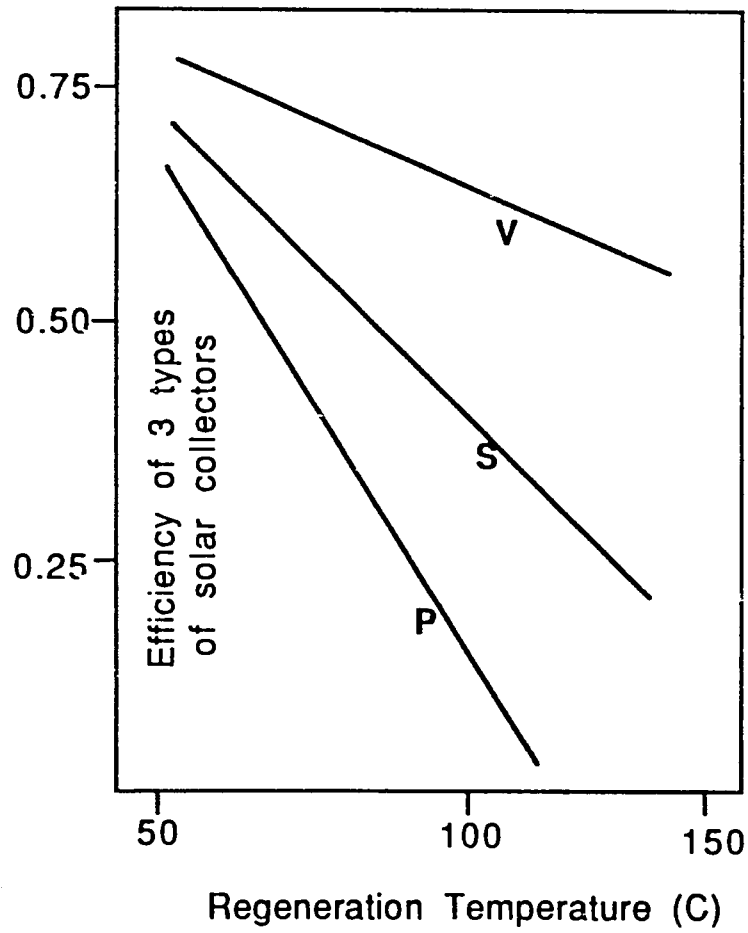$$COP = (Q_L - Q_1)/(Q_{ad} + Q_s + Q_r) \qquad (3.8)$$

Figure 3.3: Typical Vurves COP vs Temperature [16]

Figure 3.3 [16] shows the typical curve COP vs T_{re}. In this figure C_0 is the COP of an ideal trithermal machine operating between T_{re}, T_{ad} and T_{ev}, i.e. $[T_{ev}(T_{re}-T_{ad})]/[T_{re}(T_{ad}-T_{ev})]$. C_0' is the COP of an ideal quadrithermal cycle operating between T_{re}, T_{ss}, T_{co} and T_{ev}, i.e. $[(1/T_{re})-(1/T_{ss})]/[(1/T_{co})-(1/T_{ev})]$. C_1 is the COP obtained by neglecting the collector thermal capacity and a solar efficiency of unity. C_2 is the COP obtained by taking into account the thermal capacity of the collector but still an efficiency of 1. Finally the curves S and V are obtained by taking the efficiency of the collector into account. The letters P, S and V refer to a simple plane collector, a collector with selective surface and an evacuated collector respectively.

It is evident that when the efficiency of the solar collector is taken into account, the COP reaches a maximum value of about 0.25-0.38 at a certain optimum value of T_{re} before declining. Equation (3.8) shows that the COP depends on the operating temperatures, the properties of the pair adsorbent-adsorbate used and the efficiency of the solar collector. A comparison of several pairs by Guilleminot & al. [16] proved that no pair is appropriate for all applications. In particular they found that the pair Activated Al-H_2O is more efficient for air-conditioning with a water cooled condenser whereas Zeolite 13X-H_2O is better with an air-cooled condenser. The use of other refrigerants such as methanol instead of water permits evaporator temperatures below freezing and decreases the value of T_s (which is favorable to COP)
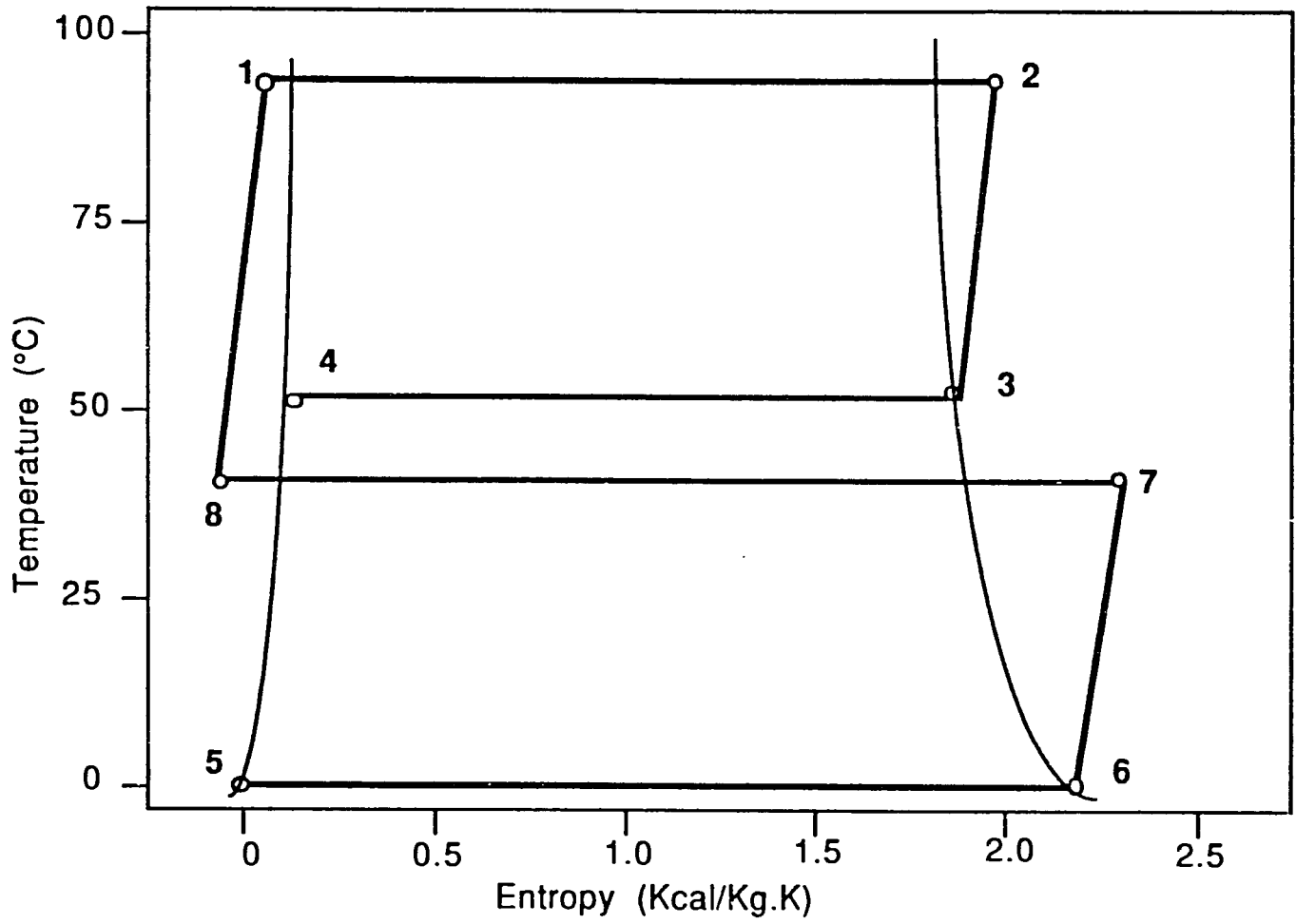
Figure 3.4: Representation of an Adsorption Cycle on the Entropy Diagram [23]

but the overall COP with the Zeolite 13X-Water pair is larger than with Zeolite 13X-Methanol. The effect of the solar collector was also found to be very important: at low values of the difference $(T_{co}-T_{ev})$, the use of a plane collector is sufficient whereas at large values of this parameter, it is necessary to use a more efficient collector at high temperatures.

Chang and Roux [18] confirmed the above observations about the factors influencing the COP. They also showed that the slope of the isosters in $\log(p_s$) vs $1/T$ diagram (which as seen in Chapter 1 determines the heat of adsorption) has competing effects on the COP. A large value of the slope decreases T_s and therefore T_{re} allowing high efficiency of the collector . But at the same time the efficiency of the cooling cycle is decreased thus lowering the overall COP of the machine.

As a mean of reducing the heat losses, Guilleminot & al. [16] proposed the possibility of recovering the sensible heat used during the regeneration phase. A fluid is heated up by circulation throught the hot collector and can be used for domestic purposes.

3.3.2 **Second Law Analysis of Adsorption Cycles**. An other representation of adsorption cycles was adopted by Dahome & Meunier [23]: They plotted the entropy of the working fluid (water in their case) versus its temperature as it follows the cycle (figure 3.4). The entropy in the adsorbed phase was calculated from the heat of adsorption q_{st} as follows:

$$S = S(T_1 , p_1) + q_{st} (T_1 , p_1)/T \qquad (3.9)$$

The COP was defined by:
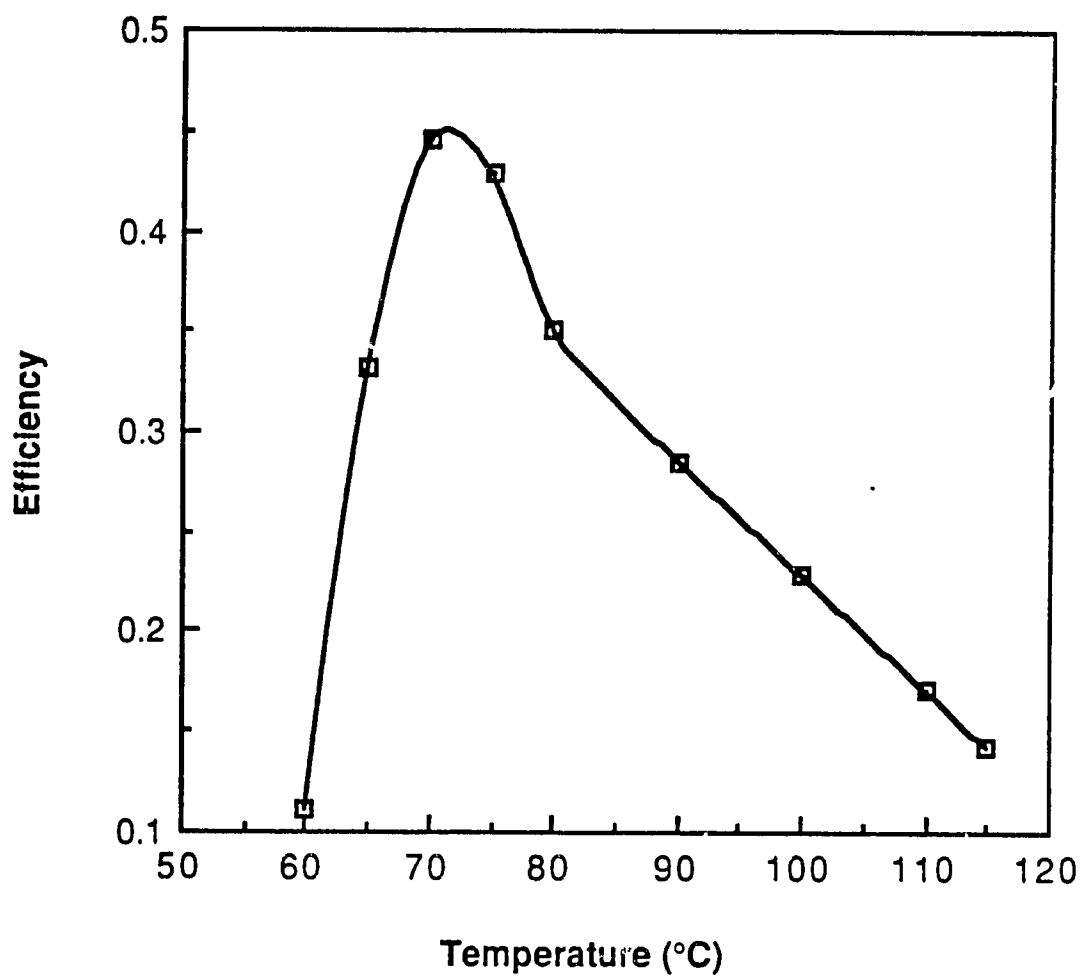
Figure 3.5a: Cooling Efficiency for Zeosorb 5.0A
with Input Power Density of 1 Kw/m2 [13]
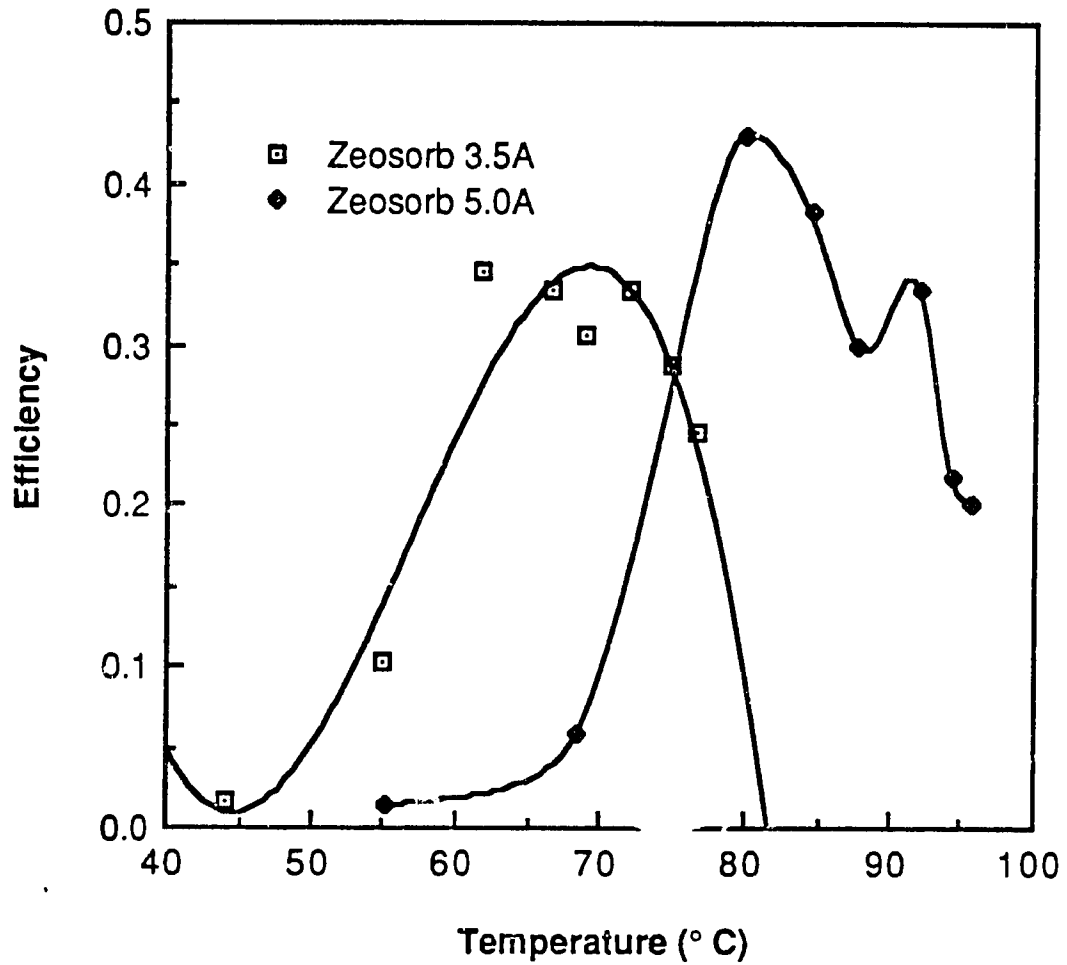
Figure 3.5b : Experimental Efficiencies for the Pairs
 Zeosorb 5.0A-Water and Zeosorb 3.5A-Water
 with Solar Heat [13]

$$COP = (Q_{4-5} + Q_{5-6})/(Q_{8-1} + Q_{1-2}) \qquad (3.10)$$

The heat quantities Q's are defined by:

$$Q_{4-5} = \int_{T_2}^{T_4} C(T) \, dT \qquad (3.11)$$

$$Q_{5-6} = L(T_4) \qquad (3.12)$$

$$Q_{8-1} = \int_{T_3}^{T_1} C_s(T) \, dT \qquad (3.13)$$

$$Q_{1-2} = H_2 - H_1 = q_{st}(T_1, P_1) \qquad (3.14)$$

The authors compared the actual adsorption cycle to an ideal quadri-thermal cycle operating between T_1, T_2, T_3 and T_4 and found that they are close but not identical. This result gives credit to the analysis of section 3.3.1 and comfirms that adsorption cycles are suitable to energy storage, cooling and heat transforming processes.The influence of internal irreversibilities was also examined in terms of "discontinuities" of the pressure and the temperature at the interfaces of phase change. The results how that irreversibilities have little effect on the COP but cause a significant drop of the ratio COP/COP_{ideal} and an important loss of available energy ("noncompensated energy").

3.4 EXPERIMENTAL RESULTS

Tchernev [13] presented experimental efficiencies of solar energy powered adsorption refrigerators using natural zeolites Zeosorb 3.5A and 5.0A as adsorbents. His results given in

Solar Time	Upper Plate Temp.	Lower Plate Temp	T_z^*	COP1	COP2
11.30-12	889	70	65	0.43	0.096
12.00-13	97	78	75	0.48	0.23
13.00-14	104	85	82	0.52	0.32
14.00-15	110	92	87	0.52	0.36
15.00-16	108	98	91	0.48	0.39
16.00-17	107	104	94	0.52	0.40
17.00-18	100	101	95	0.52	0.41
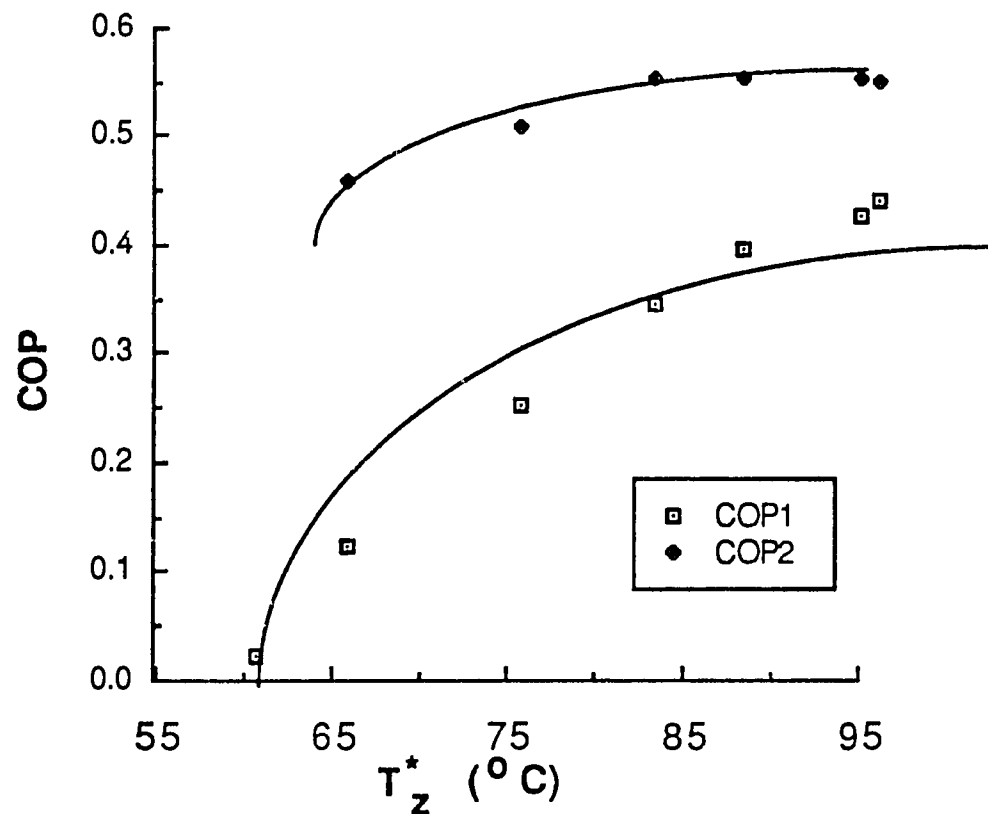
Figure 3.6 : Experimental Upper and Lower Plate Temperature, T_z^* (Apparent Zeolite Temperature) and the COP.
COP1 & COP 2 are the Instantaneous and the Cumulative COP.

figure 3.5 show a maximum value of the efficiency of about 0.40-0.45 reached around 75°C temperature. The efficiency given in [13] is not clearly defined, but the given values suggest that it is equal to the cycle COP, as defined in by equation (3.8), and does not take into account the losses at the solar collector. The shape of the efficiency curve is similar to the theoretical curve of figure 3.3a except at low temperatures of desorption. The Dubinin approach, discussed in Chapter II and known to be inadequate at the limits $\theta \approx 0$ and $\theta \approx 1$, which is used by the theoretical investigators, is probably the cause of this discrepancy. It is also evident from figure 3.5 that the pair Zeosorb 5.0-H_2O exhibits a large maximum efficiency (at about T=80°C) whereas the pair Zeosorb 3.5A-H_2O has a better efficiency at lower adsorption T_{ad} between 50 and 70°C.

Guilleminot and Meunier [8] tested a refrigerator using the pair Zeolite 13X-H_2O. Their results given in figure 3.6 show a clear difference between the calculated and the measured temperatures of the upper and lower plates of the collector-adsorber. This lead the authors to define an apparent adsorption temperature T_z^{*} which agrees with the theoretical analysis. However the experimental COP of about 0.44 is well predicted by the relatively simple theory presented in section 3.2. This demonstrates the little effect of the irreversibilities due to heat and mass transfer which are neglected in the theory of this type of experiments which are characterized by a slow periodidity and a favorable integration of the adsorber into the collector.

Adell [22] gave experimental results obtained with the pair

Zeolite 13X-H_2O. He found a solar COP of about 0.08-0.09 (all losses included). His exergy analysis which neglects some causes of irreversibilities such as mass diffusion and temperature gradients in the zeolite gave a COP of 0.095.

3.5 OTHER STUDIES

The discrepancies between the theoretical value of the COP obtained from the exergy analysis and the experimental COP lead normally Adell [20] to consider the non-uniformity of the temperature in the adsorber. An analytic model was developed assuming the dependency $T=T(z,t)$ where z is the coordinate normal to the adsorbent layer and other simplifying approximations. The model was used to predict the heat diffusivity of the "mixture" zeolite 13X -adsorbed water and the " apparent diffusivity" during during desorption. Fair agreement with the experimental profiles of temperature was obtained but the model predicts a value for a parameter defined in a linearized representation of equilibrium data which is much larger than its experimental value.

Monnier and Dupont [19] used a finite difference scheme to solve the equation of transient heat and mass transfer. Their calculation assumed as in [22] variations of temperature in the z-direction only. Their results seemed to correlate well the measured temperature profiles only in the first hours of the desorption phase. An interesting finding of their study was the existence of an optimum zeolite thickness (4 cm in their case) for which the COP is maximum.

Adell [21] presented a theoretical investigation of a possible application of adsorption cooling in agriculture in tropical

regions. He showed in particular how the daily periodic change in temperature can be controlled to allow better conditions for the plants using a very simple technology. This study predicted a COP of about 0.15.

3.6 THE CONCEPT OF REGENERATIVE HEAT EXCHANGE APPLIED TO ADSORPTION SYSTEMS

The systems described above are all based on single effect intermittent-cycles. These systems are characterized by COP's less than 1 (as small as 0.1 for the solar COP). Tchernev [10] used the idea of a regenerative heat to recover the heat generated during the adsorption phase and the sensible heat stored in the zeolite container as a means to increase the COP. His system consists of two zeolite containers working alternatively in adsorption and desorption mode. An appropriate choice of the period of each mode allows recycling of most the energy used in the desorption phase. In addition, the two-container machine provides continuous cooling (or heating in the case of a heat pump). A most detailed description of Tchernev's system along with a mathematical model for its analysis will be presented in Chapter V. A schematic representation of this system is given in figure 4-1. The author claims a potential increase of the COP to about 2.0. Note that Tchernev's system does not use solar energy as heat source therfore the increase of COP has to be compared with the value of about 0.6 obtained with single container machines when the efficieny of the solar collector is equal to unity.

A prototype was tested and an experimental cooling COP of 1.2 obtained (figure 3.7a). Another important result of Tchernev's
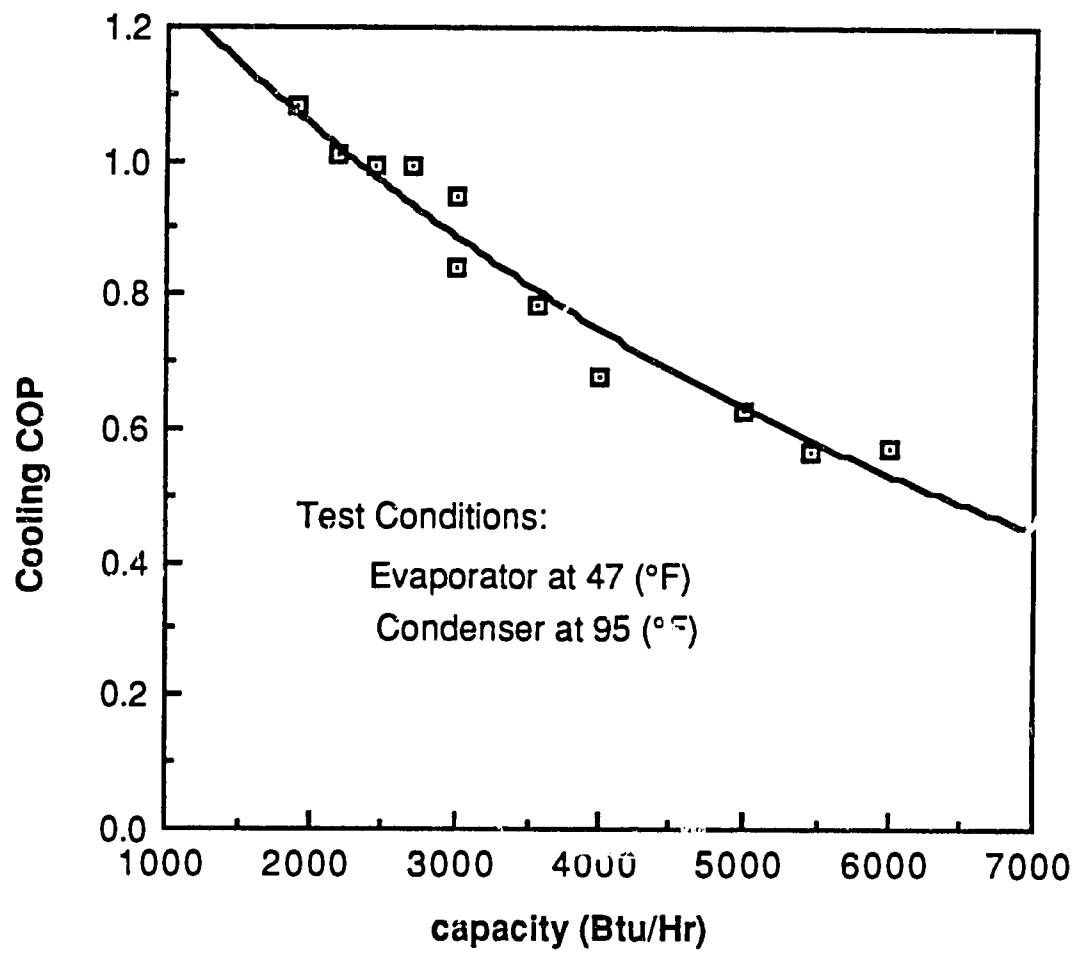
Figure 3.7a: Experimental Cooling COP vs Capacity [10]
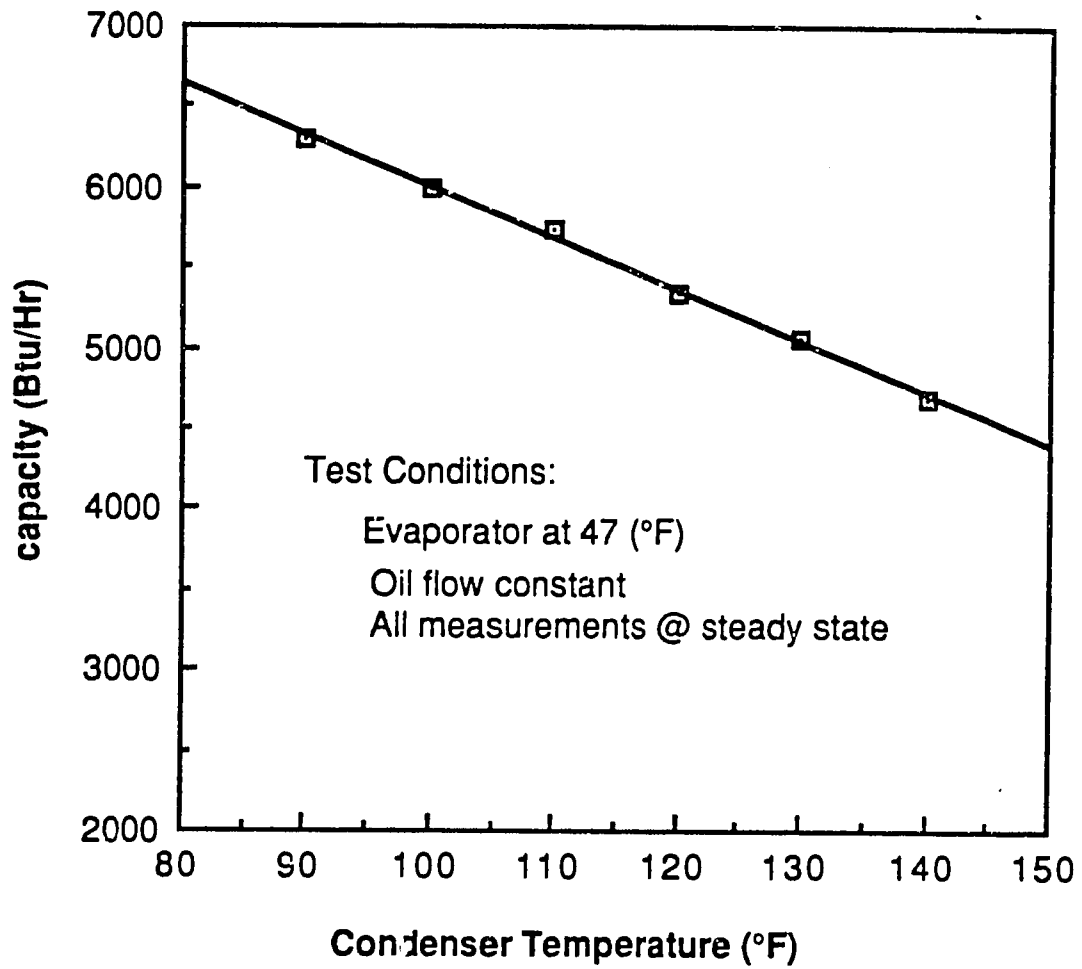
Figure 3.7b: Capacity as Function of the Condenser
Temperature [10]
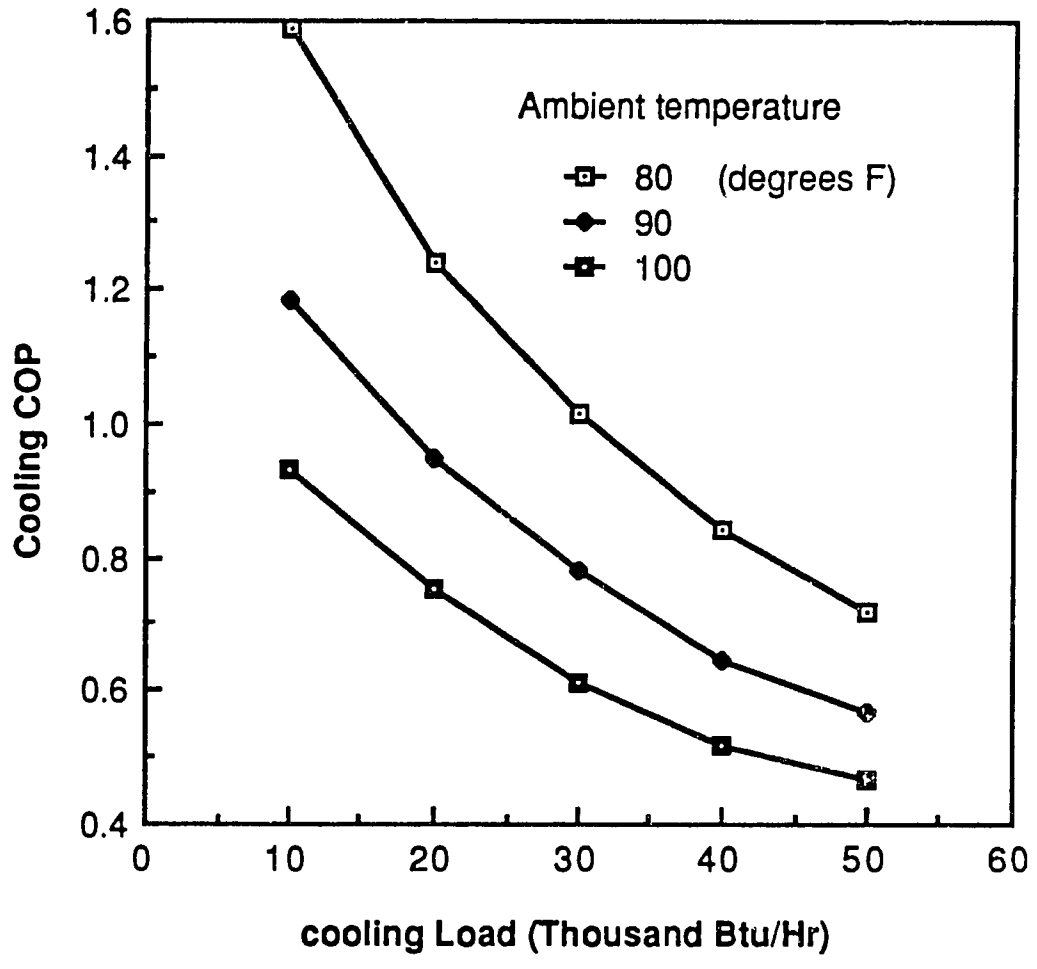
Figure 3.8: Simulation Results Giving COP vs
the Cooling Load [10]

tests was confirming the weak dependency of the system performance on the condenser temperature; which demonstrates the possibility of using air cooled condensers even in hot weather conditions (figure 3.7b). The pair used in the tests was Zeolite 13X-H_2O.

Tchernev [10] indicated the major lack of information on zeolite physical properties as well as on heat and mass transfer in regenerators with non-linear temperature dependency of the thermal properties and equilibrium relationships. A first attempt was made by the author and partial results of his unpublished analysis are shown in figure 3.8.

3.8 CONCLUSIONS

The literature survey indicates that the use of zeolites in low grade energy powered adsorption cooling and heating has been proved, both theoretically and experimentally, to yield cycle coefficients of performance of order of 0.5. The thermodynamic analyses of adsorption systems have thus far relied on the representation of the adsorption cycle in the (T_s, T) diagram. This justifies the need for a complete dynamic analysis of a closed-cycle adsorption system which will determine the effects of various design parameters and operating conditions on the system performance. This task is undertaken in Chapter IV.

The novel adsorption systems based on the concept of heat regeneration can have significantly increased performance. A first parametric analysis of such system is presented in Chapter VI.

CHAPTER IV

DYNAMIC ANALYSIS OF THE SOLAR COLLECTOR

IN A CLOSED-CYCLE ADSORPTION REFRIGERATOR

4.1 INTRODUCTION

The critical component of a closed-cycle adsorption refrigerator is the collector. The latter accomplishes the combined functions of receiving solar energy and regenerating the adsorbent material. Previous analyses of closed-cycle machines considered only an idealized cycle on the (T_s, T) diagram [15,16,18]. Although this type of analysis reasonably predicts the system performance in terms of its COP, it does not allow the study of the effect of design parameters and weather conditions. Thus, a dynamic analysis of a real system is useful from the view point of design optimization and also gives more insight into the sorption mechanisms in such systems.

The analysis of solar collectors in general presents unique problems of changing ambient temperature, wind conditions and solar radiation [25]. Besides these problems, an adsorbing collector adds the difficulty associated with adsorption phenomena. Given this complexity, several simplifying assumptions are made in this study:

1. The adsorbent is always assumed to be at thermodynamic equilibrium, i.e., the moisture content w, the temperature T and the pressure of the vapor phase p are related by:

$$T_s(p) = F(T,w) \qquad (4.1)$$

This assumption seems reasonable since the system operates on a daily cycle (long time periodicity).

2. The temperature is uniform across the collector. Although it is known that temperature gradients exist [19,20], this assumption is not expected to significantly affect the results of this analysis.

3. The values of specific heats are constant and the specific heat of adsorbed species is taken equal that of the bulk liquid adsorbate.

4.2 THE GOVERNING EQUATIONS

We assume the adsorbent material and the inert parts of the collector to be at a uniform temperature T and the glass cover at T_g. The geometry and design data of the collector are shown in figure 4.1.Two differential equations are derived by writing the energy balances for a unit area of the collector. For the adsorbent, the fraction $(\tau\alpha)_e$ of the incident solar flux ι is transformed into:

- sensible heat

- heat of sorption

- heat lost by convection and radiation to the glass cover.

The energy balance is expressed as follows:

$$(\tau\alpha)_e \, \iota = (M_c C_c + M_a C_a + w M_a C_s)(dT/dt) - q_{st}(T,w)(dw/dt)$$

$$+ (h_{r,a\text{-}g} + h_{c,a\text{-}g})(T - T_g) \qquad (4.2)$$

For the glass cover, the inlet energy increase is the sum of the absorbed solar flux and the net heat gain by convection and radiation from the adsorbent and ambient air. Therefore we obtain:

Ambient Temperature $T_a(t)$

Solar radiation $\iota(t)$

Adsorbent
M_a , C_a

Glass Cover
M_g , C_g
α_g , ε_g

Inert metal
M_c , C_c
α_c , ε_c

Insulation

β
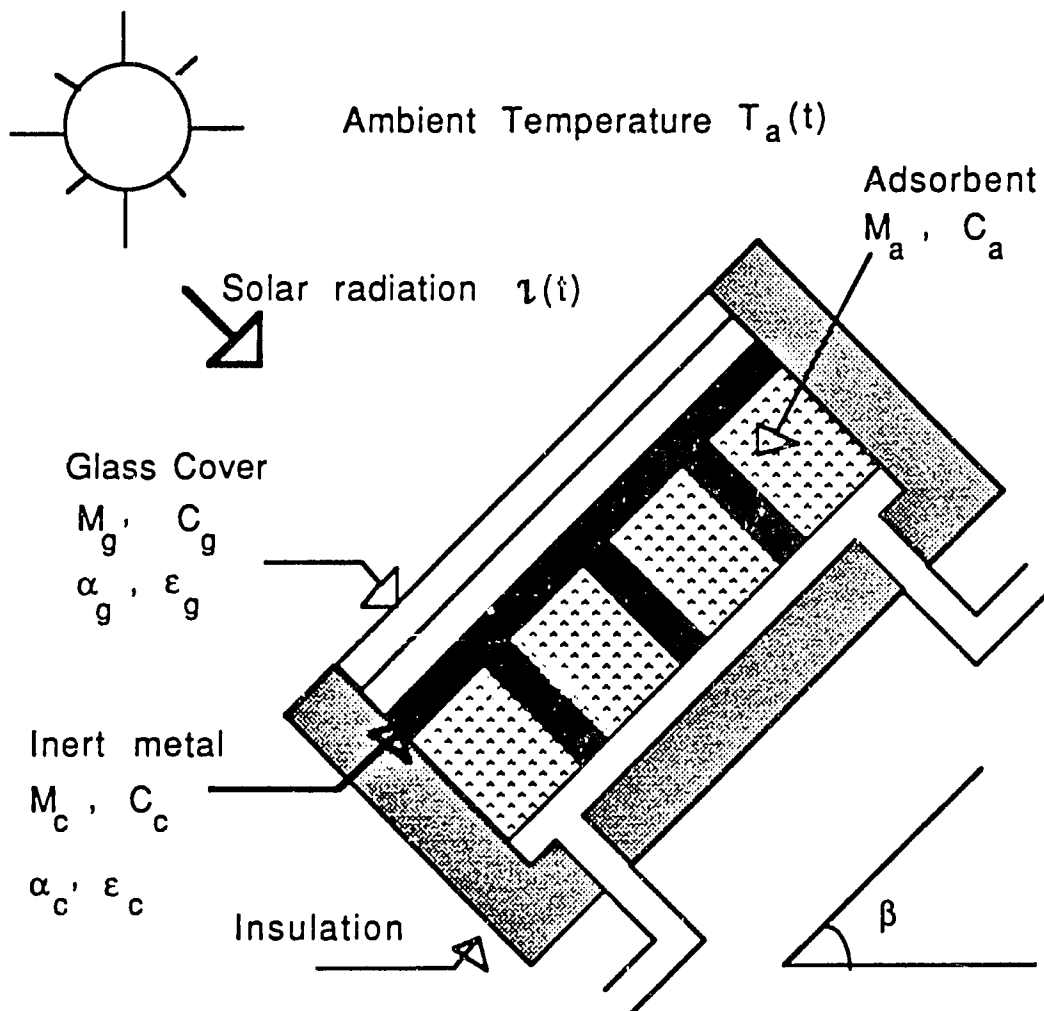
Figure 4.1 : Geometry and Design Data of the Solar Collector
in an Adsorption Cooling System

$$\alpha_g \iota + (h_{r,a\text{-}g} + h_{c,a\text{-}g})(T - T_g) = M_g C_g\ (dT_g/dt)$$

$$+ (h_{r,g\text{-}\infty} + h_{c,g\text{-}\infty})(T_g - T_\infty) \qquad (4.3)$$

Equation (4.1) can be modified to eliminate the term (dw/dt) by introducing the function **G** introduced in Chapter I which satisfies:

$$dw = G(T,w)\ dT \qquad (4.4)$$

Equations (4.2) and (4.3) can be rewritten in a more convenient form for numerical solution as follows:

$$\frac{dT}{dt} = \frac{(\alpha\tau)_e\, \iota\ -\ (h_{r,a\text{-}g} + h_{c,a\text{-}g})(T - T_g)}{M_a (C_a + wC_s)\ +\ M_c C_c\ -\ q_{st} M_a G(T,w)} \qquad (4.2')$$

$$\frac{dT_g}{dt} = \frac{\alpha_g\, \iota + (h_{r,a\text{-}g} + h_{c,a\text{-}g})(T - T_g)\ -\ (h_{r,g\text{-}\infty} + h_{c,g\text{-}\infty})(T_g - T_\infty)}{M_g C_g} \qquad (4.3')$$

Expressions of the function **G** and the relations describing the phases of an adsorption cycle are derived in Chapter I. We recall here the formulas obtained for uniform conditions:

During a constant-volume process:

$$\frac{L_o}{R\, T_s (t)} + Ln \left\{ \frac{T(t)\{\dfrac{m_v (0)}{\rho_a\, \nu_a} - [w(t) - w(0)] \}}{[T_s (t)]^{a_L / R}} \right\} = Const \qquad (4.4)$$

$$G_v = \frac{-\left(\frac{\partial F}{\partial T}\right)w + \dfrac{R}{L(T_s)}\dfrac{F^2(T,w)}{T}}{\left(\frac{\partial F}{\partial w}\right)_T + \dfrac{R}{L(T_s)}\dfrac{F^2(T,w)}{\dfrac{m_v(0)}{\rho_a \nu_a}} \cdot [\, w(t) - w(0)\,]}$$ (4.5)

During a constant-pressure phase we have:

$$T_s = \text{Constant}$$ (4.6)

$$G_p = -\,A(w)\,/\,[\,A'(w)\,T + B'(w)\,]$$ (4.7)

4.3 NONDIMENSIONLIZATION OF THE GOVERNING EQUATIONS

The important parameters influencing the performance of a solar adsorption refrigerator are better seen in the dimensionless form of the governing equations. This form is obtained after introducing the following parameters and functions:

$$\eta = t\,/\,t_0$$

$$E_0 = M_c C_c / M_a C_a \quad , \quad E_1 = C_s / C_a \quad , \quad E_2 = M_g C_g / M_a C_a$$

$$E_3 = L_0 / C_a (T_{re} - T_{ad}) \quad , \quad E_4 = h_0 A t_0 / M_a C_a \quad , \quad E_5 = r T_{ad} \rho_a / \varepsilon \rho_{ev}$$

$$E_6 = T_{re} / T_{ad} \quad , \quad E_7 = p_{co} / p_{ev} \quad , \quad E_8 = T_{co} / T_{ev} \quad , \quad E_9 = T_{co} / T_{ad}$$

$$E_{10} = L_0 / r T_{ev} \quad , \quad E_{11} = C_L / C_a \quad , \quad E_{12} = \mathbf{1}_0 A t_0 / [M_a\, C_a (T_{re} - T_{ad})]$$

$$\theta = (T - T_{ad}) / (T_{re} - T_{ad}) \quad , \quad \theta_g = (T_g - T_{ad}) / (T_{re} - T_{ad})$$

$$\theta_\infty = (T_\infty - T_{ad}) / (T_{re} - T_{ad}) \quad , \quad I(\eta) = \mathbf{1}(t)\,/\,\mathbf{1}_0$$

$$\theta_s = (T_s - T_{ev}) / (T_{co} - T_{ev}) \qquad \Phi(\theta,w) = (F(T,w) - T_{ev}) / (T_{co} - T_{ev})$$

$$\varphi(\theta,w) = q_{st}(T,w) / L_0 \quad , \quad \lambda(\theta_v) = L(T_v) / L_0 \quad , \quad \gamma(\theta,w) = G(T,w) / (T_{re} - T_{ad})$$

where t_o, h_o, L_o and G_o are characteristic values of t, h, L and G respectively. The governing equations therefore become:

$$\frac{d\theta}{d\eta} = \frac{E_{12}^{(\alpha\tau)} e^{I(\eta)} - E_4 h^*_{a-g} (\theta - \theta_g)}{1 + E_o + E_1 w - E_3 \varphi(\theta, w) \Gamma(\theta, w)} \tag{4.2'*}$$

$$\frac{d\theta_g}{d\eta} = \frac{E_{12}^{(\tau)} g^{I(\eta)} + E_4 [h^*_{a-g} (\theta - \theta_g) - h^*_{g-\infty} (\theta_g - \theta_\infty)]}{E_2} \tag{4.3'*}$$

$$w = w_o + \mu_o \left\{ 1 - \frac{[(E_8 - 1)\theta_s + 1]^\beta}{[(E_6 - 1)\theta + 1]} \frac{1}{C} \exp\left[-\frac{E_{10}}{[(E_8 - 1)\theta_s + 1]}\right] \right\} \tag{4.4'*}$$

where C and μ_o are defined by:

$$C = \frac{[(E_8 - 1)\theta_{so} + 1]^\beta}{[(E_6 - 1)\theta_o + 1]} \exp\left[-\frac{E_{10}}{[(E_8 - 1)\theta_{so} + 1]}\right]$$

$$\mu_o = \frac{T_{ad}}{T} \frac{P_o}{P_{ev}} \frac{1}{E_5}$$

4.4 METHOD OF NUMERICAL SOLUTION

The first order nonlinear differential equations (4.2,3) can be solved using the following explicit scheme:

$\theta_o = 0$ $\qquad\qquad$ $\theta_{g,o} = 0$ $\qquad\qquad$ $\theta_{s,o} = 0$

$$\theta_{n+1} = \theta_n + \frac{E_{12}(\alpha\tau)_e I_n \cdot E_4 h^*_{z-g} (\theta_n - \theta_{g,n})}{1 + E_0 + E_1 w - E_3 \varphi(\theta_n, w_n) \Gamma(\theta_n, w_n)} \Delta\eta$$

$$\theta_{g,n+1} = \theta_{g,n} + \frac{E_{12}(\tau)_g I_n + E_4 [h^*_{a-g} (\theta - \theta_g) - h^*_{g-\infty} (\theta_{g,n} - \theta_{\infty,n})]}{E_2} \Delta\eta$$

W_{n+1} and $\theta_{s,n+1}$ are obtained differently depending on whether $\theta_s < 1$ ($T_s < T_{co}$, constant volume phase) or $\theta_s = 0,1$ ($T_s = T_{co}$, T_{ev} constant pressure phase):

If $\theta_s < 1$, $\theta_{s,n+1}$ and w_{n+1} are solved using the following iterative procedure: - First a value of w_{n+1} is guessed (say w_n).

- Equation (4.1) gives $\theta_{s,n+1} = \Phi(\theta_{n+1}, w_{n+1})$

- Equation (4.4'*) gives a corrected value of w_{n+1}:

$$w_{n+1} = w_0 + \mu_0 \left\{ 1 - \frac{[(E_8 - 1)\theta_{s,n+1} + 1]^\beta}{[(E_6 - 1)\theta_{n+1} + 1]} \frac{1}{C} \exp\left[- \frac{E_{10}}{[(E_8 - 1)\theta_{s,n+1} + 1]}\right] \right\}$$

- This new value of w_{n+1} is compared to the previous one and iterations are continued until w converges. Once θ_s reaches the value 1, it remains constant for the remaining portion of the process. The quilibrium equation (4.1) is then used to determine w_{n+1} for a known θ_{n+1}.

4.5 CORRELATIONS FOR HEAT TRANSFER COEFFICIENTS

4.5.1 Natural Convection Between the Collector Plate

and the Glass Cover. It is known from the theory of hydrodynamic stability that free convection between a horizontal plate heated from below occurs at a certain critical value of Rayleigh Number of about 1708. Below this value, the heat transfer is by conduction. Thus:

$$Nu_L = 1 \qquad\qquad (Ra_L < 1708)$$

For larger values of Ra_L, the following relation due to Hollands et al. [27] is widely used:

$$Nu_L = 1 + 1.44 \ (1 - \frac{1708}{Ra_L \cos\beta})^* \ [1 - \frac{1708(\sin\beta)^{1.6}}{Ra_L \cos\beta}]$$

$$+ \ (\frac{Ra_L \cos\beta}{5830} - 1)^* \qquad\qquad (4.8)$$

The symbol (*) means here that if the term between brackets is negative, it should be taken equal to zero. This formula is valid for large aspect ratios ((H/L)>12) and for 0<β<70°. These ranges adequately cover the actual operating conditions for solar collectors. Other formulas are reported by Incropera [28] for different ranges of inclination angle and aspect ratio.

4.5.2 Natural Convection From a Heated Plate to

Ambient Air.

4.5.2.1 **Natural Convection Heat Transfer.** In absence of wind, only natural convection should be considered for heat transfer between the plate and ambient air. Although the horizontal and vertical plate configurations were extensively studied, there are

few results for intermediate inclinations. For a horizontal plate, Lloyd and Moran [26] suggest:

$$Nu_L^* = 0.76\ Ra^{0.25} \qquad \text{for} \qquad 2.6 \times 10^4 < Ra_L^* < 10^7 \qquad (4.9a)$$

$$Nu_L^* = 0.15\ Ra^{1/3} \qquad \text{for} \qquad 10^7 < Ra_L^* < 10^{11} \qquad (4.9b)$$

where $L^* = 4(\text{area})/\text{perimeter}$.

For a vertical plate, the following relationship suggested by Churchil and Lou [29] has the advantage of representing the data in the entire range of Ra:

$$Nu_L = \left\{ 0.825 + \frac{0.387\ Ra_L^{1/6}}{[\ 1+(0.492/Pr)^{9/16}\ ]^{8/27}} \right\}^2 \qquad (4.10)$$

For the intermediate inclinations, Churchil and Lou suggested that the above formula be used for $30 < \beta < 90°$ and $Ra_L > 10^9$. For Ra_L less than 10^9 they gave the following expression:

$$Nu_L = 0.68 + \frac{0.67\ (Ra_L\ \sin\beta)^{1/4}}{[\ 1+(0.492/Pr)^{9/16}\ ]^{8/27}} \qquad (4.11)$$

For small angles of inclination, no correlation could be found. However in the case of turbulent natural convection, the inclination has little effect, therefore the horizontal plate formula can be used. For the case of smaller Ra, we expect fair results from the same formula if Ra is replaced by Ra $\cos\beta$. The above discussion can be summarized in table 4.1 where all fluid properties are evaluated at the film temperature $T_f = (T_g + T_\infty)/2$.

4.5.2.2 Forced Convection. In windy conditions, the heat transfer by forced convection cannot be neglected. To calculated

Nusselt Number in laminar conditions Sparrow et al. [32] gave the expression:

$$Nu_L{}^* = 0.86 \ (Re_L{}^*)^{1/2} \ (Pr)^{1/3} \qquad\qquad Re < 5 \times 10^5 \qquad (4.12)$$

Table 4.1: Formulas for Heat Transfer Coefficient in Natural Convection Between a Heated Plate and Ambient Air

$0 < \beta < 30°$	$2.4 \times 10^4 < Ra_L{}^* < 10^7 \qquad Nu_L{}^* = 0.76 \ (Ra_L{}^* \cos\beta)^{1/4}$
	$10^7 < Ra_L{}^* < 10^{11} \qquad Nu_L{}^* = 0.15 \ (Ra_L{}^*)^{1/3}$
	where $L^* = A/P$
$30 < \beta < 90°$	$Ra_L < 10^9 \quad Nu_L = 0.68 + \dfrac{0.67 \ (Ra_L \sin\beta)^{1/4}}{[\ 1+(0.492/Pr)^{9/16}\ ]^{8/27}}$
	$Ra_L > 10^9 \quad Nu_L = \left\{\ 0.825 + \dfrac{0.387 \ Ra_L{}^{1/6}}{[\ 1+(0.492/Pr)^{9/16}\ ]^{8/27}}\ \right\}^2$

At larger values of $Re_L{}^*$ Assouad [30] proposed the formula:

$$Nu_L{}^* = 0.0479 \ (Re_L{}^*)^{0.8} \ (Pr)^{1/3} \qquad Re_L{}^* > 5 \times 10^5 \qquad (4.13)$$

Noting the lack of detailed information about the combined natural and wind convection, Sucec [31] recommended that both pure free convection and pure wind convection heat transfer coefficients be calculated and the larger value adopted. Criterias which enable a

determination of the relative importance of free and forced convection are also presented.

4.5.3 Radiation Heat Transfer Between Two Parallel

Plates. The quantity of energy transfered by radiation from a surface of area A_2 to a surface of area A_1 is given by:

$$Q_{1 \rightarrow 2} = \frac{A_1 \, \sigma(T_1^4 - T_2^4)}{\dfrac{1-\varepsilon_1}{\varepsilon_1} + \dfrac{1-\varepsilon_2}{\varepsilon_2} \dfrac{A_1}{A_2} + \dfrac{1}{F_{12}}} \qquad (4.14)$$

where ε is the emissivity, F_{12} the shape factor and $\sigma = 5.67 \times 10^{-8}$ (in S.I. Units). This formula gives in the case of two infinite parallel surfaces the following expression for the heat transfer coefficient:

$$h_{1-2} = \frac{\sigma(T_1^2 + T_2^2)(T_1 + T_2)}{\dfrac{1}{\varepsilon_1} + \dfrac{1}{\varepsilon_2} - 1} \qquad (4.15)$$

4.5.4 Radiation Heat Transfer Between a Surface and

The Surroundings. It is convenient to consider the surroundings as a black body at some temperature T_{sky} . Equation (4.14) is then applicable with $\varepsilon_2=1$ and $F_{12}=1$. Omitting the subscript 1, we obtain:

$$Q_{s-sky} = A\varepsilon\sigma(T^4 - T_{sky}^4) \qquad (4.16)$$

4.6 ANALYSIS OF SYSTEM PERFORMANCE

In order to analyze the system performance, the following

energy quantities need be defined:

- the rate of sensible heat gained by the collector,

$$Q_{sen}(t)=(M_aC_a+M_cC_c+M_awC_s)(dT/dt)$$

$$=(M_aC_a(T_{re}-T_{ad})/t_o)(1+E_o+E_1w)d\theta/d\eta \qquad (4.17)$$

- the rate of energy used in desorption,

$$Q_{ads}(t)=-q_{st}M_a(dw/dt)=-q_{st}M_aG(dT/dt)$$

$$=-[L_oM_a/t_c(T_{re}-T_{ad})]\varphi\ (w,\theta)\ \Gamma(w,\theta)(d\theta/d\eta) \qquad (4.18)$$

- the rate of desorbed mass,

$$m_{des}(t)= -M_a(dw/dt)=-M_aG(dT/dt))$$

$$=-[M_a/t_o\ (T_{re}-T_{ad}\ )](\ \Gamma(w,\theta)(d\theta/d\eta) \qquad (4.19)$$

- the rate of solar energy input to the collector:

$$Q_{sol}(t) = A\tau\ (t) = A\tau_oI\ (\eta) \qquad (4.20)$$

- the rate of cooling effect produced at the evaporator :

$$Q_{ev}(t)=[L(T_{ev})\ -C_L(T_{co}-T_{ev})]\ m_{des}$$

$$=-[L_oM_a/t_o\ (T_{re}-T_{ad}\ )]\ [\lambda(\theta_{ev})-E_{11}(E_8-1)/E_{10}]\ \Gamma(w,\theta)(d\theta/d\eta) \qquad (4.21)$$

The following COP's are defined:

- the instantaneous cycle COP:

$$COP_{cycle1}=Q_{ev}(t)\ /\ [Q_{sen}(t)+Q_{ads}(t)] \qquad (4.22a)$$

- the cumulative cycle COP:

$$COP_{cycle2}=\int Q_{ev}(t)dt\ /\ (\int Q_{sen}(t)dt\ +\ \int Q_{ads}(t)dt) \qquad (4.22b)$$

- the instantaneous solar (or system) COP:

$$COP_{solar1}=Q_{ev}(t)\ /\ Q_{sol}(t) \qquad (4.23)$$

- the cumulative solar COP:

$$COP_{solar2} = \int Q_{ev}(t)dt \; / \; [\; \int Q_{sol}(t)dt]$$ (4.24)

The range of integration is from t=0 (begining of the desorption phase) to time t at which the quantity is wanted. The difference between the cycle COP and the solar COP is that the latter takes into account the efficiency of the solar collector, whereas the former is specified by the cycle operating temperatures: T_{ad}, T_{re}, T_{co} and T_{ev}. If we denote the collector efficiency by η_{solar}, we obtain :

$$COP_{solar} = COP_{cycle} \; \eta_{solar}$$ (4.25)

4.7 RESULTS OF THE NUMERICAL SIMULATION

A computer program COLLECTG (given in Appendix A) was written to solve for the profiles of the adsorbent temperature, the uptake and the system performance as functions of time. The purpose was to examine the influence of the operating conditions on the dynamic behaviour of a solar adsorption machine as well as the effect of the parameters E_0, E_1, E_2...etc found in the nondimensionalization of the governing equations. To achieve this objective, profiles of ambient temperature and solar radiation shown in figure 4.2 are assumed and a number of runs were made to analyze the effects of different parameters. The type of solar collector and the following data are also common to all the runs :

M_a=23.3 (kg) C_a=836.0 (J/kg.K) C_c=607.1 (J/kg.K)

M_g=4.58 (kg) C_g=750.0 (J/kg)

$(\tau\alpha)_e$=0.81 ε_c =0.80 ε_g=0.93 α_g=0.085
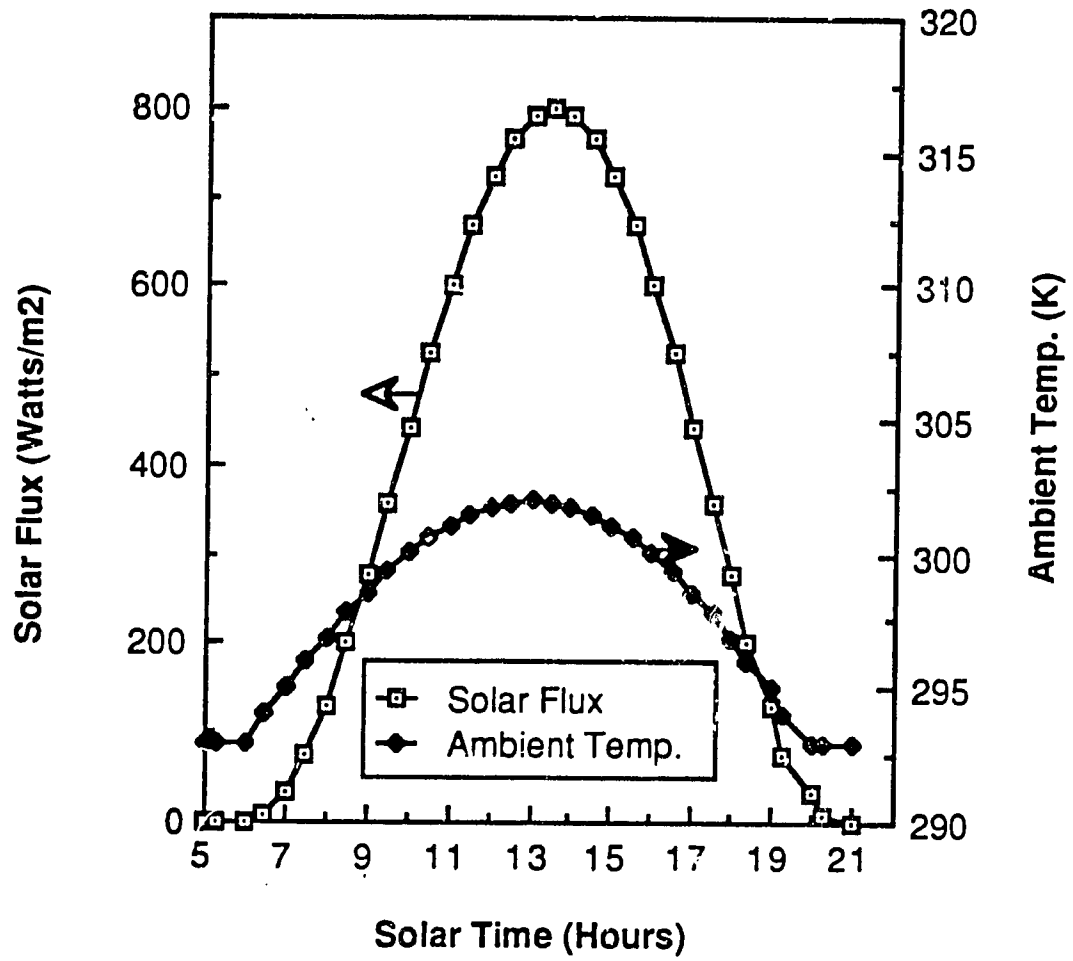
Figure 4.2: Profiles of Solar Flux and Ambient Temperature Used in the Simulation

For the cases in which the adsorbate is H_2O, we used the following:

$C_s = C_L = 4180.0$ (J/kg.K) $r = 462$(J/kg.K)

$L_o = 3171.2 \times 10^3$ (J/Kg) $a_L = -2.4425 \times 10^3$ (J/Kg.K)

For the cases in which the adsorbate is methanol, we used:

$C_s = C_L = 2500.0$ (J/Kg.K) $r = 259.5$ (J/Kg.K)

$L_o = 1718.4 \times 10^3$ (J/Kg) $a_L = -1.8288 \times 10^3$ (J/Kg.K)

4.7.1 General Considerations. To discuss the general aspects of the dynamic behaviour of a solar adsorption refrigerator, the following case is chosen:

Pair adsorbent-adsorbate: Zeolite13X-H_2O (data of [15]).

Evaporator temperature: 0°C

Condenser temperature: 50°C

4.7.1.1 Convergence and stability of the numerical

scheme. It was found that the method is stable for a time step $\Delta t < 20$mn, and that the temperature profile obtained with $\Delta t = 15$mn is only improved by less than 1% by taking $\Delta t = 7.5$mn. Thus the former time step was adopted. Also the system attains a "periodic" regime after about three "transient" cycles.

4.7.1.2 System performance. Figures 4.3a,b show the variations of the COP's with the solar time. In the early hours of the day, the solar energy input is used to increase the temperature of the collector and its content thus practically no mass is desorbed and the COP's are all equal to 0. As the desorption begins, after T_s has reached T_{co}, the instantaneous COP's rapidly increase to finite
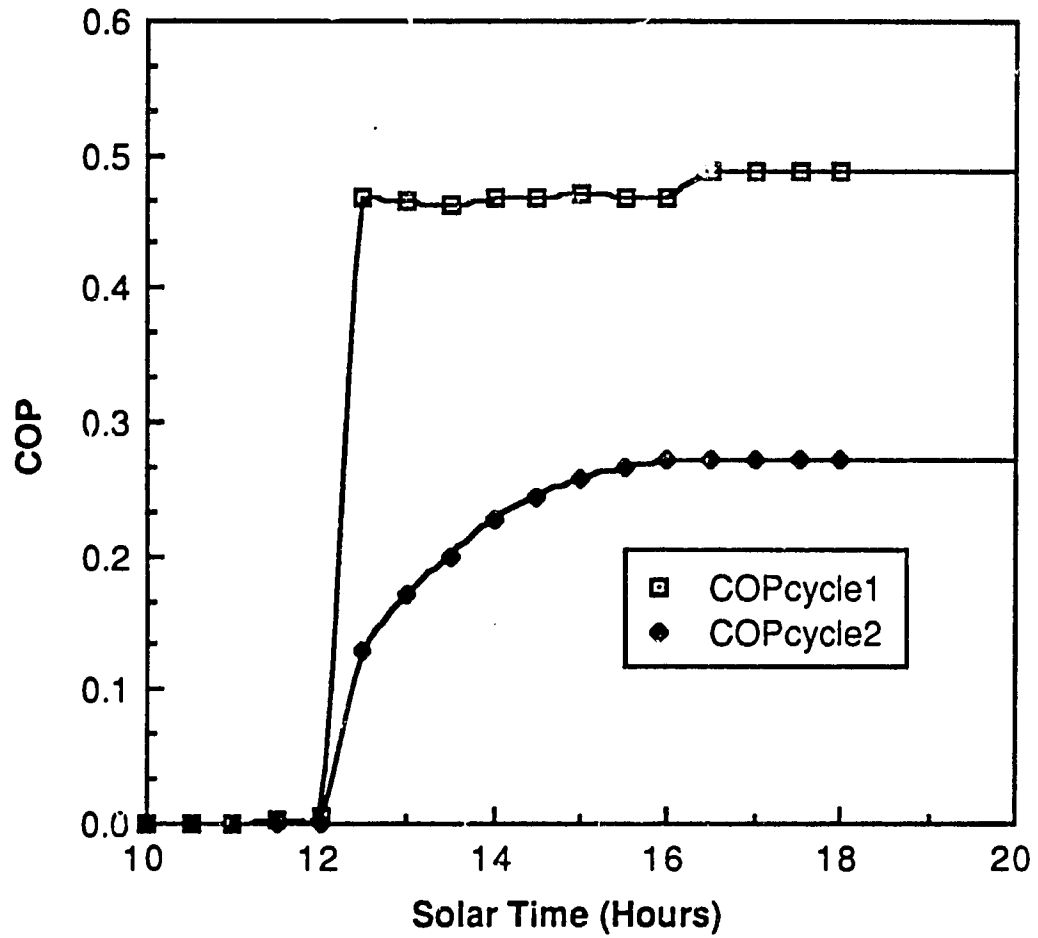
Figure 4.3a: Profiles of the Cycle Instantaneous and
Cumulative COP's
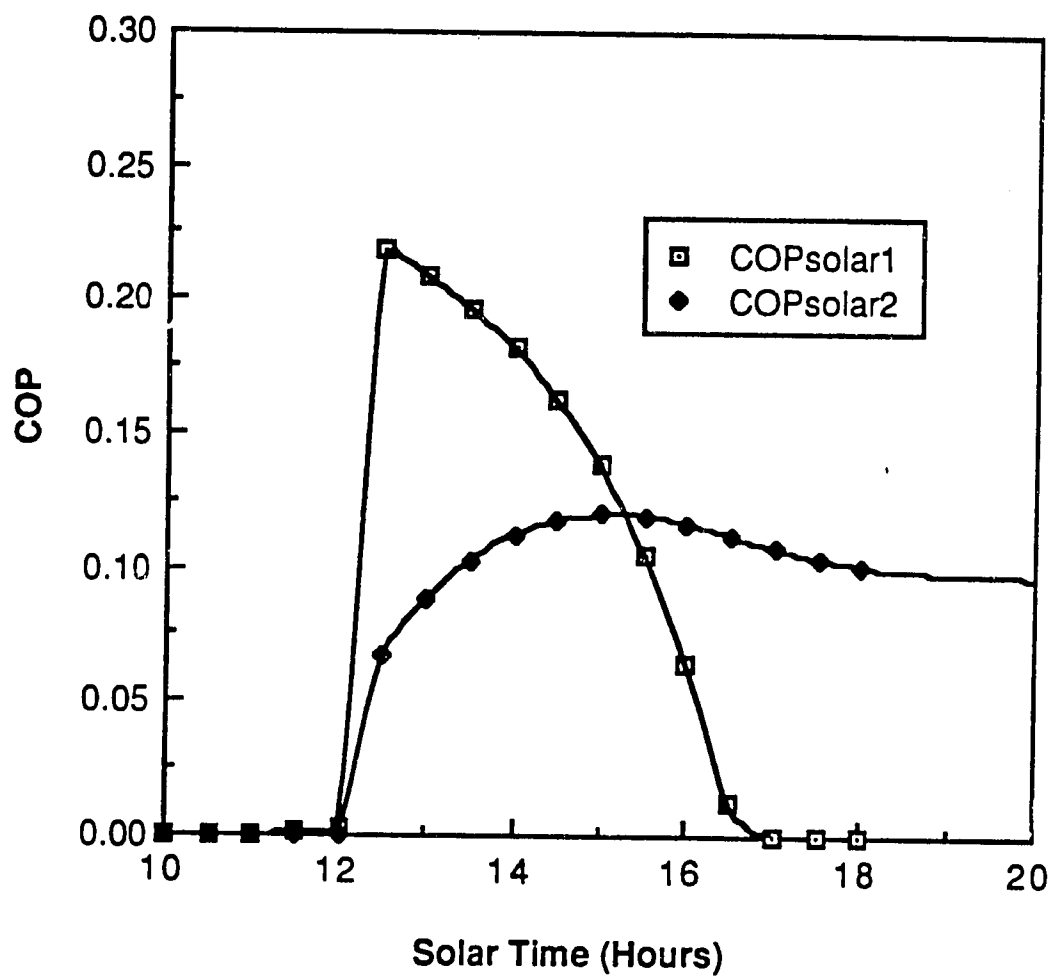
Figure 4.3b: Profiles of the Solar Instantaneous and Cumulative COP's

4.18

values: about 0.46 for COP_{cycle1} and 0.22 for COP_{solar1}. This occurs between 11:30 and 12:00. Desorption continues until the collector has reached its maximum temperature of about 139 °C. As the collector temperature rises, it's efficiency decreases causing a decline of COP_{solar1}. As a consequence, COP_{solar2} increases up to a maximum of about 0.11 before coming down to a final value of about 0.095 which constitutes the daily performance of the machine. Note that an improvement of the collector efficiency to a value of unity will not make the machine performance, COP_{solar2}, exceed the value of COP_{cycle2} which is about 0.50.

4.7.1.3 <u>Profiles of T, w and T_s and G</u>. Figure 4.4 shows the adsorption cycle in the form of T_s vs T. During the constant-volume phases, the variations of the uptake w are of the order of 10^{-5} which is smaller than the accuracy on the experimental determination of adsorption isotherms and constitues a rigourous proof of the usual assumption that the constant-volume phase is isosteric.

Figure 4.5a shows the adsorption cycle in the w-T diagram. We notice here again that the constant-volume phase is approximately a horizontal line except at the end of the phase where a sensible deviation can be seen. This figure shows also an interesting linear variation of the uptake with the adsorbent temperature which suggests that the ratio $[T_s-B(w)]/A(w)$ is a linear function of w (at constant T_s). The parameters $A(w)$ and $B(w)$ are the functions introduced in equation (1.32). This remark implies
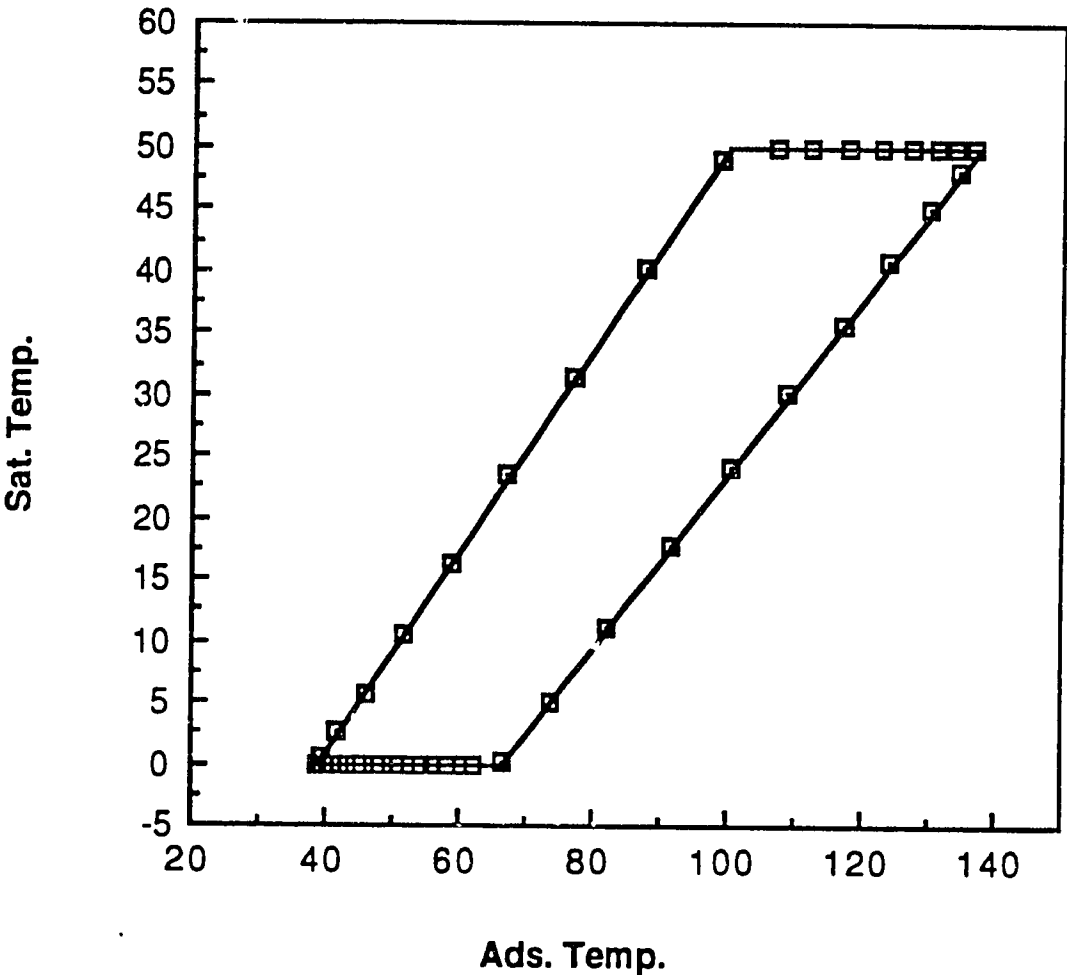
Figure 4.4: Adsorption Cycle for the Set of Data Chosen
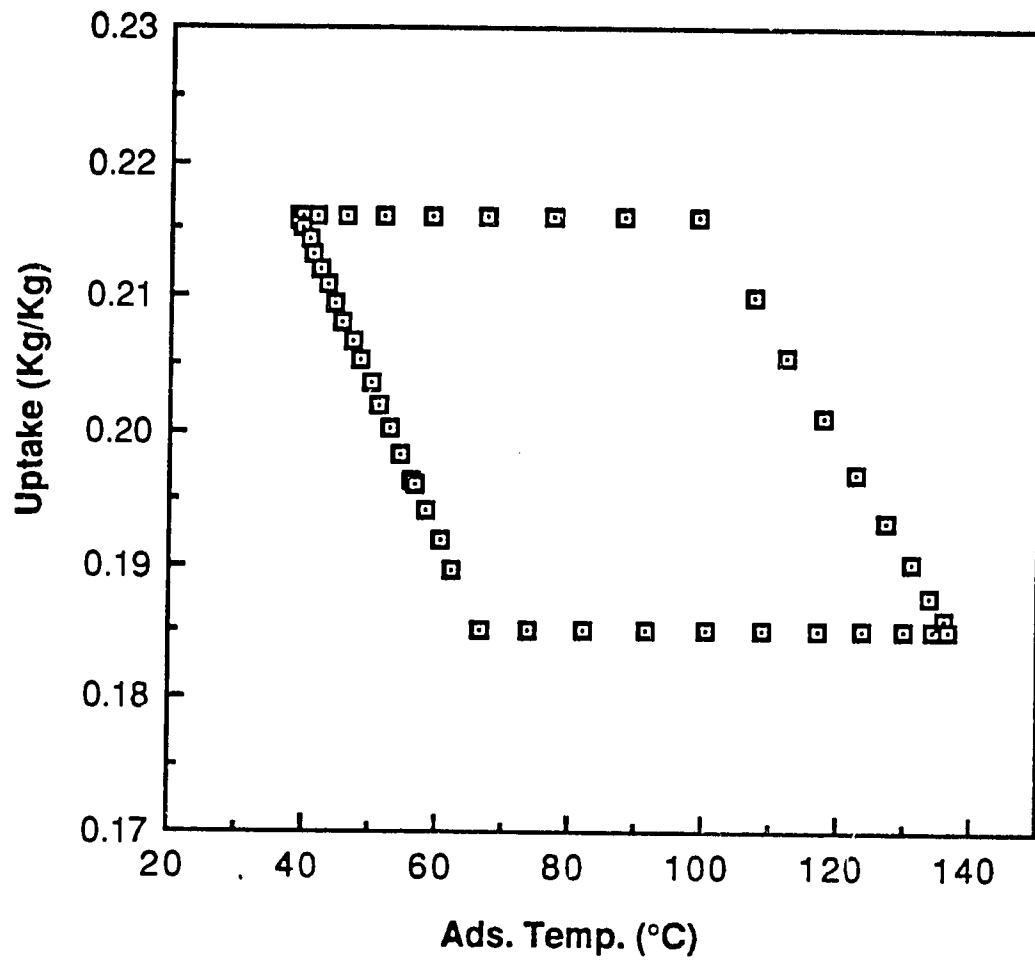
Figure 4.5a: Variation of w with Adsorbent Temperature
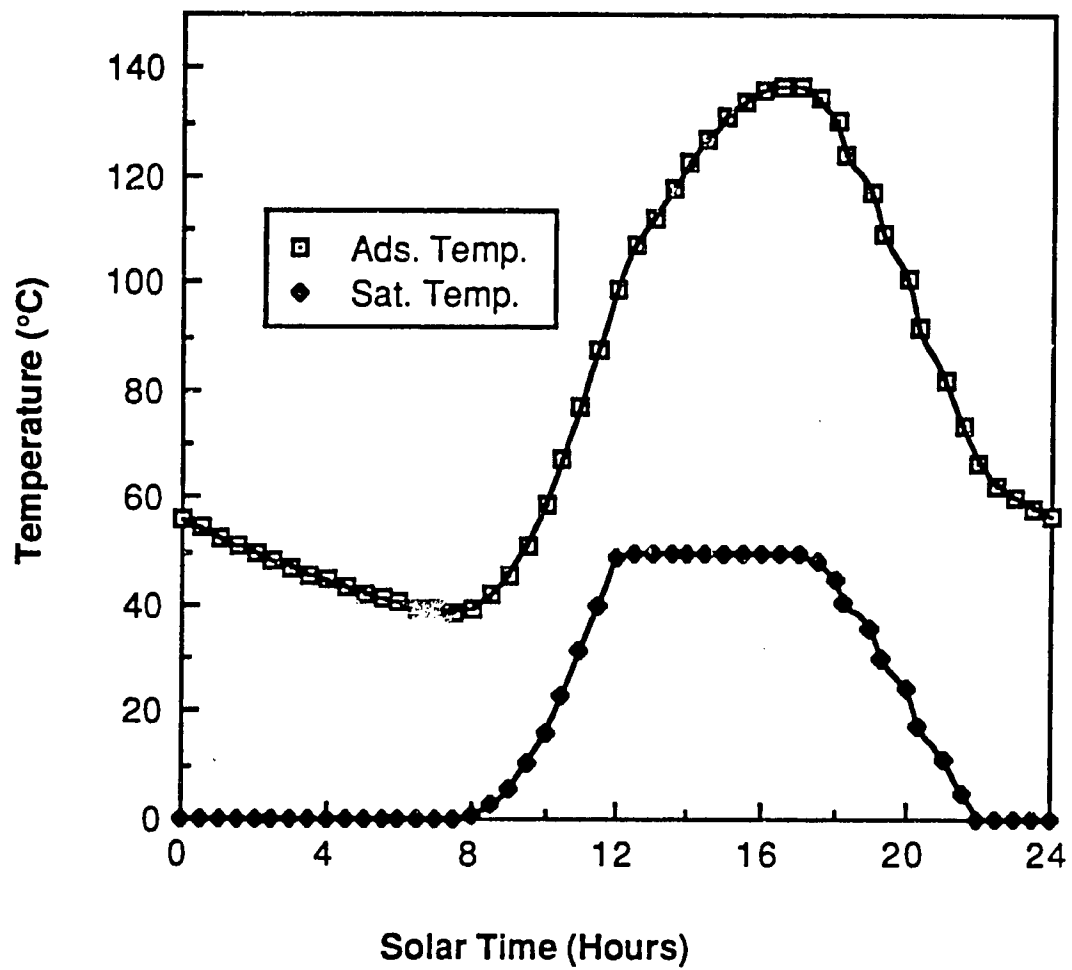
Figure 4.5b: Variation of the Adsorbent Temperature and the
Saturation Temperature with Time

also that the adsorptivity function $G(w,T)$ should be essentially constant.

Figure 4.5b shows the variations of the adsorbent temperature and the saturation temperature with time. The temperature at the end of adsorption T_{ad} is reached around 7:30 and is equal to about 38°C. The relatively large increase in temperature during the early hours of desorption is due not only to the fact that the energy is mainly transformed to sensible heat but also to the fact that the heat losses are smaller at low temperature. The maximum value T_{re} of adsorbent temperature is about 138°C and is reached around 17:00.

Figures 4.6a,b,c present the variations of the adsorptivity function G with time (or indirectly with adsorbent temperature) , uptake w and the saturation temperature respectively. These curves show the relative constancy of G during the constant-pressure phases at a value of approximately 1.1×10^{-3} (kg/kg.K). It is also seen that $Ln(G_v)$ varies almost linearly with T_s during the constant-volume phases with values ranging from about 2.0×10^{-7} to 2.0×10^{-6} (Kg/Kg.K) and slightly larger during desorption.

4.7.2 Effects of E_o , ε , T_{co} and T_{ev}. To perform a parametric study of the closed-cycle adsorption cooling system, the pair Synthetic zeolite-H_2O was chosen and the parameters Eo, ε,T_{co} and T_{ev} were varied. The results are summarized in table 4.2.

E_o is the ratio of the thermal capacity of the inert metal contained in the collector to that of the adsorbent material. The role
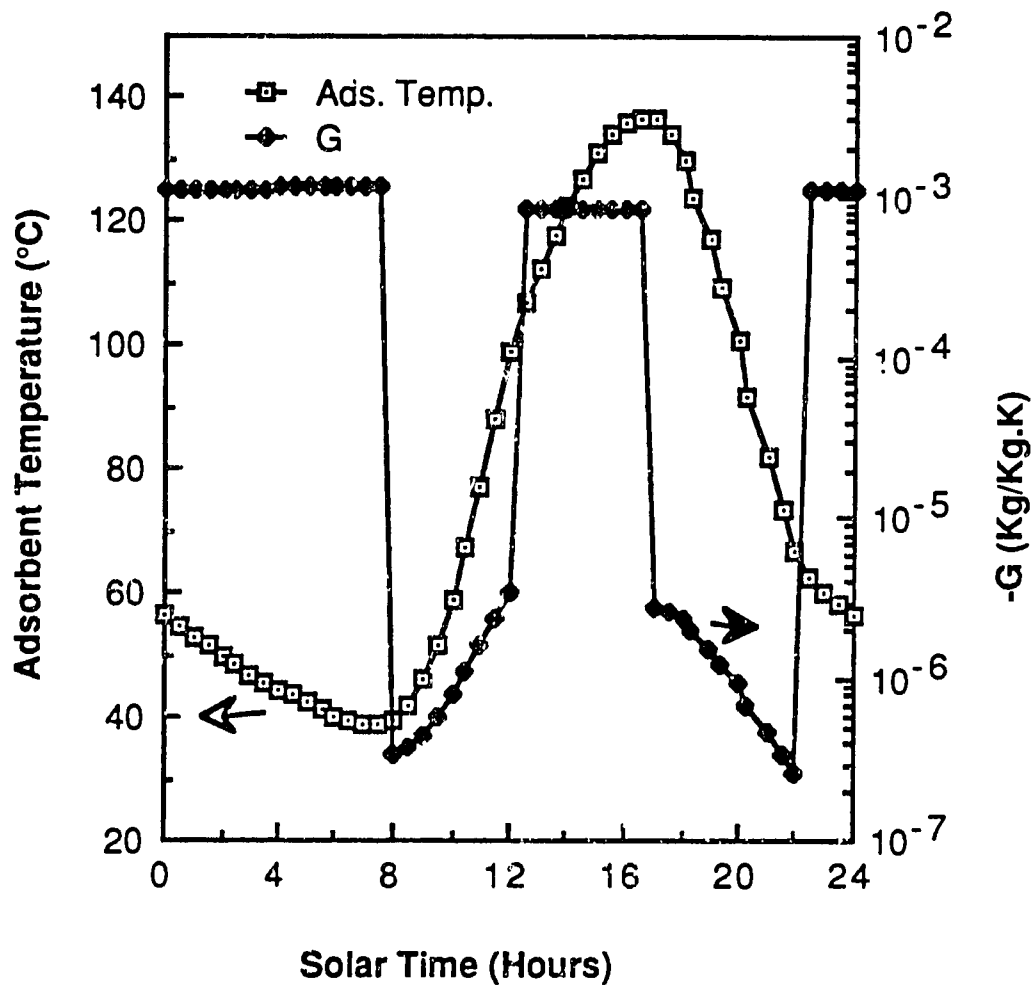
Figure 4.6a: Variations of G with Adsorbent Temperature
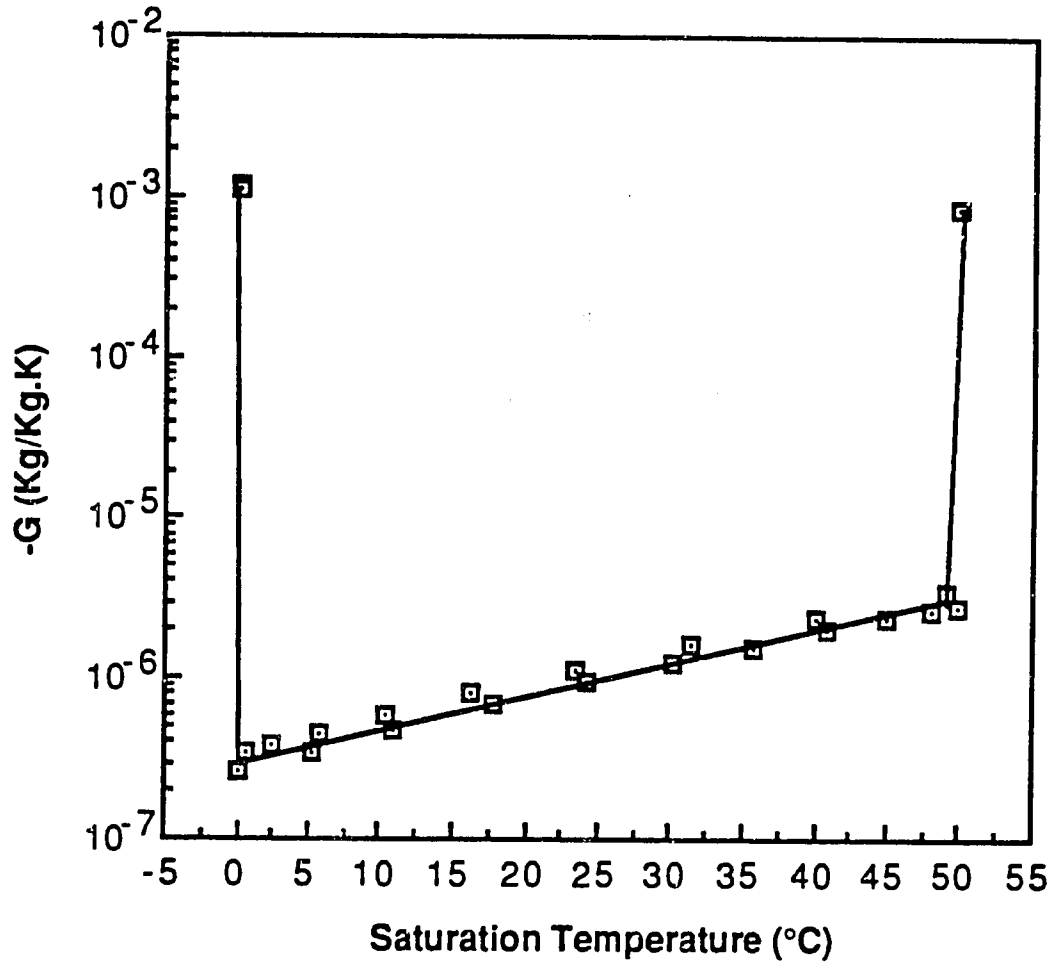
Figure 4.6b: Variation of G with of the Saturation Temperature
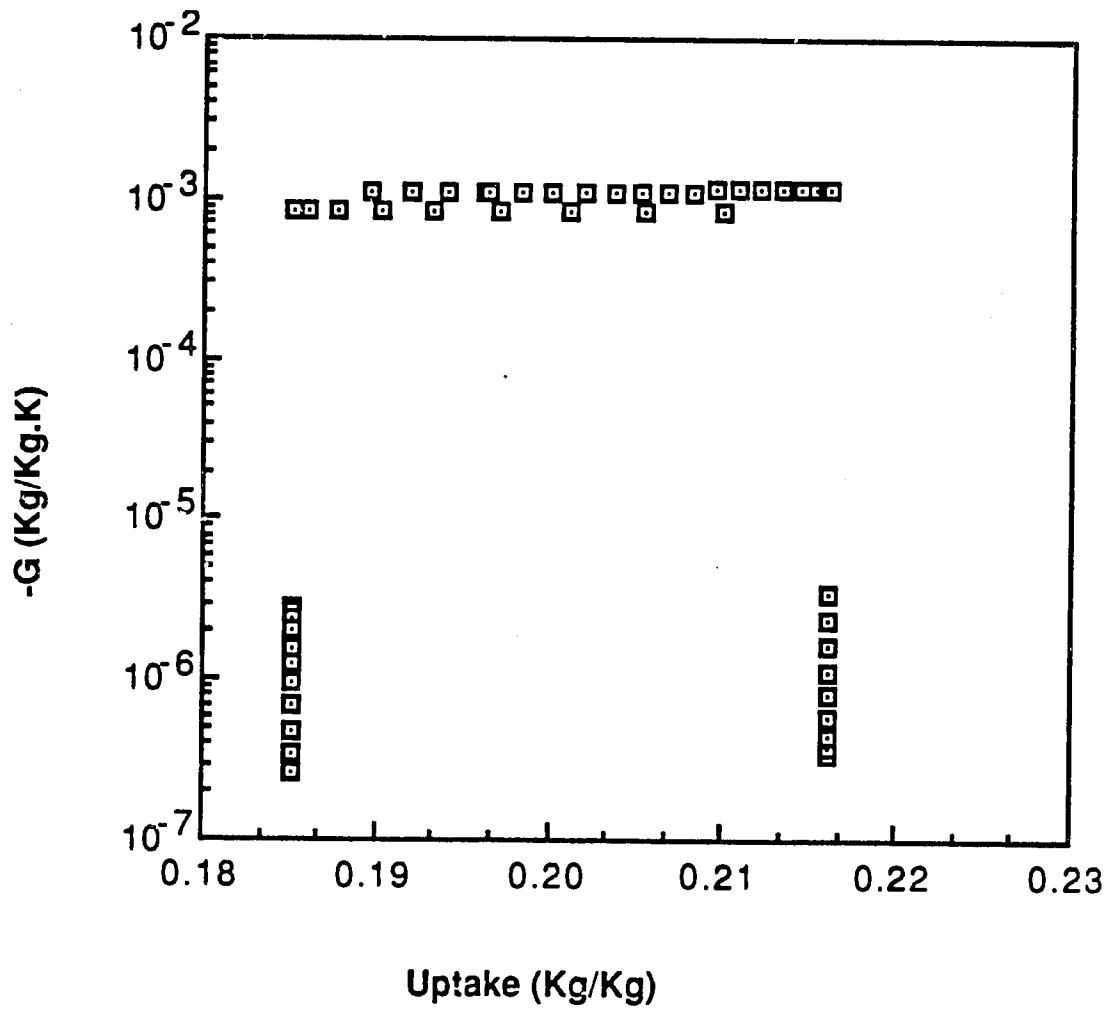
Figure 4.6c: Variation of G with the Uptake w

Table 3.2 : Effects of T_{∞}, T_{ev}, E_o and ε on the Performance of an Adsorption Cooling System

T_{∞}	T_{ev}	E_o	ε	COP cycle2	COP solar2	T_{ad}	T_{re}	w min	w max
20				0.4608	0.18873	45.0	121.7	.1519	.2090
30				0.3983	0.15172	43.2	128.6	.1643	.2111
40	0	.237	1.0	0.3283	0.12042	40.7	133.2	.1761	.2139
50				0.2727	0.09676	38.8	136.9	.1851	.2161
	0			0.3643	0.13678	41.3	130.9	.1707	.2133
35	5	.237	1.0	0.3723	0.14520	42.7	128.4	.1735	.2185
	10			0.4040	0.16099	43.2	127.1	.1749	.2247
		.000		0.3874	0.14173	41.4	132.3	.1689	.2131
		.474		0.3188	0.12384	42.4	128.4	.1734	.2120
35	0	.949	1.0	0.2748	0.10901	44.5	126.4	.1757	.2096
		1.897		0.2063	0.0866	47.3	121.3	.1801	.2065
35	0	.237	0.5	0.3646	0.13687	41.3	130.9	.1707	.2133
			1.5	0.3641	0.13673	41.3	130.9	.1707	.2133

of the metal is not only to hold the collector structure but also to permit good heat transfer through the adsorbent. However the presence of the metal reduces the fraction of heat used for desorption thus penalizing the COP. Table 4.2 shows that an increase of 0.24 in E_o causes COP_{solar2} to decrease by only 3.7%.

ε is the ratio of the volume of the gas phase to the volume of the adsorbent and depends on the "dead volume" allowed by the design of the collector and also on how the adsorbent is packed (the size of the particles, the interparticle voids...). The effect of ε is negligibly small. The reason is that at low pressures the amount of gas needed to increase the pressure from p_{ev} to p_{co} remains very small even for substantially larger volume the gas phase.

The effects of the T_{co} and T_{ev} - respectively imposed by the condenser and the evaporator - are more important. At constant T_{ev}, COP_{solar2} is improved by about 22% for a 10°C decrease of T_{co} and at constant T_{co}, a 5°C increase of T_{ev} causes an improvment of 8%. The difference $(T_{co}-T_{ev})$ seems to be more decisive in determining the machine performance as seen in figure 4.7.

4.7.3 Below-freezing Evaporator Temperatures. The use of refrigerants other than water can allow evaporator temperatures below 0°C. The most used component in solid adsorption cooling is methanol (CH_3OH). The equilibrium data provided by [5] was used to analyse the performance of the pair Chabazite-Methanol and to compare it to the pair Synthetic zeolite 13X-Water. The results are given in table 4.3
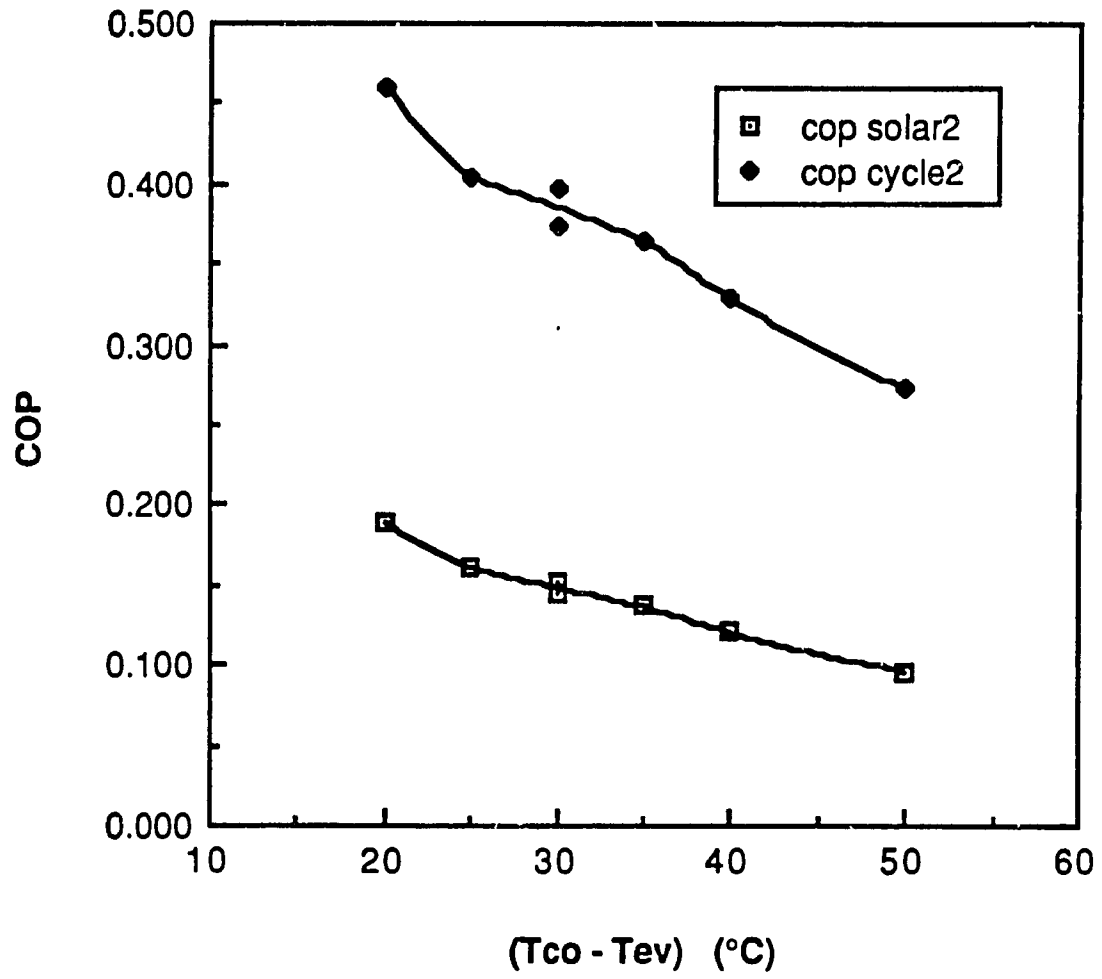
Figure 4.7: Variation of the COP with the Difference (Tco - Tev)

For comparison between the two adsorption pairs Zeolite 13X-Water and Chabazite-Methanol, figures 4.8a,b give the

Table 4.3 Effect of T_{ev} on the Machine Performance
For T_{co}=35°C, ε = 1.0, E_o = 0.237.

T_{ev}	COP_{cycle2}	COP_{solar2}
0°C	0.24741	0.08388
-5°C	0.241152	0.08132
-10°C	0.21305	0.07042

variations with time of COP_{cycle} and COP_{solar} corresponding for the two pairs at the conditions: T_{co}=30°C , T_{ev}=0°C , ε=1 and E_o=0.237. At low adsorbent temperature (early hours), the COP's of the 2nd pair are larger. But globally Zeolite-Water pair has a much better performance.

4.8 CONCLUSIONS

The dynamic performance of a closed-cycle, solar-adsorption refrigerator was modeled numerically using Zeolite 13X-Water and Chabazite-Methanol adsorbent-adsorbate pairs. The Zeolite13X-Water system, operating on a daily cycle, has a maximum instantaneous solar COP of 0.22 with a daily solar COP of
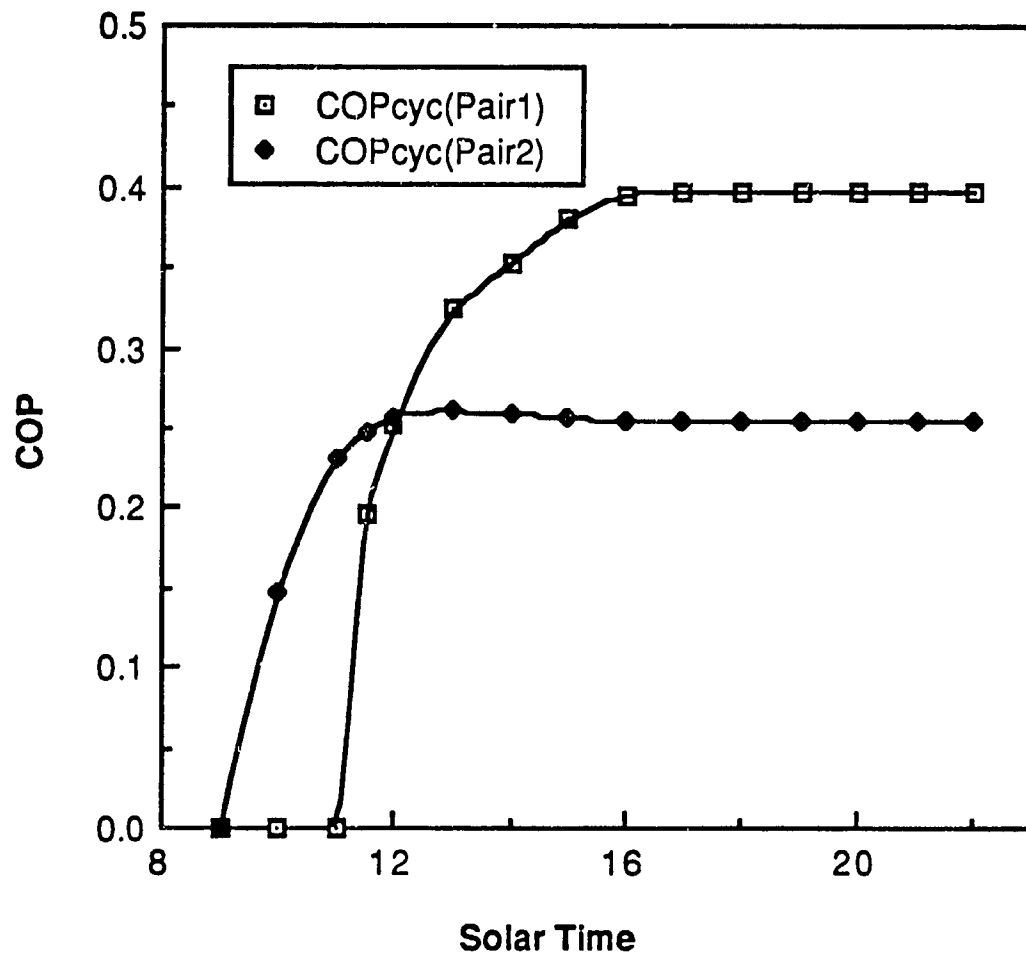
Figure 4.8a: COPcycle2 for Two Adsorption Pairs:
Zeolite 13X-Water (pair 1) and Chabazite-Methanol (pair2)
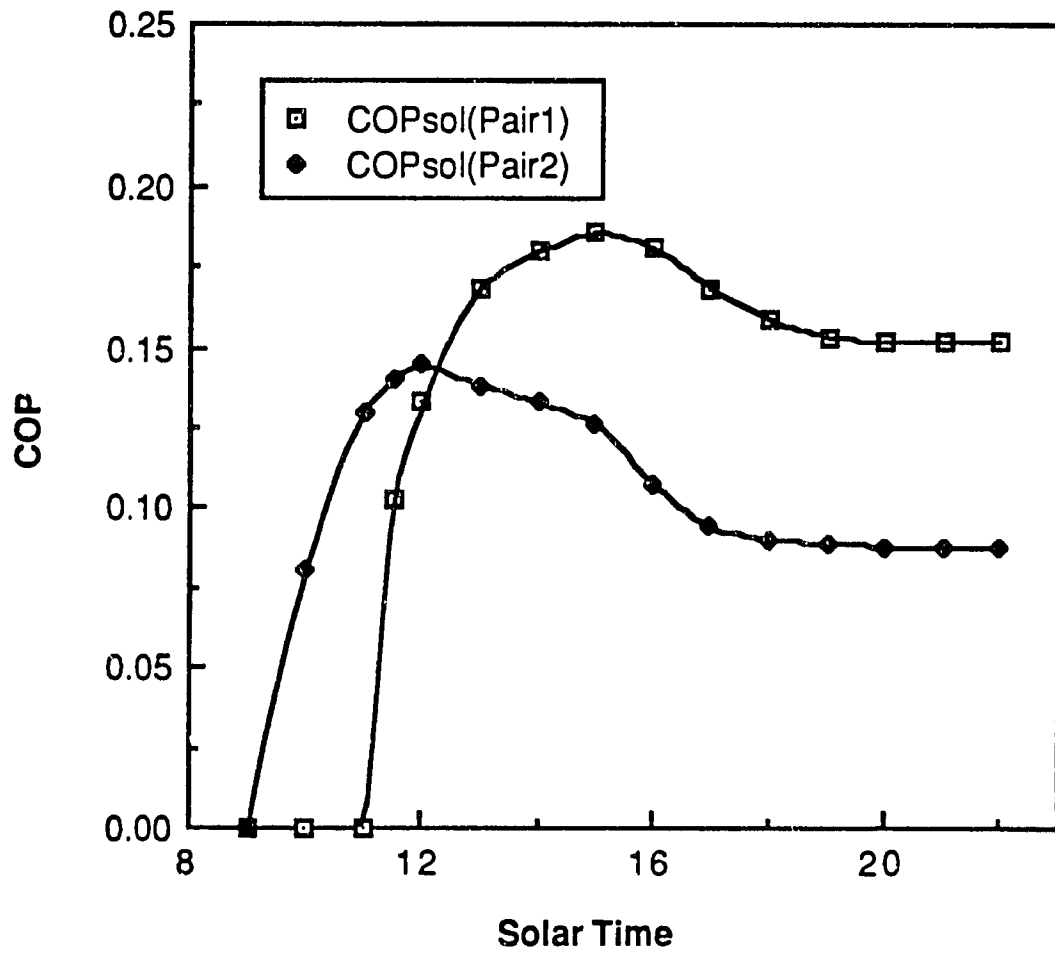
Figure 4.8b: COPsolar2 for Two Adsorption Pairs:
Zeolite 13X-Water (pair 1) and Chabazite-Methanol (pair2)

0.095. For these operating conditions, the daily cycle COP is 0.55 which is the maximum performance that could be attained if the solar collector has an efficiency of unity.

A parametric analysis to study the effect of inert material to adsorbent thermal capacity fraction, matrix porosity, evaporator and condenser temperatures was also performed. These results show that adding inert material causes a slight decrease in the daily solar coefficient of performance. Changing the matrix porosity has little effect on the performance of the system. Increasing the condenser temperature causes the performance to decrease while increasing the evaporator temperature, results in increasing the system performance.

For the same operating conditions, a system using Chabazite-Methanol was compared to a Zeolite 13X-Water system. These results show the Chabazite -Methanol has a solar COP 38% lower than the Zeolite 13X-Water system. However, the Chabazite-Methanol system allows cooling to temperatures significantly below 0°C.

CHAPTER V

APPLICATION OF THE CONCEPT OF REGENERATIVE HEAT EXCHANGER TO ADSORPTION SYSTEMS

5.1 INTRODUCTION

Closed-cycle cooling/heating systems using solid adsorbents that have been described in the literature [13,16,18] so far, are characterized by COP's smaller than unity and are generally based on daily cycles or work only intermittently. Recently Tchernev [10] suggested that by using the concept of regeneration, continuous cooling/heating can be provided and the energy used during the desorption phase can be recovered, increasing the COP significantly.

The system described in reference [10] consists of two zeolite containers which alternatively undergo adsorption and desorption. A reversible pump permits the circulation of oil from a boiler at 400°F through the zeolite containers. The oil-air heat exchangers cool the oil to the ambient or cold temperature T_c before entering the adsorbing container. Two outside fluid loops remove the heat and the cooling effect from the walls of the zeolite containers. Figure 5.1 schematically shows the system described above. A more detailed description of the operating principle is given in section 5.2 and a mathematical model is presented in section 5.3 to analyze the periodic behaviour of the system. The analysis of the system performance is made in section 5.4. The notion of an ideal regenerator is introduced in section 5.5 and finally 5.6 is devoted to the results of the numerical simulations.

5.2 OPERATING PRINCIPLE OF A REGENERATIVE ADSORPTION SYSTEM

The Zeolite-Water pair undergoes a cyclic process very similar to the other adsorption heating/cooling systems discussed in Chapter III. This cycle is conveniently shown on the (T_s, T) diagram as given in figure 5.2.

5.2.1 **The Regeneration Process (figure 5.3a).** This process starts at point (a) of the cycle where the vapor phase is at pressure p_{ev} (corresponding to the evaporator temperature T_{ev}) and the adsorbate mass fraction w is at its maximum value of the cycle. The one-way valve C_2 is closed. At this moment the pump is reversed and hot oil flows into the zeolite-oil heat exchanger. As the temperature of the adsorbent increases, desorption starts and the pressure increases closing the one-way valve C_1. Before the pressure reaches p_{co}, the process continues at constant volume. The amount of water desorbed is usually very small and the process can be represented by the isoster a-b. When the pressure p_{co} is attained the one-way valve C_2 opens and condensation starts. It continues while the walls of the zeolite container are maintained at constant temperature T_{co} by the outside loop that removes the heat of condensation to the heated space. The desorption stops when the zeolite is at its maximum temperature T_{re} (point c).

5.2.2 **The Adsorption Process (figure 5.3b).** At the end of the desorption process, the pump is reversed and cold oil flows to the zeolite container. As the temperature decreases water vapor is adsorbed and the pressure decreases. The one-way valve C_2
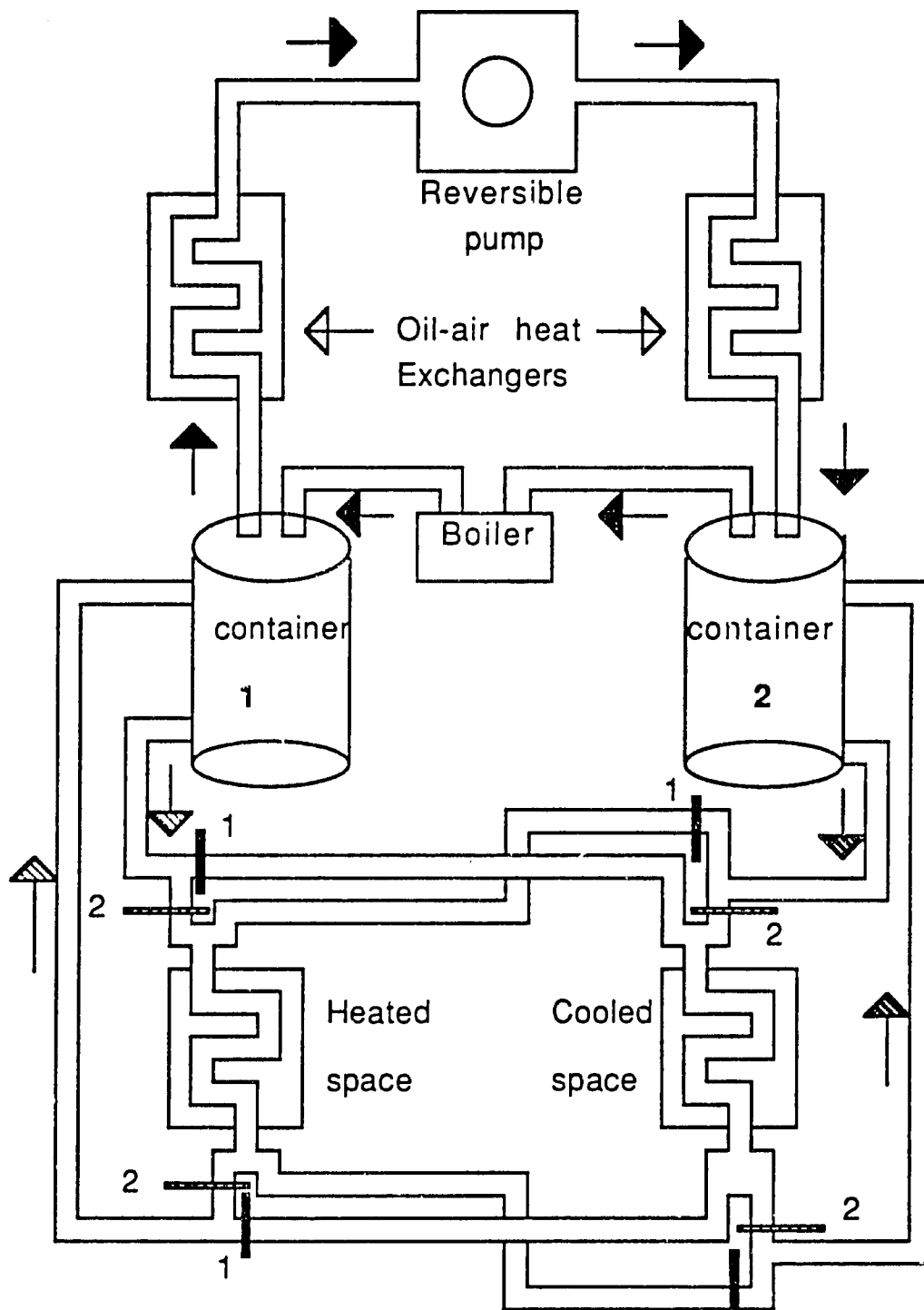
Figure 5.1: Operating Principle of a Regenerative Cooling
or Heating System: While Valves are in Position 1,
Container-1 is Desorbing and Container-2 is Adsorbing
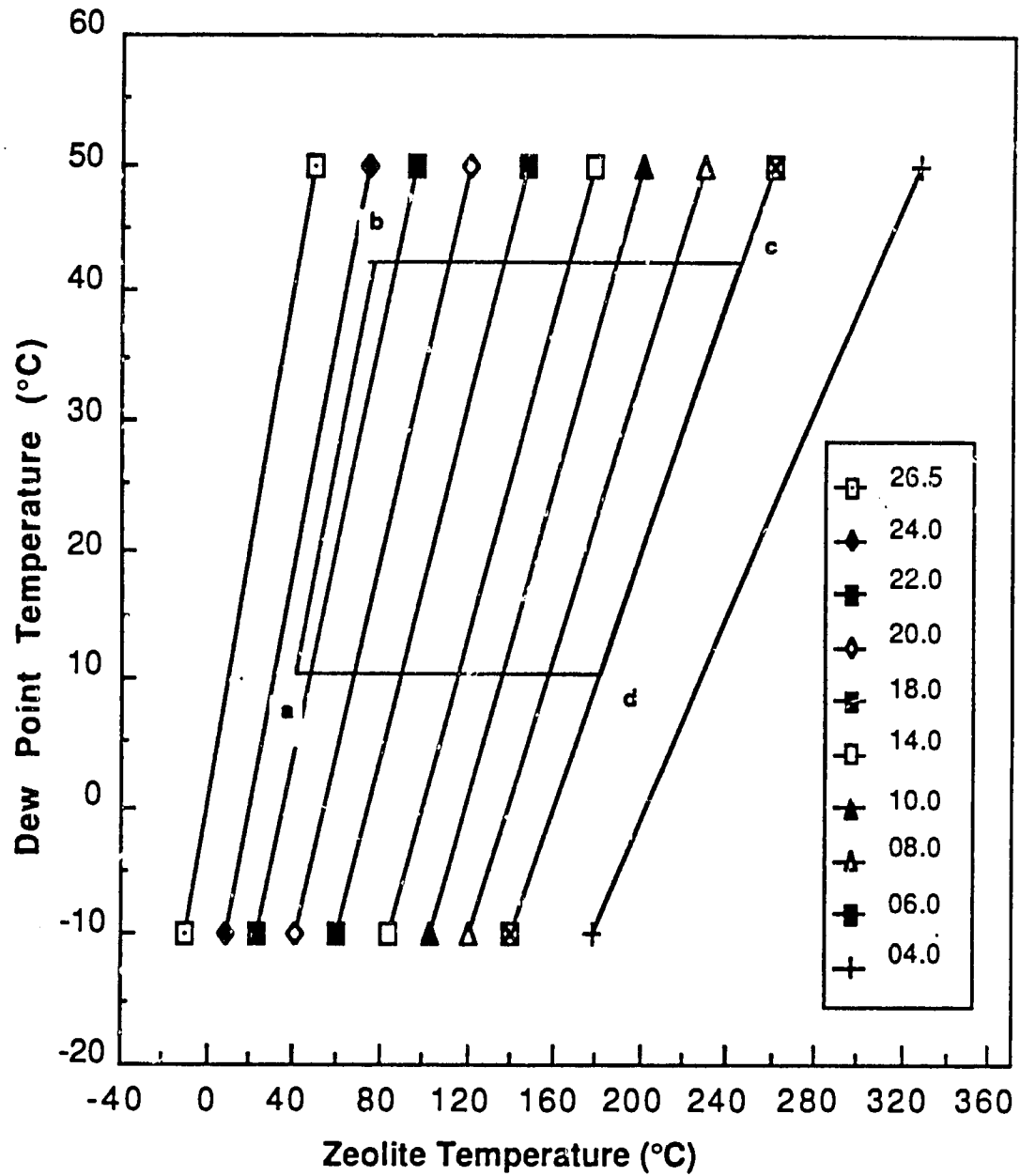
Figure 5.2: Adsorption Cycle. The Equilibrium Data are
for the Pair Zeolite 13X-Water [10]
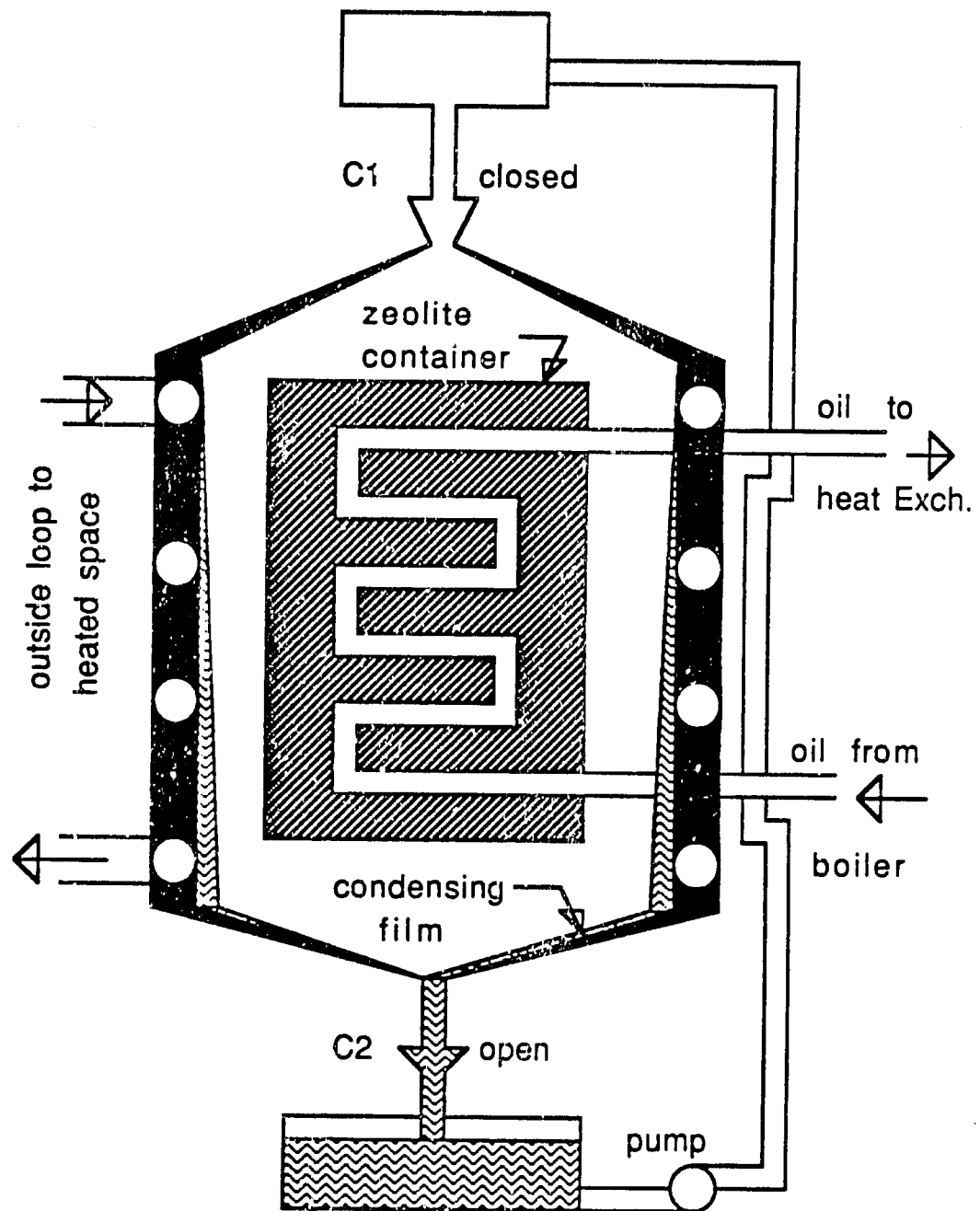
Figure 5.3a : Regeneration Phase : The walls of the
Container act as Condenser

closes and a second constant-volume process occurs which is approximated by the isoster c-d. When the pressure decreases to P_{ev}, the one-way valve C_1 opens allowing a liquid film to flow and evaporate on the walls of the zeolite container. If the pressure difference $(P_{co} - P_{ev})$ is not sufficient an auxilliary small pump should be used to bring the liquid adsorbate to the top of the zeolite container. The evaporation cooling effect is brought to the space to be cooled by a second outside loop.

5.3 DETAILED DERIVATION OF THE GOVERNING EQUATIONS OF AN ADSORPTION REGENERATOR

The energy equations of one period of solid adsorption regeneration operation are somewhat similar to those of classical (heat only) regenerator theory [34,35]. The difference lies in the term corresponding to heat of adsorption in the energy equation of the solid adsorbent and the additional difficulty due to the coupling with the nonlinear integral equation of the pressure. An element of the regenerator of length Δz (figure 5.4) is used to derive the energy and mass balances. The following additional approximations are made to simplify the problem:

1. Negligible cross-stream temperature and uptake gradients.
2. Negligible heat conductivity in the longitudinal direction.
3. Uniform liquid velocity and time independent flow rate
4. Constant densities and specific heats.
5. Constant heat and mass transfer coefficients.
6. Uniform gas phase pressure throughout the regenerator.
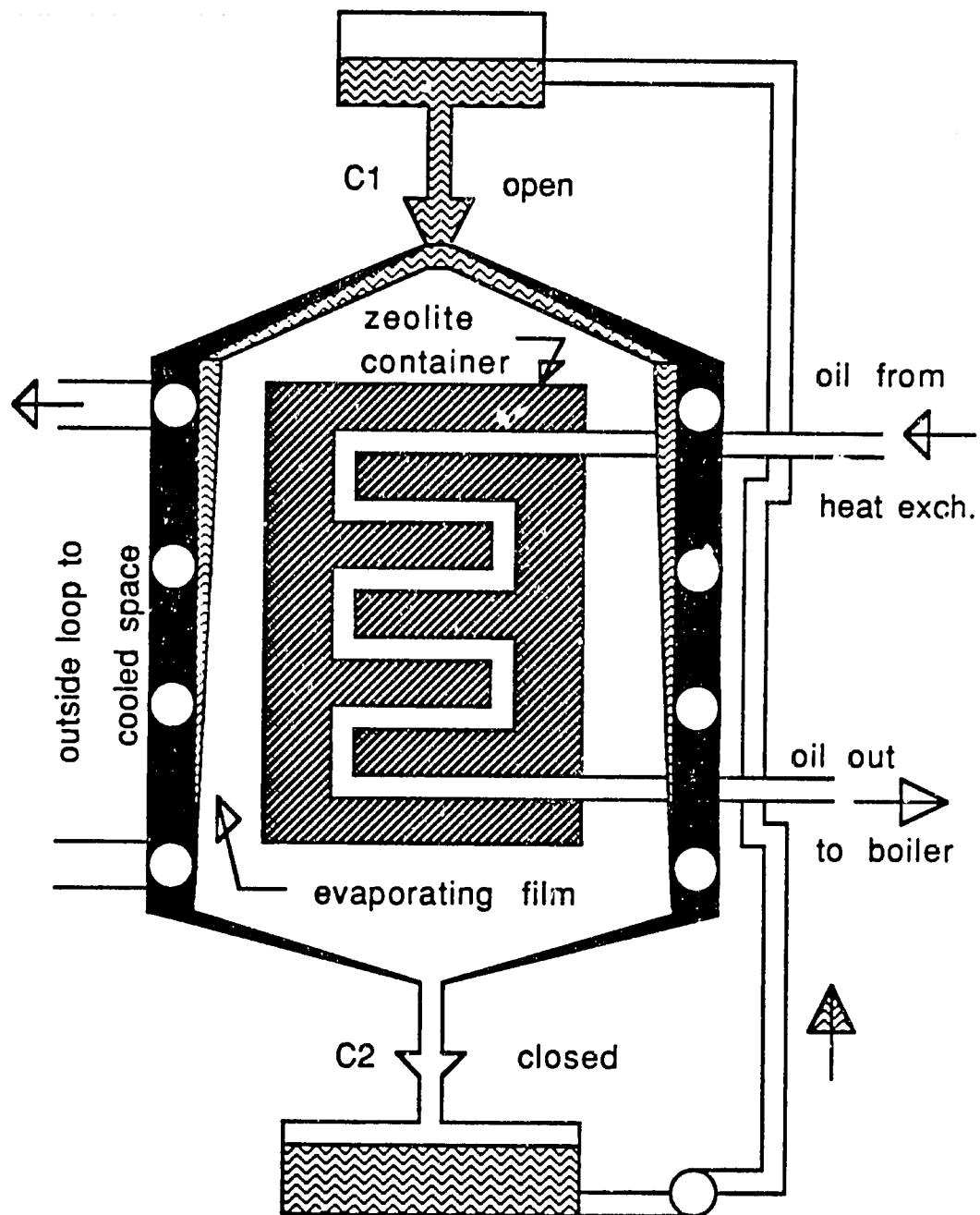
Figure 5.3b : Adsorption Phase: The Walls of the
Container act as Evaporator

5.3.1 Dimensional Form of the Equations.

The unknown quantities to be determined in the more general case where thermodynamic equilibirum is not assumed are T_f, T, T_s (or p), w and w_{eq} . Thus a set of 5 equations need be derived and simultaneously solved.

5.3.1.1 Energy balance equations.

The energy balance equations are obtained by considering the energy quantities exchanged between a small element and the flowing liquid between times t and t+Δt. These are:

δQ_{sa} sensible heat gained by adsorbent=$[\delta m_a(C_a+wC_s)+\delta m_c C_c]\Delta T$

δQ_{ads} heat of adsorption= $-q_{st}(\delta m_a)\Delta w$

δQ_{tot} heat exchanged by convection $= (P_f \Delta z) h (T_f - T)$

δQ_{sf} sensible heat gained by fluid $= (\rho_f A_f \Delta z) C_f \Delta T_f$

δQ_{adv} advective heat gained by fluid= $m_f C_f[t_f(z+ \Delta z)-T_f(z)]\Delta t$

The energy balances for the adsorbent and the fluid are as follows:

$$\delta Q_{sa} + \delta Q_{ads} = \delta Q_{tot}$$

$$\delta Q_{sf} + \delta Q_{adv} = - \delta Q_{tot}$$

Replacing each of the energy flows by their respective expressions, dividing by ($\Delta z \Delta t$) and taking the limits $\Delta z \rightarrow 0$ $\Delta t \rightarrow 0$ yields:

$$\rho_a A_a C_a [1+(C_s/C_a)W+\frac{\rho_c A_c C_c}{\rho_a A_a C_a}] \frac{\partial T}{\partial t} - \rho_a A_a q_{st} \frac{\partial w}{\partial t}$$

$$= P_f h(T_f-T) \qquad (5.1)$$
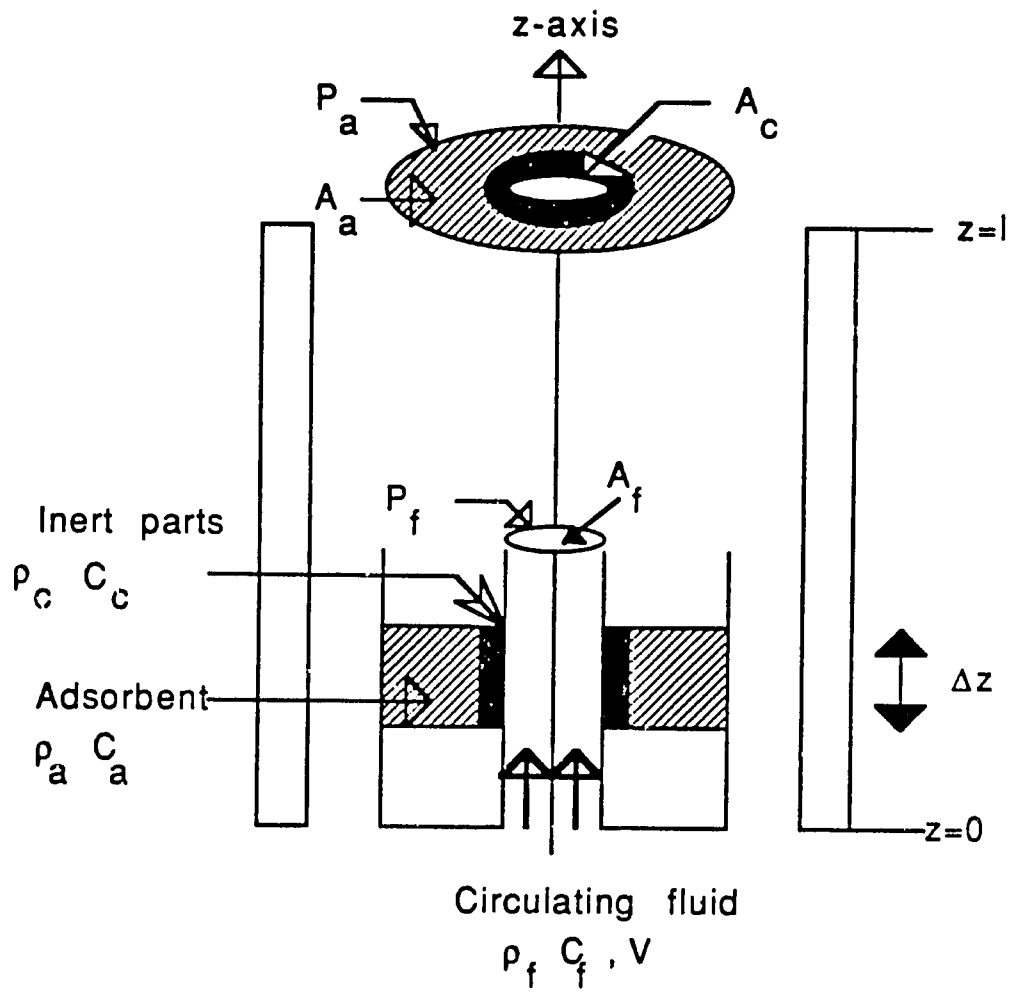
Figure 5.4 : Elements of the Mathematical Model for the
Adsorption Regenerator

$$\rho_f \, A_f \, C_f \, (\frac{\partial T_f}{\partial t} + V \frac{\partial T_f}{\partial z}) = P_f \, h \, (T - T_f) \qquad (5\text{-}2)$$

5.3.1.2 Mass Balance Equation. To obtain a general formulation, thermodynamic equilibrium is not assumed. Deviation from equilibrium can be expressed in many ways. We only consider here the simple model in which the driving force for mass transfer is the deviation from equilibrium, $(w_{eq} - w)$. We introduce a constant mass transfer coefficient h_m such that:

$$\rho_a A_a (\partial w / \partial t) = h_m \, (w_{eq} - w) \qquad (5.3a)$$

w_{eq} is the equilibrium value of the uptake at (T, T_s) thus:

$$T_s = F(T, w_{eq}) \qquad (5.3b)$$

5.3.1.3 Relation Giving the Pressure Variations. A final equation is needed which relates the variation of the pressure in the gas phase to those of T and w. We showed in Chapter II that the form of such an equation depends on the nature of the process being modeled. We will consider the two cases of constant-pressure and constant-volume processes.

1. For a constant-pressure process, p (or T_s) is known thus:

$$T_s = F(T, w_{eq}) = \text{Constant} \qquad (5.4)$$

2. For a constant-volume process, equation (2.60) yields:

$$\frac{\partial T_s}{\partial t} = \frac{R \, T_s^2 \int_0^1 \{-\frac{\rho_a}{\epsilon \, p} \frac{\partial w}{\partial t} + \frac{1}{T^2} \frac{\partial T}{\partial t}\} \, dz}{L(T_s) \int_0^1 \frac{dz}{T}} \qquad (5\text{-}5)$$

5.3.1.4 <u>Initial and Boundary Conditions</u>. To start the computations, we assume uniform temperature and uptake. Iterations continue until a periodic steady-state operation is achieved. The inlet fluid temperature is known and assumed to be time independent. Thus we can write:

For the regeneration period :

at z=0 $\qquad T_f(0,t)=T_h$

at t=0 $\qquad T_f(z,0)=T_{ad}$, $\qquad w(z,0)=w_{eq}(z,0)=w_{eq}(T_{ad},T_{ev})$

For the following adsorption period:

at z=l $\qquad T_f(l,t)=T_c$

at t=τ $\qquad T(z,\tau)$ and $w(z,\tau)$ known from the previous period

5.3.2 <u>Nondimensional Governing Equations</u>. The previous equations can be simplified by introducing the following dimensionless parameters and variables:

$\zeta=z/l$ where l is the length of the regenerator.

$\eta=t/\tau_0$ where $\tau_0=l/V$ is a characteristic time

$\theta=(T-T_c)/(T_h-T_c)$; $\quad \theta_f=(T_f-T_c)/(T_h-T_c)$; $\quad \theta_s=(T_s-T_{ev})/(T_{co}-T_{ev})$

$\pi=(p-p_{ev})/(p_{cc}-p_{ev})$; $\quad \varphi(\theta,w)=q_{st}(T,w)/L_0$; $\quad \lambda(\theta_s)=L(T_s)/L_0$

$\Phi(\theta,w)=[F(T,w)-T_{ev}]/(T_{co}-T_{ev})$; $\qquad \gamma(\theta,w)=G(T,w)\cdot(T_h-T_c)$

where L_0 is a characteristic values of q_{st} and L .

$\Pi_h=\tau_h/\tau_0$ $\qquad$ the dimensionless time of the "hot" period

$\Pi_c=\tau_c/\tau_0$ $\qquad$ the dimensionless time of the "cold" period

$$E_o = (\rho_c A_c C_c)/(\rho_a A_a C_a) \qquad E_1 = C_s/C_a \qquad E_2 = (\rho_f A_f C_f)/(\rho_a A_a C_a)$$

$$E_3 = L_o/[C_a(T_h - T_c)] \qquad E_4 = hP_f t_o/(\rho_a A_a C_a) \qquad E_{4m} = h_m t_o/(\rho_a A_a)$$

$$E_5 = r\rho_a T_c/(\epsilon p_{ev}) \qquad E_6 = T_h/T_c \qquad E_7 = p_{co}/p_{ev} \qquad E_8 = T_{co}/T_{ev}$$

$$E_9 = T_{co}/T_c \qquad E_{10} = L_o/(rT_{ev}) \qquad E_{11} = C_L/C_a$$

The governing equations of section 3.1 become:

$$(1 + E_o + E_1 w)(\partial\theta/\partial\eta) - E_3\varphi(\tau,w)(\partial w/\partial\eta) = E_4(\theta_f - \theta) \qquad (5.1^*)$$

$$(\partial\theta_f/\partial\eta) + (\partial\theta_f/\partial\zeta) = (E_4/E_2)(\theta - \theta_f) \qquad (5.2^*)$$

$$(\partial w/\partial\eta) = E_{4m}(w_{eq} - w) \qquad (5.3a^*)$$

$$\theta_s = \Phi(\theta, w_{eq}) \qquad (5.3b^*)$$

$$\Phi(\theta, w_{eq}) = \begin{cases} 0 & \text{during adsorption} \\ 1 & \text{during desorption} \end{cases} \qquad (5\text{-}4^*)$$

$$\frac{\partial\theta_s}{\partial\eta} = \frac{[\theta_s(E_8-1)+1]^2}{(E_8-1)E_{10}\,\lambda(\theta_s)} \cdot \frac{\displaystyle\int_0^1 \left\{ \frac{-E_5}{[\pi(E_7-1)+1]}\frac{\partial w}{\partial\eta} + \frac{(E_6-1)}{[\theta(E_6-1)+1]^2}\frac{\partial\theta}{\partial\eta} \right\} d\zeta}{\displaystyle\int_0^1 \frac{d\zeta}{\theta(E_6-1)+1}} \qquad (5.5^*)$$

The choice of the set of equations to solve depends on the type of process under consideration. For a constant-volume process, the unkowns θ, θ_f, w, w_{eq} and θ_s are obtained by solving the set $\{(5.1^*,2^*,3a^*,3b^*,5^*)\}$. For a constant-pressure process, the unkowns θ, θ_f, w, and w_{eq} are obtained by solving the set $\{(5.1^*,2^*,3^*,3b^*)\}$.

5.4 ANALYSIS OF PERFORMANCE

If we analyze the overall cooling/heating system and consider the quantities of energy exchanged with the outside elements (figure 5.5), the following global energy balance can be written:

$$Q_{bo} + Q_{ev} = Q_{ex} + Q_{co} \qquad (5.6)$$

The system coefficients of performance are defined as:

$$COP_{cool} = Q_{ev} / Q_{bo} \qquad (5.7)$$

$$COP_{heat} = Q_{co} / Q_{bo} \qquad (5.8)$$
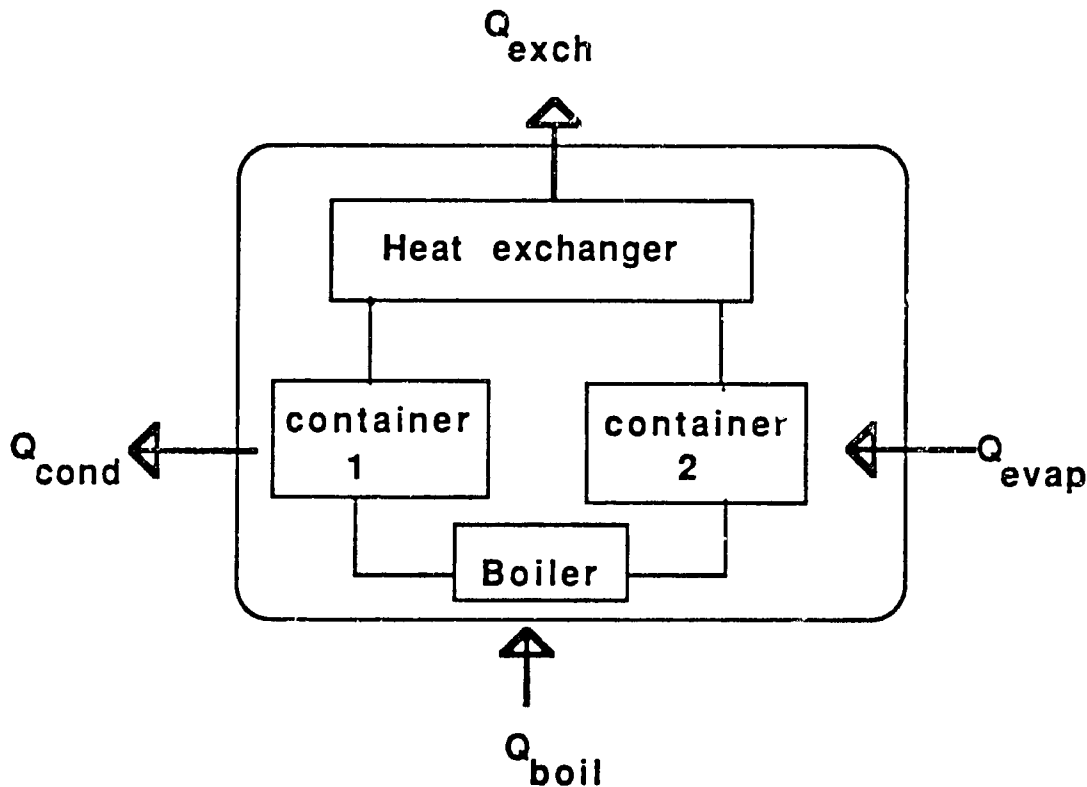
Figure 5.5: Sketch for the Overall Energy Balance of the System

In order to express both COP's in terms of the profiles of temperature and uptake, the following quantities need to be defined and calculated: ·

• The amount of desorbed species during desorption process:

$$m_{des} = -\int_0^{\tau_h} [\int_0^l \rho_a (\partial w/\partial t)\, A_a\, dz]\, dt = -\rho_a A_a \int_0^l [w(z,0) - w(z, \tau_h)]\, dz \quad (5.9)$$

• The cooling effect obtained in the evaporator:

$$Q_{ev} = [L(T_{ev}) - C_L(T_{co} - T_{ev})]\, m_{des} \quad\quad (5.10)$$

• The sensible heat gained by the desorbing container:

$$Q_{sens} = \int_0^{\tau_h} [\int_0^l (\rho_a A_a C_a + w\rho_a A_a C_a + \rho_c A_c C_c)(\partial T/\partial t)\, dz]\, dt \quad (5.11)$$

• The heat of desorption:

$$Q_{des} = -\int_0^{\tau_h} [\int_0^l \rho_a\, (\partial w/\partial t)\, A_a\, q_{st}\, dz]\, dt \quad\quad (5.12)$$

• The total heat exchanged between the fluid and the solid part, of the desorbing container:

$$Q_{flui} = -\int_0^{\tau_h} [\int_0^l h P_f\, (T_f - T)\, dz]\, dt \quad\quad (5.13)$$

• The energy generated during the adsorption process:

$$Q_{gene} = \rho_f C_f A_f V \int_0^{\tau_c} [T_h - T_f(0,t)]\, dt \quad\quad (5.14)$$

The energy balance for the desorption period can be written as:

$$Q_{flui} = Q_{sens} + Q_{des} \quad\quad (5.15)$$

Note that this equation can be obtained directly by integrating

equation (5.1) on the domain $[0,l] \times [o,\tau_h]$. The cooling COP of the cycle is given by:

$$COP_{cycle} = Q_{ev} / Q_{flui} \qquad (5.16)$$

Similar heat quantities can be defined for the adsorption phase. The expressions are identical to (5.9,14) except for a minus sign that needs be added. We introducing the non-dimensional integrals I_1, I_2, I_3, I_4, I_5 and I_6 defined by:

$$I_1 = -\int_0^{\Pi_h} \left[\int_0^1 (\partial w/\partial \eta) \, d\zeta \right] d\eta \qquad (5\text{-}17a)$$

$$I_2 = \int_0^{\Pi_h} \left[\int_0^1 (1+E_o+E_1 w)(\partial \theta /\partial \eta) \, d\zeta \right] d\eta \qquad (5\text{-}17b)$$

$$I_3 = -\int_0^{\Pi_h} \left[\int_0^1 \varphi (\partial w/\partial \eta) \, d\zeta \right] d\eta \qquad (5\text{-}17c)$$

$$I_4 = \int_0^{\Pi_h} \left[\int_0^1 (\theta_f - \theta) \, d\zeta \right] d\eta \qquad (5\text{-}17d)$$

$$I_5 = \int_0^{\Pi_h} \theta_f (1,\eta) \, d\eta \qquad (5\text{-}17e)$$

$$I_6 = \int_0^{\Pi_c} [1 - \theta_f (1,\eta)] \, d\eta \qquad (5\text{-}17f)$$

Equations (5.7) to (5.15) can then be simplified to:

$$COP_{cool} = [\lambda(\theta_{ev}) - Const] \, I_1 / (I_6/E_3) \qquad (5.7^*)$$

where $Const = E_{11} (E_8-1) / [E_3 E_8 E_9 (E_6-1)]$

$$COP_{heat} = \lambda(\theta_{co}) \, I_1 / (I_6/E_3) \qquad (5.8^*)$$

$$m_{deso} = M_a I_1 \qquad (5.9^*)$$

$$Q_{evap} = M_a L_o [\lambda(\theta_{ev}) - Const] \, I_1 \qquad (5.10^*)$$

$$Q_{sens} = M_a C_a (T_h - T_c) I_2 = M_a L_o /(I_2/E_3) \qquad (5.11^*)$$

$$Q_{deso} = M_a L_o I_3 \qquad (5.12^*)$$

$$Q_{exch} = M_a C_a (T_h - T_c) I_4 = M_a L_o (I_4/E_3) \qquad (5.13^*)$$

$$I_4 = I_2 + I_3 E_3 \qquad (5.14^*)$$

$$COP_{cycle} = [E_3 \lambda(\theta_{ev}) - const] (I_1/I_4) \qquad (5.15^*)$$

5.5 NOTION OF IDEAL REGENERATOR

The "ideal regenerator" is characterized by infinite heat and mass transfer coefficients. Consequently the local temperatures of the solid adsorbent T and the liquid T_f are equal and thermodynamic equilibrium exists ($w=w_{eq}$). In this case, the governing equations (5.1) and (5.2) are combined to yield the following energy equation:

$$\rho_a A_a C_a [1+(C_s/C_a)W + \frac{\rho_c A_c C_c}{\rho_a A_a C_a}] \frac{\partial T}{\partial t} - \rho_a A_a q_{st} \frac{\partial w}{\partial t}$$

$$= \rho_f A_f C_f (\frac{\partial T_f}{\partial t} + V \frac{\partial T_f}{\partial z}) \qquad (5.18)$$

or in dimensionless form:

$$(1 + E_0 + E_2 + E_1 w)(\partial\theta/\partial\eta) - E_3\varphi(\tau,w)(\partial w/\partial\eta) = - E_2 (\partial\theta/\partial\zeta) \qquad (5.18^*)$$

The boundary conditions are:

$\theta(0,\eta)=1$ during the desorption process

$\theta(0,\eta)=0$ during the adsorption process

The initial conditions at the begining of each period are:

$\theta_h(\zeta,0) = \theta_c(1- \zeta, \tau_c)$ for the desorption process

$\theta_c(\zeta,0) = \theta_h(1- \zeta, \tau_h)$ for the adsorption process

The ideal regenerator model gives a good approximation for the case of large transfer coefficients and provides also a useful upper limit for the performance that a real machine can achieve. The latter can be analyzed by the ratio of their COP to COP_{ideal} as function of the dimensionless transfer parameters E_4 and E_{4m}.

5.6 NUMERICAL SOLUTION OF THE GOVERNING EQUATIONS

This section is devoted to the discussion of the results of the numerical solution of the equations derived in the previous sections. The method and difficulties of the simulation will be first presented and the results of the numerical study will be given in terms of the dimensionless parameters introduced in section 5.3.2.

5.6.1 Wendroff's Scheme for First Order Hyperbolic

Equations. The governing equations (5.1) and (5.2) are of hyperbolic type. A general formulation of such system of equations can be made in the following matricial form:

$$A \frac{\partial U}{\partial \zeta} + B \frac{\partial U}{\partial \eta} = C \qquad (5.19)$$

where U is the unknown vector and A,B and C are specified functions of U, ζ and η. Wendroff's scheme consists of approximating the derivatives at point P (see figure 5.6) using the following central differences:

$$\frac{\partial U}{\partial \zeta}\bigg|_P = \frac{1}{2}\left[\frac{\partial U}{\partial \zeta}\bigg|_H + \frac{\partial U}{\partial \zeta}\bigg|_F \right]$$

$$= \frac{1}{2}\left[\frac{U_C - U_D}{\Delta\zeta} + \frac{U_B - U_A}{\Delta\zeta} \right]$$

$$\frac{\partial U}{\partial \eta}\bigg|_P = \frac{1}{2}\left[\frac{\partial U}{\partial \eta}\bigg|_G + \frac{\partial U}{\partial \eta}\bigg|_E \right]$$

$$= \frac{1}{2}\left[\frac{U_D - U_A}{\Delta\eta} + \frac{U_C - U_B}{\Delta\eta} \right]$$

Substituting in equation (5.19) and rearranging yields the following:

$$U_C = U_A + (pA + B)^{-1} (pA - B)(U_C - U_B)$$

$$+ 2(\Delta\eta)(pA + B)^{-1} C \qquad (5.20)$$

where $p=\Delta\eta/\Delta\zeta$. This scheme is explicit for initial-boundary value problems for which U is specified at $\eta=0$ and $\zeta=0$. When no boundary condition is prescribed at $\zeta=0$, an other scheme should be used at the first node of the finite-difference mesh before equation (5.20) can
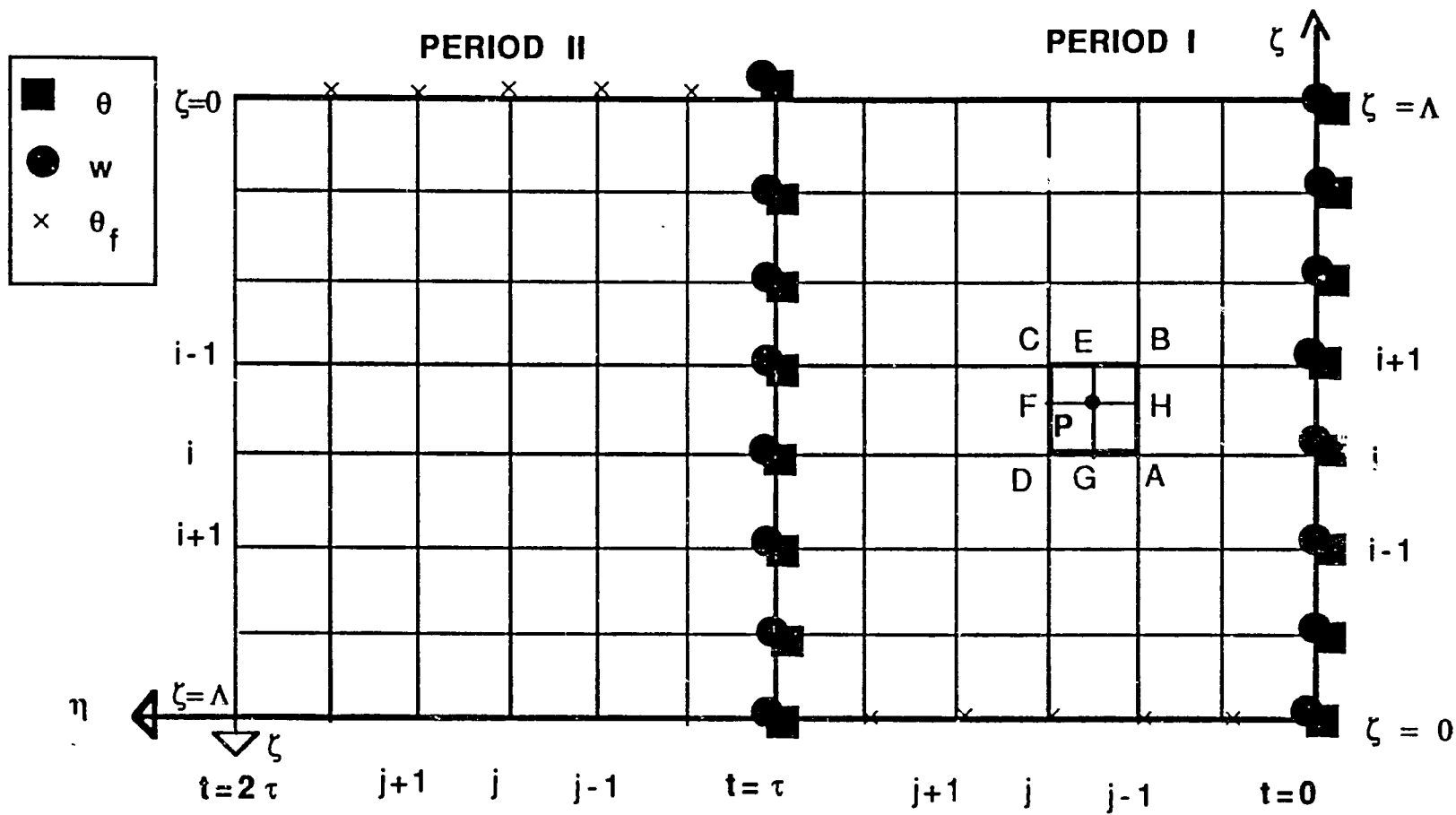
Figure 5.6: Grid Used for the Explicit Numerical Method. The initial and Boundary Conditions and the Principle of the Method are Shown

be implemented. For the case of a single equation with constant coefficients, Wendroff's scheme has the advantages of being of 2nd order accuracy, explicit and unconditionally stable [35].

5.6.2 Finite Difference Form of the Governing Equations of an Ideal Regenerator.

Equation (5.18) is of the form of (5.19) with scalar coefficients $A=(1+E_0+E_2+E_1w)$, $B=-E_2$ and $C=E_3\varphi(\theta,w)(\partial w/\partial\eta)$. Equation (5.20) gives:

$$\theta_{i+1}^{j+1} = \theta_i^j + \frac{B - Ap}{B + Ap}(\theta_i^{j+1} - \theta_{i+1}^j) + \frac{2\,\Delta\eta}{B + Ap}\,C \qquad (5.21)$$

The coefficients A,B and C which depend on θ and w are evaluated at point P using the average values:

$$w_P = (w_i^j + w_{i+1}^j + w_i^{j+1} + w_{i+1}^j)/4$$

and

$$\theta_P = (\theta_i^j + \theta_{i+1}^j + \theta_i^{j+1} + \theta_{i+1}^j)/4$$

For example A is calculated using:

$$A=[1 + E_0 + E_2 + E_1 \frac{(w_i^j + w_{i+1}^j + w_i^{j+1} + w_{i+1}^j)}{4}]$$

During a constant-volume process, equation (5.5*) is solved using the explicit scheme:

$$\theta_s^{j+1} = \theta_s^j + \frac{[\theta_s^j (E_8 -1)+1]^2}{(E_8 -1)E_{10}\,\lambda(\theta_s^j)}\,\frac{S_1^j + S_2^j}{S_3^j} \qquad (5.22)$$

where the quantities S_1, S_2 and S_3 are the approximated integrals:

$$S_1^j = \frac{-E_5}{[\pi (E_7 -1)+1]^j} \sum_{i=1}^{i=N} (w_i^{j+1} - w_i^j) \, e_i \, \Delta\zeta$$

$$S_2^j = (E_6 -1) \sum_{i=1}^{i=N} \frac{(\theta_i^{j+1} - \theta_i^j) \, e_i}{[\theta^j (E_6 -1)+1]^2} \, \Delta\zeta$$

$$S_3^j = \sum_{i=1}^{i=N} \frac{1}{[\theta^j (E_6 -1)+1]} \, \Delta\zeta$$

where the coefficients e_i depend on the in the integration scheme.

During the constant-pressure phase, θ_s is given by:

$$\Phi(\theta_{i+1}^{j+1}, w_{i+1}^{j+1}) = \begin{cases} 0 & \text{during adsorption} \\ 1 & \text{during desorption} \end{cases} \qquad (5.23)$$

The equilibrium relation (3b*) is written in the form:

$$\theta_s^{j+1} = \Phi (\theta_{i+1}^{j+1}, w_{i+1}^{j+1}) \qquad (5.24)$$

5.6.3 **Method of Numerical Solution.** A Fortran program IDEAL, given in Appendix B, is written to simulate the behaviour of an ideal adsorption regenerator. The grid used for the finite-difference solution is shown in figure 5.6 and the flowchart of the program is given in figures 5.7a,b. The procedure of calculations for a constant-volume phase can be summarized as follows:

1. θ_s at at the $(j+1)^{th}$ η-step is estimated.

2. θ and w at the $(j+1)^{th}$ η-step are estimated in order to evaluate A,B and C.

3. A corrected value of θ^{j+1} is calculated using the boundary condition or equation (5.21).

4. Equation (5.24) is used to calculate a corrected w^{j+1}.

5. The calculated values of θ^{j+1} and w^{j+1} are compared to their estimated values at step (2). If the difference is larger than ε, "new estimations" of θ^{j+1} and w^{j+1} are made and steps (3,4) are repeated.

6. If the difference is smaller than ε, equation (5.22) is used to calculate a corrected value θ_s at step η-step $(j+1)$. If the difference is larger than ε a "new estimation" is made and steps (2-6) are repeated.

8. If the difference is smaller than ε, the solution proceeds to the next η-step.

For a constant-pressure phase, θ_s is known and steps 1,6,7 and 8 are not necessary.

5.6.4 Intermediate Estimations and Numerical Stability.

The stability of the numerical solution is strongly dependent on the estimations needed at steps (5) and (6). A simple use of the calculated value is not appropriate to guarantee stability. To overcome this problem, procedures of intermediate estimations based on physical arguments are developed.
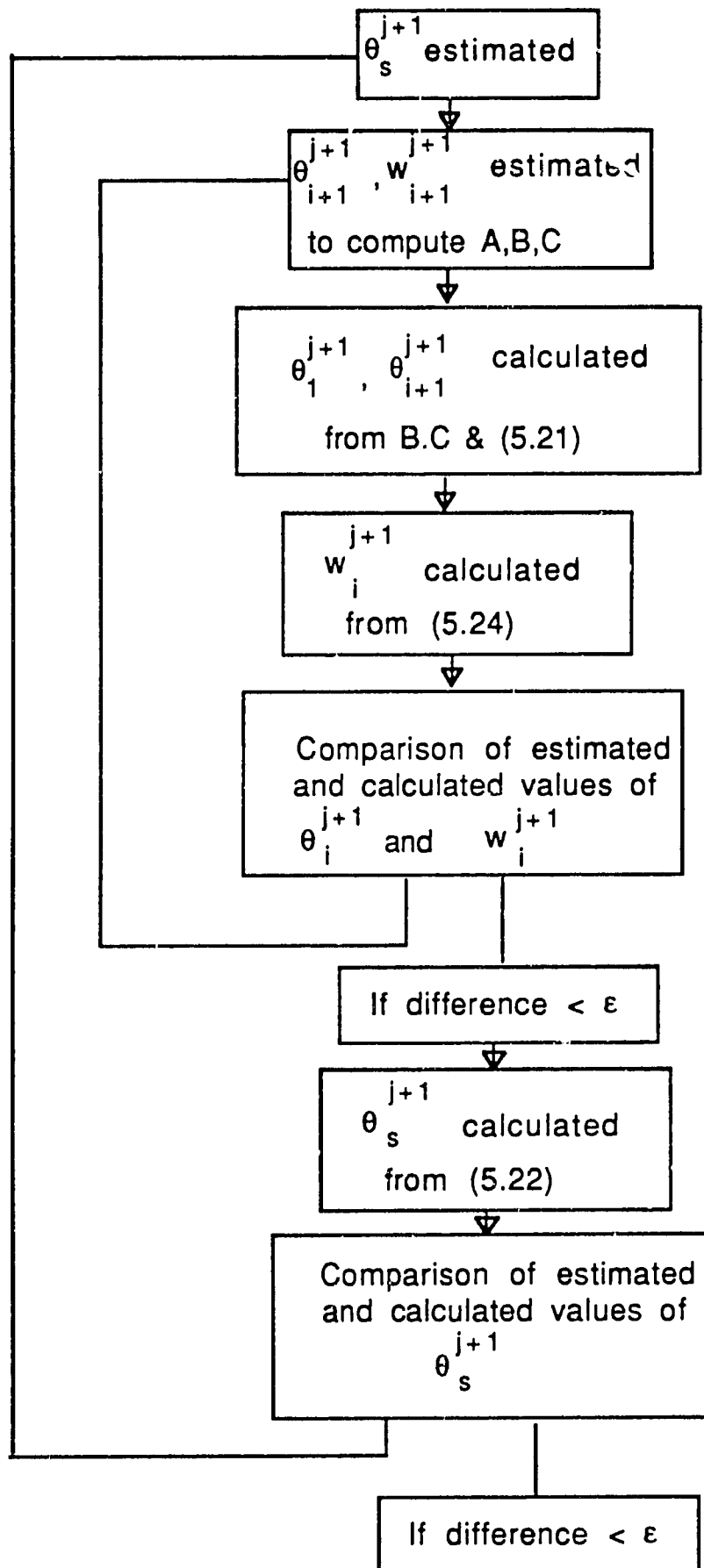
Figure 5.7a: Flowchart for the Simulation of a Constant-volume Phase

θ_{i+1}^{j+1}, w_{i+1}^{j+1} estimated to compute A,B,C

θ_1^{j+1}, θ_{i+1}^{j+1} calculated from B.C & (5.21)

w_i^{j+1} calculated from (5.24)

Comparison of estimated and calculated values of θ_i^{j+1} and w_i^{j+1}

If difference $< \epsilon$
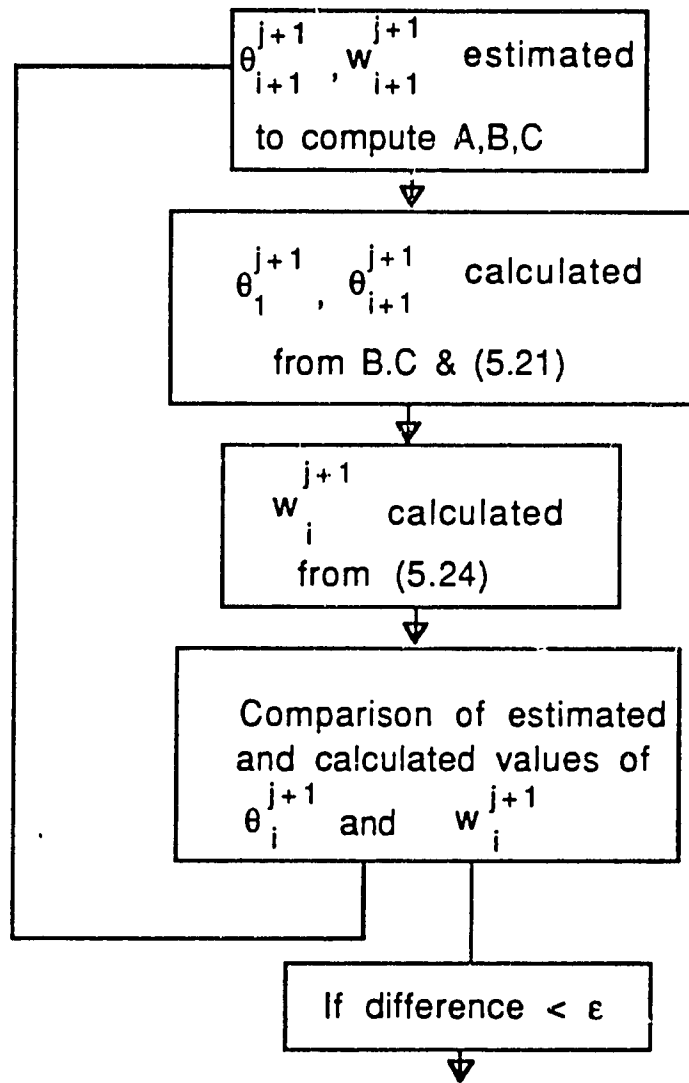
Figure 5.7b: Flowchart for the Simulation of a Constant-pressure Phase

5.6.4.1 <u>Estimation of</u> w^{j+1} <u>and</u> θ^{j+1}. The term C in equation (5.21), corresponding to the heat of adsorption, is very important compared to the rest of the terms in the energy balance. But when $\dot{w}^{j+1}$ is approximated by w^j at step (2), the term C is neglected. This leads to an overestimated value of θ^{j+1} (during desorption) and an under estimated value of w^{j+1} which cannot be used as new estimations. The following method is used to choose new estimations which lead to a converging scheme: w^j (θ^j) and the value w^{j+1} (θ^{j+1}) obtained by neglecting the adsorption term C are limits for the exact value of w^{j+1} (θ^{j+1}). A natural estimation is thus the average of these values. Note also that when exact value of w^{j+1} is used, the calculated θ^{j+1} satisfies the equilibrium equation (5.24). When w^{j+1} is underestimated the calculated value of θ^{j+1} is larger than its equilibrium value. The opposite is true when w^{j+1} is overestimated. This allows a convergent interval-halving method. Figure 5.8a is a graphical illustration of this iterative method.

5.6.4.2 <u>Estimation of</u> θ_s^{j+1} <u>During a Constant-volume</u> <u>Phase</u>. Equation (5.22) is very sensitive to the estimation of the difference (w^{j+1} - w^j). An overestimation by a very small amount leads to values of much larger than unity during desorption. These values cannot be used in the following iteration. To guarantee convergence, a similar interval-halving method as in section 5.6.4.1 is used. The upper limit for θ_s^{j+1} during desorption for example is $\min(\theta_{s,estim}^{j+1},1)$ and its lower limit is $\max(\theta_{s,estim}^{j+1},0)$. Figure 5.8b is a graphical illustration of this
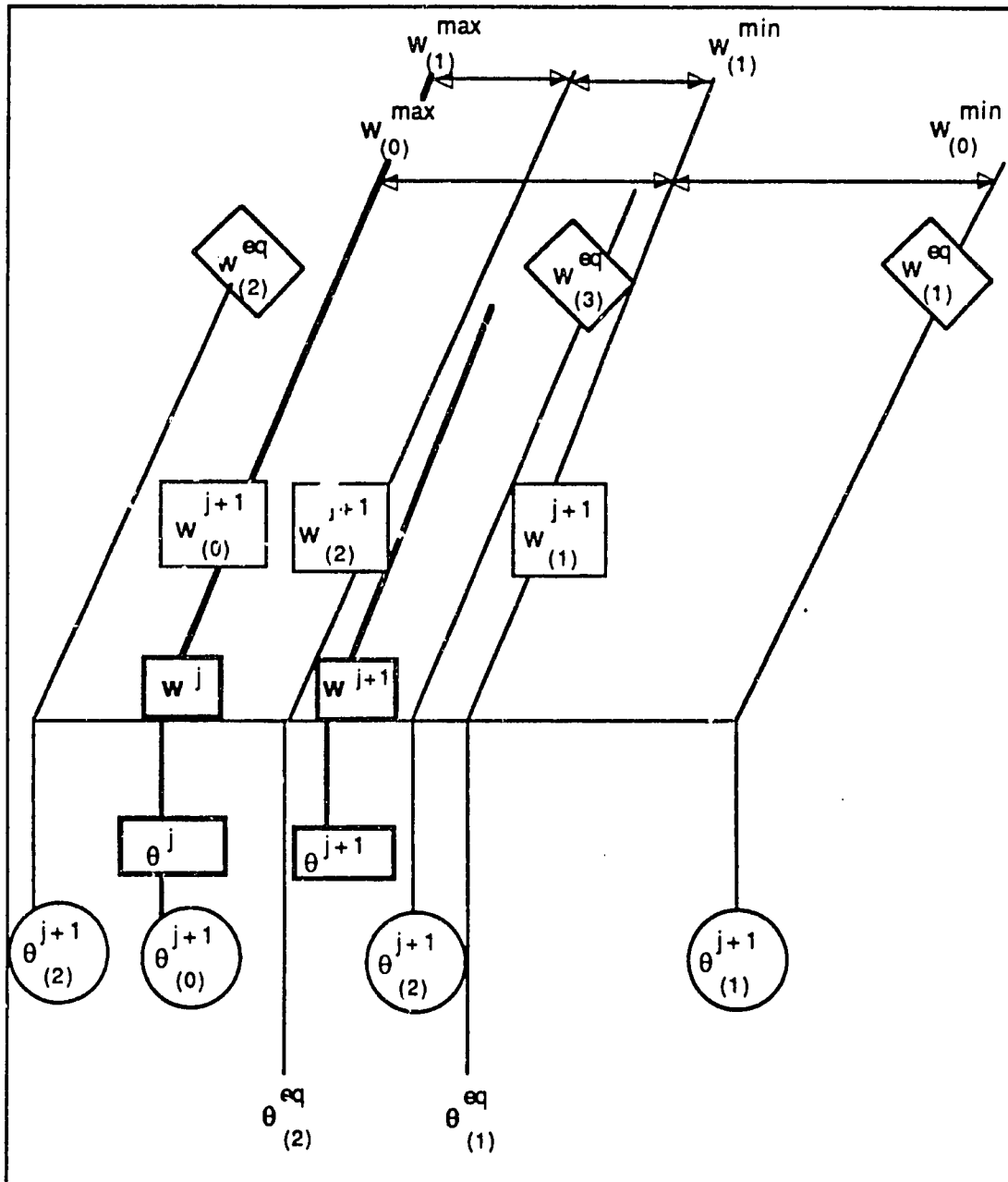
Figure 5.8a: Method of Estimating the Intermediate Values of θ^{j+1} and w^{j+1} in the Iterative Numerical Method Shown on the (θ_s, θ) Diagram
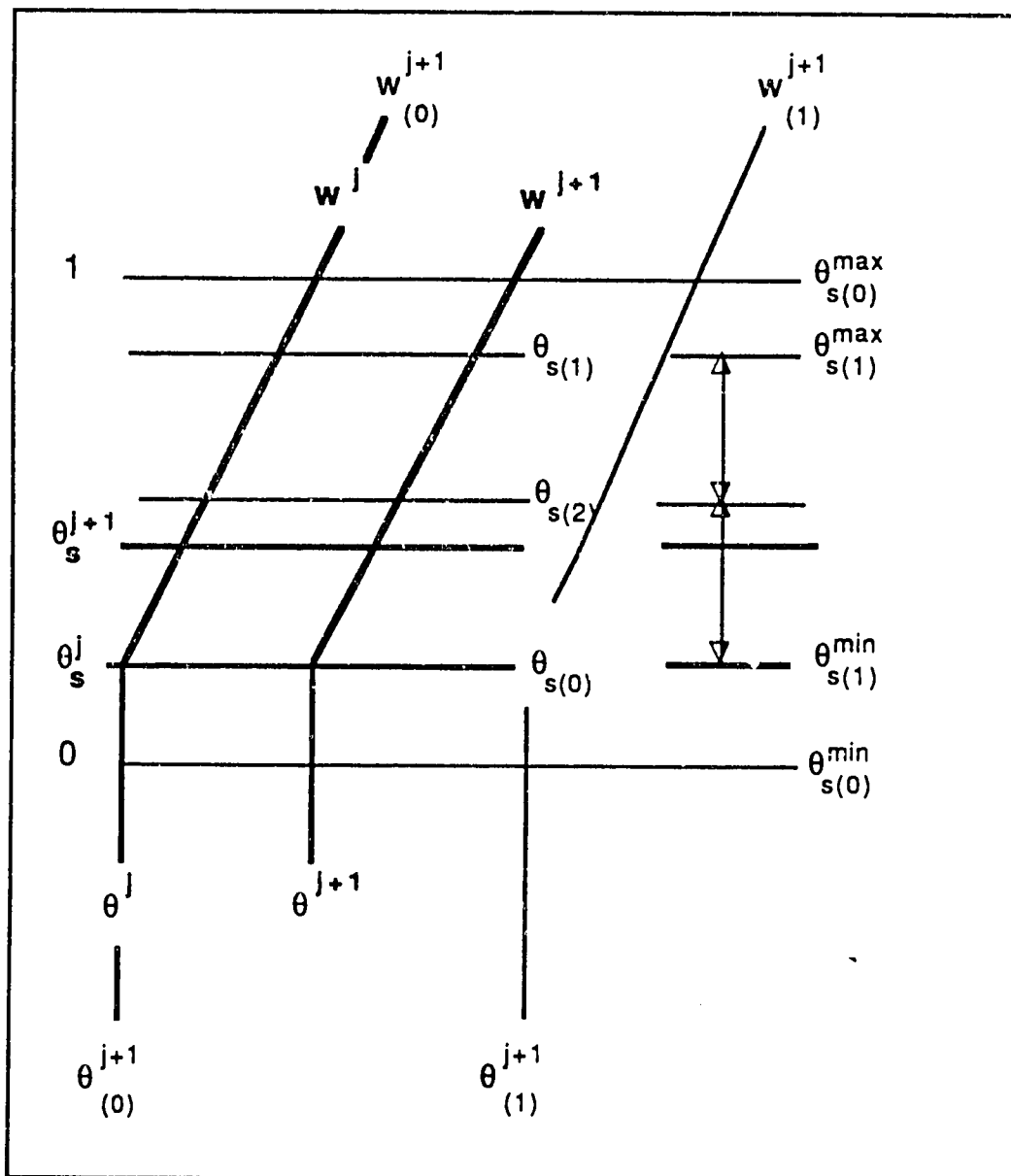
Figure 5.8b: Method of Estimating the Intermediate Values of θ_s^{j+1} in the Iterative Numerical Method Shown in (θ_s, θ) Diagram

method.

5.6.5 General Aspects of the Numerical Solution

5.6.5.1 Stability and Convergence. The procedure discussed in section 5.6.4 caused the iterative method converge to a solution of the governing equations. Another question is how this solution is affected by the size of the steps $(\Delta\zeta)$ and $(\Delta\eta)$. To check this dependence, several combinations of these parameters have been used. The two cases of constant-pressure and constant-volume are considered separately since the equation that governs the pressure variations is different. For the constant-volume process, large oscillations are observed below a critical value of $(\Delta\eta)$ which depends on $(\Delta\zeta)$. For example:

with $(\Delta\zeta)=1/20$ $\quad\quad\quad 0.125 < (\Delta\eta)_{cr} < 0.25$

with $(\Delta\zeta)=1/40$ $\quad\quad\quad 0.0625 < (\Delta\eta)_{cr} < 0.125$

This suggests that a stability condition exists and is approximately expressed by: $(\Delta\eta/\Delta\zeta) > 2.5$. Table 5.1 shows that when $(\Delta\eta)=0.25$ no major change in the solution is obtained by decreasing $(\Delta\zeta)$ from 1/40 to 1/60 .

For the constant-pressure phase the step $(\Delta\eta)$ can be made much smaller. With $\Delta\zeta=1/40$, the results given in table 5.2 show that the profiles of temperature corresponding to $\Delta\eta=0.025$ and $\Delta\eta=0.0125$ agree to about 0.01. An even better agreement is obtained when an integral quantity, such as the desorbed mass or the cooling effect, is calculated.

Based on the above observations, we used the following steps in the study of the influence of different parameters on the systen

Table 5.1 : Comparison of the Results obtained with $\Delta\zeta = 1/40$ and $\Delta\zeta = 1/60$ ($\Delta\eta = 0.25$)

		$\eta = 0.25$	$\eta = 0.50$	$\eta = 0.75$	$\eta = 1.00$
$\Delta\zeta = 1/40$	θ_s	0.131	0.543	0.791	1.000
	$\theta\ (0.0, \eta)$	1.0000	1.0000	1.0000	1.0000
	$\theta\ (0.1, \eta)$	0.0159	0.0666	0.1524	0.5599
	$\theta\ (0.2, \eta)$	0.0158	0.0639	0.0916	0.1140
	$\theta\ (0.3, \eta)$	0.0158	0.0639	0.0916	0.1135
	$\theta\ (0.4, \eta)$	0.0158	0.0639	0.0916	0.1135
	$\theta\ (0.5, \eta)$	0.0158	0.0639	0.0916	0.1135
	$\theta\ (0.6, \eta)$	0.0158	0.0639	0.0916	0.1135
	$\theta\ (0.8, \eta)$	0.0158	0.0639	0.0916	0.1135
	$\theta\ (0.9, \eta)$	0.0158	0.0639	0.0916	0.1135
	$\theta\ (1.0, \eta)$	0.0158	0.0639	0.0916	0.1135
$\Delta\zeta = 1/60$	θ_s	0.146	0.508	0.825	1.0000
	$\theta\ (0.0, \eta)$	1.0000	1.0000	1.0000	1.0000
	$\theta\ (0.1, \eta)$	0.0181	0.0695	0.1891	0.5116
	$\theta\ (0.2, \eta)$	0.0177	0.0600	0.0955	0.1160
	$\theta\ (0.3, \eta)$	0.0177	0.0599	0.0953	0.1136
	$\theta\ (0.4, \eta)$	0.0177	0.0599	0.0953	0.1136
	$\theta\ (0.5, \eta)$	0.0177	0.0599	0.0953	0.1136
	$\theta\ (0.6, \eta)$	0.0177	0.0599	0.0953	0.1136
	$\theta\ (0.8, \eta)$	0.0177	0.0599	0.0953	0.1136
	$\theta\ (0.9, \eta)$	0.0177	0.0599	0.0953	0.1136
	$\theta\ (1.0, \eta)$	0.0177	0.0599	0.0953	0.1136

Table 5.2 : Comparison of the Temperature Profiles at 3 ζ Positions and the Dimensionless Desorbed Mass for Δη =0.025 and 0.0125. (Δζ =1/40)

η	θ (0.1, η)		θ (0.5, η)		θ (1.0, η)		Desorbed mass/M_a	
	Δζ =.025	.0125	Δζ =.025	.0125	Δζ =.025	.0125	Δζ =.025	.0125
0.00	0.0000	0.0000	0.0000	0.0000	0.0000	0.0000	6.143e-4	6.143e-4
0.25	0.0159	0.0159	0.0158	0.0158	0.0158	0.0158	-4.587e-4	-4.587e-4
0.50	0.0666	0.0666	0.0639	0.0639	0.0639	0.0639	5.437e-4	5.437e-4
0.75	0.1524	0.1524	0.0916	0.0916	0.0916	0.0916	2.283e-3	2.283e-3
1.00	0.5599	0.5599	0.1135	0.1135	0.1135	0.1135	3.471e-3	3.471e-3
1.50	1.0081	1.0080	0.0777	0.0912	0.0891	0.0880	0.0124	0.0122
2.00	1.0001	1.0001	0.1494	0.1433	0.1400	0.1471	0.0218	0.0216
2.50	1.0000	1.0000	0.1344	0.1227	0.1021	0.1194	0.0312	0.0310
3.00	1.0000	1.0000	0.1953	0.1924	0.1348	0.1290	0.0406	0.0403
3.50	1.0000	1.0000	0.0045	0.0024	0.0905	0.0843	0.0500	0.0499
4.00	1.0000	1.0000	0.2974	0.3003	0.0789	0.0762	0.0595	0.0593
4.50	1.0000	1.0000	0.6160	0.6150	0.0961	0.0825	0.0688	0.0686
5.00	1.0000	1.0000	0.9941	0.9937	0.1457	0.1403	0.0782	0.0779
5.50	1.0000	1.0000	1.0000	1.0000	0.1438	0.1412	0.0879	0.0876
6.00	1.0000	1.0000	1.0000	1.0000	0.0555	0.0515	0.9720	0.0969
6.50	1.0000	1.0000	1.0000	1.0000	0.1926	0.1957	0.1065	0.1063
7.00	1.0000	1.0000	1.0000	1.0000	0.0350	0.0291	0.1159	0.1156
7.50	1.0000	1.0000	1.0000	1.0000	0.0975	0.0972	0.1261	0.1259
8.00	1.0000	1.0000	1.0000	1.0000	0.3107	0.3161	0.1344	0.1342

performance:

For a constant-volume phase: $\Delta\zeta=1/40$ $\Delta\eta=0.25$

For a constant-pressure phase: $\Delta\zeta=1/40$ $\Delta\eta=0.025$

5.6.6 **An Example**. To discuss the profiles of temperature, uptake , energy and mass quantities...etc, the following example has been chosen:

$M_a=20.4$ (kg) $C_a=836.0$ (kj/kg.K) $\rho_a=735.0$ (kg/m^3)

$M_c=10.2$ (kg) $C_c=400.0$ (kj/kg.K)

$M_f=5.0$ (kg) $C_f=2300$ (kj/kg.K)

$T_{ev}=281.3$ (K) $T_{co}=310.8$ (K)

$T_c=310.8$ (K) $T_h=477.0$ (K)

Adsorption pair: Synthetic zeolite 13X-Water (data of [10])

Starting from an initial state at which $\theta=0$, a number of iterations are performed (3 to 4) before the periodic regime is reached. Figure 5.9 shows the profiles of temperature as function of ζ as the wave travels along the regenerator. Figure 5.10 shows the variations with η of the temperature at the ends of the reactor. The areas under these curves are directly related to the regenerated energy and the energy lost at the air/oil heat exchanger. Figure 5.11 plots the dimensionless amount of adsorbate cyled versus time. There we choose $\Pi=10$ to show that after a certain time, the mass cycled remains constant. This time corresponds approximately to the optimum value of Π. It is seen that after the temperature wave has crossed the regenerator, the desired effect doesn't increase
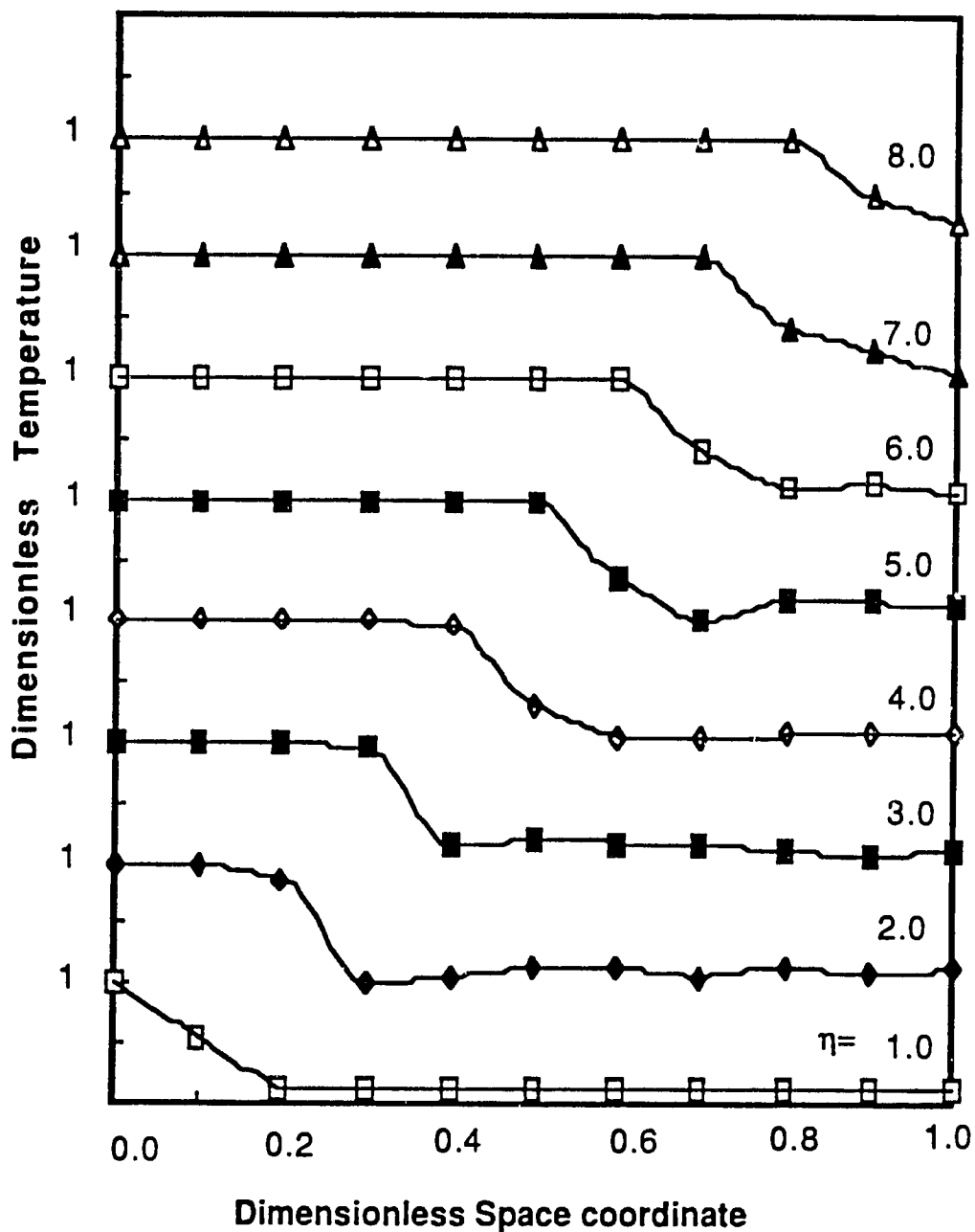
Figure 5.9: Profiles of Dimensionless Temperature versus
Space Coordinate ζ for Different Values of η
During the Transient Regime of a Desorption Phase
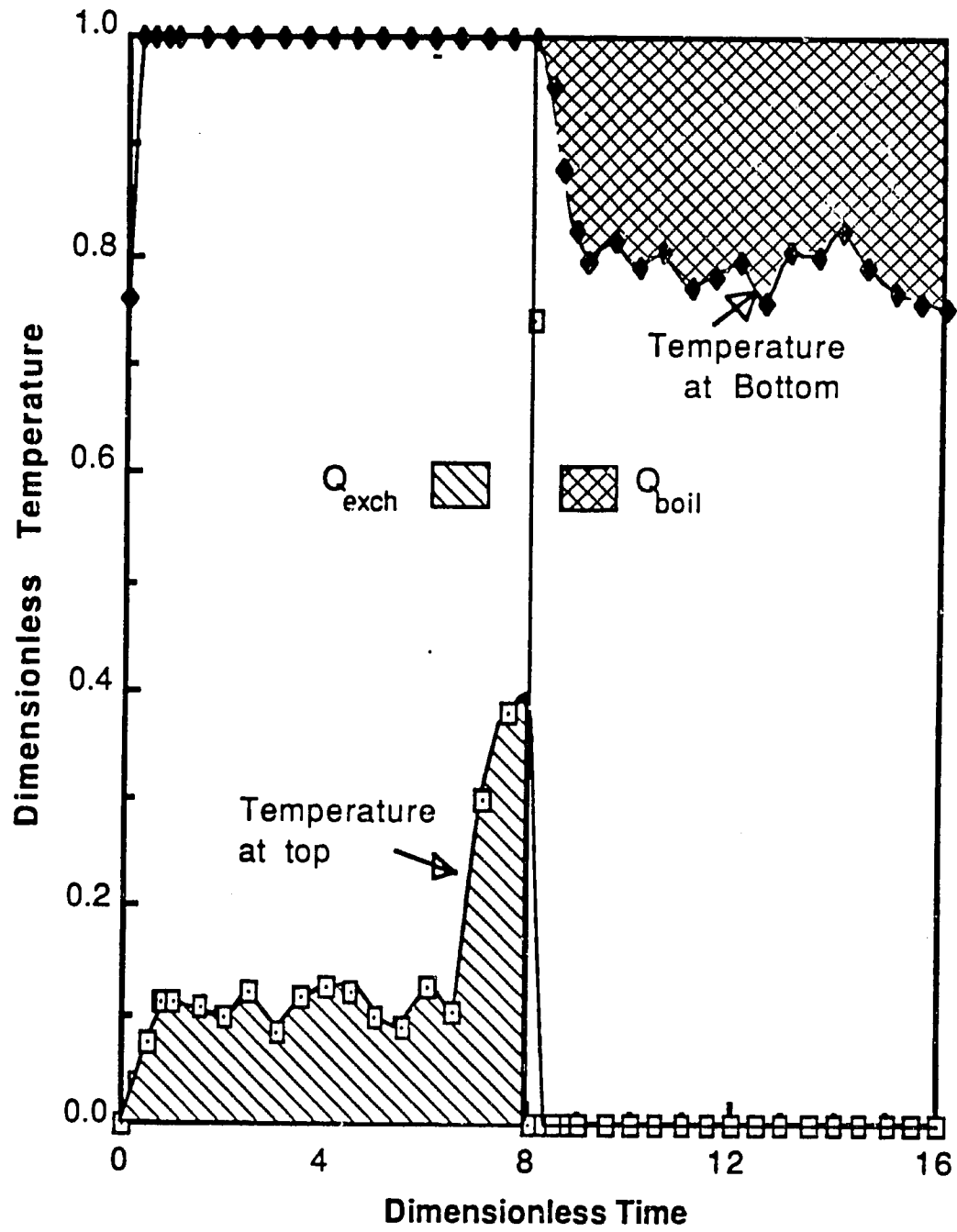
Figure 5.10: Profiles of Temperature at the Two Ends of
Each Container During One Complete Period
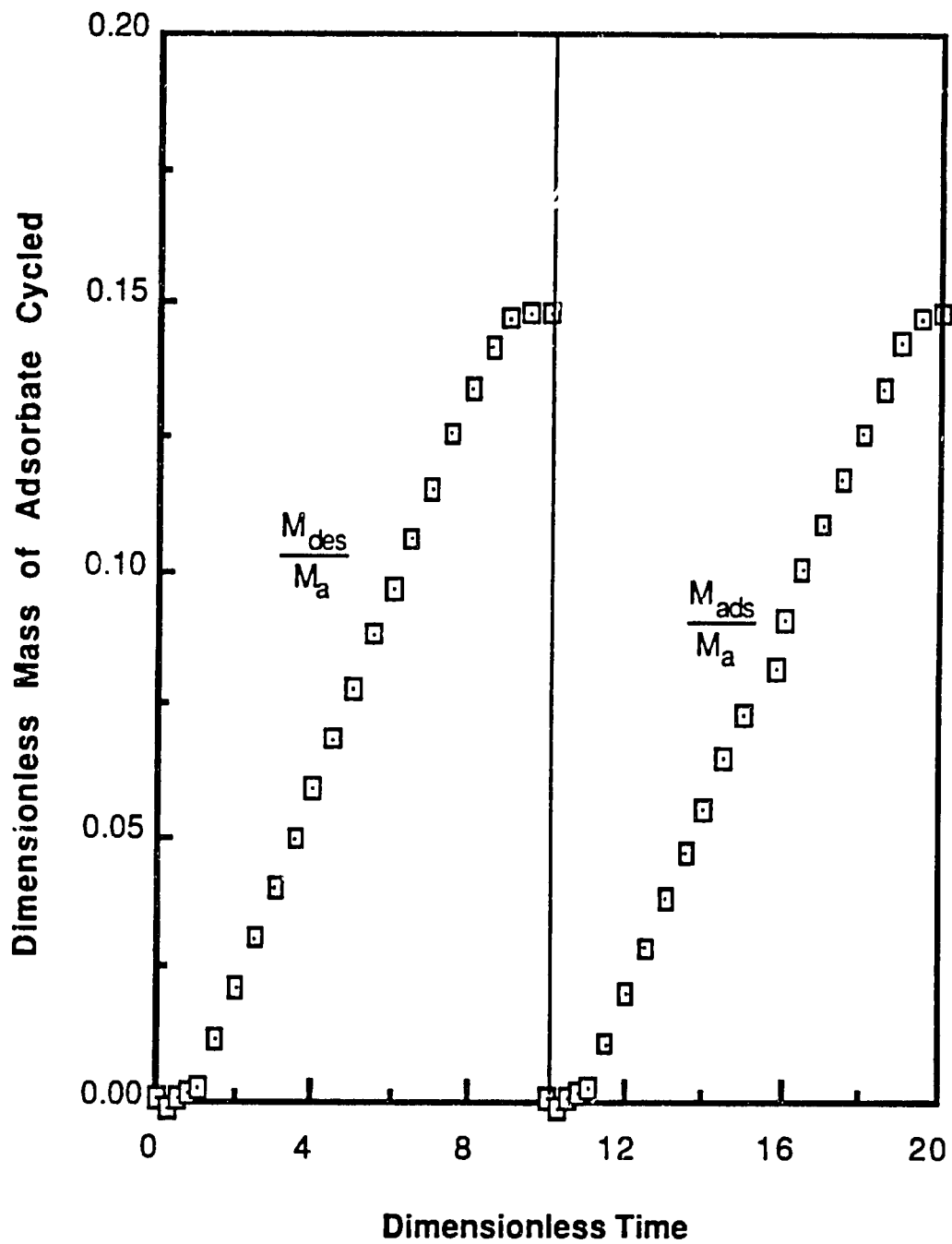
Figure 5.11 : Dimensionless Mass of Adsorbate Cycled as Function of Dimensionless Time (Π =10)

while the heat lost at the heat exhanger increases causing the system COP to decline as seen in figure 5.12. The follwing dimensionless energy quantities have been calculated:

Q_{co}=0.098358 Q_{ev}=0.09385

Q_{bo}=0.04583 Q_{ex}=0.036458

$Q_{co} + Q_{ex}$ = 0.13482 $Q_{ev} + Q_{bo}$ =0.13968

We verify that the global energy balance is satisfied to about 3.5% .

5.6.7 **Influence of the Operating Conditions.** Several runs of the program IDEAL are performed to analyze the effect of changing the operating conditions on the system performance. Table 5.3 shows the results obtained by varying the temperatures T_{co}, T_{ev} and T_c. The temperature difference (T_{co}- T_{ev}) between the condenser and the evaporator has a relatively important effect on the system performance since a 5°C decrease of this parameter causes 16-20% improvement of the system cooling COP. The effect of T_c is not as important and decreasing it by 5°C leads to an increase of the system cooling COP by only 5%. Figure 5.13 is a plot of the system cooling COP as function of the dimensionless period Π. As expected the curve shows a value of Π for which the performance is optimum. The effect of the thermal capacity of the inert parts of the reactor which is expressed by E_o is studied on the transient first period only in oreder to minimize the computing time. The results show a very weak decrease in the system cooling COP from 2.00 with E_o=0 to 1.90 with E_o=0.96.
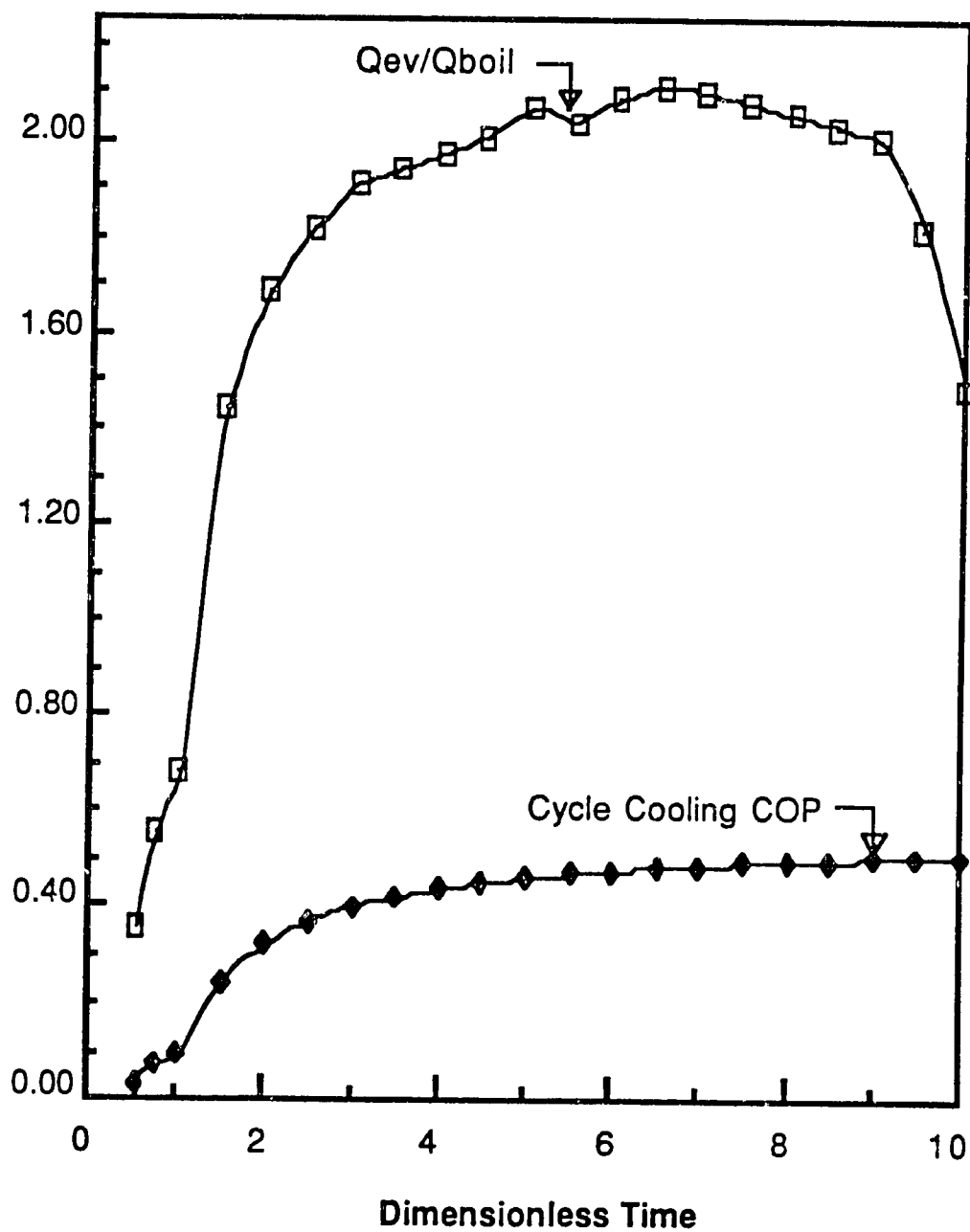
Figure 5.12: Variation of the Ratio (Qev/Qboil) and the Cycle Cooling COP's with Dimensionless Time (Π = 10)
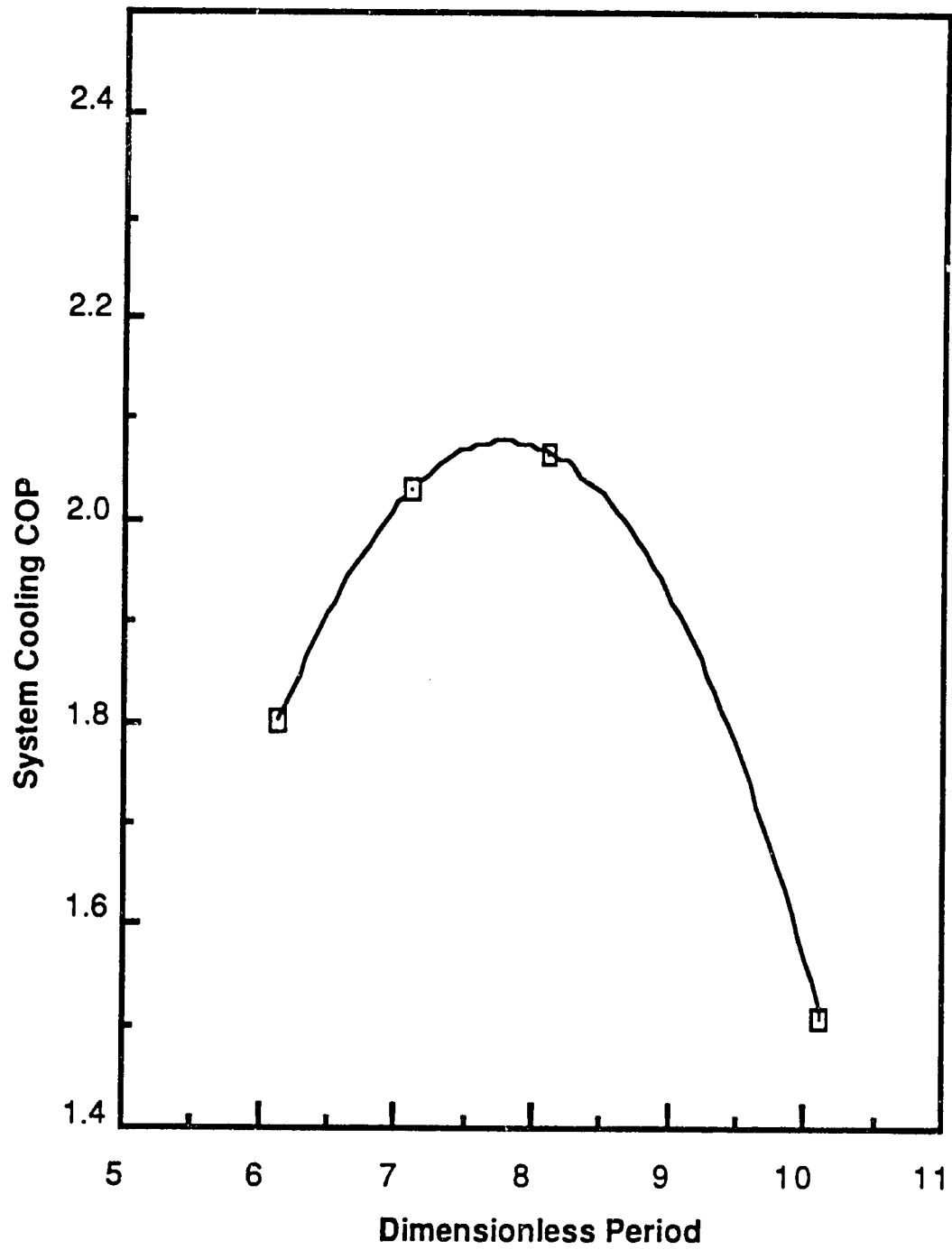
Figure 5.13 : Effect of the Dimensionless Period π
on the System Cooling COP

Table 5.3: Effect of Different Parameters on the System Performance (a) Effect of T_{co}, T_{ev} and T_c (b) Effect of E_o

T_{co}	T_{ev}	T_c	COP_{cool}	COP_{heat}
300.8	276.3	310.8	2.13	2.17
310.8	276.3	310.8	1.61	1.67
310.8	281.3	310.8	2.05	2.15
305.8	281.3	310.8	2.39	2.48
310.8	281.3	315.8	2.03	2.06

(a)

E_o	0.00	0.239	0.478	0.957
COP_{cool}	1.82	1.75	1.69	1.69
COP_{heat}	2.00	1.97	1.92	1.90

(b)

5.6.6 The Case of Actual Regenerator with Finite Heat Transfer Coefficient.

In actual systems, heat transfer coefficient is finite and the temperature of the solid adsorbent is not equal to that of the fluid. If we assume that mass transfer is infinitely fast -which is a valid assumption in heat transfer controlled adsorption- then w is equal to w_{eq} and the unknowns to be determined are θ, θ_f, w and θ_s. The equilibrium relation and the pressure equation are similar to the case of ideal regenerator. The finite difference form of the energy balance equations to solve for θ and θ_f is:

For i=1:

$$\theta_{f,1} = \begin{cases} 1 & \text{during desorption} \\ 0 & \text{during adsorption} \end{cases}$$

$$\theta_1^{j+1} = \frac{A\,\theta_1^{j} + B\,(\theta_{f,1}^{j+1} + \theta_{f,1}^{j} - \theta_1^{j}) + E_3\,\varphi\,(w_1^{j+1} - w_1^{j})}{A + B} \quad .$$

where,

$$A = 1 + E_0 + E_1\,(w_1^{j+1} + w_1^{j})/2$$

$$B = E_4\,(\Delta\eta)/2$$

For $1 < i \leq (n-1)$

$$A11\,\theta_{i+1}^{j+1} + A12\,\theta_{f,i+1}^{j+1} = C1$$

$$A21\,\theta_{i+1}^{j+1} + A22\,\theta_{f,i+1}^{j+1} = C2$$

where,

$$A11 = 1 + E_o + E_1 \, w_P + E_4 \, (\Delta\eta)/2$$

$$A12 = - E_4 \, (\Delta\eta)/2$$

$$A21 = - E_4 \, (\Delta\zeta)/(2E_2)$$

$$A22 = 1 + E_4 \, (\Delta\zeta)/(2E_2)$$

$$C1 = E_3 \, \varphi \, (w_{i+1}^{j+1} - w_{i+1}^{j} + w_{i}^{j+1} - w_{i}^{j})$$

$$+ \, (1 + E_o + E_1 \, w_P)(\theta_{i+1}^{j} + \theta_{i}^{j} - \theta_{i}^{j+1})$$

$$+ \, [\, E_4 \, (\Delta\eta)/2 \,](\theta_{f,i}^{j+1} + \theta_{f,i+1}^{j} + \theta_{f,i}^{j} - \theta_{i}^{j+1} - \theta_{i+1}^{j} - \theta_{i}^{j}$$

$$C2 = [1 - E_4 \, (\Delta\zeta)/(2E_2)] \, (\theta_{f,i}^{j+1} + \theta_{f,i}^{j})$$

$$- \, [1 + E_4 \, (\Delta\zeta)/(2E_2)] \, \theta_{f,i+1}^{j+1}$$

$$+ \, E_4 \, (\Delta\zeta)/(2E_2)(\theta_{i}^{j+1} + \theta_{i+1}^{j} + \theta_{i}^{j})$$

The equations governing the pressure and uptake variations are similar to those of the ideal regenerator case.

A computer program REALG, given in Appendix C, is developed to obtain a numerical solution to the above equations. The numerical procedure used is similar in most aspects to the ideal case. The effect of the heat transfer coefficient is analyzed by changing the parameter E_4 for a fixed set of data (the other data are those given in the example of section 5.6.4). It was in particular verified that by increasing the value of E_4, the solution tends in the limit to the

ideal case solution. Table 5.4 gives the variations of the cooling/heating effects and the system COP's with increasing E_4. These results illustrate the important effect of the rate of heat transfer. The cooling COP, for example, is increased by 60% when E_4 is increased from 10 to 100.

Table 5.4: Effect of Heat Transfer Coefficient on the System Performance

E_4	COP_{cool}	COP_{heat}	$Q_{ev}/(M_oL_o)$	$Q_{co}/(M_oL_o)$
10	0.89	0.92	0.0736	0.0761
10^2	1.43	1.48	.08588	0.0888
10^3	1.87	1.95	0.0922	0.0962
10^4	2.03	2.13	0.0937	0.0984
∞	2.05	2.15	0.0938	0.0986

5.7 CONCLUSIONS

The operating principle of a regnerative closed-cycle adsorption system is presented. A mathematical model is developed

to analyze the effect of various design parameters and operating conditions on the performance of such systems. The nonlinear set of hyperbolic governing equations is solved using a finite-difference method based on Wendroff's scheme and a procedure developed to overcome serious divergence problems.

The analysis demonstrates that the concept of regenerative heat exchanger can increase the COP of adsorption systems from 0.5 to more than 2.0.

The temperature difference between the condenser and the evaporator has a relatively important effect on the system performance since a 5°C decrease of this parameter causes 16-20% improvement of the system cooling COP. Whereas decreasing the cold or ambient temperature by 5°C leads to an increase of only 5% of the system cooling COP. The system performance presents a maximum value at an optimum value of the dimensionless adsorption or desorption period. The effect of the thermal capacity of the inert parts of the adsorbent container which is expressed by E_o is relatively weak. There is a decrease of the system cooling COP from 2.00 with $E_o = 0$ to 1.90 with $E_o = 0.96$. The rate and area of heat transfer, expressed by the parameter E_4, has a very strong effect. The cooling COP is increased by 60% when E_4 is increased from 10 to 100.

AIT

Asian Institute of Technology
Bangkok   Thailand

RESEARCH AND DEVELOPMENT OF SOLAR-POWERED DESICCANT
REFRIGERATION FOR COLD-STORAGE APPLICATIONS
(Grant No. DPE-5542-G-SS-4057-00)

Final Report

by

Prof. R. H. B. Exell
Professor

Dr. S. C. Bhattacharya
Associate Professor

and

Y. R. Upadhyaya
Research Associate

Asian Institute of Technology
P.O. Box 2754, Bangkok 10501
Thailand

1987

CONTENT

I   REQUIREMENT OF COLD STORAGE IN THAILAND

1.   Introduction

The need of refrigeration and cold/cool storage in the developing countries is mainly for the storage of foodstuffs such as for milk chilling, storage of fish, meat, fruits and vegetables and the storage of medical supplies.

Most of the rural areas of the world produce ample foodstuffs but losses are high due to lack of proper preservation facilities like refrigeration. The losses have been reported to be substantial and sometimes of the order of 50% in the interval between production and consumption (FAO, 1984). One of the acute needs of cold/cool storage is for the fruits and vegetables both in the temperate and tropical areas of the developing countries. In a temperate climate much of the production of the fruits and the vegetables is confined to short growing seasons and storage is essential to supply products after harvesting seasons. In a tropical climate the production can be extended but storage is still needed mainly due to the following reasons:

i.   To remove the field heat immediately after harvesting to prevent overripening, deterioration and ultimate destruction of the fruits and vegetables.

ii.   For short term storage around the production areas before being transported to big cold storages or for distribution.

iii.   To extend the marketing period and increase the value of sales.

iv.   To wait for a favorable market response.

Around two billion people, about half of the world population, live in the rural areas and villages of the developing countries. In most of the developing countries living conditions of the majority are poor and there is not only malnutrition but very high incidence of disease. Infant mortality is particularly high in the rural areas; it is surprising to note that in some countries, more than one-third of the children die before the age of four (Derrik and Durand, 1986). This is because from six months of age until the fourth year of life infections and parasitic disease play a significant role in the high infant and child mortality rate. Much of this can be controlled through mass immunisation before infection occurs. The vaccines for immunisation require refrigeration during transport and storage. According to WHO, vaccines for measles, yellow fever and oral polio has to be stored at a temperature between -15°C and -25°C, and others such as DPT, Tetanus Toxoid, DT and BCG need storage temepratures between

0°C and 8°C (EPI, 1986). But there is a great dearth of refrigeration systems in rural areas of the developing countries as they do not have access to mains electricity, and other sources of fuels are either scarce or expensive. This problem has been well recognised by World Health Organisation (WHO) for storage and transportation of vaccines for their Expanded Programme of Immunisation (WHO, 1981). They also have recognised the potential of solar refrigeration for vaccine Cold Chains in remote areas where solar energy is the only reliable source of energy. Most of the work to-date has been on the use of the photovoltaic refrigerator which unfortunately are expensive. A unit of photovoltaic solar refrigerator having capacity of four litres of vaccine storage costs more than US\$ 6000 (Uppal and others, 1986). Moreover, in over 40% of the field tests done by WHO, breakdowns occurred and trivial repairs needed posed serious problems in remote areas due to lack of maintenance facilities. So there is a great scope for thermally powered systems which are reliable and available at lower cost.

1.1 Requirement of Refrigeration and Cold Storage in Thailand

Thailand is an agricultural country with a population of about 60 million. Agricultural crops, fish and meat are abundant in Thailand in comparison to the other developing countries of the world. Thailand is one of the largest fishing nations of the world and ranks third largest in the region after Japan and Peoples Republic of China. The most important fruit crops are mango, durian, pomeloes, custard apple, mangosteen, orange, lime, pineapple, water melon, lichee, papaya, banana, jackfruit, guava, tamarind and rambutan. The main vegetable crops of the country are shallot, chinese radish, tomato, cabbage, cucumber, pumpkin, white gourd, taro, etc.

The demand of the tropical and sub-tropical exotic fruits like mangoes, papayas, passion fruits, tamarinds, soursop, cashew apples, cherries, jackfruits, pineapples, lichees, longans, avocados, guavas, mangosteens is rising in several countries of the west (Vandendriessche, 1976). With its central location and favorable natural resources, Thailand has the potential to become a leading exporter of tropical and sub-tropical fruits of southeast Asia. The Royal Thai Government is very aware of this potential and intensive development of agriculture, and particularly increase of production of the cash crops to increase export earning and reduce the trade deficit is a prime element of Government policy.

The major fruit and vegetable producing area is the stretch of land west of Bangkok city but now the Government is incouraging this policy throughout the country. A particular emphasis has been given to the northern mountaineous region of Thailand under the Royal Northern Project, established in 1969 (Devapriya, 1984). This area is within the so called 'Golden Triangle' considered as one of the principal opium growing areas

of the world. This Project was established under Royal patronage to persuade the local hillpeoples to cease the practice of shifting cultivation and opium growing. The area under this project is approximately 40 square kilometres. Some of the replacement crops introduced are temperate-zone fruits and vegetables, and cut flowers which sell for relatively high prices in local markets (Boon-Long, 1983). After cutting and packing in the morning, the flowers must be kept cool at 0 -- 5°C before loading into refrigerated trucks for transportation from the hills in the afternoon or next day.

To evaluate the need for cold storages in Thailand a survey of the existing cold storages was carried out. There are altogether 46 cold storages in Thailand (Saisithi, 1982), of which 24 are situated at and around Bangkok and rest are scattered in the provinces. Most of the privately owned cold stores do not have 'cool stores' to store vegetables and fruits as they are designed for the storage of frozen meats and fish for export. The details of the activities of these private cold stores are not available. So informations ere sought from the Government Cold Storage Organisation of Thailand.

The Cold Storage Organisation is a state enterprise under the control and supervision of the Ministry of Agriculture and Co-operatives. This organisation has altogether eleven plants at Bangkok and different provinces in the country. The cold stores in the provinces are located in the suburbs to make them accessible to producers of vegetables and fruits. The cold stores in provinces render freezing, cold and cool storage facilities to farmers and traders. The cool stores have temperature 0 to 10^0C and relative humidity above 95%. The main products stored in the cool stores are fruits, vegetables, dried fresh water and marine fish, and dried lizard etc., for local consumption and export. The fresh fish is also stored temporarily in cool stores during an intermediate waiting period for better utilization of limited freezer capacity. According to Kasemsap, (1985), the Deputy Director of the organization, the market share of the organization is approximately 20%. The privately owned cold stores are generally small, having 30 to 100 ton holding capacities. According to him, there is a great need for small cool stores having storage temperature 0 to 10^0C and relative humidity above 95% located close to the production areas. The holding capacities of these units can be of the order of 10 to 30 cubic metres. Such units should be available in the North, North-East, East and the central region of Thailand. These units would be used to store fruits and vegetables for retaining the freshness and quality for better distribution and sale in the local market, or as temporary store before being transferred to bigger stores for long term storage and distribution in a wider market or for export.

These units will be of great value for farmers in the mountaineous northern region of Thailand where vegetables, fruits

and flowers are grown as a part of crop replacement program to reduce deforestation and opium growing by hillpeoples. Emphasis has been placed on high-priced vegetables which could not be grown well or could be grown only during limited periods in the lowlands. But very heavy post-harvest losses have been reported mostly due to lack of proper storage conditions. Losses up to 75% on the route from Chiang Mai to Bangkok (a distance of 700 km) have been reported (Boon-Long, 1983). The major reason for this has been cited as lack of pre-cooling before transportation. So the small cool stores could be used as pre-coolers shortly after harvesting or a short term storage. These units might as well help in the proper utilization of 'cool store' capacities of the existing big plants, only 30 to 40% of whose total holding capacities are utilized at present.

To implement such projects in different parts of country government incentive is needed in terms of soft and sub-loans with the special purpose of developing rural areas. According to Kasemsap (1985) such loans could be channelled through the Government Cold Storage Organisation which has expertise and manpower to initiate and implement such projects.

The number of villages which had no access to mains electricity was about 47,725 during the year 1979, and in spite of the rural electrification programs of the Provential Electricity Authority this number is expected to increase to 55,000 by 1999 (Chantavorapap, 1979). The health posts of these villages are supplied with vaccines by the nearby hospitals or health centres with electricity and transported in ice boxes.

II SUMMARY OF THE FIRST YEAR'S WORK

2. Brief Summary

During the first year, a hybrid system which combines a solar powered intermittent ammonia-water absorption refrigeration cycle, a solid desiccant cooling cycle to cool the condenser, and positive ventilation with ice bank cooling to use the ice produced effectively, was studied.

The solid desiccant cycle can reduce the temperature of the condenser and increase the ammonia generation approximately by 50%. This also means increase in the yield of ice by the same proportion. The collector/generator of the ammonia-water system then operates at lower temperatures, which gives a better solar collection efficiency. Other indirect benefits of this system would be on the life of the collector/generator as it would be subjected to lower temperature and pressure induced stresses.

If the solid desiccant cycle is used to cool the condenser, the amount of ice increases, but at the cost of a lot of extra hardware like desiccant beds, solar air heaters, air blowers and the evaporative condenser. This system will have moving parts such as complex air switching arrangements which will need parasitic power. Such a system cannot be used in places which do not have an electricity supply.

Although the technology of the ammonia-water system is proved it has certain practical disadvantages: (1) the high pressure and consequent heaviness of the equipment, (2) the corrosiveness of the fluid, (3) the problem of rectification (removing water from the ammonia during generation), and (4) as the efficiency of the cycle decreases with a increased condenser temperature an air cooled condenser cannot be used, especially in hot countries.

These problems can be avoided by using solid adsorption systems. A literature survey of solid adsorption refrigeration revealed the development of the zeolite 13X-water systems in France(Meunier and Mischer, 1979). But this pair could only produce an evaporation temperature of $0^{\circ}C$ at heat sink temperatures of $50^{\circ}C$, typical of the air cooled condensers in tropical climate. For ice making, the zeolite 13X-CH_3OH pair was reported to be suitable and it was possible to achieve an overall COP of 0.13. Bechec and others (1981) reported the design of a system using zeolite 13X-CH_3OH pair. But a later study by Guilleminot and others(1981) found the above pair chemically unstable due to a catalytic reaction which forms dimethyl ether.

Synthetic zeolites such as zeolite 13X, zeolites 3A to zeolite 10 A have ordered crystalline structure, uniform pore size, and can be tailor-made to suit a particular use. But for solar refrigeration natural zeolites are preferred as the heat of

adsorption of water on zeolites is about 2791 kJ/kg compared to a value of about 4187 kJ/kg in the case of the synthetic zeolites. Moreover, natural zeolites are reported to be about ten times cheaper than the synthetic ones (Tchernev, 1978).

Dehydrated natural zeolites, especially chabazite crystals, rapidly adsorb many kinds of refrigerant gas, ranging from water vapour and ammonia to carbon dioxide, freons, methyl alcohol ethyl alcohol, and formic acid, etc. According to Tchernev (1984) the amount of any refrigerant adsorbed by the zeolites is about 30% by weight and the adsorption phenomenon is reversible especially in the case of chabazite and modernite.

The adsorption isotherms of the zeolites have an extremely non-linear pressure dependence while silica gel has almost linear pressure dependence (Tchernev, 1978). So the zeolites can adsorb large quantities of refrigerant vapour at ambient temperature and low partial pressures. When heated, they can desorb a large amount of the refrigerant vapour even at the high condenser temperatures, i.e. at the higher pressures in air cooled condensers. For the extreme condensation and evaporation pressures of 7.3 kPa and 0.5 kPa, respectively, the differential water loading of most natural zeolites is about 7% by weight between ambient temperature and 120°C, which is about the maximum temperature attainable with flat-plate collectors with a selective surface. The daily integrated efficiency of the zeolite water pair (total cooling/daily total solar radiation) has been experimentally found by Tchernev to be in the range 12 to 15% with a peak at 30%.

Considering the merits of zeolites in solar cooling, a survey of the availability of the natural zeolites was conducted to look for the possible sources for future use in this region.

2.1 Occurrence of Zeolite Minerals

Zeolites, generally occur in sedimentary rocks and in basaltic igneous and volcanic rocks. Selected examples of the sedimentary zeolites are tabulated in Table 2.1. The different natural zeolites with the countries of their occurrences are given in Table 2.2 (Breck, 1974).

Although there are more than thirty-four known zeolite minerals and about 100 types of synthetic zeolites, only a few have practical significance either because of the dehydration irreversibility, or because of structural collapse, or because they do not occur in sufficient quantities. Out of these thirty-four zeolite minerals only seven --- modernite, clinoptilolite, ferrerite, chabazite, erionite, phillipsite, and analcime --- occur in sufficient quantity and purity to be individually considered as viable mineral resources (Vaughan, 1978). Among the seven zeolite minerals, phillipsite is one of the more abundant mineral species in the earth. Over large areas of the

Table 2.1: Sedimentary Zeolite Deposits.

Age	Location	Zeolites	Depositional Environment
1 Some typical zeolites in deposits of saline, alkaline nonmarine environments			
Recent sediments	Lake Natron, Tanzania	Analcime	Sodium carbonate lake of high salinity
Recent-late Pleistocene	Teels Marsh, Nevada	Phillipsite, clinoptilolite, analcime	Sodium carbonate lake
Late Pleistocene	Owens Lake, California	Phillipsite, clinoptilolite, erionite, analcime	Saline, alkaline lake
Late Pleistocene	Olduvai Gorge, Tanzania	Analcime, chabazite, phillipsite	Playa Lake
Middle Pliocene to Middle Pleistocene	North Central Nevada	Erionite, phillipsite	Saline, alkaline lake
Pliocene	Central Nevada	Erionite, clinoptilolite, phillipsite	Saline, alkaline lake
Early and Middle Eocene	Wyoming	Analcime	Saline, sodium carbonate lake
Triassic	New Jersey	Analcime	Saline lake, soda-rich
Early Carboniferous	Tuva, Siberia	Analcime, laumontite	Saline and alkaline lake or lagoon
2 Zeolites deposited in marine and fresh-water environments			
Recent sediments	Gulf of Naples	Analcime	Shallow marine
Recent and Pleistocene	Pacific and Indian Oceans	Phillipsite, harmotome clinoptilolite, natrolite	Deep-sea floor
Recent and late Pleistocene	Atlantic Ocean	Clinoptilolite	Deep-sea floor
Late Miocene and Pliocene	Central Nevada	Clinoptilolite	Lacustrine
Oligocene to early Pliocene	North Central Nevada	Clinoptilolite	Lacustrine
Miocene	Northern Honshu	Clinoptilolite, mordenite	Marine and lacustrine
Oligocene	South Dakota and Wyoming	Clinoptilolite, erionite	Fluvial
Cretaceous	Ural Mountains	Mordenite	Marine
Cretaceous	New Guinea	Laumontite	Marine
Early to late Triassic	New Zealand	Analcime, heulandite, clinoptilolite, laumontite	Marine
Carboniferous	England	Analcime	Land surface
Early Paleozoic or Precambrian	Georgia, USA	Laumontite	Subaerial and subaqueous

Table 2.2: A List of Zeolite Minerals.

Name	Structure Group	Year Discovered	Typical Occurence in Igneous Rocks	Examples of Occurence in Sedimentary Rocks
Analcime	1	1784	Ireland, New Jersey	Extensive; Wyoming, etc. Deep sea floor
Bikitaite	6	1957	Rhodesia	
Brewsterite	7	1822	Scotland	
Chabazite	4	1772	Nova Scotia, Ireland	Arizona, Nevada, Italy
Clinoptilolite	7	1890	Wyoming	Extensive; Western U. S., Deep sea floor
Dachiardite	6	1905	Elba, Italy	
Edingtonite	5	1825	Scotland	
Epistilbite	6	1823	Iceland	
Erionite	2	1890	Rare, Oregon	Nevada, Oregon, U.S.S.R.
Faujasite	4	1842	Rare, Germany	
Ferriente	6	1918	Rare, British Columbia, Italy	Utah, Nevada
Garronite	1	1962	Ireland, Iceland	
Gismondine	1	1816	Rare, Italy	
Gmelinite	4	1807	Nova Scotia	
Gonnardite	5	1896	France, Italy	
Harmotome	1	1775	Scotland	
Herschelite	4	1825	Sicily	Arizona
Heulandite	7	1801	Iceland	New Zealand
Kehoeite	1	1893	Rare, South Dakota	
Laumontite	1	1785	Nova Scotia, Faroe Islands	Extensive; New Zealand, U.S.S.R.
Levynite	2	1825	Iceland	
Mesolite	5	1813	Nova Scotia	
Mordenite	6	1864	Nova Scotia	U.S.S.R., Japan, Western U.S.
Natrolite	5	1758	Ireland, New Jersey	
Offretite	2	1890	Rare, France	
Paulingite	1	1960	Rare, Washington	
Phillipsite	1	1824	Ireland, Sicily	Extensive, Western U.S., Africa, Deep sea floor
Scolecite	5	1801	Iceland, Colorado	
Stellerite	7	1909		
Stilbite	7	1756	Iceland, Ireland, Scotland	
Thomsonite	5	1801	Scotland, Colorado	
Viseite	1	1942	Rare, Belgium	
Wairakite	1	1955	New Zealand	
Yugawaralite	1	1952	Japan	

Pacific Ocean sediments have been found that contain over 50% phillipsite (Breck, 1974).

Extensive deposits of various zeolites occur in North and Central America, Central and Southern Europe, Russia, Japan, Korea and New Zealand. A wide variety of the zeolite minerals like chabazite, thomsonite, natrolite, clinoptilolite and stilbite are reported to be available in abundance in Deccan Traps(specially Poona, India) by Wadia (1975) and Marel & Beutelspacher (1976). Small deposits of fibrous zeolites are reported to be found at Mount Wyatt, Upper River Madai, middle reaches of River Tingakayu, Salagan Island and abundant deposits have been found in Kalunpang in Simporna Peninsula of North Borneo (Kirk, 1962). Abundant high grade natural zeolites such as clinoptilolite, heulandite, mordenite, ferririte, erionite, analcinite, chabazite, mesolite, and natrolite are found in the Yeongil area, South Korea (Noh and Kim. 1986). Significant deposits of the natural zeolites of importance as given by Marel and Beutelspacher (1976) are given in Table 2.3.

Table 2.3: The countries having significant deposits of natural zeolites.

Zeolite Type	Country of Origin
Chabazite	Hungary, Faroe Islands, Ireland; Bohemia, Czechoslovakia; Global Station, Oregon, New Jersey and Nova Scotia.
Clinoptilolite	Hector, California.
Stilbite	Banat Csiklova, Roumania; Hanz, West Germany; Iceland, Faoer Islands, Nova Scotia.

2.2. Occurrences of Natural Zeolites in Japan

In this region, Japan, India and Korea are the likely potential sources for natural zeolites. Zeolite mineral was originally discovered in sedimentary rock in Japan (Ota and Sudo, 1979). The most commonly found zeolite tuffs (Zeolite having particle size smaller than 4mm in diameter), modernite and clinoptilolite, are both abundant in Japan. Both the modernite and the clinoptilolite-tuff are reported to show excellent adsorptive properties compared with commercial adsorbents, such as synthetic zeolites 5A, silica gel, and activated alumina. Because of high affinity for water, clinoptilolite-tuff is primarily used as a desiccant. About 5000 to 6000 tons of these

zeolites per month, are mined from the different open-pit mines in Japan. Some of the zeolite mines in Japan are listed in Table 2.4 (Minato, and Tamura, 1978).

Table 2.4: Zeolite Mines in Japan.

Mine	Prefecture	Amount of ore (t/month)	Zeolite
Osiyamambe	Hokkaido	100–200	Clinoptilolite
Futatsui	Akita	150–300	Clinoptilolite
Yasawagi	Akita	100–200	Clinoptilolite and mordenite
Itado	Akita	Spot (about 300 t)	Mordenite
Itaya	Yamagata	4000–5000	Clinoptilolite
Shiroishi	Miyagi	100–200	Mordenite
Ten'ei	Fukushima	100–200	Mordenite
Maji	Shimane	Spot (about 300 t)	Mordenite
Iwami mine	Shimane	50–100	Clinoptilolite

III Zeolite-Water Solar Refrigerator

3. Introduction

Some zeolite-water solar refrigerators were built and tested mainly in the cold countries like USA and France but none of them have been tested in a tropical climate. It is essential to evaluate the performance of such systems in this climate to find out their suitablity for possible future use. So, a zeolite-water solar refrigerator manufactured by Zeopower Company, USA was imported and tested at Asian Institute of Technology. This is a closed cycle intermittent adsorption type refrigerator which has natural zeolite as adsorbent and water as the refrigerant. A schematic diagram of this refrigerator is shown in Fig. 3.1. It consists of a selectively coated solar collector with a single glass cover. The solar collector is a rectangular copper pan with a lid, and contains about 25.63 kg of dehydrated natural zeolite about 50mm deep. The tilt angle of the solar collector is 14° which is almost equal to the latitude of AIT. This system consists of an air cooled condenser placed under the solar collector. A glass bottle graduated in BTU's, and housed in an insulated box acts as the receiver/evaporator. These components are connected by copper tubes. This system operates below the atmospheric pressure, so it was evacuated, leak tested, filled with about 8.4 kg of water and hermetically sealed before being shipped for testing at AIT. The specifications supplied by the Zeopower Company, USA are as follows:

3.1 Specifications of the frigerator

Type: Liquid with Solid/Gas Adsorption System.
Model : SR-4
Gross Collector Dimensions : 29" x 47" = 0.8786 m²
Net Collector Absorbing Surface Area : 25" x 43" = 0.6935 m²
Overall Dimensions:

Height	46 1/4"	(1.175 m)
Width	30 1/2"	(0.7742 m)
Depth	48 1/2"	(1.232 m)

Refrigeration Capacity : 4 Cubic feet = 0.112 m³
Ice Making Capacity : 15 lbs or 6.803 kg per day.
Storage Capacity : Three days of bad weather after collector surface has been exposed to a series of three or more sunny days.
Maintenance Requirements : None.
Moving Part : None except the door of the refrigerator box.
Total Weight : 215 lbs (97.505 kg).

3.2 Experimentation, Test Results and Conclusions

During intial testing, the refrigerator was instrumented with a few calibrated k-type temperature sensors which were attached to the top and bottom of the condenser, top and bottom of the
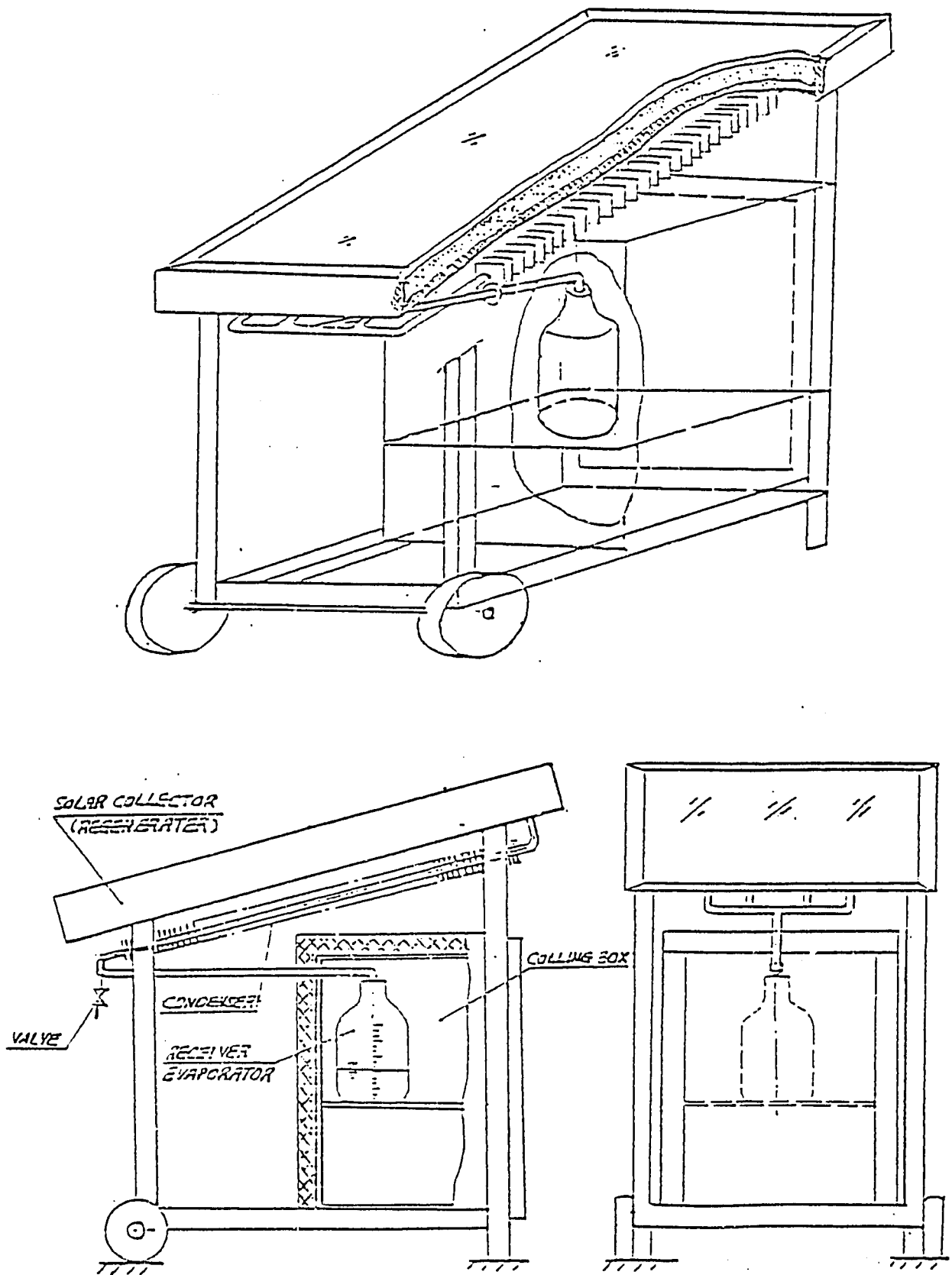
Fig. 3.1: Schematic diagram of the Zeolite-Water Refrigerator.

glass bottle (receiver/evaporator), and one senser was left hanging in the cooling chamber. These temperature sensors were connected to a Fuji Chart Recorder and values were recored continuously. Integrated and the instanteneous values of solar radiation incident on the surface of the collector were measured by a calibrated diffused type pyranometer with integrator, and hourly values were read from a digital display. The amount of heat rejected by the condensing water during desorption was estimated by taking the difference of water level in the morning and late afternoon from the glass bottle, calibrated in BTU's by the manufacturer. Similarly, the difference of readings between late afternoon and the early morning gives the net cooling produced by evaporation of water from the glass bottle during night. The water level in the receiver/evaporator bottle was read every hour until 24:00 hours.

The refrigerator was in transit for a couple of weeks and the zeolite had adsorbed approximately 7.9 kg of water (30.71 wt. %, dry basis) out of about 8.37 kg charged into the system. During the days of average insolation, water started to desorb between 10:00 and 11:00 hours and the desorption continued until the peak temperature for the day was reached generally by 15:00 hours. The zeolite, although, starts to adsorb water immediately after peak collectr temp rature but noticeable change in water level was observed only after 18:00 hours. During first few days comparatively large quantities of water desorbed as the zeolite was saturated with water during transit, but only a fraction of desorbed water was adsorbed during subsequent nights. The system took several days to achieve near equilibrium condition as could be seen comparing the amount of heat rejected and cooling produced from Table 3.1. The cooling produced during night varied from 316 to 844 kJ. It was observed that the condenser temperature was very high and reached up to 57°C. During 5, 6, and 7 November 1986 two blowers were used to cool the condenser. Although the use of blowers did not help to reduce the condenser temperature significantly but the average condenser temperacure was lower and the integrated efficiency or Solar COP (cooling produced/total daily incident solar radiation) was between 6.1% and 6.7% which are higher.

As stated by the manufacturer, the system should be able to produce about 6.8 kg of ice during a clear day. To produce that much ice the system should cycle more than 1 kg of water. But even after several days of operation, the receiver/evaporator bottle contained only about 2.45 kg of water (estimated by the measurement of the external dimensions of the glass receiver/evaporator); and only a fraction of this (approximately 130 to a maximum of 360 gm of water) was readsorbed during cooling period. The system was not able to produce ice and the sensor attached to the bottom of the glass bottle recorded temperatures always above 4°C. Moreover, the condensation starts in the glass bottle, as it is the coldest and it continues

Table 3.1. The summary of test results of Zeolite-Water Solar Refrigerator (22 Oct. 1986 -- 16 May 1987).

Date d/m/y	Ambient Temp. Max. (C)	Temp. Min. (C)	Evaporator Temp. Minm. (C)	Zeolite Temp. Max. (C)	Temp. Min. (C)	Condenser Temp. Max. (C)	Heat Rejected (kJ/day)	Cooling Produced (kJ/day)	Solar Radiation (MJ/day)	Solar COP (%)	Remarks
22/10/86	31.0	27.5	7.2	--	--	48.0	3166.2	527.0	12.029	4.4	
23/10/86	30.6	27.7	7.2	--	--	48.7	369.3	485.5	7.520	6.5	
24/10/86	33.4	27.7	7.2	--	--	55.9	1224.3	580.5	11.122	5.2	
25/10/86	33.0	28.3	7.1	--	--	47.4	52.8	527.7	6.002	8.8	Initial
26/10/36	33.0	28.3	5.8	--	--	55.0	949.9	580.5	11.561	5.0	Testing
27/10/86	31.3	28.5	6.6	--	--	57.0	369.4	527.7	8.568	6.2	without
28/10/96	34.1	27.3	5.8	--	--	51.0	527.7	527.7	9.172	5.8	any
30/10/86	28.4	25.8	5.1	--	--	47.0	527.7	316.6	9.612	3.3	modifications.
31/10/86	29.9	26.4	6.4	--	--	45.1	316.6	369.4	9.030	4.1	
1/11/86	32.0	27.3	7.2	--	--	52.0	949.8	474.9	11.918	4.0	
2/11/86	31.7	27.0	3.7	--	--	52.0	633.2	633.2	12.248	5.2	
3/11/86	33.7	27.7	4.1	--	--	61.0	738.8	633.2	11.726	5.4	
4/11/86	33.7	25.9	3.8	--	--	57.0	686.0	686.0	13.099	5.2	
5/11/86	33.4	23.5	6.0	--	--	50.0	633.2	791.5	11.754	6.7	Tests
6/11/86	36.2	23.8	6.0	--	--	52.0	791.6	738.8	12.029	6.1	with
7/11/86	32.7	24.1	5.1	--	--	48.0	897.1	844.3	12.173	6.9	two blowers.
9/12/86	29.6	21.0	8.8	105.0	26.3	46.6	622.1	400.9	11.369	3.5	
10/12/86	29.0	18.7	6.6	109.0	22.8	48.1	506.4	316.5	12.056	2.6	Tests after
23/12/86	32.0	18.6	10.6	109.0	21.8	49.9	422.0	316.5	11.232	2.8	the loss of
24/12/86	32.1	19.7	9.3	111.0	24.8	50.8	527.5	422.0	11.946	3.5	Inert Gas.
25/12/86	34.6	19.4	8.8	112.0	24.3	54.1	474.8	474.8	12.221	3.9	
15/5/87	36.2	24.7	10.2	114.0	26.8	44.2	1022.5	279.1	10.661	2.6	With mirror
16/5/87	37.5	26.1	8.0	127.0	29.0	40.9	930.4	325.6	14.056	2.3	boosters

Note:

1. Heat rejected by the condenser is equal to the latent heat of water condensed in the receiver.

2. The Zeolite temperature was assumed equal to mean container temperature.

3. Cooling produced at night is equal to the heat extracted by the evaporation of water, while the latent heat of evaporation of water is 2326 kJ/kg (Tchernev, 1979).

until the temperature of the bottle reaches the ambient temperature. This has serious consequences as the ice produced by the system is not removable and part of the cooling produced during night will be used to condense the water vapour.

After this initial testing, some sensors were attached to the top and bottom of the absorber plate to measure the approximate collector and zeolite temperatures. During this modification due the defective valve in the supplied system, some air leaked into the system which was evacuated immediately after the pressure gauge and isolation valves assembly was soldered. The temperature of the zeoloite panel(collector) during a clear day having total incident solar radiation between 18 and 19 MJ/m^2-day reached up to 105°C; even then it was not high enough to give significant desorption. The amount of water cycled was found less than 1%. Since the performance of the system became worse, it was decided to evacuate the system as completely as possible and recharge again. The system was further modified and tested by Zhu (1987). In one important modification, two mirror boosters each having about 0.812 m^2 area were attached along the length of the system (Fig. 3.2). The solar collector was heated using mirror boosters and evacuated during late morning until late afternoon almost for a month. The minimum concentration of water in the zeolite reached about 16.5% from 31.71 wt. % initially charged into the system. Then the system was charged with a small quantity of water in steps over of sevaral days. The charging system with isolation valves is shown in Fig. 3.3. The performance of the recharged system (water content in the zeolite about 21.4 wt. %, dry basis) is shown in Table 3.1 (8-16 May, 1987). During these days, the average collector temperature was found higher than the average found earlier as there was less water charged into the system, but the amount of water cycled was less and surprisingly zeolite did not adsorb more than 22 wt.%, (dry basis) in subsqent charging. It is seen from Table 3.1 that the solar COP of the recharged system varied between 2.3 and 2.6%, which is lower than the unmodified system. We came to know about a small amount of inert gas initially charged into the system the supplier (Worek, 1986) which unfortunately escaped during first modification. Since, no further information about the type and the quantity of the inert gas was available, and since the system did not perform as well when the inert gas was intact, no further tests were carried out.
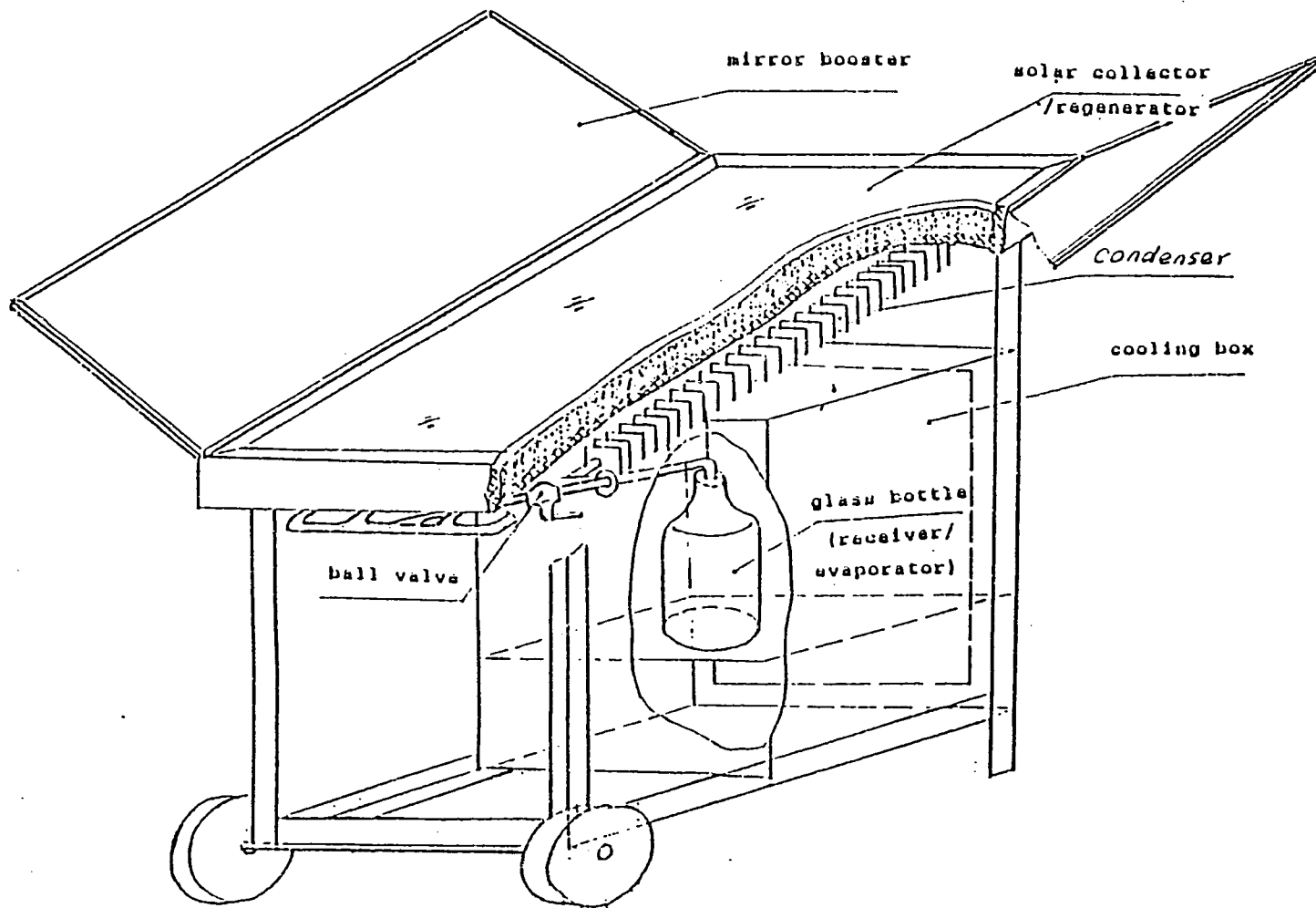
Fig. 3.2: Modified Zeolite-Water Refrigerator.
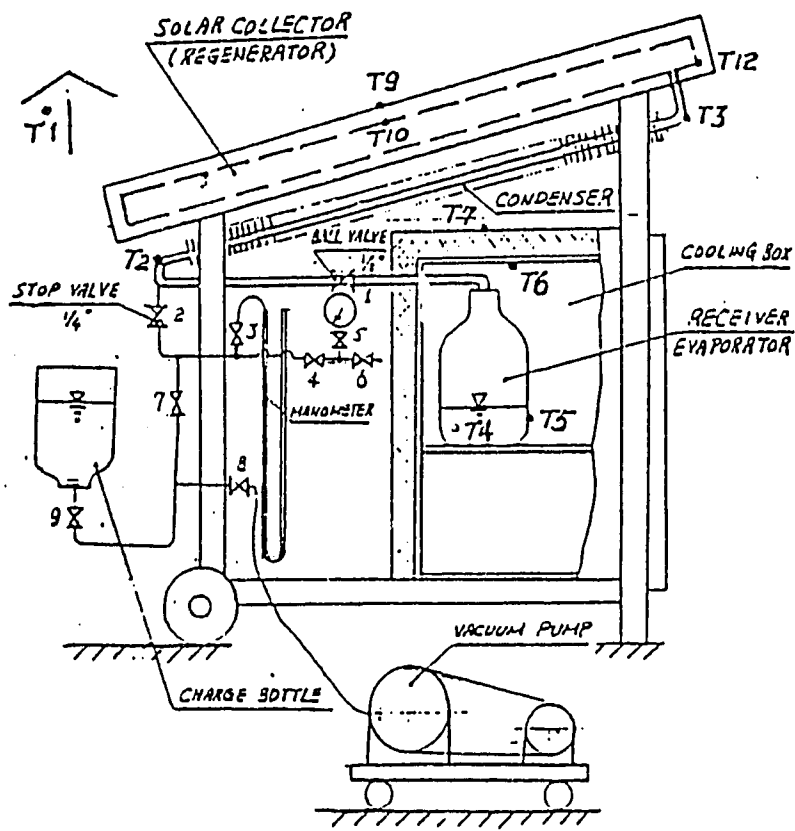
Fig. 3.3: Modified Charging System.

IV Work Carried out at AIT on the Charcoal-Methanol Pair

4. Introduction

The performance of the zeolite-water solar refrigerator was found not very promising during the initial testing and further research was done to investigate other pairs.

The comparison of synthetic zeolite 5A, 13X and activated charcoal(AC) with different refrigerants R11, R12, R22, and R114 done by Critoph and Vogel (1986) proved charcoal as the preferable adsorbent for solar cooling. We also became aware of the study done by Grenier and Pons(1983), Meunier and others (1986) on synthetic zeolite-methanol and the charcoal-methanol pairs. Their study revealed that charcoal-methanol gives a better COP generally, but that when the night-time ambient temperature-evaporating temperature is particularly high then a zeolite-water combination is better. However this will require a higher generating temperature from the solar collector during the day. The comparison of zeolite 13X-water and AC 35-methanol done by Meunier and others(1986) suggest that zeolite combinations will only be superior when the temperature lift (difference between adsorption and the evaporating temperatures) exceeds 45°C. The COP is based on heat input to the adsorbent rather than the solar collector and so the reduced solar collector efficiency at higher temperatures may actually make charcoal-methanol combinations superior even at higher temperature lifts.

The others reasons for preferring activated charcoal are as follows:

1. Activated charcoals are cheaper than zeolites.
2. Activated charcoals can be made with properties to suit particular applications by varying the activation time and temperature, etc.
3. Activated charcoals (particularly coconut shell charcoal) can be manufactured in the country of origin and use.

Because of above advantages and the encouraging French results it was decided to investigate the methanol-charcoal system under the terms of the USAID contract.

The properties of the activated charcoals such as porosity, pore size, and surface area for adsorption depends upon the raw material used, the activation process and the degree of activation. Accordingly, we carried out tests to investigate the adsorption properties of some imported and locally available charcoal samples for their possible use in solar refrigeration.

4.1 Experimental Setup and Procedure

The test rig (Fig. 4.1) used to determine the equilibrium data has a brass container A which was filled with a known quantity of a activated charcoal sample (usually 100 gms), a
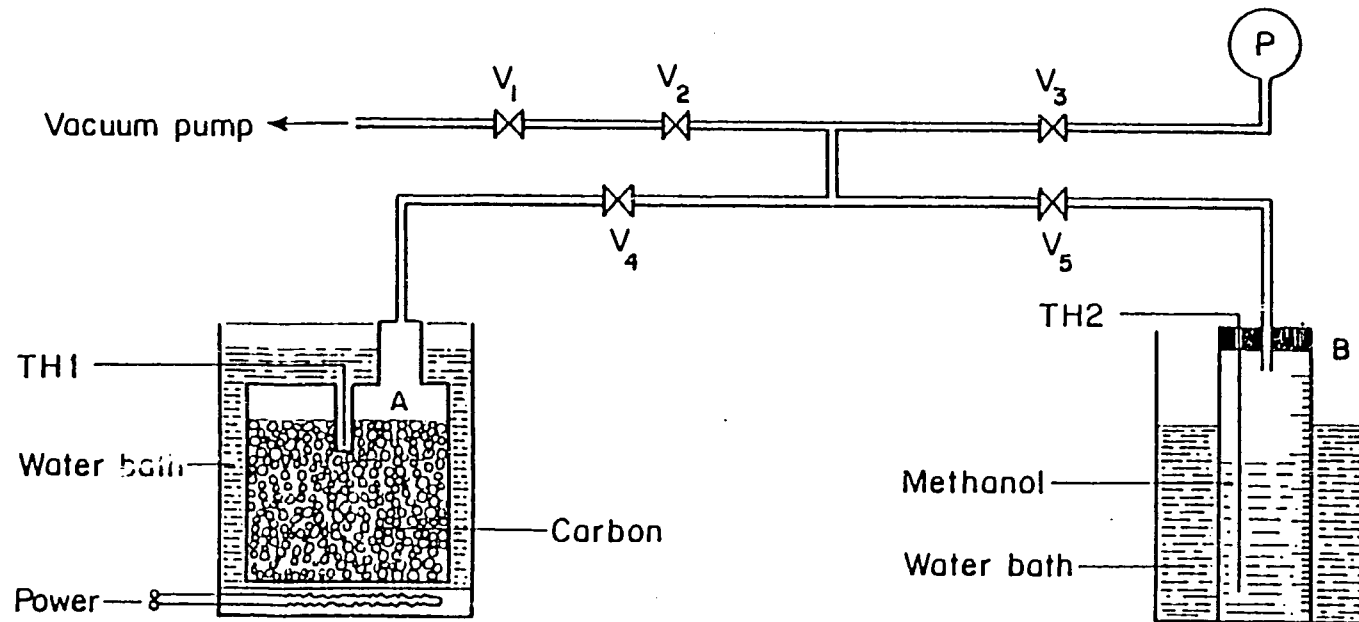
A — Activated carbon container
B — Methanol receiver cum evaporator
P — Vacuum gauge
THI — Thermocouple conn. for carbon temp.
TH2— Thermocouple conn. for methanol temp.
V_1.....V_5 — Isolation valves.

Fig. 4.1: Schematic of the Experimental Setup.

graduated glass vessel B for containing methanol, and a vacuum
gauge P. The methanol level can be read from the graduations of
B and the quantity of methanol in the charcoal can thus be
calculated at any time. The temperatures of the charcoal and
methanol can be read from two calibrated k-type thermocouples
TH1 and TH2. The components A, B, and P were separated by
isolating valves V1 through V5 to facilitate evacuation of each
components separately and checking leaks. The piping was of
1/4" soft copper and all valves were soldered to successfully
maintain the system vacuum tight.

The activated charcoal was degassed over at least two days by
heating the charcoal at about 100°C and continuously evacuating
it. This was done to drive out impurities present in the deep
pores before actual adsorption/desorption takes place.
Similarly, methanol contained in vessel B was separately
evacuated and a small amount of methanol was allowed to boil out
to ensure no dissolved air remains in the methanol. Equilibrium
data were obtained along two isobars (0.13 bar and 0.04 bar)
keeping the methanol in B at constant temperature while varying
charcoal temperatures. To obtain the desorption data, charcoal
saturated with methanol at about 30°C was heated in steps of
10°C approximately to 100°C. Sufficiently long time was allowed
to reach the near equilibrium and at each step pressure,
temperature and concentration were measured. Similarly
adsorption data were obtained cooling the charcoal in the steps
of 10°C back to 30°C. For each sample, to get the better data
points, up to three such adsorption/desorption cycles were
repeated at each isobar. In case of slight deviation, the
latest data were taken as correct.

In total, eight samples of activated charcoal, six imported
and two local were tested. The specifications for the
charcoals supplied by the manufacturers are listed in Table 4.1.

4.2 Data Analysis and Results

The data obtained along two isobars can be used easily, when
plotted on a ln P versus -1/T graph, for applications like
refrigerations etc. The ideal cycle, which consists of two
isobars and two isosters can be easily traced in such diagrams.
Since we can determine the state points on this diagram, the
performance of such systems can be determined. Moreover, the
slopes of the straight lines (isosters) directly give the heat of
adsorption/desorption. The pressure-temperature-concentration
(p-T-x) diagrams for charcoals tested are shown in Fig. 4.2
through Fig. 4.6. For three charcoals the p-T-x diagrams are not
presented, due to lack of consistent data points at both the
pressures.

4.2.1 Applications of the Dubinin Equation

The best established description of adsorption in activated

Table 4.1: Manufacturer's Data.

SUTCLIFFE CARBONS CO. LTD., U. K.

COCONUTSHELL BASED CARBONS

GRADE	SURFACE AREA m²/g B.E.T N2	BULK DENSITY g/cc	CTC %	ASH %
203C	700 — 800	0.55 — 0.59	20 — 30	1.0 — 2.0
205C	900 — 1000	0.53 — 0.57	35 — 45	2.0 — 2.5
207C	1100 — 1200	0.49 — 0.53	50 — 60	2.5 — 3.0
208C	1200 — 1300	0.47 — 0.51	60 — 70	3.0 — 4.0
† 607	1100 — 1200	0.49 — 0.53	50 — 60	0.5 — 1.0
610	1300 — 1500	0.40 — 0.44	80 — 90	3.0 — 4.0

† Type 607 is a specially prepared acid washed carbon with low ash and high ignition temperature for use in solvent recovery or condensate de-oiling.

* The bulk density is carried out on dry base carbon with nominal mesh size 7-18BSS.

IMPREGNATED & MISCELLANEOUS SPECIAL CARBONS

207E3(EXTRUDED)	1100 — 1200	0.45 — 0.49	55 — 65	4.0 — 8.0
207E4(EXTRUDED)	1100 — 1200	0.45 — 0.49	55 — 65	4.0 — 8.0

UDP CHEMICAL CO. LTD., BANGKOK.

TYPICAL APPLICATIONS : MD-G 7746

MD-G 7746 is designed for removal of odourous atmosphere in industrial processes and in air conditioning systems, including a variety of purification and separation processes in the chemical industries.

GENERAL SPECIFICATIONS AND PROPERTIES

Mesh Sizes _____ 4 x 6
Iodine Number Min. _____ 1050
Methylene Blue Number Min. _____ 200
Abrasion Number Min. _____ 80
Hardness Number Min. _____ 90
Moisture as packed Max. % _____ 3
Residue on Ignition. Max: % _____ 3
pH _____ 8-9
Surface Area (N₂-B.E.T.) _____ 1100-1200
Bulk Density. g/cc. _____ 0.40-0.45

TYPICAL APPLICATIONS : MD-W 7830

MD-W 7830 is recommended for water purification both in municipal and industrial use. It is also popular in a variety of separation and purification processes in the organic chemical industries.

GENERAL SPECIFICATIONS AND PROPERTIES

Mesh Sizes _____ 8 x 30
Iodine Number Min. _____ 1050
Methylene Blue Number Min. _____ 220
Abrasion Number Min. _____ 80
Hardness Number Min. _____ 90
Moisture as packed Max. % _____ 3
Residue on Ignition. Max. % _____ 3
pH _____ 8-9
Surface Area (N₂-B.E.T.) _____ 1150-1250
Bulk Density. g/cc. _____ 0.50-0.55
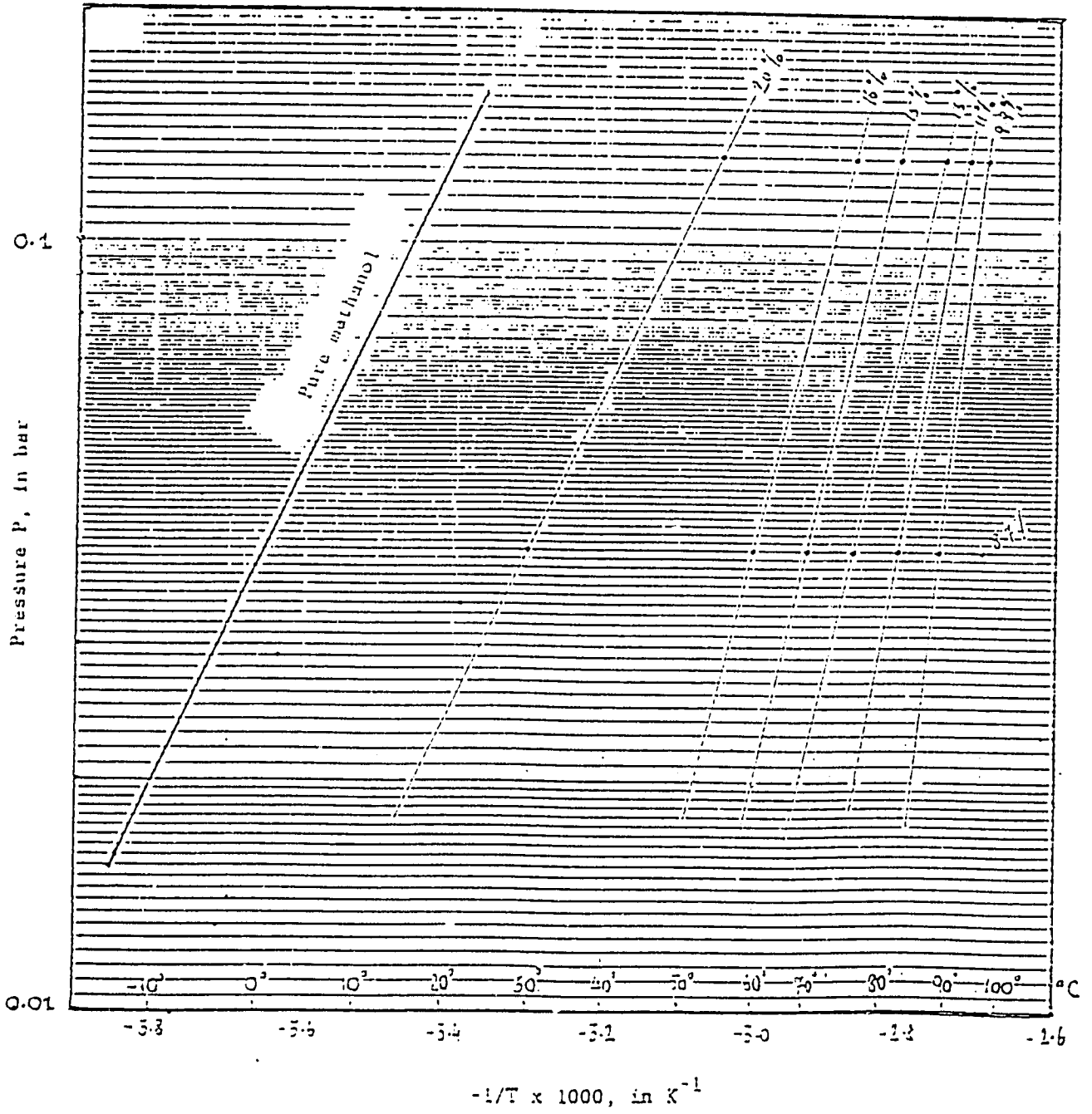
Fig 4.2: Experimental isosteres on a ln P versus -1/T plot.

(a) Carbon 207C
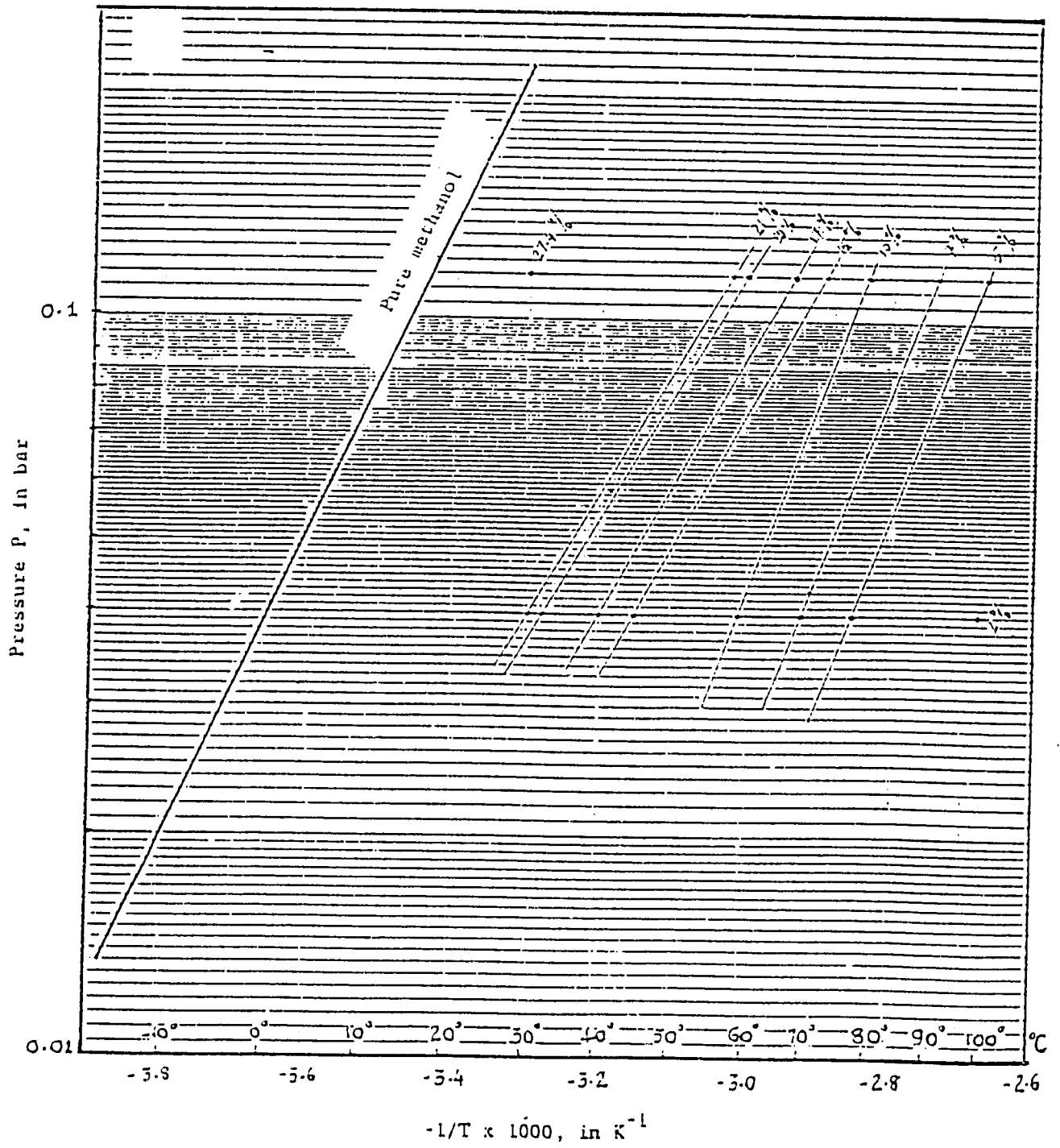
Fig 4.3: Experimental isosteres on a ln P versus -1/T plot.

(b) Carbon 207E
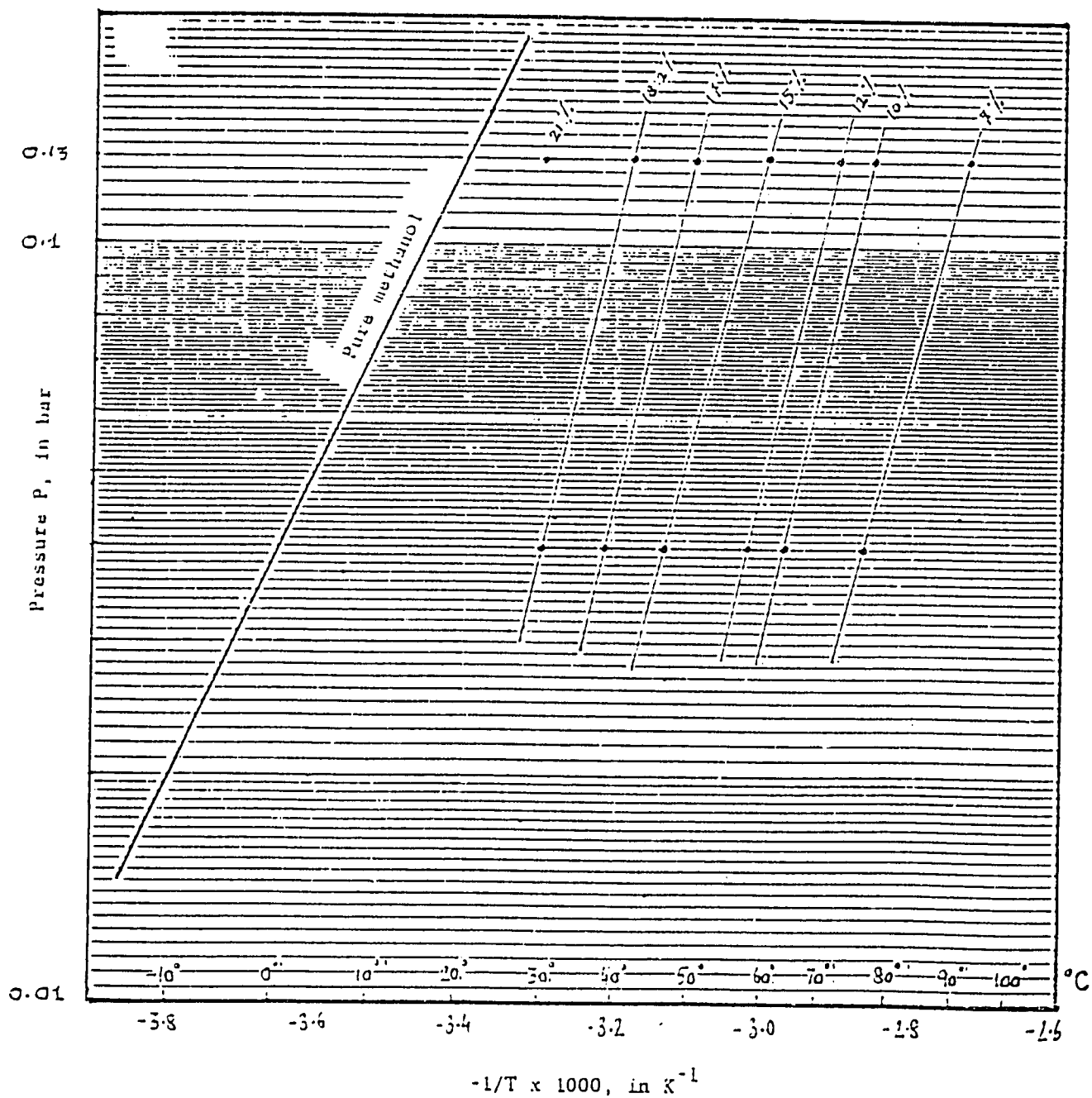
Fig 4.4: Experimental isosteres on a ln P versus -1/T plot.

(d) Carbon 610
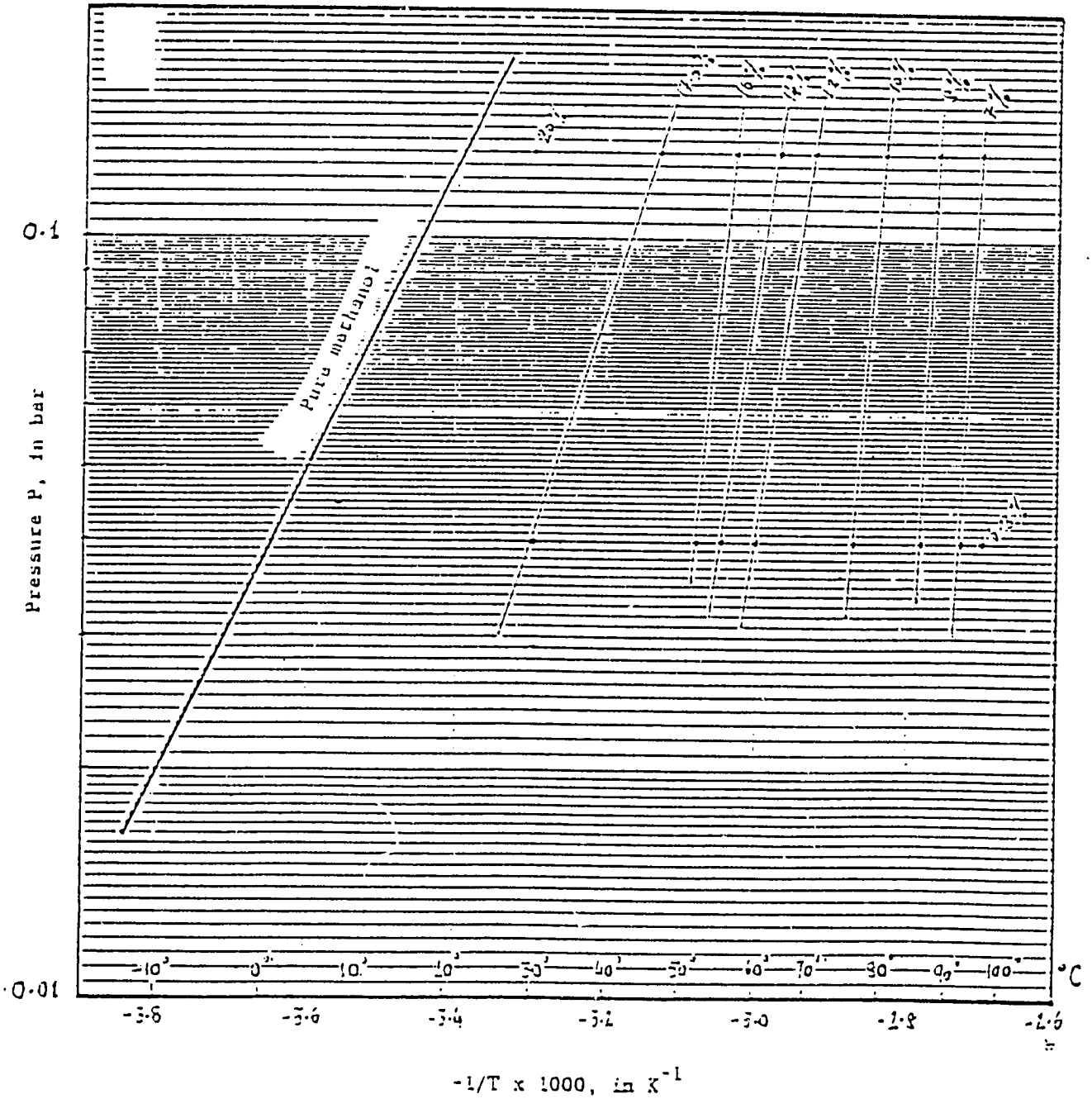
Fig 4.5: Experimental isosteres on a ln P versus -1/T plot.

(e) Carbon THAI-1
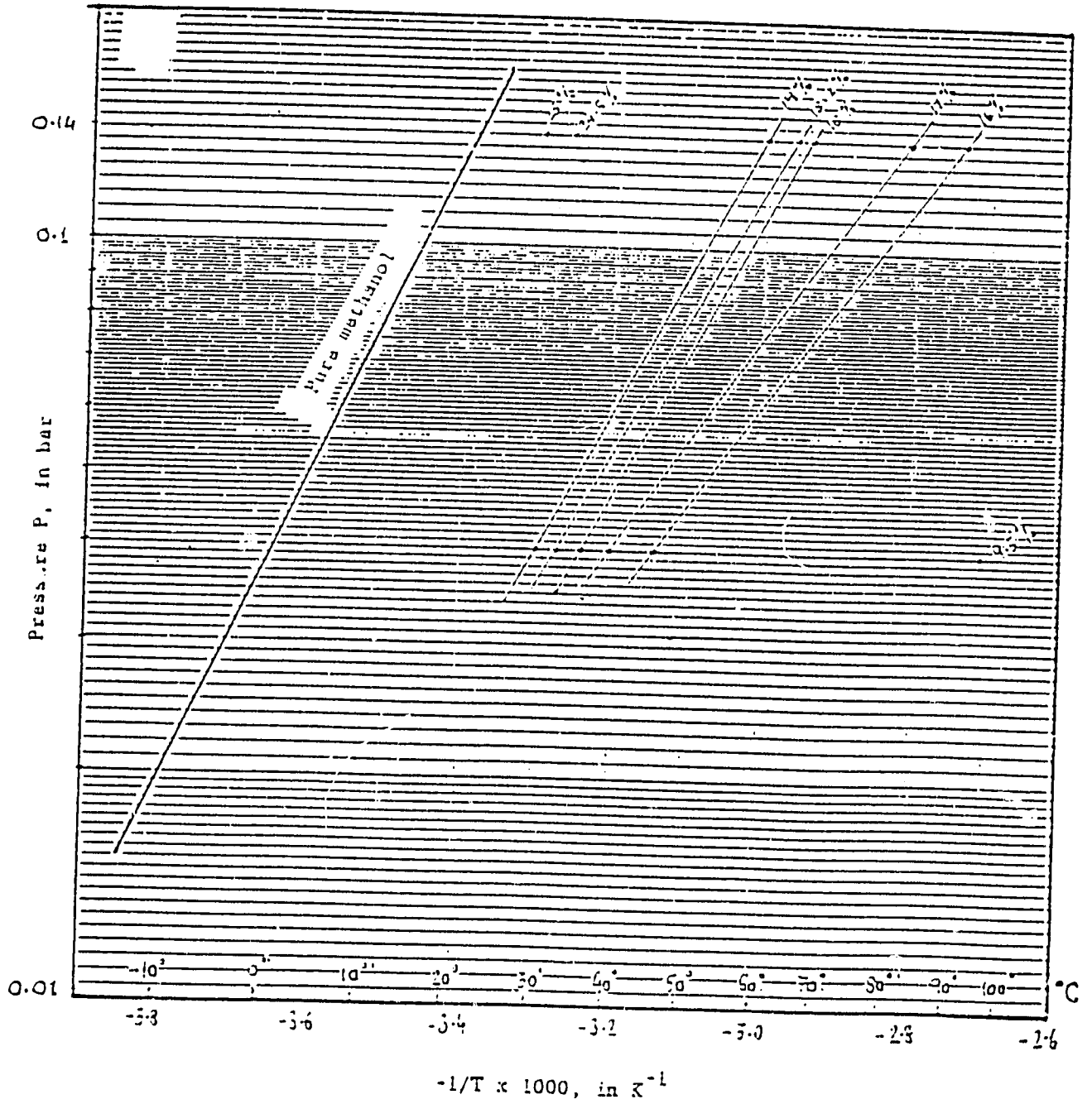
Fig 4.6: Experimental isosteres on a ln P versus -1/T plot.

(f) Carbon THAI-2

charcoal as proposed by Polayani(1970) is based on the potential theory. But the analytical form for the adsorption isotherm was by given Dubinin(Smisek, and Cerny, 1970). This theory of volume filling of micropores applies over a large range of relative pressures, and the fundamental equation originally proposed by Dubinin and Radushkevich(D-R equation) can be expressed as (Smisek and Cerny, 1970):

$$W = W_o \exp(-k \ (RT \ln P_s/p)^2) \tag{4.1}$$

where
  W = Volume filled by the adsorbate,
  W_o = Maximum volume of the adsorption space,
  k = A parameter which primarily depends upon the number and size distribution of micropores and also upon the adsorbate, as adsorbents have different affinities for different adsorbates,
  R = Gas constant,
  T = Absolute temperature,
  Ps = Saturated vapour pressure of adsorbate at temp. T,
  P = Equilibrium pressure.

The above equation is valid for temperatures sufficiently below the critical temperatures T_c (T < 0.8 T_c or T < $T_{b.p.}$). If we consider k' is the same parameter for the standard vapour whose affinity coefficient β is equal to 1 , then $k = k'/\beta^2$. Thus k now will be function of the structure of the adsorbent only and its value will not depend on the adsorbate as the difference in adsorption properties of different vapours from those of the standard vapour (normally benzene) is accounted by β; which is a function of adsorbate only. The D-R equation can thus be written as:

$$W = W_o \exp(- B \ (T/\beta \ln P_s/P)^2) \tag{4.2}$$

where B is a function of the adsorbent microstructure, the more the microporous the charcoal is, the smaller is B.

The density of the adsorbed phase in the above case can be assumed to be same as that of liquid adsorbate at the same temperature provided that temperature is well below the critical temperature.

The usefulness of this equation lies in the separation of adsorbate and adsorbent properties, since affinity coefficient which is the ratio of adsorbate molar volume at T to that of reference gas at the same temperature T, can easily be determined. The affinity coefficient of different adsorbates on activated charcoal is given in Table 4.2(Smisek and Cerny, 1970). The two parameters Wo and B can be determined by plotting the experimental data in the linear form. Unfortunately, some deviations from linearity were observed by Marsh and Rand (1970). So, the Dubinin and Astakhov (D-A) equation (1970), which

Table 4.2: The Affinity Coefficient β for some vapours on Charcoal.

	β		β
Benzene	1.00	Dichloromethane	0.66
Cyclobenzane	1.04	Ethyl Chloride	0.76
Toluene	1.25	Ethyl Ether	1.09
Propane	0.78	Acetone	0.88
n-Butane	0.90	Formic acid	0.61
n-Pentane	1.12	Ammonia	0.28
n-Hexane	1.35	Nitrogen	0.33
n-Heptane	1.59	Carbon Disulphide	0.70
Methanol	0.40	Acetic acid	0.97
Ethanol	0.61	Xenon	0.50
Methyl Chloride	0.57	Krypton	0.37
Methyl Bromide	0.56	Chloroform	0.86

introduces a third variable n in the parameter to improve the fit of the experimental data, is given as:

$$W = W_O \exp(- D \{ T \ln P_S/P)^n)$$ (4.3)

Writing this in the linear form we obtain:

$$\ln W = \ln W_O - D (T \ln P_S/P)^n$$ (4.4)

When $n = 2$, the D-A equation is equivalent to the D-R equation.

The p-T-x data when plotted in the D-R form gives a straight line if adsorption follows the theory of volume filling of micropores. Thus plotting $\ln W$ versus $(T \ln P_S/P)^2$ the values of Wo and D can be determined. The D-R plots for the different charcoals tested are shown in Fig. 4.7 through 4.10.

If the D-R equation applies, the experimental points determined at two isobars theoretically merge to a single straight line. But over some part of the experimental range distinct disagreement has been observed as seen from the D-R plots. This has been attributed to the not so sophisticated experimental setup and also due to presence of mesopores in some charcoals. In some cases the data obtained along one of the two isobars was found inconsistent even when it was repeated to several cycles and the D-R plots are for the data points along one isobar. But most of the charcoals tested showed results close to ideal ones, and linear plots having correlation coefficient r between 0.96 and 0.97 were obtained with the exception of Thai-2 which has the correlation coefficient equal to 0.87. The values of Wo, D and correlation coefficient r are given in Table 4.3. It is seen that charcoal 607 has the highest value for Wo followed by 207E3, which means their adsorption capacities for methanol are larger. Other charcoals have also shown significant adsorption capabilities expect for Thai-2 which showed the lowest value, although Thai-1 and Thai-2 were from two different batches from the same manufacturer. This might be due to different degrees of activation in different batches.

4.3 COP Calculations

Since we know the constants for the Dubinin equation Wo and D, the relationship between p, T, x is known, where x is the concentration of the refrigerant adsorbed (kg/kg of charcoal). Once this relation is known, with the knowledge of any two parameters the third can be calculated, and thus the coefficient of performances (COPs) for different applications can be calculated.

4.3.1 Ideal Cycle

The ideal cycle operating this type of system consists two

(a)
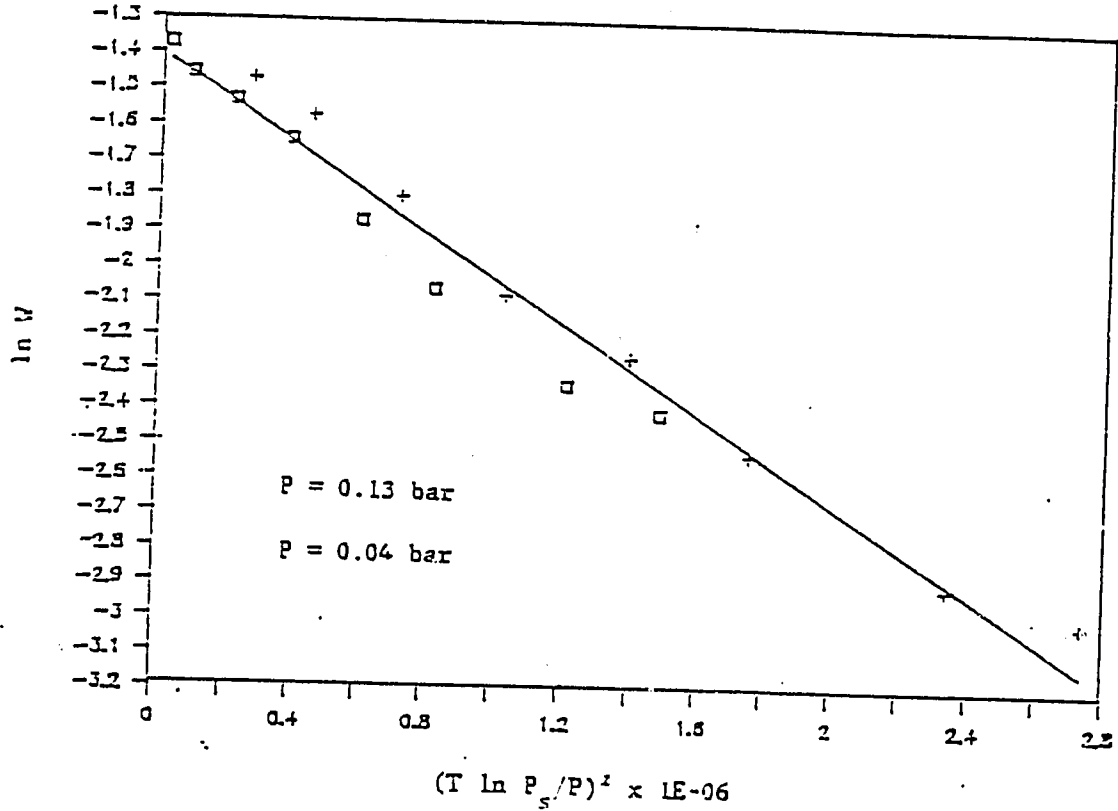
(b)
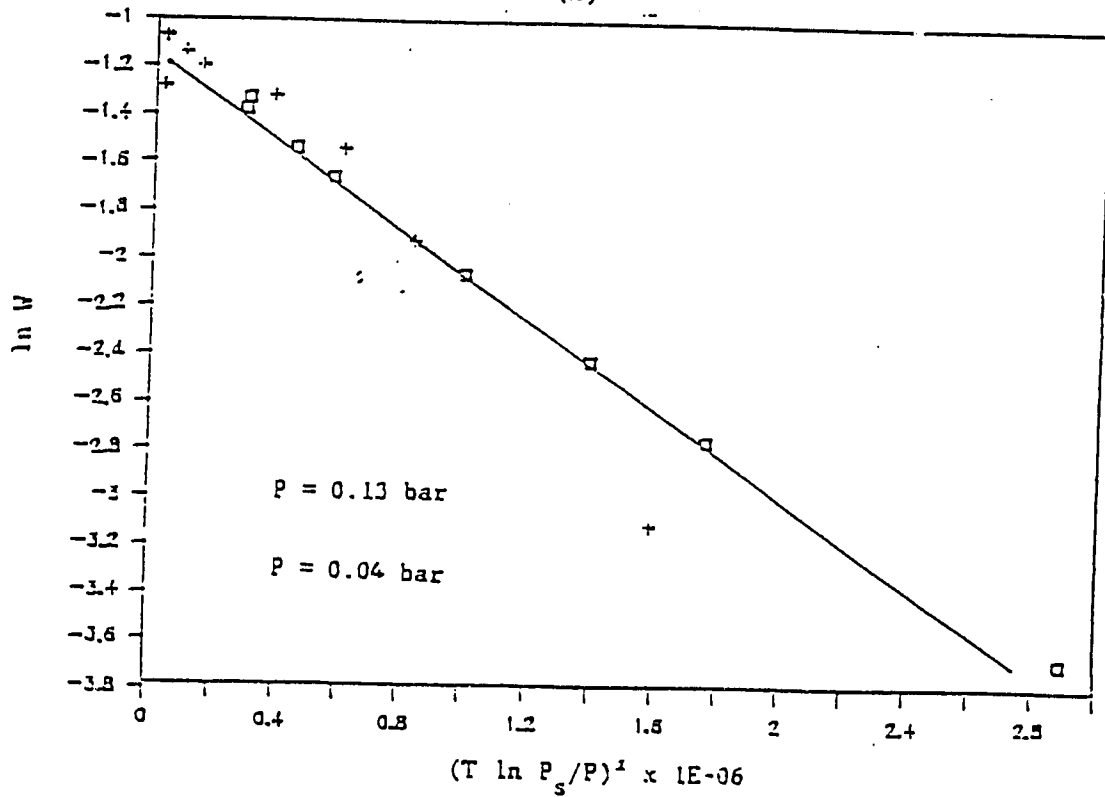
Fig 4.7: Characteristic curve obtained on a D-R plot.
(a) Carbon 207C   (b) Carbon 207E
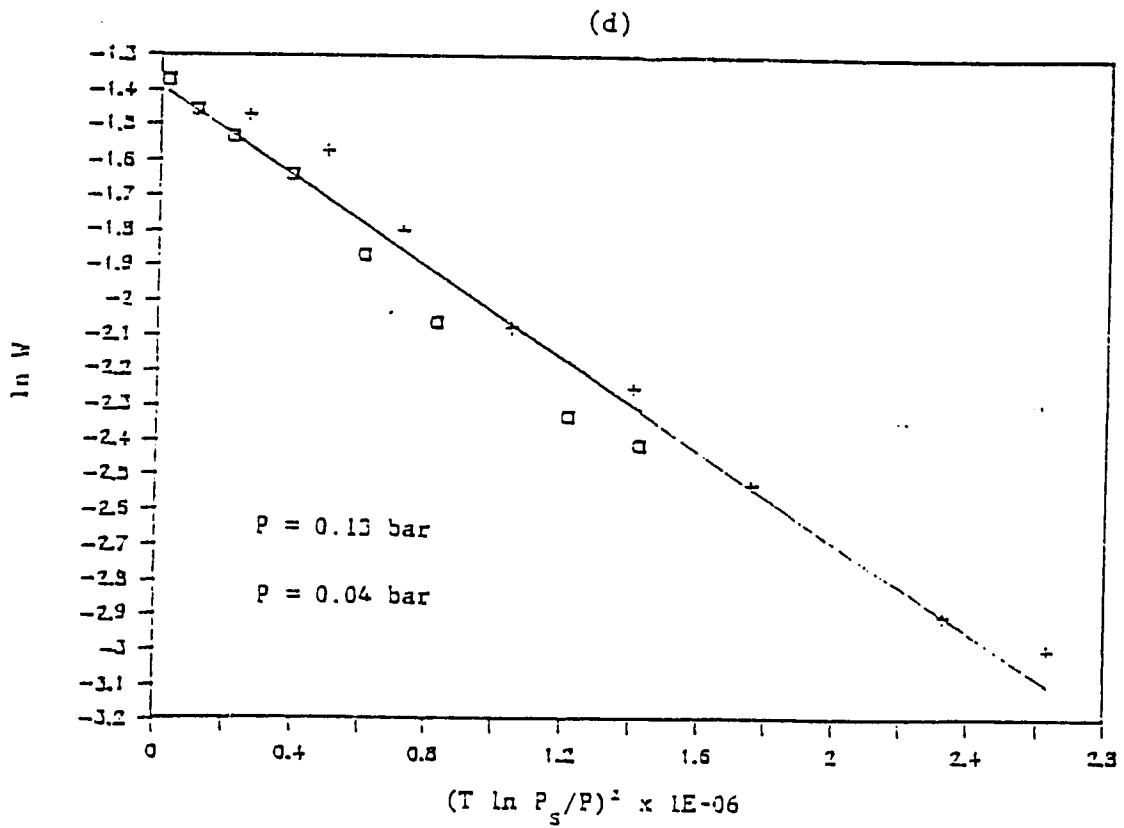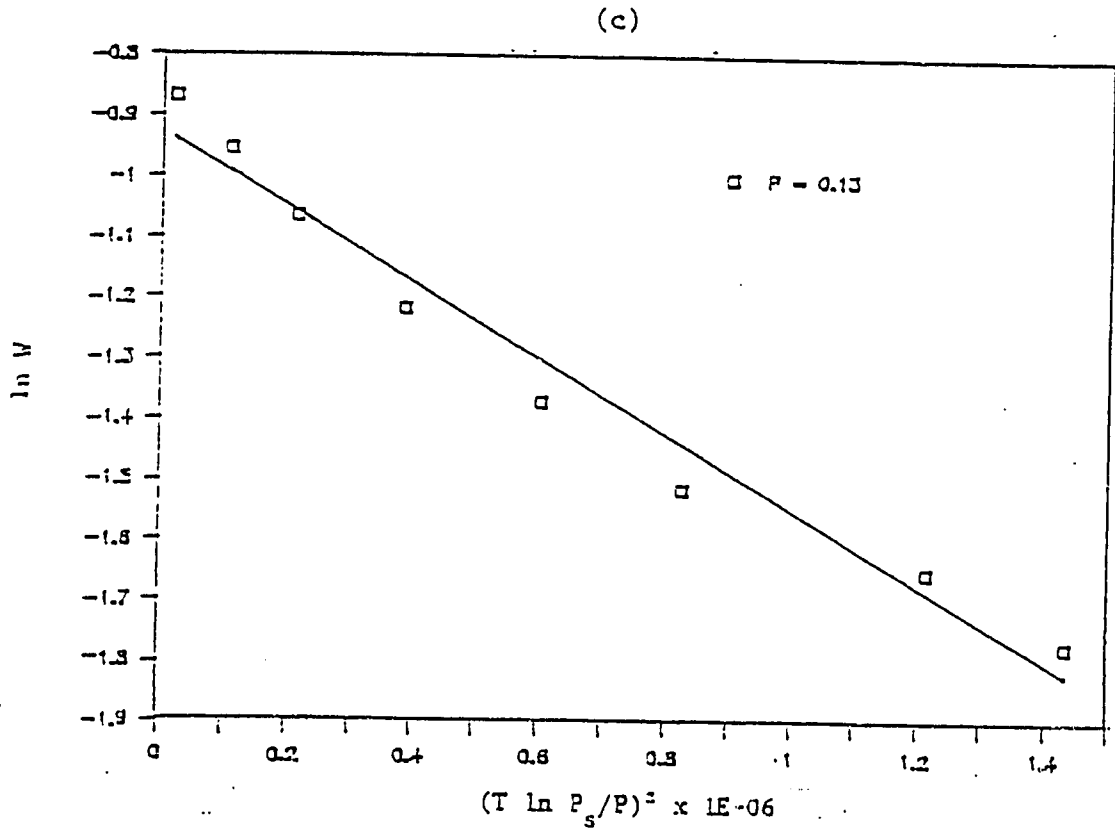
Fig. 4.8: Characteristic curve obtained on a D-R plot.
(c) Carbon 607C   (d) Carbon 610

(e)

$P = 0.13$ bar

$(T \ln P_s/P)^2 \times 1E\text{-}06$

(f)

$P = 0.13$ bar

$P = 0.04$ bar

$(T \ln P_s/P)^2 \times 1E\text{-}06$
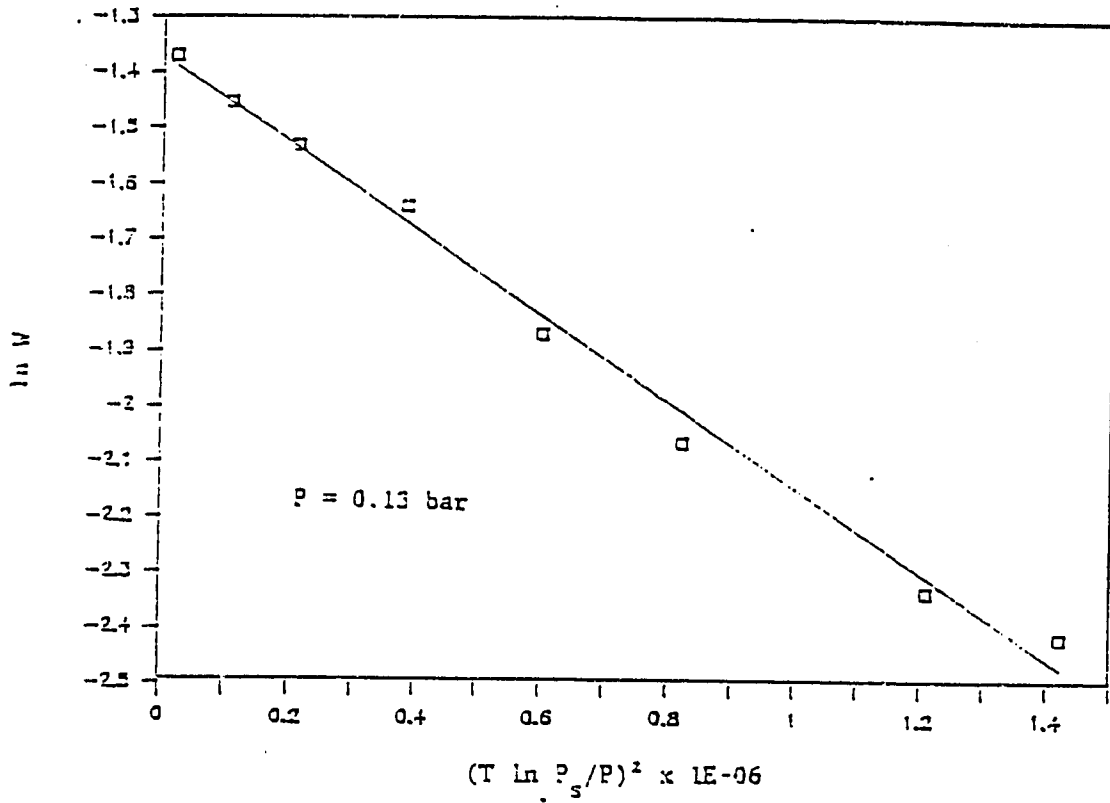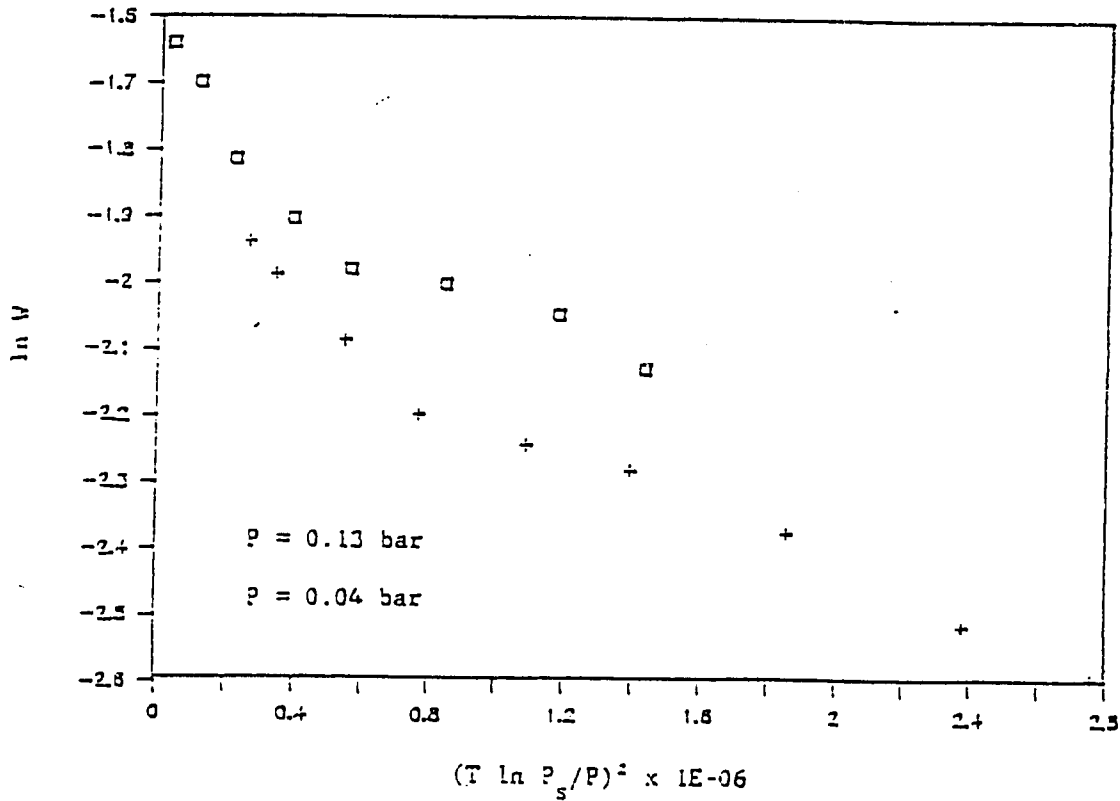
Fig 4.9: Characteristic curve obtained on a D-R plot.
(e) Carbon THAI-1 (f) Carbon THAI-2

(g)

(h)
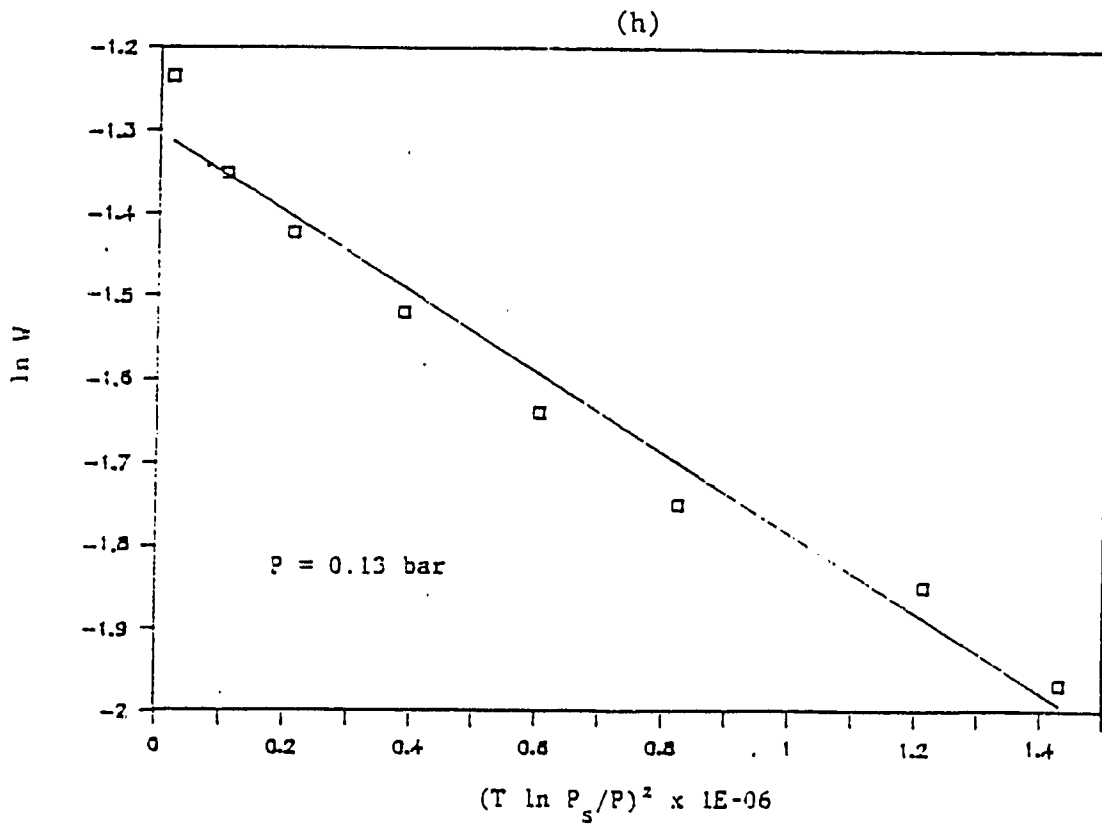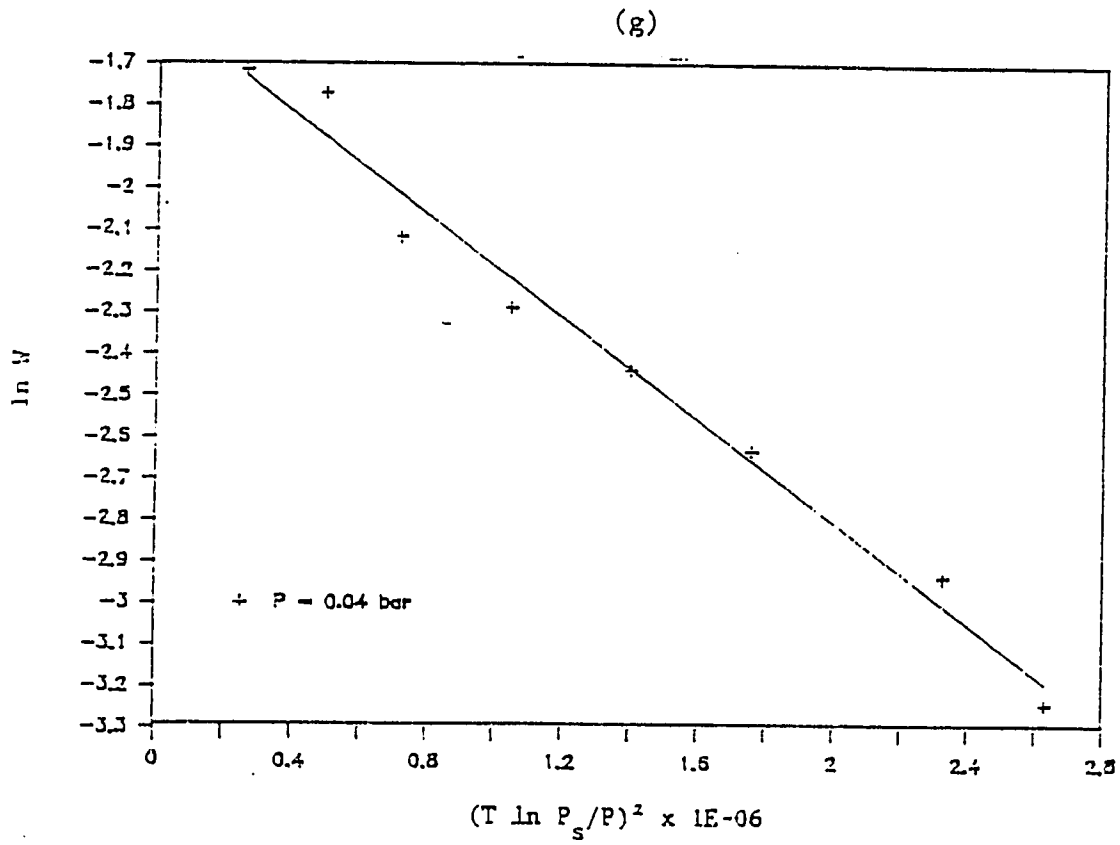
Fig 4.10:Characteristic curve obtained on a D-R plot.
   (g) Carbon 203C   (h) Carbon 205C

isosters and two isobars. The sensible heating and sensible cooling before and after generation follow two isosters; and the

Table 4.3:   Values of W_O, D and r in the D-R
Equation for the Charcoals Tested.

Charcoal	W_O (lit/kg)	D x 1E+06	Correlation Coefficient (r)
207E	0.3339	0.9645	0.96
207C	0.2458	0.6329	0.97
203C	0.2060	0.6134	0.98
205C	0.2710	0.4820	0.97
607	0.3962	0.6258	0.97
610	0.2485	0.6502	0.97
THAI-1	0.2531	0.7731	0.99
THAI-2	0.1666	0.3064	0.87

generation and the adsorption processes follow the isobars. The cycle can best be illustrated in the p-T-x diagram of Fig. 4.11.

a. Sensible Heating 1-2

The process starts at point 1, where the charcoal adsorbs the maximum amount of adsorbate, the concentration is x_{max} at temperature T_1. Starting in the morning, charcoal having a rich concentration of adsorbate is heated from temperature T_1 till the pressure P_2 (condenser pressure) is reached. Since no desorption has taken place yet, and the concentration being the same at x_{max}, T_2 can be evaluated.

b. Generation Process 2-3

Desorption starts at point 2 at a constant pressure corresponding to the condenser temperature and the adsorbent becomes more and more dilute. This continues until the maximum temperature attainable, T_{max} for the day is reached. Since we know the pressure and the temperature T_{max}, the new concentration x_{min} at point 3 can be calculated.
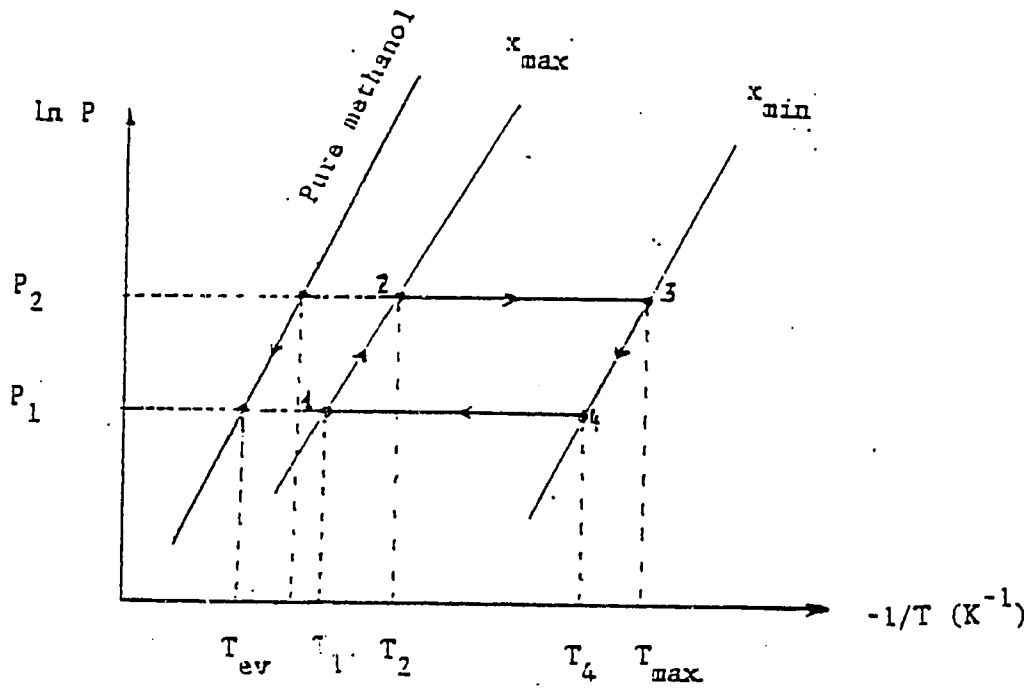
Fig 4.11: Adsorption Cycle.

c. Sensible Cooling 3-4

Cooling of the collector/generator takes place, at constant concentration x_{min} from 3 to 4 till the evaporator pressure P_1 is reached. Since P_1 and x_{min} are known, we can calculate T_4.

d. Adsorption 4-1

Adsorption starts at point 4 and continues until the concentration of refrigerant in the adsorbent reaches its maximum value x_{max}. Thus the cycle is complete.

4.3.2 Heat Balances in the Cycle

Process 1-2

The total heat used during this part of cycle is the sensible heating of the adsorbent and adsorbed refrigerant:

$$Q_{1-2} = (CP_a + CP_r \; x_{max}) \; (T_2 - T_1) \tag{4.5}$$

where

    CP_a, CP_r are the specific heats of the adsorbent and the refrigerant respectively,
    Q_{1-2} is the sensible heat during the process from state point 1 to 2.

Process 2-3

The heat supplied during the process consists of (i) sensible heating of the adsorbent from T_2 to T_3, (ii) sensible heating of the mean mass of the adsorbate from T_2 to T_3; and (iii) the heat of desorption.

$$Q_{2-3} = (CP_a + CP_r \; (x_{max} + x_{min})/2.) \; (T_3 - T_2)$$
$$+ \; (x_{max} - x_{min}) \; H_{des}, \tag{4.5}$$

where the heat of desorption/adsorption H_{des} is the average value of the two extreme values calculated from the slope of the two isosters calculated using the Clausius-Clapeyron equation:

At x_{max},

$$H1_{des} = (R/M) \; (\ln P_2/P_1) \; / \; (1/T_1 - 1/T_2),$$

Similarly, at the isoster, x_{min},

$$H2_{des} = (R/M) \; (\ln P_2/P_1)/(1/T_4 - 1/T_3),$$

where R is the universal gas constant,
       M is the molecular weight of the adsorbate.

Thus the average heat of desorption $H_{des} = (H1_{des} + H2_{des})/2$.

Cooling Produced

Assuming the refrigerant first cools from temperature T_1 to the evaporator temperature T_{ev}, and then evaporates, and also assuming the latent heat of evaporation L is constant, the cooling produced is:

$$Q_c = (x_{max} - x_{min})(L - CP_r(T_1 - T_{ev})),\qquad(4.7)$$

and the coefficient of performance is

$$COP_{th} = Q_c/(Q_{1-2} + Q_{2-3}).\qquad(4.8)$$

4.3.3 Computation of COPs and Results

Based on the type of application the evaporator temperature will be fixed, and the condenser temperature can be assumed known based upon the type of condenser used. The values of specific heats of the adsorbent CP_a and CP_r are known. The heat of adsorption/desorption H_{des} can be calculated, knowing condenser and evaporator temperatures, latent heat of evaporation L for an adsorbate can be calculated. Thus the COPs can be calculated.

It is clear from the heat balances that the thermal mass of the container has not been taken into account and the heat input is directly to the adsorbent and the refrigerant. A computer program written in Fortran Language was used to compute the COPs of the different charcoal samples tested. This computer program utilizes the data determined for charcoal-methanol adsorption presented in Section 4.2. The possible cases investigated include evaporator temperatures of $-10^{\circ}C$ and $5^{\circ}C$, typical for ice-making and cool storage respectively. The condenser temperatures modeled in above cases are $35^{\circ}C$ and $25^{\circ}C$. The results of this computer simulation are shown in Figs. 4.12 through 4.15.

Charcoal 607 has shown the best performance with methanol for ice-making followed by Charcoal 207E3; but at lower condenser temperatures and higher evaporator temperatures, Charcoal 207E3 is better. The COPs for Charcoal 207E3 at a generation temperature of about $110^{\circ}C$, condenser temperatures of $35^{\circ}C$ and $25^{\circ}C$, and evaporator temperature of $-10^{\circ}C$ were 0.41 and 0.52 respectively. The COPs for the local samples THAI-1 at the above temperatures were 0.36 and 0.47; while for THAI-2 were 0.25 and 0.35 (Sridhar, 1987). Similarly, Charcoals 607 and THAI-1 have been paired with other refrigerants for ice making purposes $(T_{evap} = -10^{\circ}C, T_{con} = 35^{\circ}C)$ shows better COPs compared to methanol (Figs. 4.16 and 4.17). But other practical difficulties, such as high pressure and corrosion, in the case of ammonia must be considered.
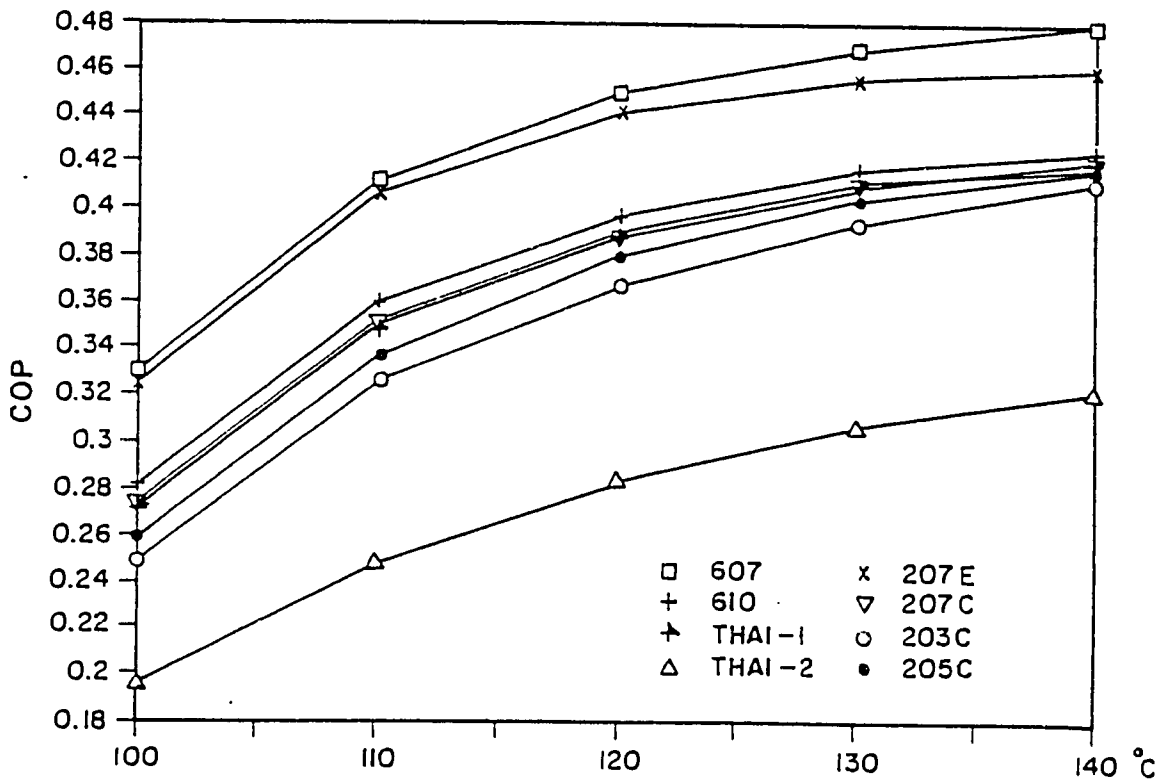
Fig.4-12:COP versus maximum temperature for the different carbons $T_{evap} = -10°C$; $T_{cond} = 35°C$.
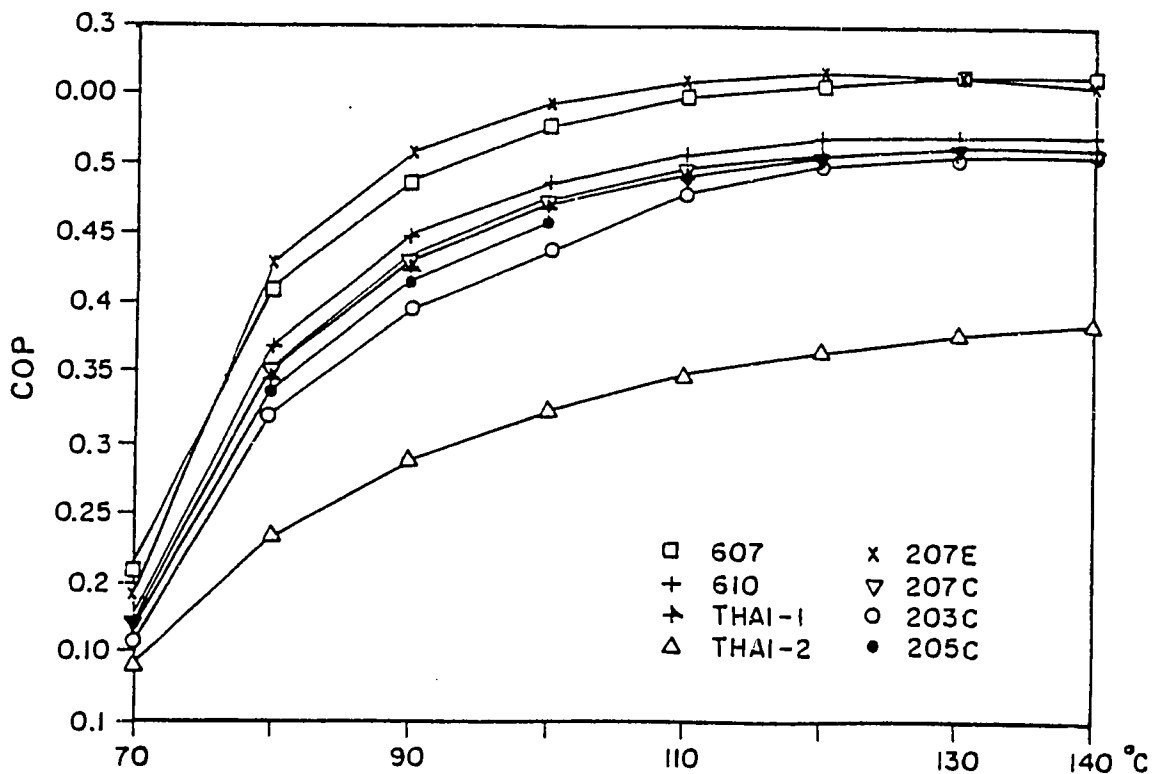
Fig.4.13: COP versus maximum temperature for the different carbons $T_{evap} = 5°C$, $T_{cond} = 35°C$.
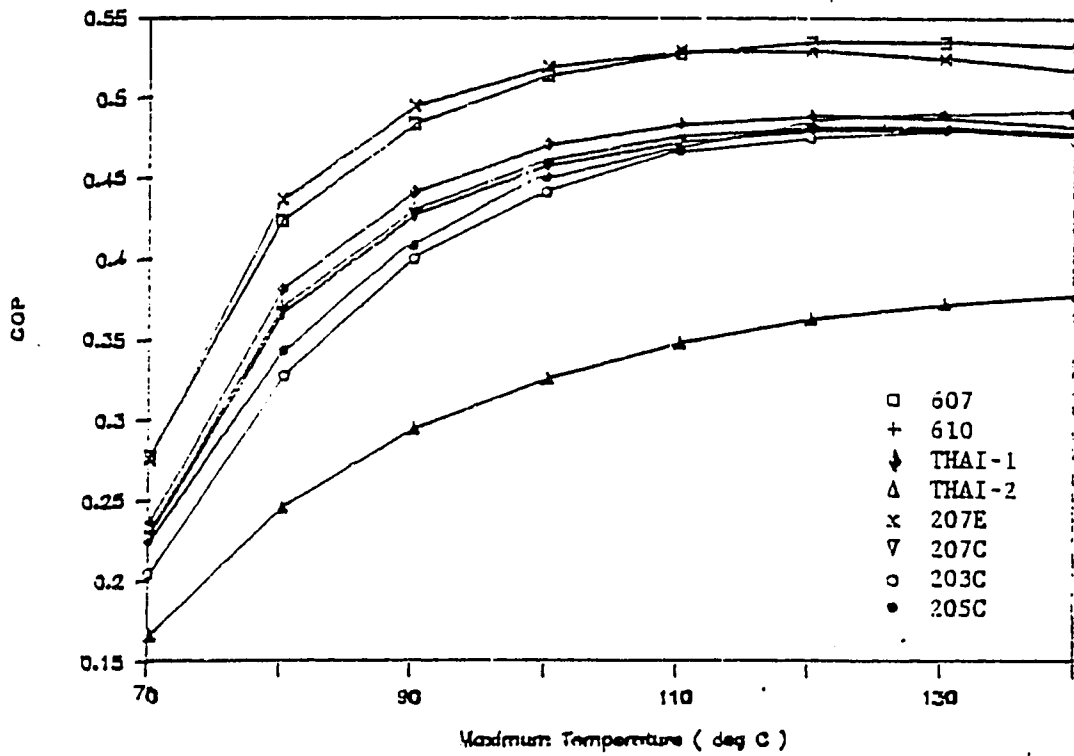
Fig 4.14: COP versus maximum temperature for the different carbons
$T_{evap} = -10\,^{\circ}C$; $T_{cond} = 25\,^{\circ}C$
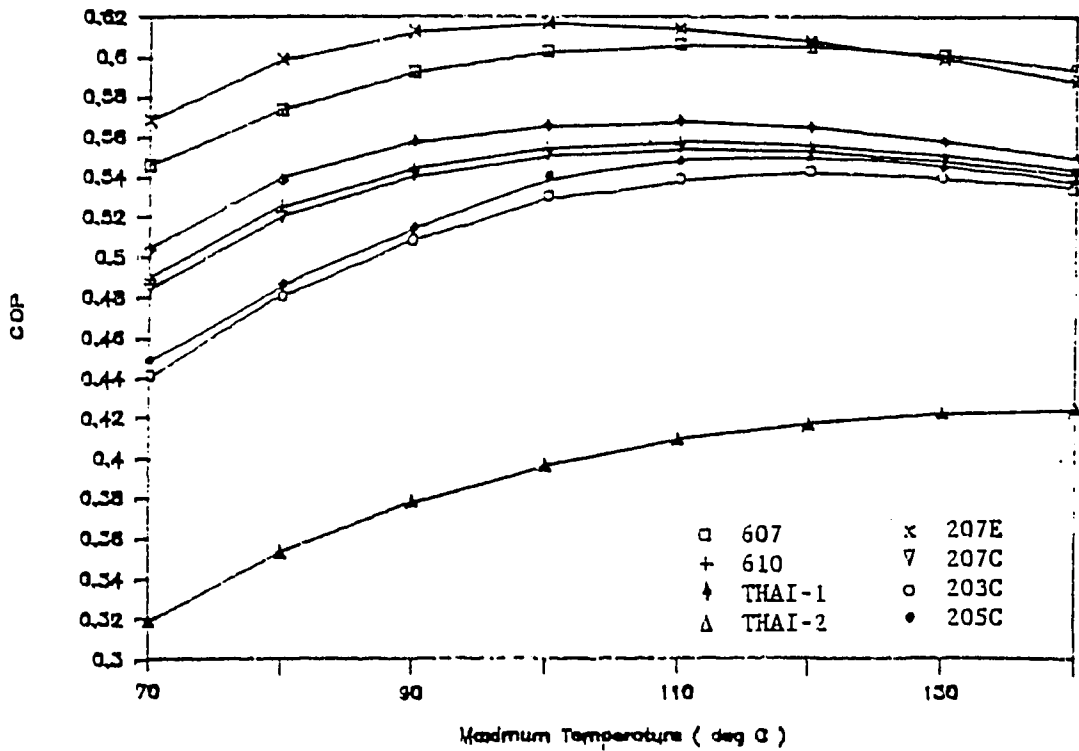
Fig 4.15: COP versus maximum temperature for the different carbons.
$T_{evap} = 5\,^{\circ}C$; $T_{cond} = 25\,^{\circ}C$
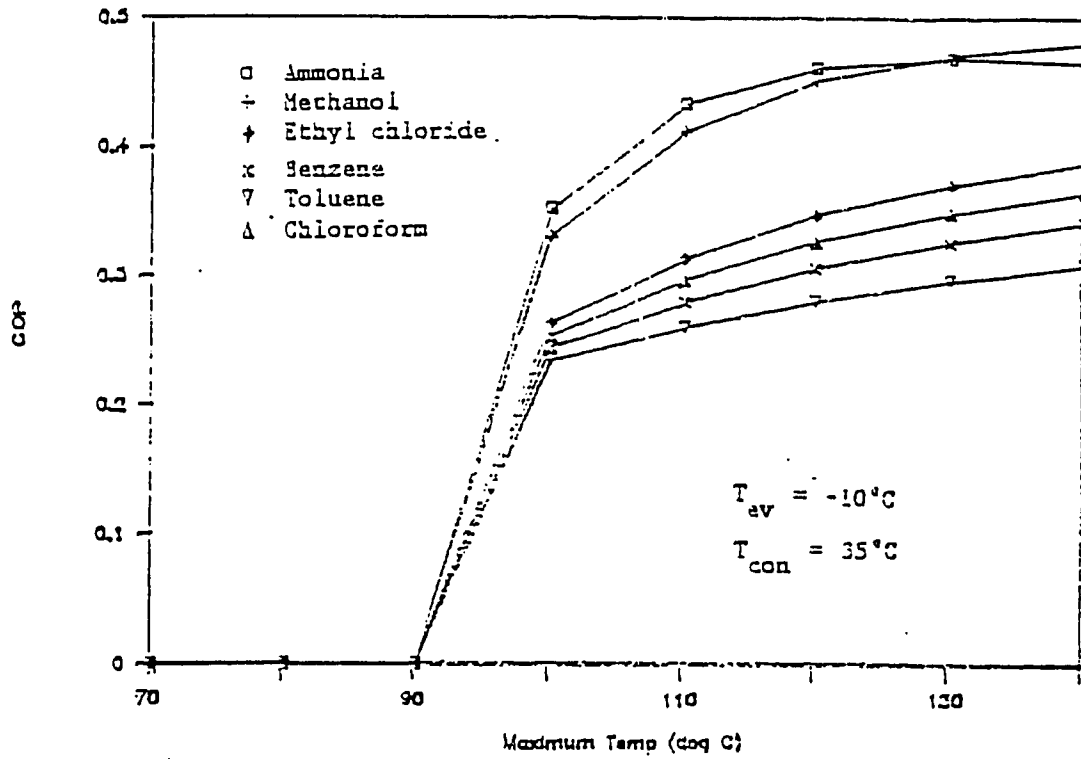
Fig 4.16: Carbon 607C with different refrigerants.
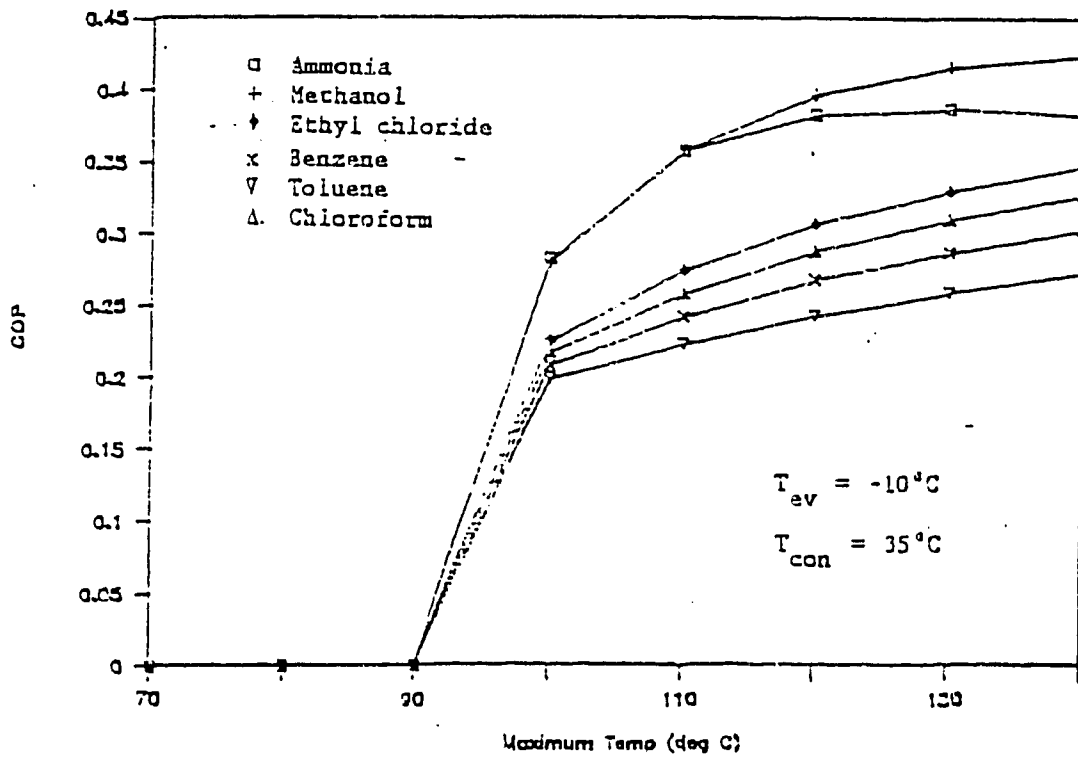
Fig 4.17: Carbon THAI-1 with different refrigerants.

V AIT Charcoal-Methanol Solar Refrigerator

5. Introduction

An intermittent solar activated charcoal-methanol adsorption refrigerator has been designed and tested at AIT. The design of the system is based on p-T-x data determined with our laboratory measuring equipment for one of the eight charcoal samples, (extruded type 207E3) from Sutcliffe Speakman Carbons Ltd., U. K. Two samples of the activated charcoal from a local factory in Thailand were also tested. Those samples were able to adsorb and desorb methanol, but large hysteresis was observed during adsorption and desorption especially at low evaporator pressure. So, the local charcoal was not used in this system.

5.1. Design of the System

The ideal cycle plotted on an Ln P versus -1/T chart for the selected charcoal is shown in Fig. 5.1. The following is the method used to trace the state points on this diagram.

The evaporation temperature T_{ev} depends on the applications; for ice production it has to be in the range of -10°C. T_{con} is the condensing temperature which should be as near to the ambient temperature as heat transfer and economics will allow. Similarily T_1 should be as low as possible so that the rich concentration x_{max} is as high as possible. This maximizes the concentration change thus minimizing the quantity of charcoal that must be (wastefully) heated and cooled with the adsorbed refrigerant. But T_1 depends on the night-time ambient temperature and also the heat transfer characteristics of the collector. For design calculations it has been assumed equal to 30°C. Thus the point corresponding to the evaporation temperature of -10°C and adsorber temperature of 30°C fixes point 1 in the p-T-x diagram. The concentration corresponding to it is about 15% by weight. This system has a water cooled condenser and condensing temperature assumed equal to 30°C. By following the 15% isoster and condensation pressure corresponding to 30°C, point 2 can be located, which corresponds to the generator temperature of 86°C. Assuming a generator temperature T_3 equal to 100°C, typical of the flat-plate solar collector and condensation at 30°C, point 3 can be located. Thus the final concentration of the methanol remaining in charcoal is 7%. This gives a concentration change of 8 wt. %. Similarly the generator has to be sensibly cooled down until it reaches the point 4, corresponding to temperature equal to 60°C, before the adsorption starts at a pressure corresponding to the evaporation at -10°C. This adsorption process starts late at night and continues until next morning. This fixes the ideal cycle on which the design is based.
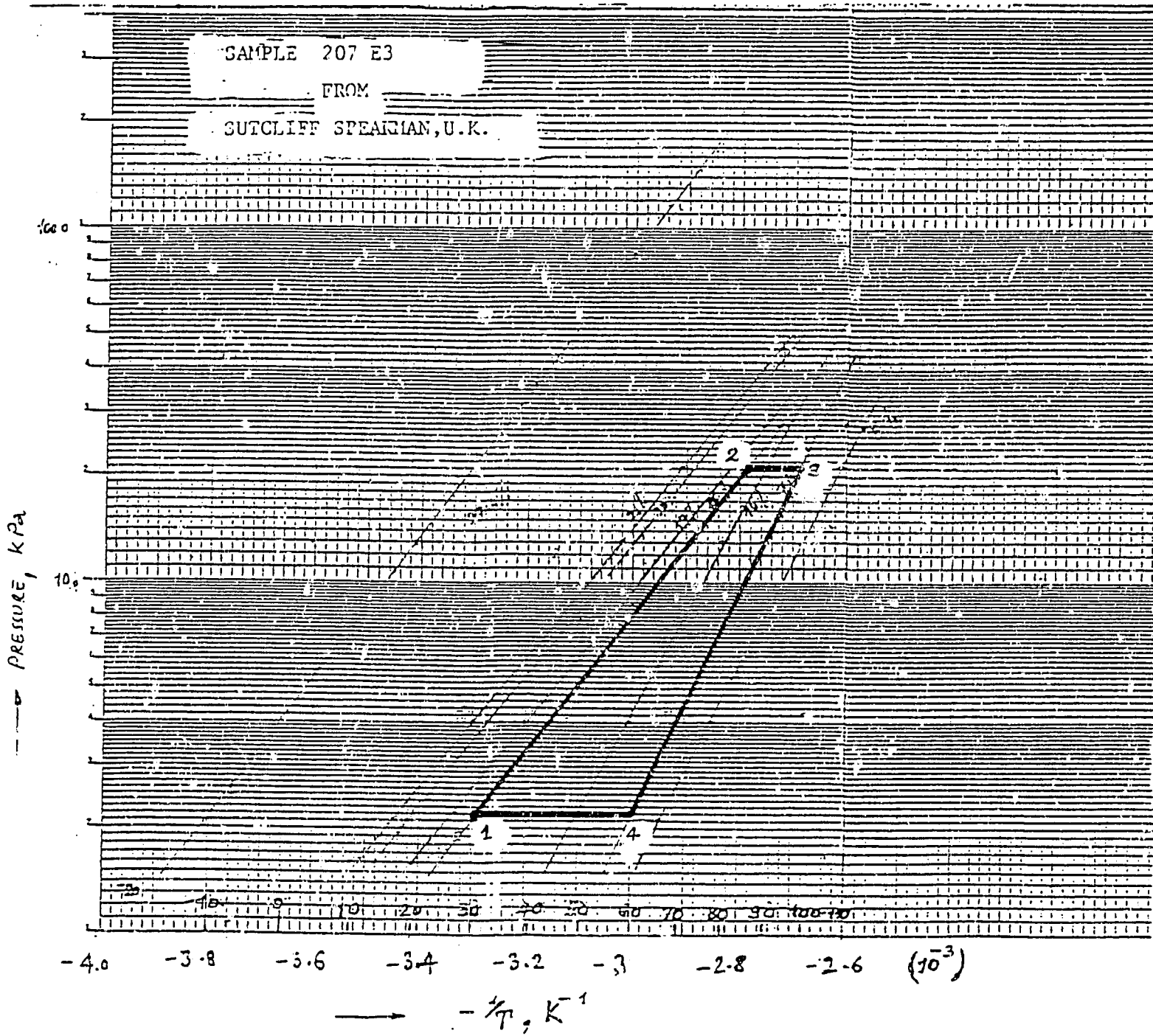
Fig. 5.1: Ideal Cycle in Ln P v. 1/T diagram.

5.1.1 Heat Transfer in the Cycle

Let m_c and m_a be the mass of the collector/generator and adsorbent (charcoal) contained in the collector respectively. Let CP_c and CP_a be the respective specific heats of the collector material and the charcoal. The specific heat of the adsorbed phase has been assumed equal to that of the liquid phase and denoted by CP_r. Assuming the collector, charcoal and the adsorbed phase are at the same temperature, the heat to be supplied during the sensible heating Q_{1-2} from temperature T_1 to T_2 can be estimated as:

$$Q_{1-2} = (m_c\ CP_c + m_a\ CP_a + m_a\ x_{max}\ CP_r)\ (T_2 - T_1). \qquad (5.1)$$

where X_{max} is the rich concentration (kg of methanol/kg of charcoal).

The desorption or generation process starts once the temperature reaches T_2 and continues until the highest temperature of the day T_3 is reached. After this, heat loss from the collector becomes greater than the heat input and generation stops. Thus heat supplied during the generation process includes sensible heating of the collector grid, charcoal, the adsorbed phase and also the heat of desorption. Assuming the specific heat of the adsorbed phase is equal to that of the liquid phase and sensible heating of the desorbed phase is equal to that needed to raise the mean mass of the adsorbate during desorption to the final temperature T_3, the heat needed to be supplied Q_{2-3} can be approximated as:

$$Q_{2-3} = (m_c\ CP_c + m_a\ CP_a + m_a\ (X_{max} + X_{min})/2)\ CP_r)\ (T_3 - T_2)$$
$$+ m_a\ (X_{max} - X_{min})\ H_{des}. \qquad (5.2)$$

where X_{min} is the weak concentration at the end of generation, and H_{des} is the heat of desorption which has been assumed equal to the heat of adsorption.

The total heat that has to be supplied during the sensible heating and the generation process is approximately the sum of the quantities given by equations (5.1) and (5.2).

The heat that has to be lost from the collector during the sensible cooling process T_3 to T_4 can be calculated as:

$$Q_{3-4} = (m_c\ CP_c + m_a\ CP_a + m_a\ x_{min}\ CP_r)\ (T_3 - T_4). \qquad (5.3)$$

The heat needed to be rejected by the collector during adsorption process Q_{1-2} can be approximated as:

$$Q_{4-1} = (m_c\ CP_c + m_a\ CP_a + m_a\ (x_{max} + x_{min})/2\ CP_r)\ (T_4 - T_1)$$
$$+ m_a\ H_{Ads}\ (X_{max} - X_{min}). \qquad (5.4)$$

The useful cooling Q_c that can be produced by this system

during night can be approximated as:

$$Q_c = m_a \ (x_{max} - x_{min}) \ (L - CP_r \ (T_{con} - T_{ev})). \qquad (5.5)$$

where L is the average latent heat of the refrigerant liquid leaving the evaporator (kJ/kg).

Thus the thermal coefficient of performance of the system is given as follows:

$$COP_{th} = Q_c \ /(Q_{1-2} + Q_{2-3}). \qquad (5.6)$$

Since this calculation is based on the heat used by the collector, the overall coefficient of performance the the system will be equal to the thermal coefficient of performance multiplied by efficiency of the solar collector/generator.

5.1.2   Design of the Components

(a)   Solar collector

The solar collector consists of an array of 15 copper tubes $2^1/8$"(53.97 mm O.D.), 0.528" (1.47mm)thick and 1.2 m long. This configuration provides an effective collection area of about 1 m^2. Although calculations were done on the different materials such as brass, stainless steel, aluminum tubings and also aluminum sections, M-type copper tube was chosen for the following reasons:

- availability of the material and fittings,
- ease of fabrication such as by soft soldering, silver brazing etc.,
- low specific heat but high conductivity of the material of the tubing.

Each copper tube contains a centrally placed perforated gauge tube of 3/8" diameter which is connected to the common header at the bottom of the collector. This was done to ensure even distribution of the methanol vapour in the charcoal and to reduce the pressure drop. Once the charcoal was filled, the top ends of the collector tubes were sealed by soldering brass plates. The lower ends of collector tubes have flare joints which can be assembled to the bottom header. The arrangement is shown in Fig. 5.2. The collector as fabricated has 38 kg of copper in tubes containing charcoal, header and gauge tubes, the 3.85 kg of brass in end caps, nipples, and flared joints. The total weight of the collector grid is 59.6 kg and contains 17.8 kg of charcoal.

The collector has a single glass cover, 4mm thick at a distance of 32 mm from the top surface of the collector tubes. One glass cover was choosen based on the previous experience at AIT (Exell and Kornsakoo, 1981). The top surface of the collector array is covered with selective Maxorb Solar Foil (Inco
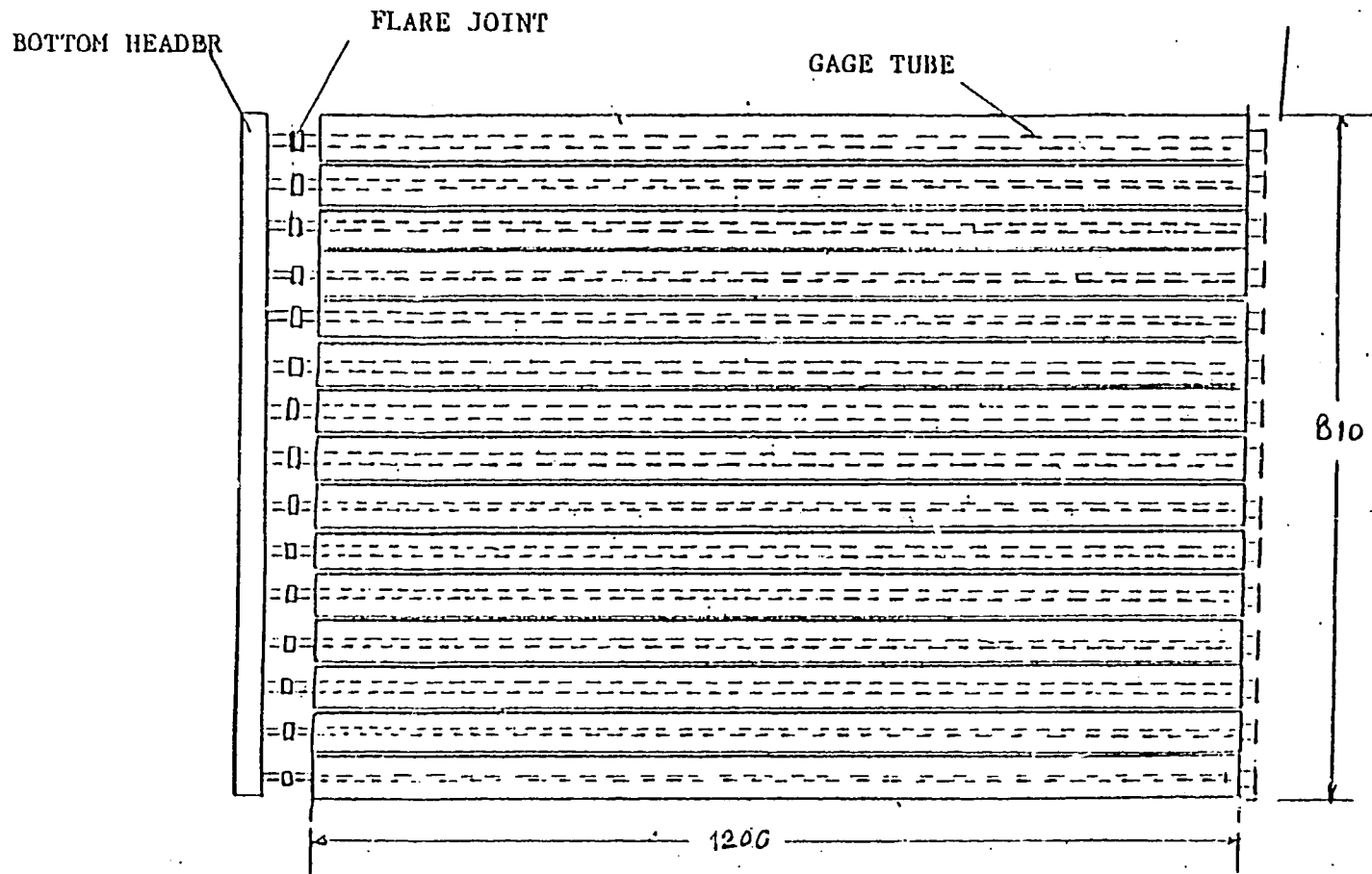
Fig. 5.2: Solar Collector Grid.

Dimensions are in mm.

Selective Surfaces, U.K.) coated with a special pressure-sensitive adhesive which can be used at high temperatures.

The assembly is housed in a galvanized iron sheet case of size 1.5m x 1 m. Polyurethane foam is used for insulating the pipes. The insulation fills in the casing and forms a mould about 90 mm thick. The back insulation of the collector can be opened by lowering the back of the casing which is hinged at the bottom and bolted in position at the top. The panel is tilted at an angle of 14° facing south. This collector at 30 to 35% collection efficiency can provide heat needed to desorb approximately 1.4 kg of methanol and has sufficient area to dissipate the heat of adsorption when the back of the collector is lowered. The properties of the materials used are given in Table 5.1 and the detailed calculations are given in appendix.

Table 5.1: Properties of different materials used in the design.

Methanol Properties		
Average Specific Heat of Liquid	2.55	kJ/kg-K
Average Density of Liquid	791.00	kg/m^3
Average Latent Heat of Evaporation of Methanol Vapour	1200.00	kJ/kg
Average Heat of Adsorption/Desorption	1500.0	kJ/kg
Charcoal Properties		
Bulk Density	500.0	kg/m^3
Average Specific Heat	0.7	kJ/kg-K
Other Properties		
Average Specific Heat of Copper	0.380	kJ/kg-K
Average Specific Heat of Brass	0.385	kJ/kg-K

(b) Condenser

The design of the condenser is based on the condensation of 1.4 kg of methanol vapour at 30°C to methanol liquid at the same temperature. The total amount of heat to be released in the condenser can be calculated as follows:

From the methanol property tables (Liney, 1982), the enthalpy of the methanol vapour at 30°C is 1776.5 kJ/kg and the enthalpy of the methanol liquid at the same temperature is 613.85 kJ/kg. So, a total of 1627.7 kJ has to be released in the condenser. Supposing condensation takes place during the period of four

hours, the heat rate is 113.03 W.

The heat transfer area for the condenser can be calculated as:

$$A_{con} = 113.03/(U \, \Delta t), \, m^2 \qquad\qquad (5.7)$$

where U is the overall heat transfer coefficient in W/m^2-K and Δt is the temperature difference in degrees.

The overall heat transfer coefficient by natural convection in the static water tank with some fouling was estimated to be 170 W/m^2-K from previous experience (Exell and Kornsakoo, 1981). Assuming a 2^oC temperature difference between the vapour and the cooling water, a heat transfer area of 0.332 m^2 is required. The condenser, fabricated from 1/2" and 1 3/8" hard copper tubing is shown in Fig. 5.3. This configuration has about 0.35 m^2 heat transfer area.

Since the total heat to be released in the static water tank is about 1627.7 kJ, and allowing a temperature rise of 1.5^oC, the amount of water needed in the tank is 260 kg. The water tank is made from of mild steel sheets and has dimensions 1m x 0.7m x 0.4m; it can contain 279 kg of water.

(c) Receiver

The methanol is contained in a brass container 150mm in diameter and 180mm long, and it can hold about 3 litres of methanol liquid. The tubing connecting the receiver and the evaporator, and the evaporator together can hold about 0.5 litre of methanol. So, the total methanol that can contained in the assembly is about 3.5 litres which is approximately 15.6 wt. % of the methanol cycled. The total weight of receiver is about 2 kg.

(d) Evaporator

The design of the evaporator is based on the following assumptions:

1. The amount of methanol to be evaporated is 1.4 kg.
2. The refrigeration process takes 12 hours.
3. The evaporator temperature is -10^oC.
4. The average latent heat of evaporation of the methanol vapour between 30 to -10^oC is 1200 kJ/kg.
5. The conductivity of the ice layer is 2.2 W/m-K.
6. The average specific heat of methanol liquid is 2.55 kJ/kg-K.

It follows from the above assumptions that the maximum amount of ice that could be produced by this system (neglecting the thermal mass of the container and the heat leak to the ice

VAPOUR INLET

TOP HEADER

BOTTOM HEADER

SCALE : 1:5

CONDENSATE OUTLET
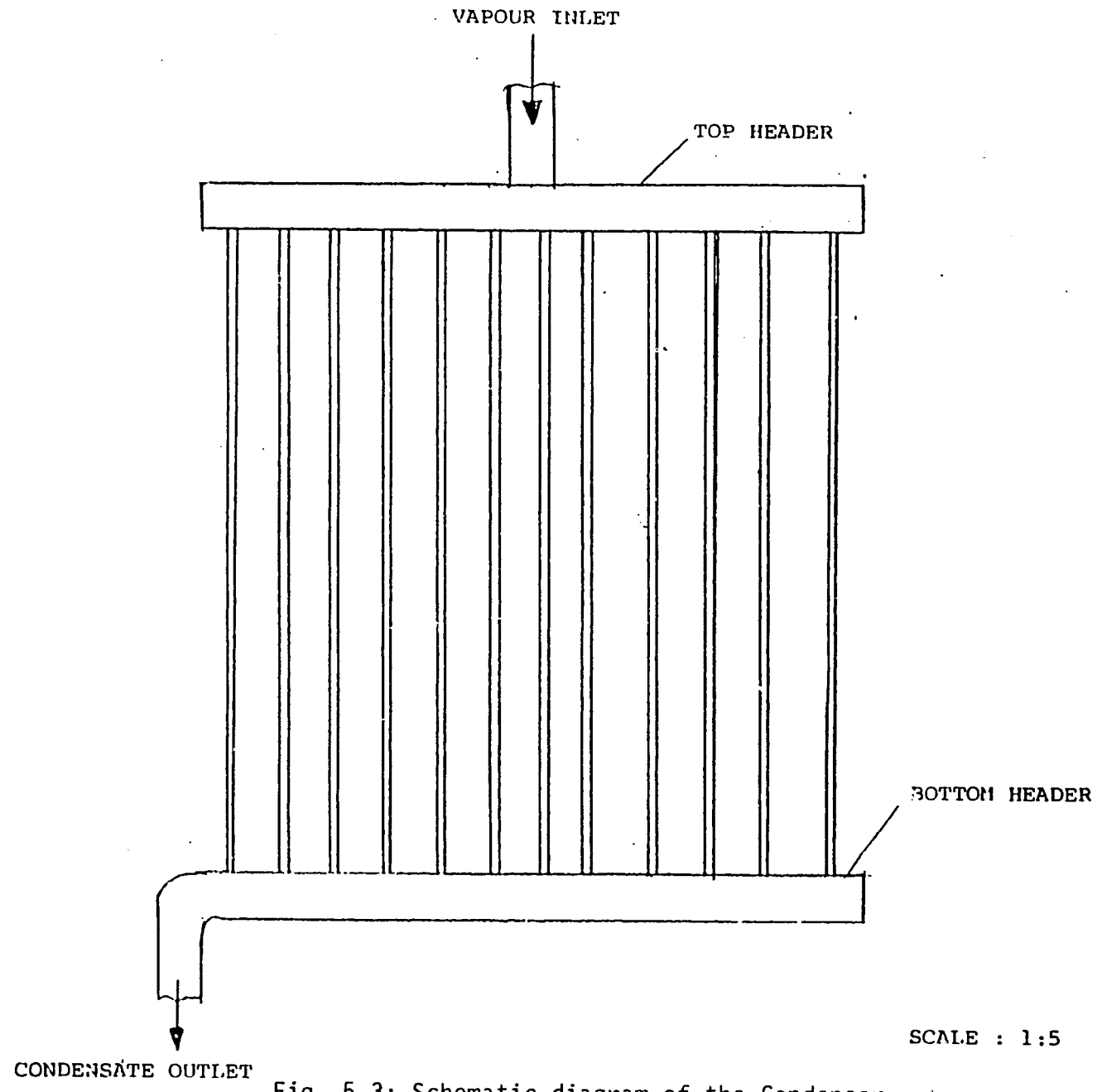
Fig. 5.3: Schematic diagram of the Condenser.

box) from water initially at $30^{\circ}C$ is about 3.35 kg. The total cooling produced is 1537 kJ and the heat flow rate required is 35.6 W. This heat flow rate must be maintained by the freezing water until the last bit of ice is formed in the cycle. Thus,

$$35.6 = 2.2 \ A_{ev} \ \Delta T/x, \tag{5.8}$$

where

A_{ev} = Heat transfer area of the evaporator, m^2,
ΔT = Temperature difference between evaporator
and water surrounding the evaporator $10^{\circ}C$,
x = Thickness of ice, m.

From equation (5.8), $A_{ev}/x = 1.62$ m. (5.9)

The specific volume of ice at $0^{\circ}C$ is 0.001091 m^3/kg and the total volume of 3.35 kg of ice is 0.00365 m^3 which gives:

$$A_{ev} \ x = 0.00365 \ m^3. \tag{5.10}$$

Solving equations (5.9) and (5.10), gives the surface area of heat transfer equal to 0.077 m^2, and the maximum thickness of the ice is 47.5 mm. After several trials a trapezoidal section has been selected for the evaporator. This section provides an effective surface area of about 0.131 m^2, and from equation (5.10) the effective thickness of ice reduces to 27.8 mm. The evaporator was made out of the brass sheet and has a total mass of 2.0 kg, including the copper tubing connecting receiver and the evaporator. Moreover, this configuration allows easy removal of ice. The receiver/evaporator assembly is shown in Fig. 5.4, and the sectional view of the refrigerator is shown in Fig. 5.5.

5.1.3 Pressure Drop in Connecting Tubes and Charcoal

The worst possible case that might be encountered is a temperature of 260 K ($-13.15^{\circ}C$) during evaporation, the specific volume of methanol vapour at this temperature is 39.49 m^3/kg and the corresponding pressure is 1700 Pa. Since the total amount of vapour to be cycled is about 1.4 kg in twelve hours, the average mass flow rate is 3.24 x 10^{-5} kg/s. The average velocity of the methanol vapour V can be calculated as:

$$V = \dot{m} \ \nu / \ A_f \tag{5.11}$$

where,

m = Methanol vapour rate, kg/s,
ν = Specific volume, m^3/kg,
A_f = Cross-section area of flow, m^2.

To keep the pressure drop in the connecting pipe low a smooth drawn $1^3/8"$ (32.8 mm I.D.) copper tube has been choosen. This tube has a flow area of 0.0008296 m^2 and the average

LEVEL GLASS

RECEIVER

EVAPORATOR

.Fig. 5.4: Receiver/Evaporator Assembly.

Solar collector

Bottom header

Removable insulation

Condenser

Static water tank

Insulated box
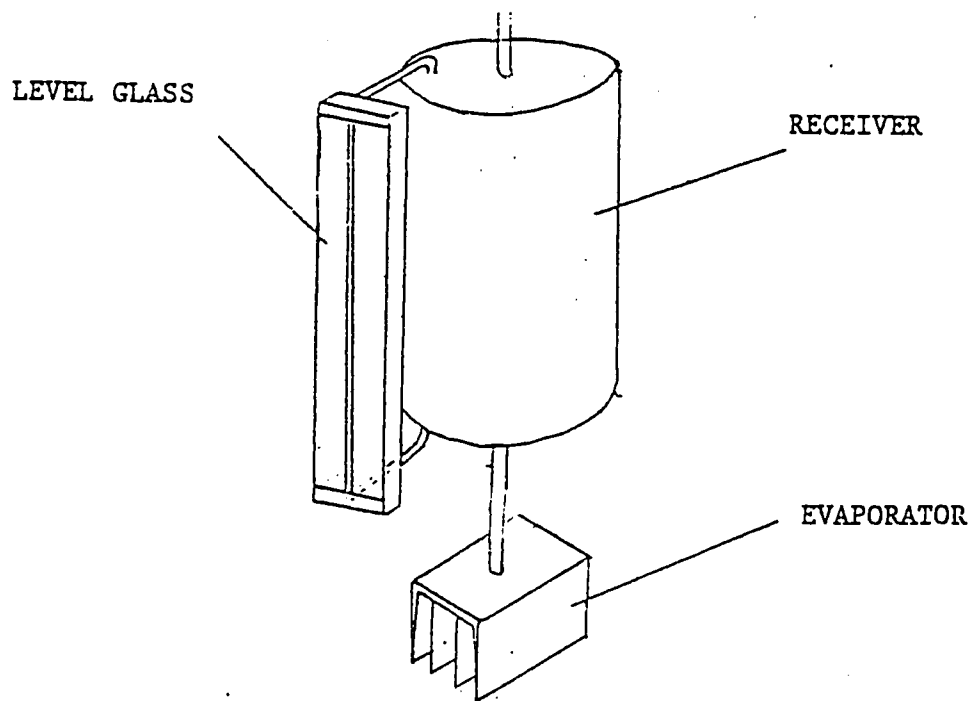
Receiver

Evaporator
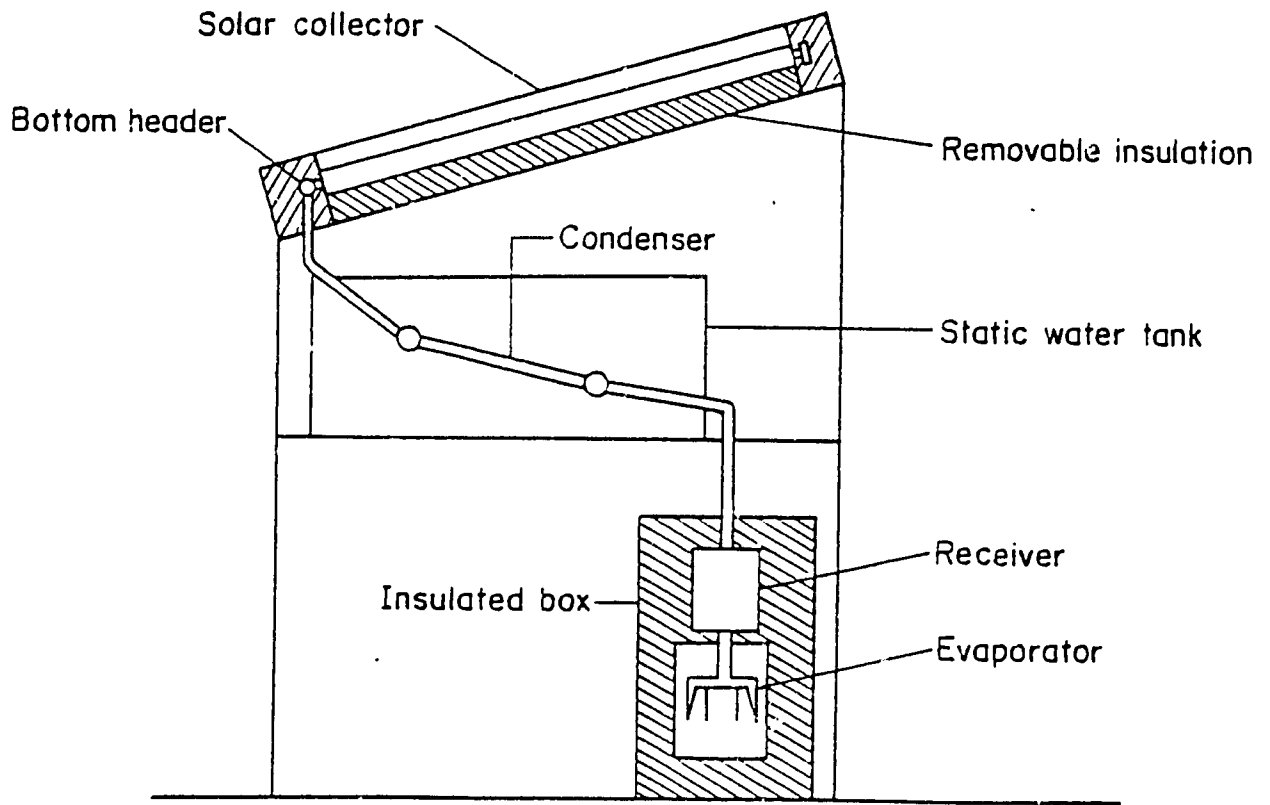
Fig. 5.5: The sectional view of the Solar Refrigerator.

velocity of vapour flow in the tube is 1.54 m/s. Assuming the average viscosity of the methanol vapour μ is equal to 10.1×10^{-6} Ns/m^2, the Reynold's number R_N is given as:

$$R_N = 4 \, \overset{\bullet}{m} \, /(\pi D_i \, \mu) \simeq 126 \qquad (5.12)$$

where

D_i = Internal diameter of vapour transport tube(m).

Since the Reynold's number is less than 2000, the flow is laminar and the Fanning's friction factor f is equals to $16/R_N$ (Perry and Chilton, 1973), and the pressure drop ΔP (Pa/m) in the connecting tubes can be calculated as:

$$\Delta P = 1/2 \, (f \, \rho \, v^2) \, /D_i \qquad (5.13)$$

For the 1 3/8" connecting tubes, the pressure drop is equal to 0.1161 Pa/m and the pressure drop in gauge tubes is 1.9 Pa/m, which is satisfactory.

The flow is laminar and the pressure drop in the bends is small but the bends and sudden changes in the internal diameter of flow have been kept to minimum.

Since gauge tubes have been used in this system, the effective thickness of charcoal in the tube in the radial direction is only 21 mm and the pressure drop in the charcoal will be negligible.

5.2 Preparation for Tests

5.2.1 Calibration of Level Glass of Receiver/Evaporator

The receiver/evaporator assembly consists of a level glass to measure the liquid level inside the receiver. The level glass was calibrated by filling a known quantity of water into the receiver/evaporator in small increments. The volume V of the liquid in the receiver can be calculated from the level glass reading as follows:

$$V = 34.17 + 192.16 \ H - 0.55 \ H^2, \ cm^3 \qquad (5.14)$$

where H is the level glass reading (cm) and the above equation is valid for $3 \leqslant H \leqslant 19.1$.

The lowest value that can be read from the level glass is 3 and the highest level is 19.1 cm. The evaporator and the tube connecting the evaporator and the receiver contains about 600 cm^3 of methanol liquid.

5.2.2 Overall Heat Loss Coefficient of Receiver/Evaporator Box

The receiver/evaporator is housed in a box (700 mm x 460 mm x 460 mm) well insulated by polyurethane foam. To determine the overall heat loss coefficient of the box, the receiver/evaporator was filled with ice-cold water and the temperatures at different points (Fig. 5.6) were recorded continuously.

TR_1 = Receiver top temperature, $^{\circ}C$
TR_2 = Receiver bottom temperature, $^{\circ}C$
TR = Mean receiver temperature, $^{\circ}C$
TE_1 = Temperature of the tube connecting
 receiver/evaporator, $^{\circ}C$
TE_2 = Evaporator temperature, $^{\circ}C$
TE = Mean evaporator temperature, $^{\circ}C$
TW = Water temperature, $^{\circ}C$
TC = Mean cover temperature, $^{\circ}C$.
and,
$m_R \ C_R$ = Thermal mass of the receiver, $kJ/kg-^{\circ}C$,
$m_E \ C_E$ = Thermal mass of the evaporator, $kJ/kg-^{\circ}C$,
$m_W \ C_W$ = Thermal mass of water filled in the
 receiver/evaporator, $kJ/kg-^{\circ}C$.

The heat balance of the receiver/evaporator can be written as:

$$m_R \ C_R \ dTR/dt + m_E \ C_E \ dTE/dt + m_W \ C_W \ dTW/dt =$$

$$3.6 \ U \ A_C \ (TC - (TR + TE)/2) \qquad (5.15)$$

where,
U = Overall heat loss coefficient with respect
 to outside surface area of the cold box, $W/m^2-^{\circ}C$,
A_C = Total outside heat transfer area of the cold box, m^2.
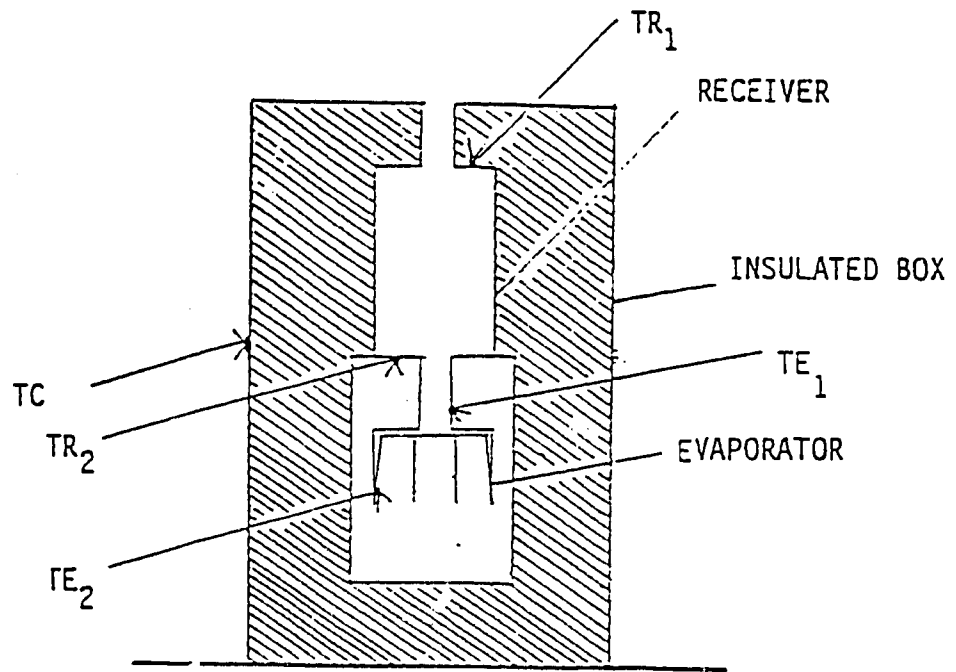
Fig. 5.6: Positions of sensors to determine
         Overall Heat Loss Coefficient.

$$U = (m_R \, C_R \, dTR/dt + m_E \, C_E \, dTE/dt + m_W \, C_W \, dTW/dt)/(3.6 \, AC \, (TC$$

$$- (TR + TE)/2) \tag{5.16}$$

The mean cover temperature of the cold box TC varies in a sinusoidal pattern, but for small time interval it was represented by the curve

$$TC = 33.65 - 0.44 \, t + 0.01 \, t^2, \tag{5.17}$$

where t is the time (h).

The temperature difference between the cover and the cold box decreases exponentially with time according to the Newton's law of cooling. The linear regression curves fitted are:

$$\ln (TC - TR) = 3.16 - 0.08 \, t, \tag{5.18}$$

$$\ln (TC - TE) = 3.15 - 0.07 \, t, \tag{5.19}$$

$$\ln (TC - TW) = 3.19 - 0.07 \, t. \tag{5.20}$$

Thus from (5.17), and (5.18), (5.19) and (5.20) we get,

$$TR = 33.65 - 0.44 \, t + 0.01 \, t^2 - 25.57 \, e^{-0.08 \, t}, \tag{5.21}$$

$$TE = 33.65 - 0.44 \, t + 0.01 \, t^2 - 25.57 \, e^{-0.07 \, t}, \tag{5.22}$$

$$TW = 33.65 - 0.44 \, t + 0.01 \, t^2 - 24.29 \, e^{-0.07 \, t}. \tag{5.23}$$

Differentiating equations (5.21), (5.22), (5.23) with respect to time t and substituting in equation (5.16), the hourly values of overall heat loss coefficient can be computed. The computed values are shown in Table 5.2.

Table 5.2:   Results of the Overall Heat Loss Coefficient
              Calculation for the Receiver/Evaporator Box.

Local Time, (Hr)	Time (Hr)	TR (C)	TE (C)	TW (C)	TC (C)	U (W/m^2-C)
16	1	11.98	12.41	11.86	33.73	0.14
17	2	13.13	12.88	12.40	32.77	0.15
18	3	13.89	13.19	12.91	31.83	0.15
19	4	14.85	13.99	13.80	31.60	0.14
20	5	15.42	14.45	14.25	31.57	0.14
21	6	15.99	14.79	14.60	31.55	0.13
22	7	16.94	16.09	15.85	31.32	0.13
23	8	17.91	17.01	16.83	30.86	0.14
24	9	18.29	17.47	17.27	30.47	0.14
1	10	19.26	17.93	17.90	30.02	0.14
2	11	19.82	18.92	18.84	29.79	0.14
3	12	20.58	19.43	19.42	29.33	0.15
4	13	20.98	20.07	19.99	29.33	0.15
5	14	21.35	20.45	20.37	29.13	0.15

5.2.3 Leak-tightness Tests

Prior to assembling, all the components, such as collector tubes, condenser, receiver/evaporator, were tested separately under pressure as well as under vacuum conditions. Once assembled, the solar collector was exposed to the sun and evacuated. The solar collector and condenser, and the receiver/evaporator were checked separately for vacuum tightness over the period of several days, isolating them with the help of isolating valves. The isolating valves and the methanol feeding arrangement are shown in Fig. 5.7.

5.2.4 Preparation of Charcoal for Test

As a first step to remove moisture adsorbed during transit, the charcoal was put into a vacuum oven at 150°C for three days and evacuated with the help of a vacuum pump. The dry hot charcoal from the vacuum oven was filled into the collector tubes and the tubes were assembled. Degassing of the charcoal in the collector tubes was done by exposing the solar collector to the sun and evacuating it around the peak temperature, which reached up to 135°C on clear days. After several days, the charcoal was washed by letting it adsorb a small amount of methanol vapour from the methanol feeding bottle during the night, and by heating and evacuating it during the day. This was done to remove gases adsorbed into the deep pores of the charcoal and gradually replacing them by methanol. After a few such cycles, charcoal was finally ready for actual tests.

SOLAR COLLECTOR

VACUUM GAUGE

CONDENSER

BALL VALVE

LEVEL GAUGE

ICE BOX

FEEDING BOTTLE

TO THE VACUUM PUMP

MERCURY MANOMETER

X SHUT -OFF VALVES

⊗ BALL VALVE
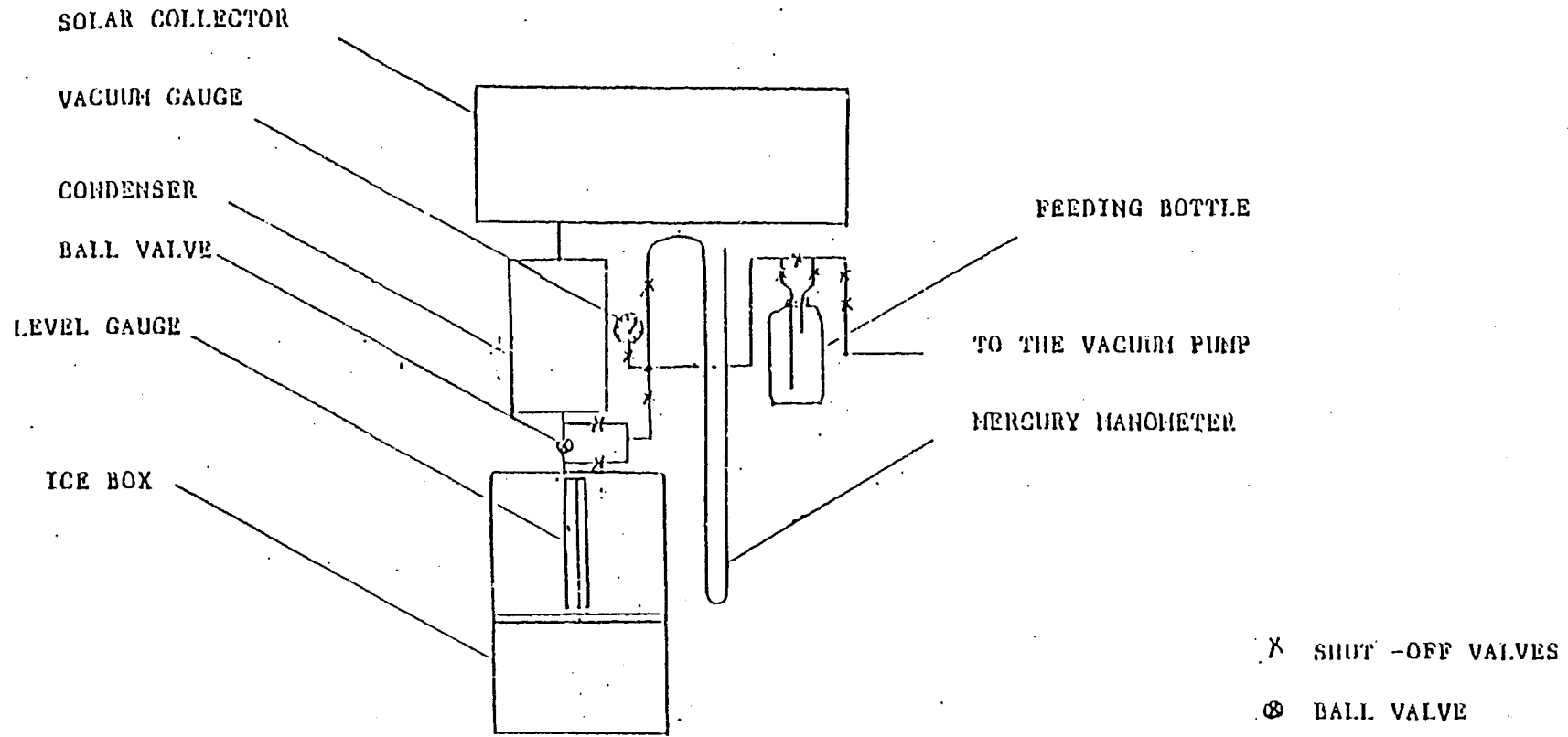
Fig. 5.7: The schematic diagram showing the isolating valves.

5.2.5 Charging of the System

Initially, the charcoal was allowed to adsorb methanol from the feeding bottle. But the adsorption from the feeding bottle was very slow and liquid methanol was therefore charged directly into the receiver/evaporator. The collector was covered during the day and the back insulation was lowered until the adsorption process was complete. The total methanol charged was four litres, all of which was adsorbed by the charcoal. The initial concentration of methanol in the charcoal was about 17.8 wt. % (dry basis).

5.2.6   Instrumentation

Temperature Measurement

The principal temperature measurements were made by twelve copper-constantan (T-Type) temperature sensors, which are designed for a temperature range between -88^0C and 370^0C. These thermocouples were calibrated against a standard mercury-in-glass thermometer having a precision of 0.1^0C. These temperature sensors were installed on the glass cover, top, inside and the bottom of the collector, the condenser, the receiver, the evaporator, and the water or ice temperature. One sensor was used to measure the ambient temperature. The positions of the sensors are shown in Fig. 5.8. These temperatures were recorded continuously by a Fuji chart recorder. Two calibrated k-type temperature sensors were used to measure condenser tube and the cooling water temperatures and those two values were read from the digital display.

Solar Radiation

A pyranometer attached to an integrator with digital display (Solar 118, Switzerland) was used to monitor the instantaneous and integrated values of solar radiation on a surface parallel to the solar collector. This pyranometer was calibrated against a standard pyranometer used at the meteorological station of the ET Park, AIT. The instantaneous and the integrated values of solar radiation were read manually.

Pressure

Besides an ordinary Bourdon gauge, a U-tube mercury manometer has been connected to the system through a system of isolating valves. The Bourdon gauge can be used to estimate the pressure range but the mercury manometer can be used to read the vacuum level to a resolution of 1 mm. One end of this manometer is exposed to the atmosphere. The atmospheric pressure can be read from the standard barometer installed at the ET Park, AIT. Thus, the system pressure at any time can be calculated.

AMBIENT TEMPERATURE

GLASS COVER

COLLECTOR TUBES

STATIC WATER TANK

CONDENSER

RECEIVER

EVAPORATOR
ICE CONTAINER
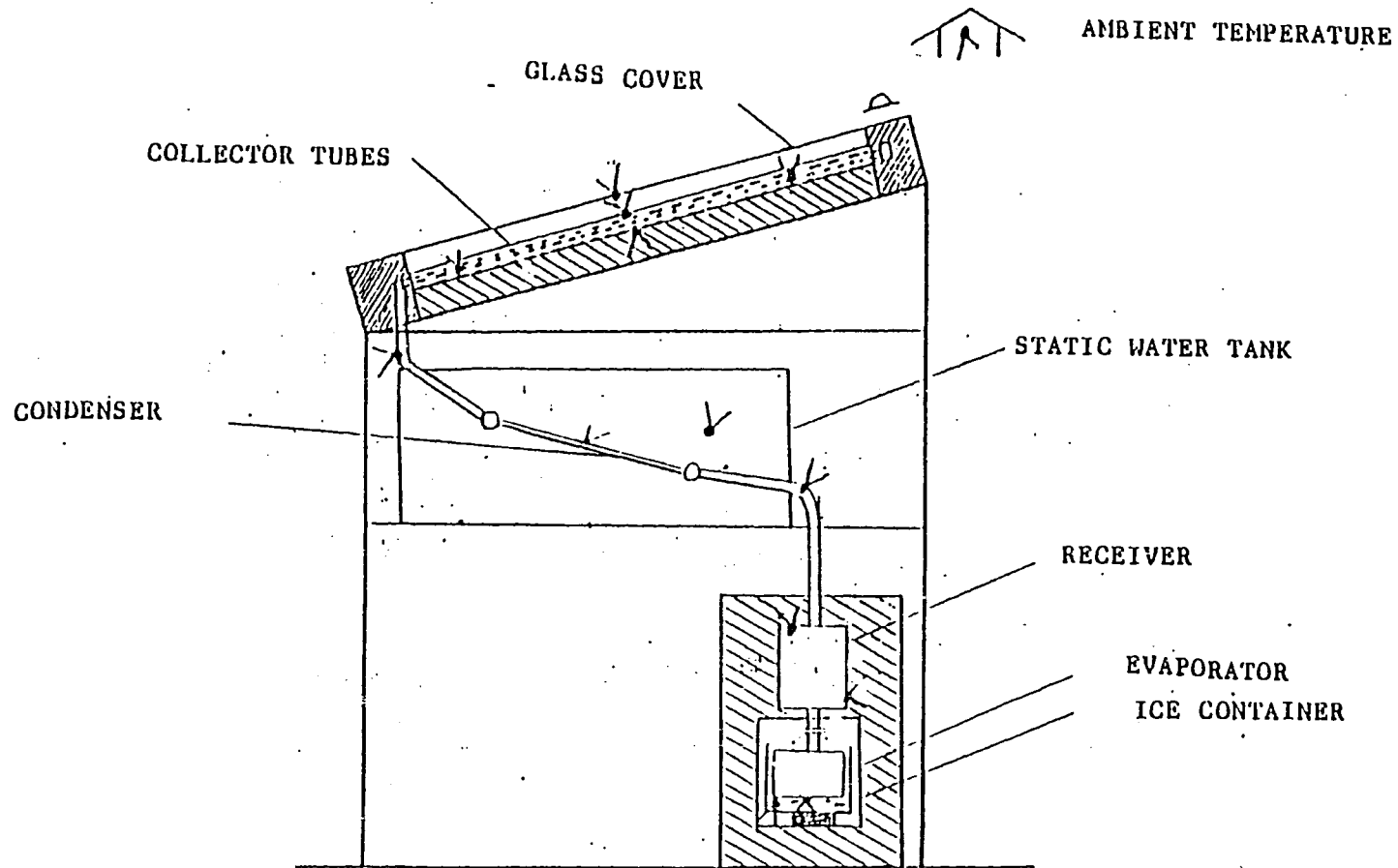
$\curlyvee$
$\curlywedge$ TEMPERATURE SENSOR

Fig. 5.8: Positions of the sensors in the solar refrigerator. $\triangle$ PYRANOMETER

Liquid Level

The volume of the methanol can be read from the level glass attach··d to the receiver. Sine the density of methanol liquid is known from the property tables, the mass of methanol in the receiver, and thus the mass cycled, can be estimated.

5.3 Testing Procedure and General Observations

The performance of the above solar refrigerator has been monitored since the beginning of October, 1987. The the weather during October was highly variable, as there were a few exceptionally clear days, as well as some cloudy and some rainy days. The experimental observations for a few days are given in Tables 5.3 through 5.5.

5.3.1 Solar Radiation

The solar radiation incident on the surface of the collector during the period of the experimentation varied between 9.4 and 23.24 MJ/m^2-day. The daily solar radiation incident on the surface of the collector for the month of October is shown in Fig. 5.9.

5.3.2 Ambient Temperature

The minimum ambient temperature recorded during October was 20°C during a cool night, and the maximum value was 34°C during clear afternoons.

5.3.3 Collector Temperature

Five sensors (2 and 5 to measure top and bottom temperatures of collector tubes, 3 and 4 to measure charcoal temperatures from the top and bottom end of tubes, 1 to measure glass temperature) were used to measure collector temperatures. The collector reached 122°C during clear days, and the minimum collector temperature was 4 -- 6°C above the minimum ambient temperature, while the charcoal temperature was 1 -- 2°C above tube temperatures. The temperature profile of the collector during a clear day and including the ambient temperature are shown Fig. 5.10.

5.3.4 Condenser Temperatures

The water in the static water tank cools down to a temperature close to the minimum ambient temperature during the night as the tank is not insulated. The maximum water temperature was about 32°C and the condensation temperature was close to the ambient temperature.

Table 5.3: The Experimental Observations of the AIT Charcoal-Methanol Solar Refrigerator (17 October, 1987).

Local Time	Amb Temp.	Collector Temperatures					Condenser Temperatures				Receiver		Evaporator		Level Glass	Incident Radiation	Remarks
		Glass	Coll. Top	Coll. Bot	Char Top	Char Bot	Vapour	Liquid	Tube	Water	Top	Bot.	Evap.	Ice			
(Hr)	(C)	(C)	(C)	(C)	(C)	(C)	(C)	(C)	(C)	(C)	(C)	(C)	(C)	(C)	(Cm)	(kJ)	
6.00	24.62	24.52	30.63	30.87	27.55	24.73	27.53	24.50	27.14	27.10	-8.80	-8.94	-2.85	-1.38	-	0.00	
7.00	26.15	27.55	32.15	30.87	32.10	32.38	27.53	26.02	27.14	27.10	1.91	-8.94	-2.85	-1.38	-	205.20	
8.00	26.15	33.61	41.24	40.05	38.16	38.50	33.59	26.02	27.34	27.10	11.09	0.24	-1.32	-1.38	-	962.20	
9.00	27.68	42.70	60.93	61.47	56.34	58.39	41.17	27.53	28.03	27.79	18.74	15.54	-1.32	-1.38	-	1809.80	
10.00	30.74	50.28	81.38	81.36	76.03	79.81	53.29	30.56	30.41	28.49	27.92	21.66	0.21	-1.38	4.00	2455.50	
10.50	33.04	54.06	86.99	87.79	80.58	85.93	60.10	30.56	31.40	28.98	27.92	19.37	0.98	-1.38	6.20	1452.30	
11.00	33.80	57.85	94.26	95.13	86.64	92.05	63.89	33.59	32.19	29.58	29.45	18.60	1.74	-1.38	9.00	1759.30	
11.50	30.74	51.79	89.72	90.54	88.15	92.05	51.77	31.32	31.40	30.17	27.92	18.60	4.80	-1.38	10.30	756.00	
12.00	30.74	45.73	85.17	85.95	85.12	87.46	47.23	30.56	31.10	30.37	26.39	17.07	4.80	-1.38	10.40	408.00	
12.50	32.27	48.76	92.75	92.07	91.18	93.58	55.56	32.08	31.60	30.66	28.69	17.84	7.10	-1.38	10.40	1101.30	
13.00	32.27	53.31	100.32	99.72	94.21	96.64	60.86	32.08	31.89	30.86	29.45	18.60	6.33	-1.38	11.90	1382.50	
13.50	33.80	57.85	106.38	105.84	100.27	104.29	63.89	33.59	32.49	31.36	30.22	26.25	7.86	-1.38	13.80	1642.20	
14.00	32.27	54.82	109.41	108.90	104.82	108.88	60.86	32.08	32.39	31.85	29.45	20.13	9.39	-1.38	15.30	1274.00	
14.50	33.04	63.91	113.20	113.49	104.82	113.47	63.89	32.83	32.78	32.15	27.92	20.13	9.39	-1.38	16.10	1340.40	
15.00	32.27	54.82	109.41	108.90	109.36	111.94	53.29	32.08	32.39	32.45	27.92	20.13	9.39	-1.38	16.60	930.80	
15.50	32.27	45.73	91.23	92.07	100.27	99.70	45.71	30.56	32.39	32.25	23.33	18.60	29.28	29.22	17.00	308.30	
16.00	29.21	45.73	80.63	79.83	86.64	87.46	44.20	29.05	-	-	15.68	17.07	20.10	21.57	15.60	653.30	
17.00	29.21	36.64	60.93	59.94	63.91	64.51	39.65	22.99	-	-	4.97	6.36	10.92	10.86	13.40	702.70	
18.00	29.21	33.61	50.33	50.76	53.31	53.80	36.62	21.47	-	-	-1.15	0.24	6.33	6.27	11.40	110.60	
19.00	29.21	30.58	42.75	43.11	45.73	46.15	33.59	24.50	-	-	-5.74	-4.35	1.74	1.68	10.10	0.00	
20.00	27.68	29.07	38.21	38.52	39.67	40.03	33.59	26.02	-	-	-5.74	-4.35	0.21	0.15	9.20	0.00	
21.00	27.68	27.55	36.69	35.46	38.16	38.50	32.08	26.02	-	-	-7.27	-5.88	-1.32	-1.38	8.30	0.00	
22.00	27.68	27.55	35.18	35.46	36.64	36.97	30.56	26.02	-	-	-8.80	-5.88	-1.32	-1.38	7.50	0.00	
23.00	26.15	26.04	35.18	35.46	36.64	36.97	30.56	26.02	-	-	-8.80	-7.41	-1.32	-1.38	6.50	0.00	
24.00	26.15	26.04	33.66	33.93	35.13	35.44	30.56	26.02	-	-	-8.80	-7.41	-2.85	-2.91	5.70	0.00	
1.00	26.15	26.04	32.15	32.40	35.13	35.44	30.56	26.02	-	-	-8.80	-7.41	-2.85	-2.91	-	0.00	
2.00	26.15	26.04	32.15	32.40	33.61	33.91	29.05	26.02	-	-	-8.80	-7.41	-2.85	-2.91	-	0.00	
3.00	26.15	26.04	32.15	32.40	33.61	33.91	29.05	24.50	-	-	-8.80	-7.41	-2.85	-2.91	-	0.00	
4.00	24.62	24.52	30.63	30.87	32.10	32.38	29.05	24.50	-	-	-8.80	-7.41	-2.85	-2.91	-	0.00	
5.00	24.62	24.52	30.63	29.34	29.07	29.32	29.05	24.50	-	-	-7.27	-7.41	-2.85	-2.91	-	0.00	
6.00	24.62	24.52	30.63	29.34	29.07	29.32	29.05	24.50	-	-	-1.15	-7.41	-4.38	-4.44	0.00	0.00[a]	

Total Incident Solar Radiation = 19265.0

[a] End of Adsorption.

Table 5.4: The Experimental Observations of the AIT Charcoal-Methanol Solar Refrigerator (27 October, 1987).

Local Time (Hr)	Lab Temp. (C)	Collector Temperatures					Condenser Temperatures				Receiver		Evaporator		Level Glass (Cm)	Incident Radiation (kJ)	Remarks
		Glass (C)	Coll. Top (C)	Coll. Bot (C)	Char Top (C)	Char. Bot (C)	Vapour (C)	Liquid (C)	Tube (C)	Water (C)	Top (C)	Bot. (C)	Evap. (C)	Ice (C)			
6.00	20.03	19.98	24.57	24.75	26.04	26.26	24.50	19.96	23.18	23.14	-11.86	-12.00	-5.91	-5.97	-	0.00	
7.00	24.62	21.49	26.09	26.28	26.04	26.26	24.50	21.47	23.87	23.93	0.38	-10.47	-7.44	-9.03	-	180.60	
8.00	26.15	26.04	33.66	32.40	32.10	33.91	27.53	22.99	23.97	23.93	6.50	-4.35	-4.38	-4.44	-	966.80	
9.00	27.68	35.13	53.36	53.82	50.28	50.74	36.62	24.50	27.64	25.22	15.68	12.48	-1.32	-1.38	-	1825.70	
10.00	29.21	44.22	76.08	76.77	69.97	73.69	48.74	26.02	28.63	25.52	24.86	20.13	-1.32	-1.38	3.90	2522.10	
10.50	29.21	47.25	82.14	82.89	76.03	79.81	53.29	26.02	29.12	26.01	23.33	15.54	-1.32	-1.38	5.80	1482.90	
11.00	29.21	50.28	88.20	89.01	82.09	85.93	56.32	27.53	29.32	26.51	23.33	14.01	-1.32	0.15	8.50	1577.50	
11.50	29.21	50.28	92.75	93.60	85.12	92.05	57.83	29.05	29.52	27.30	24.86	14.01	-1.32	0.15	11.20	1692.50	
12.00	29.21	50.28	97.29	98.19	91.18	95.11	59.35	29.05	29.12	27.60	24.86	14.01	0.21	0.15	13.90	1448.50	
12.50	29.21	47.25	98.81	99.72	95.73	99.70	53.29	29.05	29.22	28.09	24.86	14.01	-1.32	0.15	14.70	1307.30	
13.00	29.21	50.28	106.38	107.37	101.79	107.35	57.83	29.05	29.22	28.59	24.86	12.48	-1.32	0.15	16.10	1691.30	
13.50	29.21	51.79	112.44	113.49	109.36	113.47	57.83	29.05	29.12	28.68	24.86	12.48	-1.32	0.15	17.70	1635.50	
14.00	29.21	53.31	118.50	118.08	115.42	116.53	57.83	29.05	28.82	28.59	24.86	12.48	0.21	0.15	18.30	1520.10	
14.50	29.21	53.31	121.53	122.67	119.97	122.65	56.32	29.05	29.12	28.49	23.33	12.48	0.21	0.15	18.70	1368.60	
15.00	29.21	53.31	121.53	122.67	121.48	122.65	54.80	29.05	29.12	28.59	23.33	12.48	0.21	0.15	18.90	1187.50	
15.50	29.21	53.31	120.02	131.14	121.48	122.65	53.29	29.05	-	-	23.33	14.01	0.21	0.15	18.90	991.70	
16.00	29.21	53.31	113.96	115.02	116.94	118.06	53.29	30.56	-	-	23.33	17.07	15.51	15.45	16.80	797.90	
17.00	29.21	41.19	70.02	69.12	76.03	76.75	41.17	21.47	-	-	8.03	7.89	15.51	15.45	16.20	895.90	
18.00	26.15	32.10	51.84	50.76	57.85	58.39	36.62	15.41	-	-	-2.68	0.24	6.33	6.27	14.20	144.00	
19.00	26.15	27.55	42.75	41.58	45.73	46.15	33.59	19.96	-	-	-5.74	-4.35	0.21	1.68	13.10	0.00	
20.00	24.62	26.04	38.21	38.52	39.67	40.03	30.56	21.47	-	-	-7.27	-7.41	-1.32	1.68	11.60	0.00	
21.00	24.62	24.52	35.18	35.46	36.64	36.97	30.56	22.99	-	-	-8.80	-8.94	-1.32	-1.38	10.70	0.00	
22.00	23.09	23.01	33.66	33.93	33.61	33.91	29.05	22.99	-	-	-10.33	-10.47	-2.85	-1.38	8.90	0.00	
23.00	23.09	23.01	30.63	30.87	32.10	32.38	27.53	22.99	-	-	-10.33	-10.47	-2.85	-1.38	8.00	0.00	
24.00	23.09	23.01	30.63	30.87	32.10	32.38	27.53	22.99	-	-	-10.33	-10.47	-2.85	-1.38	7.30	0.00	
1.00	23.09	23.01	29.12	29.34	30.58	30.85	27.53	22.99	-	-	-10.33	-10.47	-4.38	-1.38	-	0.00	
2.00	23.09	23.01	29.12	29.34	30.58	30.85	27.53	22.99	-	-	-10.33	-10.47	-4.38	-1.38	-	0.00	
3.00	23.09	23.01	29.12	29.34	30.56	30.85	26.02	22.99	-	-	-10.33	-10.47	-4.38	-1.38	-	0.00	
4.00	21.56	21.49	27.60	27.81	30.58	30.85	26.02	21.47	-	-	-10.33	-10.47	-4.38	-1.38	-	0.00	
5.00	21.56	21.49	27.60	27.81	29.07	29.32	26.02	21.47	-	-	-10.33	-10.47	-4.38	-1.38	-	0.00	
6.00	21.56	21.49	26.09	26.28	27.55	27.79	24.50	21.47	-	-	-10.33	-10.47	-5.91	-1.38	0.00	0.00[a]	

Total Incident Solar Radiation = 23042.0

[a] End of Adsorption.

Table 5.5: The Experimental Observations of the MIT Charcoal-Methanol Solar Refrigerator (29 October, 1987).

Local Time	Amb Temp.	Collector Temperatures					Condenser Temperatures				Receiver		Evaporator		Level Glass	Incident Radiation	Remarks
		Glass	Coll. Top	Coll. Bot	Char Top	Char. Bot	Vapour	Liquid	Tube	Water	Top	Bot.	Evap.	Ice			
(Hr)	(C)	(C)	(C)	(C)	(C)	(C)	(C)	(C)	(C)	(C)	(C)	(C)	(C)	(C)	(Cm)	(kJ)	
6.00	24.62	24.52	29.12	29.34	29.07	29.32	26.02	22.99	25.16	25.12	0.38	-7.41	-5.91	-5.97	-	0.00	
7.00	24.62	23.01	29.12	29.34	29.07	29.32	27.53	22.99	25.46	25..2	4.97	-7.41	-4.38	-4.44	-	63.40	
8.00	24.62	26.04	32.15	32.40	32.10	32.38	29.05	24.50	25.46	25.52	8.03	-2.82	-2.85	-2.91	-	346.10	
9.00	26.15	35.13	50.33	50.00	47.25	47.68	35.11	26.02	25.75	25.62	15.68	9.42	-1.32	-1.38	-	1516.70	
10.00	27.68	41.19	73.05	73.71	68.46	70.63	45.71	27.53	27.04	26.11	27.92	27.78	0.21	0.15	3.90	2447.40	
10.50	29.21	44.22	79.11	79.83	73.00	76.75	48.74	27.53	29.02	26.51	26.39	18.60	-1.32	-1.38	5.80	1410.90	
11.00	30.74	47.25	85.17	85.95	80.58	84.40	51.77	29.05	29.62	26.80	24.86	17.07	-1.32	-1.38	6.70	1354.70	
11.50	30.74	47.25	86.69	87.48	83.61	85.93	51.77	29.05	30.41	27.89	24.86	15.54	-1.32	-1.38	8.80	1379.10	
12.00	30.74	50.28	94.26	95.13	88.15	92.05	56.32	29.80	30.51	28.19	26.39	15.54	-1.32	-1.38	10.40	1566.00	
12.50	30.74	50.28	94.26	95.13	91.18	95.11	54.80	29.80	30.11	28.68	26.39	15.54	0.21	0.15	12.00	1263.10	
13.00	30.74	51.79	98.81	99.72	95.73	99.76	56.32	30.56	30.41	29.28	26.39	15.54	3.27	3.21	13.90	1293.10	
13.50	30.74	54.82	103.35	104.31	100.27	104.29	56.32	30.56	30.31	29.58	26.39	15.54	4.80	4.74	14.00	1253.90	
14.00	30.74	53.31	104.87	105.84	103.30	105.82	54.80	30.56	30.11	30.37	26.39	15.54	3.27	3.21	15.00	1960.30	
14.50	30.74	57.85	110.93	111.96	107.85	110.41	60.86	32.08	31.10	30.37	27.92	15.54	4.80	4.74	16.50	1411.80	
15.00	30.74	56.34	112.44	113.49	110.88	113.47	56.32	32.08	30.90	30.76	26.39	17.07	6.33	6.27	17.00	1198.10	
15.50	30.74	51.79	109.41	110.43	110.88	111.94	50.26	30.56	-	-	26.39	17.07	7.86	7.80	16.90	748.60	
16.00	30.74	50.28	104.87	105.84	106.33	107.35	51.77	32.08	-	-	24.86	20.13	29.28	29.22	16.90	762.20	
17.00	29.21	39.67	68.51	67.59	74.52	75.22	41.17	24.50	-	-	9.56	9.42	15.51	15.45	14.50	534.30	
18.00	27.68	33.61	54.87	53.82	57.85	58.39	36.62	16.93	-	-	0.38	1.77	7.86	7.80	12.50	72.60	
19.00	27.68	30.58	45.78	44.64	47.25	47.68	35.11	16.93	-	-	-4.21	-2.82	3.27	3.21	11.00	0.00	
20.00	27.68	30.58	39.72	40.05	41.19	41.56	32.08	26.02	-	-	-4.21	-4.35	0.21	0.15	10.20	0.00	
21.00	26.62	27.55	35.18	35.46	36.64	36.97	29.05	24.50	-	-	-8.80	-7.41	-1.32	-1.38	9.20	0.00	
22.00	24.62	26.04	33.66	33.93	35.13	35.44	29.05	24.50	-	-	-8.80	-7.41	-1.32	-1.38	7.90	0.00	
23.00	24.62	24.52	32.15	32.40	33.61	33.91	29.05	24.50	-	-	-8.80	-8.94	-1.32	-1.38	7.00	0.00	
24.00	24.62	24.52	32.15	32.40	33.61	33.91	29.05	24.50	-	-	-8.80	-7.41	-2.85	-2.91	6.40	0.00	
1.00	23.09	23.01	30.63	30.87	30.58	30.85	27.53	24.50	-	-	-10.33	-10.47	-2.85	-2.91	-	0.00	
2.00	23.09	23.01	29.12	29.34	30.58	30.85	27.53	22.99	-	-	-8.80	-8.94	-2.85	-2.91	-	0.00	
3.00	23.09	23.01	29.12	29.34	30.58	30.85	27.53	22.99	-	-	-8.80	-8.94	-2.85	-2.91	-	0.00	
4.00	23.09	23.01	29.12	29.34	29.07	29.32	27.53	22.99	-	-	-8.80	-8.94	-2.85	-2.91	-	0.00	
5.00	23.09	23.01	29.12	29.34	29.07	29.32	27.53	22.99	-	-	-8.80	-8.94	-4.38	-4.44	-	0.00	
6.00	23.09	23.01	29.12	29.34	29.07	29.32	27.53	22.99	-	-	0.38	-8.94	-4.38	-4.44	0.00	0.00*	

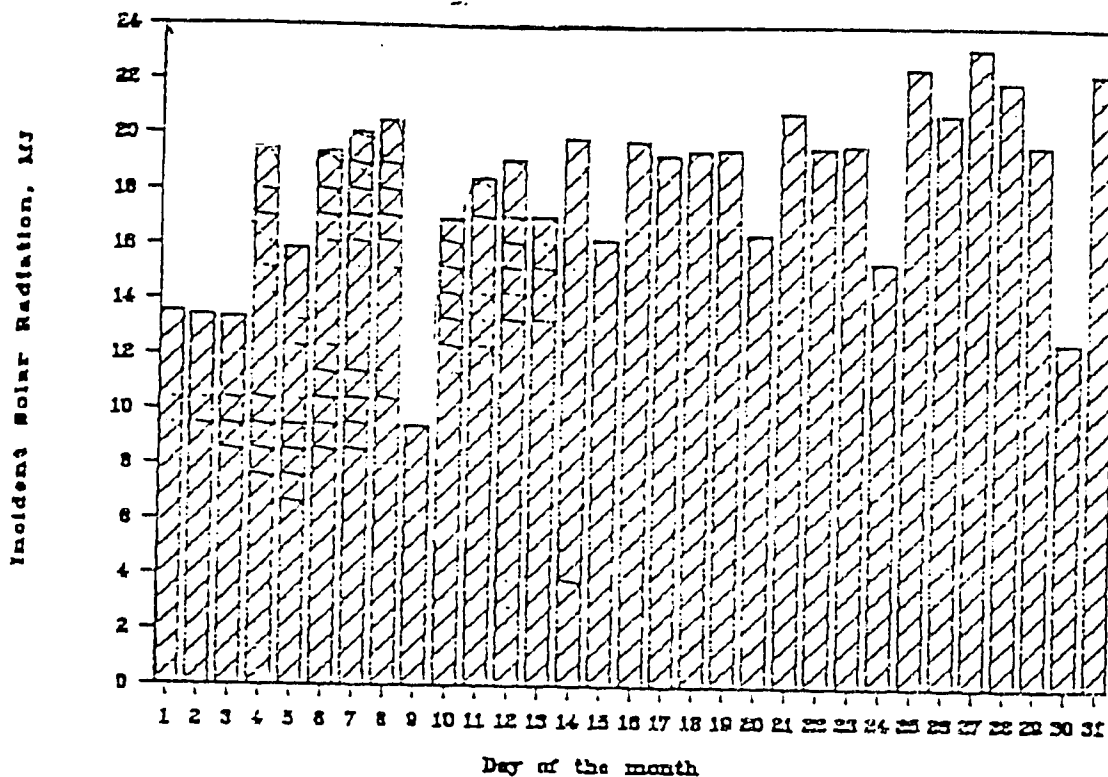Total Incident Solar Radiation = 19682.3

* End of Adsorption.

Fig.5-9: The Incident Solar Radiation on the Surface of Solar Collector for the month of October, 1987.
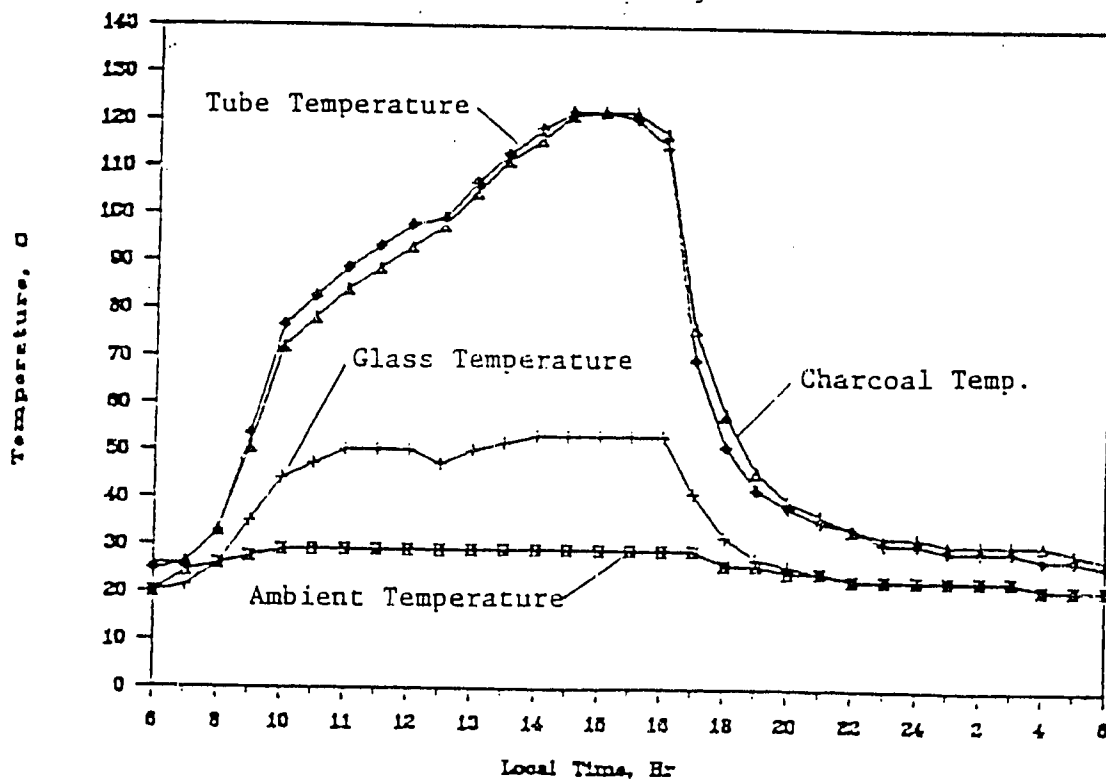

Fig. 5.10: The Temperature Profile of the Solar Collector during a Clear Day (27 October, 1987).

5.3.5 Receiver/Evaporator Temperature

Three temperature sensors(8, 9 and 10) were used to measure receiver/evaporator temperatures. The evaporator temperature is read by sensor 10, but during the cooling process it is immersed in the water and it reads a temperature intermediate between the evaporator and the water/ice temperature. The temperature measured by sensor 9, which is just above the evaporator, was taken as the evaporator temperature. The lowest evaporator temperature was -13.4°C. The temperature profile of the receiver/evaporator for a typical day is shown in Fig. 5.11. The condensation first starts in the receiver/evaporator as it is the coldest, and the temperature rises. This melts a small quantity of ice allowing the rest of the ice to be removed easily.

5.4 Experimental Data Analysis

5.4.1 Initial Analysis

The initial results calculated for the solar refrigerator were based on the heat balance at the end of desorption using the properties at the mean temperatures. The main assumptions are as follows:

1. The condenser temperature varies between 24°C and 32°C. But for this calculations, it was assumed equal to 31°C.

2. The temperature at state point 2 (beginning of the desorption), also called threshold temperature, cannot be determined accurately by observations as the first condensate collects in the evaporator and level cannot be read. So, this was determined from the p-T-x chart of the pair, and the value thus obtained was verified by calculations for T_2 using the mean properties by the Clausius Clapeyron equation as follows:

$$L(1/T_{ev} - 1/T_{con}) = H_{des} (1/T_1 - 1/T_2), \qquad (5.24)$$

where

$$\begin{aligned}
T_{ev} &= \text{Evaporator Temperature, C,} \\
T_{con} &= \text{Condenser, C,} \\
T_1 &= \text{Temperature of charcoal at the end of adsorption, C,} \\
T_2 &= \text{Threshold temperature, C,} \\
L &= \text{Latent heat of evaporation, kJ/kg,} \\
H_{des} &= \text{Heat of desorption, kJ/kg.}
\end{aligned}$$

3. The methanol liquid is assumed to evaporate at -10°C with the latent heat of evaporation L constant.

The useful heat during desorption Q_u (from state point 1 to 3) is given as:
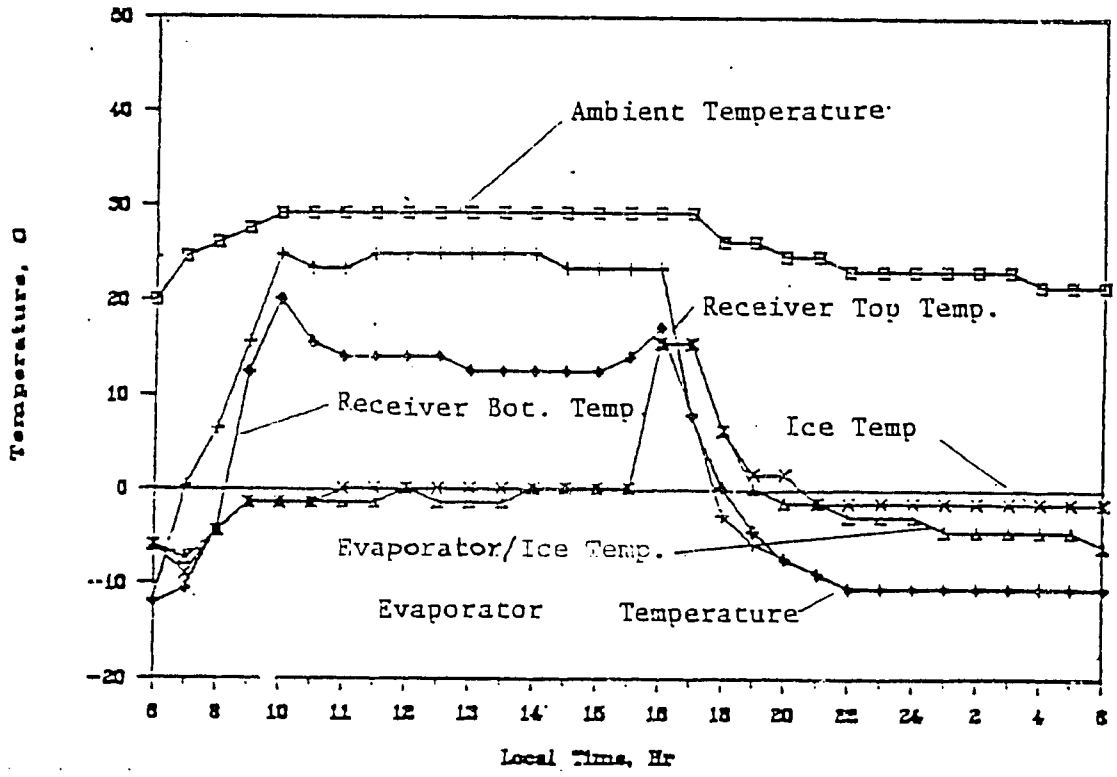
Fig. 5.14: The Temperature Profile of the Receiver/Evaporator
Box (27 October, 1987).

$$Q_u = Q_{coll} + Q_{ch} + Q_{meoh} + Q_{des} \qquad (5.25)$$

where

Q_{coll} = Total sensible heat used to raise the temperature of the collector, kJ,

Q_{ch} = Sensible heat used to heat the charcoal in the collector tubes, kJ,

Q_{meoh} = Sensible heat to the methanol liquid adsorbed in the charcoal, kJ,

Q_{des} = Total heat of desorption of the methanol, kJ.

If Q_{Ides} is the integrated value of the incident solar radiation on the surface of the solar collector at the end of desorption; then the average collector efficiency during desorption can be calculated as:

$$Coll\ Eff. = Q_u / Q_{Ides} \qquad (5.26)$$

Based on the above assumptions, the cooling produced by the methanol during adsorption can be approximated as:

$$Q_c = m_r (L - CP_{meoh} (T_{con} + 10.0)), \qquad (5.27)$$

where

m_r = Mass of the methanol cycled, kg,

CP_{meoh} = Specific heat of methanol, kJ/kg-K.

Thus, the integrated thermal coefficient of performance (COPIN) can be calculated as:

$$COPIN = Q_c / Q_u \qquad (5.28)$$

Similarly, the two integrated COPs of the system based on the amount of incident solar radiation can be calculated as follows:

COPINS (until the end of desorption) = Q_c / Q_{Ides} \qquad (5.29)

COPINS (over the day) = Q_c / Q_{Iday} \qquad (5.30)

where Q_{Iday} is the total incident radiation.

The performance of the charcoal-methanol solar refrigerator for the period of initial testing is given in Table 5.6.

5.4.2 Detailed Analysis

The above analysis gives the average performance of the system, but detailed calculations were done to determine the performance over the particular day. This analysis is based on the heat balances of the collector during desortion, and heat balances of the receiver/evaporator during adsorption. The main assumptions for the calculations are as follows:

Table 5.6: Test Results of AiT Charcoal-Methanol Solar Refrigerator (2-12 October, 1987)

Day	Hours	Incident Solar Energy (kJ)	Amb. (C)	Temperatures Coll. (C)	Char. (C)	Cond. (C)	Methanol Cycled (kg)	Evap. Temps. (C)	Useful Heat (kJ)	Total Cooling (kJ)	Avg. Coll. Eff.	COPIN	COPINS	Remarks
2/10/1987	6:00													
	13:30	12428.9	30.7	100.0	97.7	31.0	1.83	31.6	5340.8	1993.3	0.430	0.373	0.160	Clouded
	18:00	13404.6	23.1	26.9	26.9			-11.2					0.149	day
3/10/1987	6:00													
	15:00	11382.3	30.7	103.8	103.4	31.0	1.29	30.1	4649.0	1414.4	0.408	0.304	0.124	Clouded
	18:00	13315.0	26.2	28.8	29.2			-8.9					0.106	day
4/10/1987	6:00													Clear Morn.,
	15:00	16627.9	29.2	104.6	104.1	31.0	2.19	30.1	6005.7	2388.6	0.361	0.398	0.144	Rain
	18:00	19483.4	24.6	28.1	28.8			-10.9					0.123	After noon
5/10/1987	6:00													
	13:30	13398.9	31.5	109.2	105.7	31.0	2.05	30.1	5923.9	2232.8	0.442	0.377	0.167	Partially
	18:00	15844.4	23.1	28.1	28.0			-12.0					0.141	Clouded
6/10/1987	6:00													
	15:30	18523.9	33.0	116.8	116.7	31.0	2.44	29.3	6822.4	2660.4	0.368	0.290	0.144	Clear
	18:00	19307.9	24.6	27.7	27.6			-10.5					0.138	day
7/10/1987	6:00													
	14:30	18953.9	35.3	124.4	123.6	31.0	2.65	30.1	7337.3	2902.3	0.387	0.395	0.153	Clear
	18:00	20060.2	24.6	28.5	29.2			-9.7					0.145	day
8/10/1987	6:00													
	14:30	17444.8	27.6	108.0	107.6	31.0	2.40	27.8	6467.3	2634.6	0.371	0.407	0.151	Clear
	18:00	20513.8	23.9	27.7	28.0			-7.4					0.128	day
9/10/1987	6:00													
	14:30	9218.0	29.2	96.2	94.7	31.0	0.68	27.8	3466.4	746.7	0.375	0.215	0.081	Clouded
	18:00	9405.2	24.6	28.8	29.2			-8.9					0.079	day
10/10/1987	6:00													
	14:00	13288.4	33.8	109.2	105.3	31.0	1.77	27.0	5498.9	1946.2	0.414	0.354	0.146	Partially
	18:00	16905.5	23.1	28.4	28.4			-8.2					0.115	Clouded
11/10/1987	6:00													Rain
	14:00	15961.2	32.3	115.3	114.5	31.0	2.33	28.5	6543.0	2634.6	0.395	0.439	0.174	during
	18:00	18401.6	23.9	29.2	29.2			-8.9					0.138	Afternoon
12/10/1987	6:00													Clouded
	13:30	15166.3	32.3	98.5	97.3	31.0	2.40	27.1	5996.5	2634.6	0.395	0.439	0.174	Morning
	18:00	19087.0	24.6	30.8	30.7			-7.4					0.138	Clear Later

1. The methanol adsorbed in the charcoal is assumed to be at the mean charcoal temperature.

2. The properties of the collector tubes and the charcoal were assumed constant.

3. The properties of the methanol were computed as a function of temperature from the regression formulas based on published tables (Liley, 1982).

4. The heat of desorption was computed as a function of the charcoal temperature T and concentration x as follows:

$$H_{des} = (P(T) \, \nu(T)/T) \quad slope(x), \qquad (5.31)$$

where

$P(T)$ = Saturation pressure of the methanol vapour at temp. T, bar,

slope = Slope of the isosters calculated from the Clausius diagram for the charcoal-methanol based on the laboratory tests.

For the slopes for different concentrations of methanol in charcoal, x (wt. %) was represented by the following regressions:

slope = $4977.84 - 3776.07 \, x \qquad 0.15 \leqslant x \leqslant 0.21,$

slope = $11076.1 - 43996.0 \, x \qquad 0.10 \leqslant x \leqslant 0.15,$

slope = $7206.6 \; - 5366.9 \, x \qquad 0.02 \leqslant x \leqslant 0.10.$

The specific volume ν of the saturated methanol vapour can calculated as:

$$\nu(T) = 21780.3 \; \exp(-0.0304 \, T), \; m^3/kg \qquad (5.32)$$

The saturation vapour pressure of methanol was calculated using the Harlacher equation(Reid and others, 1977) as follows:

$$P(T) = \exp(HARA + HARB/T + HARC \, \ln(T) + HARD * P(T)/T^2) \qquad (5.33)$$

5. Other Properties of methanol were calculated as follows:

$$CP_{meoh} = 3.96 - 0.152 \, T + 0.000035 \, T^2 \qquad (5.34)$$

$$\rho_{meoh} = 947.7 - 0.1152 \, T - 0.0014 \, T^2 \qquad (5.35)$$

$$h_l = 121.07 + 0.7115 \, T + 0.003 \, T^2 \qquad (5.36)$$

$$h_v = 1120.35 + 3.383 \, T - 0.00401 \, T^2 \qquad (5.37)$$

here

CP_{meoh} = Specific heat, kJ/kg-K,
ρ_{meoh} = Density, kg/m^3,
h_1 = Specific enthalpy of methanol liquid, kJ/kg,
h_v = Specific enthalpy of methanol vapour, kJ/kg,
and T = Temperature, K.

6. For the COP calculations during desorption, the methanol was assumed to evaporate at -10°C with a constant latent heat L.

Desorption Period

The temperature at the state point 2 at the beginning of desorption was estimated by the method described earlier. The first heat balance starts when the methanol level can be read from the level glass. The heat used during the sensible heating up to 2, and the desorption until value could be read, were estimated from the experimental data. The heat balance of the solar collector was calculated every half an hour until the end of desorption.

The useful heat dQUsed for each period can be calculated as:

$$dQUsed = dQTube + dQChar + dQMeoh + dQDes, \qquad (5.38)$$

where

dQTube = Sensible heating of the collector tubes during the interval, kJ,
dQChar = Sensible heating of the charcoal in the tubes, kJ,
dQMeoh = Sensible heating of mean mass of methanol, kJ,
dQDes = Heat of desorption, kJ.

If dQRad is the incident radiation, during the same interval, the collector efficiency can be calculated as:

$$Coll. Eff = dQUsed/ dQRad \qquad (5.39)$$

Similarly if dQEv is the cooling that could be produced by the methanol desorbed calculated as shown earlier, the thermal coefficient of performance of the system during the period is:

$$COP_{In} = dQEv/dQUsed \qquad (5.40)$$

The coefficient of performance for the same period based on the incident solar radiation is

$$COP_{Ins} = dQEv/dQRad \qquad (5.41)$$

The accumulated value of thermal coefficient of performance up to the particular period can be calculated as:

$$\text{COP}_{\text{Intg.}} = \Sigma \, dQEv / \Sigma \, dQUsed \qquad (5.42)$$

Similarly, the accumulated coefficient of performance based on the solar radiation up to that period is :

$$\text{COP}_{\text{Intgs.}} = \Sigma \, dQEv / \Sigma \, dQRad \qquad (5.43)$$

The concentration of methanol in the charcoal was calculated reading the methanol level from the level glass, and the corresponding values calculated using Dubinin the equation and the performance of the solar refrigerator during the desorption period for a clear day is shown in Table 5.7.

Adsorption Period

The net cooling produced during the adsorption was calculated by performing hourly heat balances of the receiver/evaporator. The methanol lev.. generally could not be read after 24:00 hours (midnight). But the end of adsorption was estimated from the temperature profile of the receiver/evaporator, which generally occurred after 2:00 a.m. The evaporator temperature remains constant during the period after midnight. The last heat balance covers the time period between midnight and the end of adsorption. In each case, the properties of the methanol were evaluated at the mean temperature for the period. The net cooling produced by the system dQNet during each period can calculated as:

$$dQNet = dQc - (dQRec + dQEvap + dQLIq + dQLoss), \qquad (5.44)$$

where the heat values for the components during the period are:

dQc   = Cooling produced by the methanol cycled during the period (kJ),
dQRec   = Sensible heating/cooling of the receiver (kJ),
dQEvap = Sensible heating/cooling of the evaporator (kJ),
dQLiq   = Sensible heating/cooling of the mean mass of the liquid in the receiver/evaporator (kJ),
dQLoss = Heat lost from the receiver/evaporator box (kJ).

Thus the net solar COP, also called the overall coefficient of performance of the refrigerator, can be calculated as:

$$\text{Net Solar COP} = \Sigma \, dQNet / \Sigma \, dQRAd, \qquad (5.45)$$

where $\Sigma \, dQNet$ is the net cooling produced during adsorption period, and $\Sigma \, dQRad$ is the total incident solar radiation during the day.

The performance of the system during the adsorption period is shown in Table 5.8.

- 72 -

Table 5.7: The Performance of the AIT Charcoal-Methanol Solar Refrigerator during a Clear Day (29 October, 1987).

Local Time (Hr)	Amb. Temp. (C)	Mean Temp. Coll. (C)	Mean Temp. Char (C)	Exp. MEOH Conc.	Theo. MEOH Conc.	dQTube (kJ)	dQChar (kJ)	dQMeoh (kJ)	dMeoh (kg)	dQDes (kJ)	dQUsed (kJ)	dQRad (kJ)	dQEV (kJ)	Coll. Eff.	In	Ins	Intg.	Intgs.	Remark
6.00	24.6	29.2	29.2	.178															
10.00	27.7	73.4	69.5	.144	0.164	703.0	502.8	645.9	0.61	623.5	2475.2	4373.6	673.8	0.57	0.00	0.00	0.27	0.15	
10.50	29.2	79.5	74.9	.128	0.159	97.0	66.4	37.2	0.28	344.4	545.0	1410.9	314.1	0.39	0.58	0.22	0.33	0.17	
11.00	30.7	85.6	82.5	.120	0.142	97.0	94.9	49.5	0.13	182.2	423.5	1354.7	147.1	0.31	0.35	0.11	0.33	0.16	
11.50	30.7	87.1	84.8	.103	0.129	24.2	28.4	13.6	0.31	462.9	529.1	1379.1	336.8	0.38	0.64	0.24	0.37	0.17	
12.00	30.7	94.7	90.1	.090	0.119	121.2	66.4	27.8	0.23	376.3	591.8	1566.0	251.1	0.38	0.42	0.16	0.38	0.17	
12.50	30.7	94.7	93.1	.077	0.106	0.0	37.9	13.9	0.23	378.7	430.6	1263.1	250.1	0.34	0.58	0.20	0.39	0.17	
13.00	30.7	99.3	97.7	.069	0.095	72.7	56.9	18.6	0.14	236.1	384.3	1293.1	155.1	0.30	0.40	0.12	0.40	0.17	
13.50	30.7	103.8	102.3	.061	0.083	72.7	56.9	16.8	0.14	234.4	380.8	1253.9	154.1	0.30	0.40	0.12	0.40	0.16	
14.00	30.7	105.4	104.6	.054	0.074	24.2	28.4	7.5	0.14	232.5	292.6	1060.3	153.2	0.28	0.52	0.14	0.40	0.16	
14.50	30.7	111.4	109.1	.042	0.068	97.0	56.9	12.6	0.21	341.6	508.0	1411.8	225.4	0.36	0.44	0.16	0.41	0.16	
15.00	30.7	113.0	112.2	.038	0.061	24.2	37.9	7.1	0.07	113.3	182.7	1198.1	75.3	0.15	0.41	0.06	0.41	0.16	

Total						1333.2	1033.9	850.4	2.49	3525.9	6743.5	17564.6	2736.0						
As % of Incident Radiation						7.6	5.9	4.8		20.1	38.4								
Total % of Heat Used						19.8	15.3	12.6		52.3									

Table 5.8: The Performance of the AIT Solar Refrigerator during Adsorption Process (29 October, 1987).

Local Time	Amb. Temp.	Mean Temp.		dQRec	dQEvap	dQLiq	dQloss	dQC	dQNet	Remarks
		Rec.	Evap.							
(Hr)	(C)	(C)	(C)	(kJ)	(kJ)	(kJ)	(kJ)	(kJ)	(kJ)	
15.00	30.7	21.7	17.1							
15.50	30.7	14.4	17.07	0.00	0.00	0.00	7.14	-25.25	-32.40	
16.00	30.7	20.3	20.13	0.59	2.36	4.78	4.55	20.28	8.00	
17.00	29.2	19.2	9.42	10.01	8.25	75.46	9.43	389.56	286.41	
18.00	27.7	8.5	1.77	6.48	5.89	41.72	17.46	308.93	237.37	
19.00	27.7	2.2	-2.82	3.53	3.53	19.93	22.31	245.87	196.56	
20.00	27.7	-1.1	-4.35	0.59	1.18	3.01	25.16	134.38	104.44	
21.00	24.6	-3.4	-7.41	2.95	2.36	13.83	25.83	174.06	129.10	
22.00	24.6	-4.7	-7.41	0.00	0.00	0.00	25.66	232.15	206.49	
23.00	24.6	-4.9	-8.94	0.59	1.18	2.15	25.83	163.26	133.52	
0.00	24.6	-5.3	-7.41	0.59	1.18	1.94	26.16	109.07	79.20	
6.00	23.1	-4.9	-8.94	2.95	1.18	4.65	150.94	1226.94	1067.22	
Total				28.27	27.10	167.5	340.5	2979.2	2415.9	

Net Solar COP = 0.123

5.5 Results and Conclusions

The average efficiency of the collector varied between 33 and 44% and the peak collector temperature reached 122°C during clear days. The collector temperature was above 90°C even during cloudy days. The thermal coefficient of performance of the system was about 40% including the thermal mass of the components. The system can cycle up to 14 % wt. of methanol out of the 17.8% initially charged into the system. The integrated solar COP over the day was in the range 15%; but the net solar COP of the system during clear days including all the thermal losses in the receiver/evaporator was above 10% and reached up to 12.3%. This result is comparable to the contemporary French results. The evaporator temperature during most days was below -7°C but during some nights, it was as low as -12°C. This system was able to produce up to 4 kg of ice during clear days and the ice produced was subcooled to -4°C; most of the ice produced was removable. It was found that the heat losses in the evaporator were very high mainly due to the large heat transfer area of the box, and the longitudinal heat transfer through the connecting tubes. The solar refrigerator has outperformed our design expectations.

5.6 Cost and Economics of the System

5.6.1 Cost of the System

Table 5.9 shows the cost of the experimental unit built and tested at AIT. The cost of this unit does not contain the cost of the valves and other measuring equipments which are not needed in finished product. It is seen that the major cost of this refrigerator is the cost of the solar collector which accounts for about 60% of total costs. The break down of the solar collector cost shows that cost of the collector tubes and fittings was 31.6%, while the cost of charcoal was 22.5%, assuming the charcoal was acquired by surface mail. The other major cost is the labour cost which was assumed 25% of the material cost and is about 20% of the total cost. The total cost of the solar refrigerator was about US$ 1000.0, in December 1987. The cost of this solar refrigerator could be easily reduced using other cheaper materials such aluminum tubes or sections, and also using the locally manufactured charcoals. It must be mentioned here that the cost of imported charcoal was about ฿ 316.0/kg while the local charcoal is about seven times cheaper. The quality of the local charcoals can be tailor made for this particular application, and hopefully the cheaper local charcoals will help to reduce system costs significantly.

5.6.2 Economic Evaluation

A detailed economic evaluatiation of the solar refrigerator would be premature at this stage since this system is yet to reach a form suitable for commercial production. But a

Table 5.9: The Cost of the Experimental System.

Items	Cost (Bahts)	Cost (% of total)
1. Solar Collector		
Solar collector	8005.0	31.6
Activated Charcoal	5700.0	22.5
Selective Surface	1460.0	5.8
2. Water-cooled Condenser with static water tank	2490.0	9.8
3. Receiver/Evaporator	1260.0	5.0
4. Miscellaneous		
Methanol	500.0	2.0
MS Steel frame	840.0	3.3
Labour Cost	5064.0	20.0
Total Cost	25319.0 (about US $ 1000.0)	100.0

preliminary assessment of economic feasibility has been made using two simple economic indicators: the pay-back period, and the cost:revenue ratio.

The annual revenue from the unit is assumed to come from the sales of ice produced at the current local market prices. The retail price of ice in Bangkok is 3 bahts per kilogram, but in remote areas ice can be sold at twice the Bangkok price. So prices of 4, 5, and 6 bahts per kilogram are also considered. Although the system with slight improvement of the evaporator should be able to produce about 5 kg of ice during clear days, an average ice production of 3 kg per day has been taken for all calculations.

Table 5.10 shows the cost to revenue ratios for assumed lives of the unit from 10 years to 20 years, and assumed interest rates on the borrowed money from 10% to 17.5%. For all calculations a general inflation rate of 7% has been taken. The price of ice for this calculation is assumed to be 3 bahts per kilogram. The cost to revenue ratio varies from 0.52:1 under the most favorable conditions to 1.26:1 under the worst conditions.

Table 5.11 shows the pay-back period of the system using the break even point method. For all calculations only the initial

Table 5.10: Costs and Revenues.

Interest Rate (%)	Machine Life (years)	Initial Cost (bahts)	Present Value of Revenues (bahts)	Ratio
10.0	10.0	25319.0	27917.0	0.91
	15.0		39234.0	0.65
	20.0		49089.0	0.52
12.0	10.0	25319.0	25421.0	0.99
	15.0		34386.0	0.74
	20.0		41521.0	0.61
15.0	10.0	25319.0	22263.0	1.14
	15.0		28641.0	0.88
	20.0		33089.0	0.77
17.5	10.0	25319.0	20069.0	1.26
	15.0		24909.0	1.02
	20.0		27940.0	0.91

Table 5.11: Pay-Back Periods.

Interst Rate (%)	Pay Back Period (years)			
	Selling Price of Ice			
	3 bahts/kg	4 bahts/kg	5 bahts/kg	6 bahts/kg
10.0	8.94	6.49	5.10	4.20
12.0	9.95	7.01	5.42	4.41
15.0	12.17	8.00	5.99	4.79
17.5	15.55	9.14	6.58	5.17

cost of the equipment has been considered (maintenance not included) and present values were calculated at the general inflation rate of 7% per year.

5.6.3 Cost Comparison with the Photovoltaic Refrigerators

This solar refrigerator without much modification can be used for vaccine storage and freezing icepacks. Thus, it is reasonable to compare the cost of our system with the cost of photovoltaic refrigerators. The cost of the photovoltaic refrigerators used in the Expanded Programme of Immunization producing about 1.2 to 2 kg of ice per day range from US$ 4000.0 up to US$ 8000.0. Compared with our system these solar refrigerators are expensive. Moreover instances of failure of photovoltaic systems in field conditions have been encountered due to various reasons, such as failure of the photovoltaic panels due to temperature and wind induced stresses (Srivastava, 1987). Thus there is a great need for some cheap, reliable and robust systems, such as the system developed here.

5.7 Recommendations for the Future Work

The charcoal in the solar refrigerator is cycling more methanol compared to the sample of the same type tested in our test rig. This can be seen from the the theoretical concentrations calculated from the Dubinin equation (see Theo. MEOH Conc. in Table 5.7) and the actual values based on the experimental results (see Exp MEOH Conc. in Table 5.7). Due to the excellent methanol cycling capacity of the charcoal in the solar refrigerator, the receiver/evaporator has been undersized. At this stage, the system is partially charged, and any additional methanol charged into this system cannot be measured during clear days. So, the first improvement should be to redesign the receiver/evaporator. This receiver/evaporator should be larger in capacity, there should be a better level glass arrangement to measure the methanol cycled accurately. Moreover the receiver/evaporator box should be well insulated but compact. Some arrangements should also be made to reduce the longitudinal heat leak through the connecting tube into the receiver/evaporator. With these improvements, the system should be tested to evaluate its long term performance.

This system has performed satisfactorily during tests carried out so far. But long term performance of this system during different seasons must be monitored before possible commercial exploitation of such system in this region.

References

Bechec, M., G. Dhenain, J. Fontaine, G. Marsin, and D. Royer (1981). A Solar Ice Making and Cold Storage Machine With Intermittent Adsorption Cycle. In: Hall, D. O., and J. Mortan (Eds.). Solar World Forum, Vol. 2, Pergamon Press. pp. 1066.

Boon-Long, P. (1983) 'Crop Processing Systems in Northern Thailand', In: Devapriya, D.S. (1984), 'Location Modelling for Post-Harvest Handling Chain ' case of Perishable Crops grown in Northern Thailand' Research Study, Asian Institute of Technology, Bangkok. pp. 1-3.

Breck, D. W. (1974). Zeolite Molecular Sieve. John Wiley and Sons, New York. p. 771.

Chantavorapap, S. (1979) 'Development of Solar Energy in Thailand' Application of Solar Energy in Southeast Asia', Asian Institute of Technology, Bangkok. pp. 142.

Critoph, R. E., and R. Vogel (1986). Possible Adsorption Pairs for Use in Solar Cooling. International Journal of Ambient Energy. In press.

Derrik, A., and J. M. Durand (1986). Photovoltaic Refrigerators for Rural Health Care-Experiments. In: McNelis, B., and J. Morton (Ed.) Solar Energy for Developing Countries Power for Villages. ISES, U. K. Section. pp. 19-25.

Devapriya, D.S. (1984) 'Location Modelling for Post-Harvest Handling Chain' case of Perishable Crops grown in Northern Thailand' Research Study, Asian Institute of Technology, Bangkok. pp. 1-3.

Dubinin, M. M., and V. A. Astakhov (1970). Adv. Chem. Ser. 102. p.72.

Exell, R.H.B., and K. Saricali (1976). The Availability of Solar Radiation in Thailand, Research Report 63, Asian Institute of Technology, Bangkok, Thailand. 85 p.

Exell, R. H. B., and S. Kornsakoo (1981). Design and Testing of of a Solar Powered Refrigerator Research Report No. 126, Asian Institute of Technology, Bangkok. p. 60.

Exell, R. H. B. (1983). The Theory of Simple Solar Refrigerator. Renewable Energy Review Journal, Vol. 5, No. 2. pp. 1-17.

References (Contd.)

Expanded Programme of Immunization (1986). EPI Technical Series The Cold Chain Product Information Sheets. WHO/UNICEF/EPI.TS/86.1. pp. 9.

Food and Agriculture Organization (1984). Design and Operation of Cold Stores in Developing Countries, WHO, Rome. pp. 1.

Grenier, Ph., and M. Pons (1984). Experimental and Theoretical Results on the Use of an Activated Carbon CH_3OH Intermittent Cycle for Application to a Solar Powered Ice Maker. In S. V. Szokolay (Ed.) Solar World Congress, Vol. 1. Pergamon Press. pp. 500-506.

Guilliminot, J. J., F. Meunier, G. Marsin, and D. Royer (1981). In: Reider, D. (Ed.). Proc. of the EC Contractors Meeting, Athens. pp. 93-100.

Holman, J. P. (1981). Heat Transfer. McGraw-Hill International Book Company. pp. 283.

Kasemsap, M. (1985), Personal Communications.

Kirk, H. J. C. (1962). The Geology and Mineral Resources of the Simporna Peninsula North Borneo. Geological Survey Department British Territories in Borneo, Kuching, Sarabak. pp. 40-118.

Liney, P. E. (1982). Thermodynamic Properties of Methanol. Chemical Engineering, pp. 50-51.

Marel, H. W. van der, and H. Beutelspacher (1976). Atlas of the Infrared Spectroscopy of Clay Minerals and their Admixtures. Elsevier Scientific Publishing Company. pp. 292-298.

Meunier, F. and B. Mischler (1979). Solar Cooling through Cycles using Microporous Solid Adsorbents. In: Boer, K. W, and B. H. Glenn (Eds.), SUN II, Pergamon Press. pp. 676-680.

Meunier, F., Ph. Grenier, J.J. Guilleminot, and M. Pons (1986). Solar Powered Refrigeration Using Intermittent Solid Adsorption Cycles. To be published in the J. Solar Energy Engineering.

Minato, H., and T. Tamura (1978). Production of Oxygen and Nitrogen With Natural Zeolites. In: Sand, L. B., and F. A. Mumpton (Eds.). Natural Zeolites, Occurrences, Properties, Use. Pergamon Press Ltd. pp. 509-516.

References (Contd.)

Noh, J. H., and S. J. Kim (1986). Zeolites from Tertiary Tuffaceous Rocks in Yeongil Area, Korea. In: Murakami, Y., A. Iijima, and J. Ward (Eds.). New Developments in Zeolite Science Technology. Proc. of 7th International Conference.

Ota, S., and T. Sudo (1949). Studies in Oya-ishi Part 2, Mineralogical Composition. In: Sand, L. B., and F. A. Mumpton (Eds.). Natural Zeolites, Occurrences, Properties, Use. Pergamon Press Ltd. pp. 451-470.

Perry, R. H., and C. H. Chilton (1973). Chemical Engineer's Handbook. McGraw-Hill Kogakusha Ltd. pp. 5-22.

Polayani, M. (1970). Verh. deut. phys. Ges. In: Smisek, M., S. Cerney (Auths.). Active Carbon Manufacture, Properties and Applications. Elsevier Publishing Company. pp. 71-162.

Reid, R. C., J. M. Prausnitz, and T. K. Sherwood (1977). The Properties of Gases and Liquids. McGraw-Hill Book Company. pp. 629-679.

Saisithi, P. (1982) Present Status of Food Technology in Thailand Country Report, Institute of Food and Product Development, Kasesart University. pp. 23.

Smisek, M., S. Cerny (1970). Active Carbon Manufacture, Properties and Applications. Elsevier Publising Company. pp. 71-162.

Sridhar, K. (1987). Studies on Activated Carbon-Methanol Pairs with Relevance to Ice Making. M. Eng. Thesis, Asian Institute of Technology, Bangkok (Unpublished). p. 84.

Srivastava, N. K. (1987). Private Communications.

Tchernev, D. I. (1978). Solar Energy Application of Natural Zeolites. In: Sand, L. B., and F. A. Mumpton (Eds.). Natural Zeolites, Occurrences, Properties, Use. Pergamon Press Ltd. pp. 479-485.

Tchernev, D. I. (1984). Use of Natural Zeolites in Solar Refrigeration. ASSET, 6, NO. 5. pp. 21-24.

Uppal, A. H., B. Norton, S. D. Probert, and J. C. McVeigh (1986). Solar Adsorption-Cycle Refrigerator for Vaccine Storage. In: McNelis, B., and J. Morton (Ed.) Solar Energy for Developing Countries Power for Villages. ISES, U. K. Section. pp. 28-36.

References (Contd.)

Vandendriessche, H. (1976) 'Tropical Fruit Processing Industry: A Case studies of the industry in Developing Countries' Developing Centre of the Organisation for Economic Cooperation and Development, Paris. pp. 31-32.

Vaughan, D. E. W. (1978). Properties of Natural Zeolites. In: Sand, L. B., and F. A. Mumpton (Eds.). Natural Zeolites, Occurrences, Properties, Use. Pergamon Press Ltd. pp. 353-371.

Wadia, D. N. (1975). Geology of India. Tata McGraw-Hill Publishing Co., New Delhi. pp. 281.

Worek, W. M. (1986). Personal Communication.

World Health Organisation (1981). Specifications for Photovoltaic Refrigerator WHO EPI/9.81/CC.

Zhu, Z. (1987). Testing of a Solar Powered Zeolite-Water Refrigerator. M. Eng. Thesis, Asian Institute of Technology, Bangkok (Unpublished). p. 95.

APPENDIX A

Design Calculations

The solar collector consists of 38 kg of copper, 3.85 kg of brass. The total amount of charcoal that can be filled in the generator/collector is 17.8 kg. From the p-T-x diagram, it is clear that the rich concentration of methanol is 15% and the weak concentration will be 7% if the generator temperature reaches 100°C. If the system follows the ideal cycle, the collector, charcoal and the methanol adsorbed in the charcoal have to be sensibly heated to 86°C. Thus the heat to be supplied during the sensible heating process from initial temperature of 30° to 86°C is:

$$Q_{1-2} = (38 \times 0.38 + 3.85 \times 0.385)(86 - 30)$$
$$+ (17.8 \times 0.7 + 17.8 \times 0.15 \times 2.55)(86 - 30)$$
$$= 1970.7 \text{ kJ}.$$

Similarily, the heat supplied during the generation process from a temperature of 86°C to the maximum generator temperature of 100°C when the concentration of methanol in the charcoal decreases to 7% is:

$$Q_{2-3} = (38 \times 0.38 + 3.85 \times 0.385 + 17.8 \times 0.7 + 17.8 \times$$
$$(0.15 + 0.07)/2 \times 2.55))(100 - 86) + 17.8 \times 1500$$
$$\times (0.15 - 0.07)$$
$$= 2603.3 \text{ kJ}.$$

So the total heat to be supplied by the collector is the sum of Q_{1-2} and Q_{2-3}, and is equal to 4573.9 kJ. The total heat needed to heat the container from the state 1 to 3 is 1114.6 kJ, which is approximately 24.4% of the total heat that has to be supplied to the system.

If we assume the average efficiency of the solar collector equal to 30%, the total incident solar energy on the surface of the collector has to be 15.25 MJ. But if the efficiency of the solar collector is 35%, the above amount reduces to 13.07 MJ. Since the average solar radiation for Bangkok is about 16 MJ/m^2, the peak being approximately 20 MJ/m^2 (Exell and Sarikari, 1976) the solar collector has sufficient area to supply the required amount of heat to the system.

Estimation of the Cooling Produced

If we negelet the thermal mass of the receiver, the evaporator, and heat leak, the net cooling produced by the evaporation of about 1.4 kg of methanol is 1537.2 kJ. Thus the thermal coefficient of performance of the system is 33.6% but the overall coefficient of performance will be between 10 to 11.7%. But the thermal mass of the receiver, evaporator and the heat leak to the receiver/evaporator box will reduce this

performance further. The overall coefficient of performance of the system is expected to be around 10% and the system is expected to produce about 3 kg of ice from water initially at 30°C.

Estimation of Heat Lost by the collector during Adsorption

After the generator passes the highest temperature for the day, the back insulation of the collector can be lowered to cool the generator and the charcoal contained in it. If we assume half of the circumference of each tube to be exposed to the ambient air the total heat transfer area is approximately 1.5 m^2. The heat loss from the back of the collector will be mainly by three modes of heat transfer (i) natural convection, (ii) forced convection due to wind, and (iii) radiation.

(i) Heat Loss by Natural Convection

For a heated plate facing downward the Nusselt number Nu is given by Holman (1981) as follows:

$$Nu = 0.56 \ (Gr \ Pr \ Cos \ \theta)^{1/4}.$$

But the Grashof number $Gr = g \ \beta \ (T_W - T_\infty) \ x^3/ \nu^2$,

where

β = Volume coefficient of expansion = $1/T$, where T is in kelvins,
T_W = Wall temperature(K),
T_∞ = Free stream temperature(K),
x = Length of the plate(m),
ν = Kinematic viscosity of air = μ/ρ , (m^2/s),
μ = Dynamic viscosity (kg/m-s),
Pr = Prandl number = ν/α, and $\alpha = k/\rho \ c_p$,
k = Conductivity of air (W/m-K),
α = Diffusivity (m^2/s),
θ = Angle made by the heated plate with the vertical, (degrees).

In the above equation T is calculated as:

$$T = T_\infty + 0.25 \ (T_W - T_\infty).$$

Other properties are evaluated at temperature T_1 which is given as:

$$T_1 = T_W - 0.25 \ (T_W - T_\infty).$$

Assuming the wall temperature equal to 35°C and the free stream temperature of 30°C, β is equal to 1/304.4 and the fluid properties have to be evaluated at 29°C. This gives Gr Pr equal to $687E10^6$. Thus the convective heat tranfer coefficient

can be calculated as:

$$h_c = Nu \ k/x.$$

The above equation gives a convective heat tranfer coefficient due to natural convection h_c for 1.2 m long tube equal to 1.39 W/m^2-K.

(ii) <u>Heat Tranfer due to Wind</u>

Assuming the average wind speed of 1 m/s and applying the empirical relation of Watmuff, Charter and Procter (Exell, 1983), the convective heat tranfer coefficient due to wind flowing over the plate is:

$$h_w = 2.8 + 3.0 = 5.8 \ W/m^2-K.$$

Thus the total heat lost by natural convection and the wind blowing across the exposed area of 1.5 m^2, assuming the average temperature difference of 5°C between the back of the collector plate and ambient, is equal to 53.92 W.

(iii) <u>Radiation</u>

Assuming a temperature difference of 5°C between the collector and the ambient at 3O^{o}C, and emissivity of the back of the coated collector equal to 0.8, the heat transfer through the surface area of 1.5 m^2 is:

$$q_r = \epsilon \sigma (T_w^4 - T_a^4) \ A$$
$$q_r = 0.8 \times 5.669 \times 10^{-8}(308.15^4 - 303.15^4) \times 1.5$$
$$= 39.5 \ W.$$

Thus the total heat lost by the back of the collector by above three modes of heat transfer is equal to 93.4 W. If the time to release the heat is 12 hours, the total heat that can be lost is equal to 4036 kJ. The heat to be lost during adsorption period is equal to 2731 kJ. Thus the back of the collector can dissipate the heat during adsorption. It must be remembered that heat will also be lost from the top of the collector.

PHOTOGRAPHS
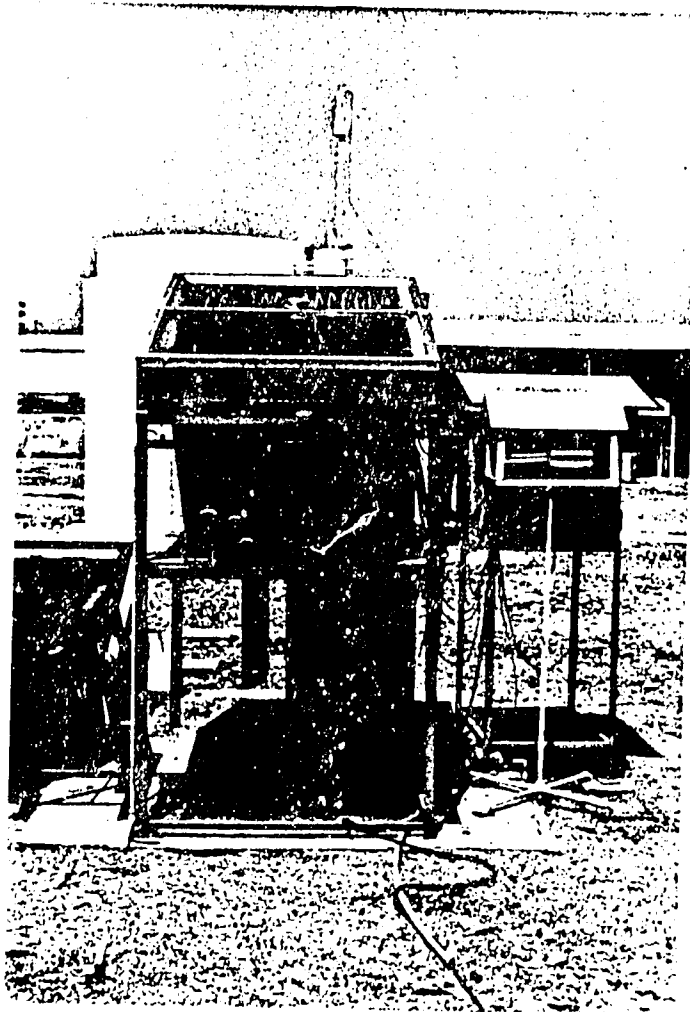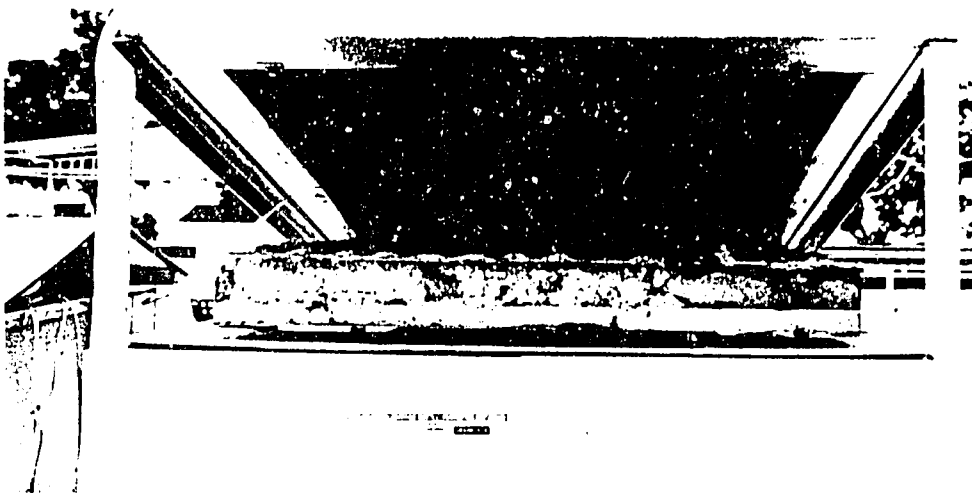
Front view of the solar refrigerator.
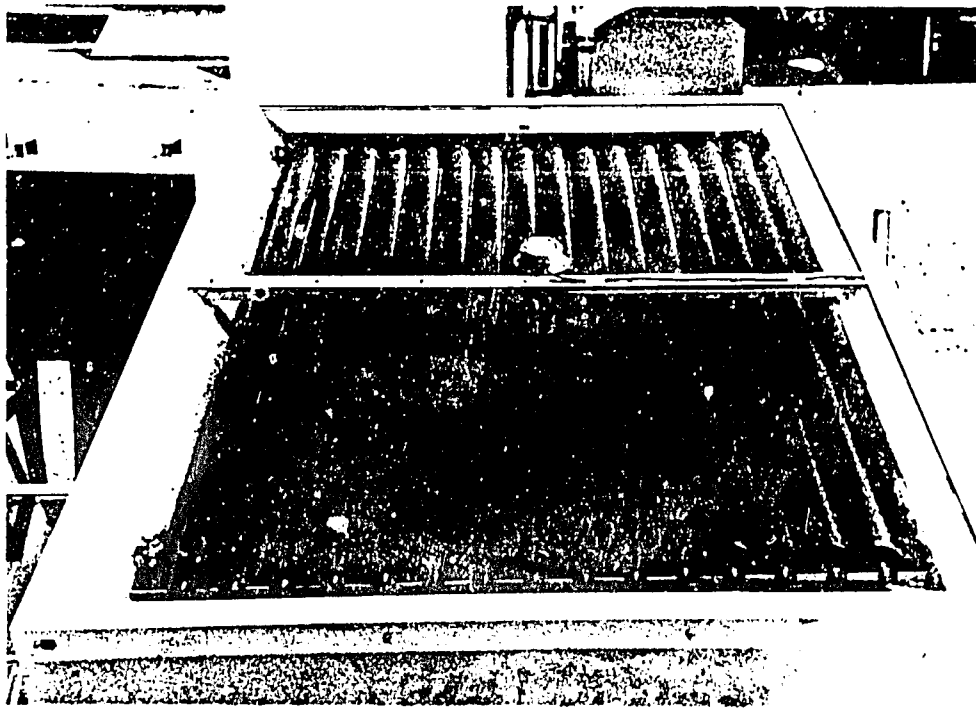
Solar collector.

Condenser

Isolation
valves
and
ice box

Back of the solar collector showing insulation
lowered.